PROTECTION OF MILD STEEL IN AGGRESSIVE MEDIA USING CARBOHYDRATE POLYMERS

Thesis Submitted
to the University of Calicut for the
award of

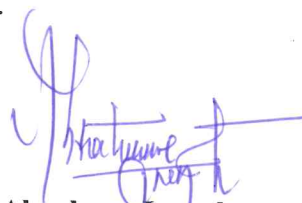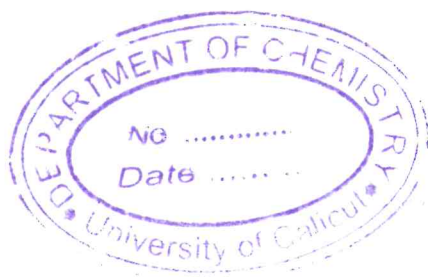## DOCTOR OF PHILOSOPHY IN CHEMISTRY

SHAMSHEERA K. O.

DEPARTMENT OF CHEMISTRY
UNIVERSITY OF CALICUT
KERALA- 673635
JANUARY 2021

Certificate

This is to certify that the thesis entitled "Protection of Mild Steel in Aggressive Media using Carbohydrate Polymers" submitted to the University of Calicut, is a record of precise research work carried out by Shamsheera K. O. at the Department of Chemistry, University of Calicut under my guidance and supervision. The contents of the thesis have been checked for plagiarism using the software 'Urkund' and the similarity index falls under permissible limit, and I further certify that the thesis or part has not previously formed the basis for the award of any degree, diploma or associate ship of any other University or Institute. The suggestions/corrections/recommendations/observations made by the adjudicators have been included in the revised thesis.

University of Calicut

Dr. Abraham Joseph
Professor

Dr. ABRAHAM JOSEPH
Professor
Department of Chemistry
University of Calicut
Calicut University P.O.
Malappuram, Kerala
Pin - 673 635

Certificate

This is to certify that the thesis entitled "Protection of Mild Steel in Aggressive Media using Carbohydrate Polymers" submitted to the University of Calicut, is a record of precise research work carried out by Shamsheera K. O. at the Department of Chemistry, University of Calicut under my guidance and supervision. The contents of the thesis have been checked for plagiarism using the software 'Urkund' and the similarity index falls under permissible limit, and I further certify that the thesis or part has not previously formed the basis for the award of any degree, diploma or associate ship of any other University or Institute. The suggestions/corrections/recommendations/observations made by the adjudicators have been included in the revised thesis.

University of Calicut

Dr. Abraham Joseph
Professor

Declaration

I, **Shamsheera K. O.,** hereby declare that thesis entitled as "Protection of Mild Steel in Aggressive Media using Carbohydrate Polymers" submitted to the University of Calicut is a bona fide record of project work done by me under the supervision and guidance of **Dr. Abraham Joseph**, Professor, Department of Chemistry, University of Calicut and it has not formed the basis for the award of any Degree/Diploma/Associate ship/Fellowship or other similar title of any other University or Institution.

University of Calicut   **Shamsheera K. O.**

Acknowledgment

*First and foremost, I would like to thank Almighty **"ALLAH"** the most merciful and the beneficent for showering limitless blessings on me for making this challenging task reach to its completion.*

Research requires a high level of planning, execution and discussion. To maximise the quality of the results obtained, we need plentiful opinions, contributions and support. A thesis is not a personal achievement but the result of an enriching experience involving more than one person.

*It is definitely a pleasing privilege for me to express my heartfelt gratitude to my supervisor **Prof. Abraham Joseph** for his constant support and encouragement throughout this work. I was fortunate enough to have him as my mentor. I greatly appreciate his ability to stay kind and the liberty he gave to carry out this work. His wisdom and reasoning abilities have been of great value for me and I hope it will continue to be so in future too. I extend my most sincere regard and thanks to him for his insightful comments, excellent advices and perceptive suggestions that eventually led to the final draft of this study.*

*I would like to express my sincere thanks to the Head of the Department, **Dr. A. I. Yahya** and former Heads of the Department, Dr. P. Raveendran and Dr. K. Muraleedharan for providing me all the facilities to carry out my research work. I express my sincere gratitude to all the faculty members and non-teaching staff in the Department of Chemistry of University of Calicut.*

I take this opportunity to thank my research colleagues Dr. Rugmini Ammal, Dr. Prajila, Dr. Anupama, Dr. Shainy K M, Anupama R Prasad, Dr. Sabeel M Basheer, Jaseela P K, Julia Garvasis, Sr. Asha Thomas, Linda Williams,

Shamsheera K. O.

Dedicated to

My Family

Table of Contents

Preface

The problem of metal corrosion and its prevention is a prime research area for investigation as economic losses due to corrosion represent a large portion of the total costs for industries every year worldwide. Iron and its alloys have attracted much attention due to high mechanical strength, recyclability, malleability, easy availability, and low cost. Mild steel is one of the most widely used industrial materials, which has been used in a variety of industries, especially for structural applications. During its application, it may come in contact with aggressive acid solutions and corrodes heavily. Proper corrosion control can not only help in avoiding huge economic losses but can also help to avoid many potential disasters that can cause serious issues to humans and the environment. The increased awareness of the toxicity and harmful effects of raw materials to human and the environment have demanded the development of cost-effective and benign remediations for corrosion prevention. Several naturally occurring, chemically stable, cost-effective, and eco-friendly macromolecules like carbohydrate biopolymers and their derivatives have been developed as effective corrosion resistant coating and inhibitors for metals in various aggressive media. The work embodied in this thesis entitled "Protection of mild steel in aggressive media using carbohydrate polymers" comprises eight chapters.

Chapter 1: Introduction and Literature Review

This chapter encompasses the general introduction which deals with the economic aspects of corrosion, mechanism of corrosion, forms of corrosion, corrosion prevention using corrosion resistant coating and

inhibitors and corrosion prevention mechanism. The non-electrochemical and electrochemical methods for monitoring the process of corrosion and the theories behind all these techniques have been included here. A detailed literature review of carbohydrate polymers like chitosan, guar gum, and pectin as corrosion resistant materials are included in this chapter.

Chapter 2: Materials and Methods

This chapter deals with the materials and methods used in this work. This chapter also includes the methods of development of coating on mild steel surface. The instrumental details of various characterization techniques used for the study are also described. The details of corrosion monitoring strategies that have been used for the corrosion protection of carbohydrate polymers studied here are also included in this chapter. Theoretical strategies and the correlation of experimental results with quantum chemical calculations using NBO analysis and Monte Carlo simulation studies are also described here.

Chapter 3: Protection of Mild Steel in Aggressive Environments Using Stearic Acid Grafted Chitosan

This chapter discusses the development of stearic acid grafted chitosan film as corrosion resistant coating for mild steel in 0.5M HCl and 3.5% NaCl. The successful grafting of stearic acid into chitosan film is experimentally confirmed using elemental analysis, water contact angle measurements, TGA, FTIR, NMR, and theoretically proven via DFT calculations. The critical micelle concentration measurement is carried out to prove the self-assembling ability of the grafted film. Weight loss measurements, electrochemical impedance spectroscopy (EIS),

potentiodynamic polarization (PDP) were carried out for monitoring the corrosion process of uncoated and coated mild steel. Surface morphological studies were carried out to ensure the effective formation of coating on mild steel using SEM and AFM.

Chapter 4: Extended protection of mild steel in saline and acidic environment using stearic acid grafted chitosan preloaded with mesoporous hydrophobic silica

This chapter describes the development of a corrosion resistant coating by loading mesoporous hydrophobic silica as nano filler into chitosan and further grafting with stearic acid. Mesoporous hydrophilic silica and mesoporous hydrophobic silica were characterized using BET analysis, FESEM, TEM, FTIR, TGA, and water contact measurements. Weight loss study, EIS, and PDP studies were used to monitor the corrosion protection performance of stearic acid grafted chitosan preloaded with mesoporous-hydrophobic silica. Corrosion studies after different immersion times in acidic and saline media were carried out. Scotch tape adhesion test was also performed to ensure the effective formation of coating on the mild steel surface. Surface morphological studies were carried to ensure the presence of coating after exposure to corrosive media.

Chapter 5: Inhibition of Mild Steel Corrosion in Acidic Environment Using Guar Gum as Inhibitor

The corrosion inhibition performance of guar gum is discussed in this chapter. The optimum concentration of guar gum is determined from the weight loss study. 200-800ppm of guar gum is introduced into the corrosive medium and the behaviour is studied by using EIS and PDP

methods at 303-318K. The stable interaction between guar gum and mild steel is verified using FTIR and XPS. The mode of adsorption of inhibitor molecules on mild steel surface was also elucidated by the determination of thermodynamic and kinetic parameters. The surface morphology of the corroded mild steel samples in the presence and absence of guar gum was evaluated using FESEM and AFM. The DFT study shows that guar gum can donate free electrons to the metal atom and hence act as a good inhibitor by forming an adsorptive layer by replacing the pre-adsorbed water molecules. The Fukui indices also specify the nucleophilic and electrophilic centres in guar gum. The adsorption of guar gum on Fe (1 1 0) plane has been carried out using Monte Carlo simulation studies.

Chapter 6: Enhanced Protection of Mild Steel in HCl Using Synergistic Interaction of Guar Gum and Non-Ionic Surfactants

This chapter deals with the synergistic effect of two non-ionic surfactants (Tween-80 and Triton-X) on the corrosion inhibition performance of guar gum for mild steel in 0.5M HCl at different temperatures. The corrosion inhibition of the synergistic pairs was carried out using weight loss study, EIS, and PDP measurements. The addition of surfactants synergistically increased the inhibition efficiency of guar gum; the effect of Tween-80 being more pronounced than Triton-X. The XPS, FESEM, and AFM images indicated the formation of thin inhibitor film on mild steel surface which is responsible for inhibiting metal dissolution. Quantum chemical calculations and Monte Carlo simulations were used to confirm the corrosion inhibition of

synergistic pairs. NBO analysis is used to confirm the higher inhibition efficiency of guar gum: Tween-80 over guar gum: Triton-X.

Chapter 7: Protection of Mild Steel in HCl Using Pectin Isolated from Jack Fruit Waste

In this chapter pectin isolated from the jack fruit peel waste was used as a green corrosion inhibitor for mild steel in 0.5M HCl. Corrosion inhibition performance of pectin was carried out using the weight loss method, EIS, and PDP measurements. The mechanism of inhibition was also investigated by calculating the thermodynamic and activation parameters. The adsorption of the inhibitor on mild steel surface obeyed Langmuir adsorption isotherm. The FESEM and AFM studies were used to judge the adsorptive nature of the pectin in the acid solution. The electronic and structural information of pectin was disclosed by DFT and Monte Carlo simulation studies.

The thesis ends up with **Summary and Future Outlook**

Introduction and Literature Review

Chapter 1

This chapter covers a brief introduction about the economic aspects of corrosion, various forms of corrosion, and corrosion control using coatings and inhibitors. The probable mechanisms of corrosion protection are also mentioned in this chapter. The experimental and theoretical aspects of various corrosion monitoring techniques are also briefly outlined in this chapter. A brief literature survey of green carbohydrate polymer as corrosion resistant material was also given in this chapter.

CONTENTS

1.1. Motivation and Background

Earth has a treasure of natural resources for metals. It is difficult to imagine today the world without metals as it became part and parcel of daily life. Owing to their excellent mechanical and physicochemical properties, humans have made-up goods from metals over a millennium. Metals are extracted from their ores by the application of energy. The metals in their metastable state revert back to its low energy state of chemically bound form. The usual way for these reversal is the process of corrosion[1, 2]. Corrosion is the word originated from its Latin counterpart corrodere, means, "to attack", or "to chew away". Corrosion is defined by Mars Fontana as the deterioration of metals or materials due to chemical or electrochemical interaction with their environment[3]. Humans have been trying to recognize and control corrosion since they have been using metals and alloys. The increased awareness of the toxicity and harmful effects of raw materials to human and environment have demanded the development of cost-effective and benign remediations for corrosion prevention. Corrosion makes severe economic consequences, social and health hazards. Thus, corrosion protection of commercial metals become a scientific task for research community, especially materials scientists and chemists, and an enduring battle for industries. It is estimated that corrosion destroys one-quarter of the world's annual steel production, which corresponds to about 150 million tons per year, or 5 tons per second. Of course, corrosion is not limited to steel but affects all materials including metals, polymers, and ceramics.

1.2. Corrosion and Global economy

Corrosion prevention is concerned with the safety, conservation, and economy. Corrosion is a process which grab huge economic liability and physical threat. Just like any other natural calamity, corrosion also can cause disastrous damage to bridges, petroleum pipelines, automobiles, etc [4-6]. Billions of dollars are spent annually for the replacement of corroded materials, machinery, and several other objects. According to study by NACE (National Association of Corrosion Engineers), the global cost of corrosion is in the order of 1 to 5 % of the gross national product (GNP) for any country. According to the "International Measures of Prevention, Application and economics of Corrosion Technology (IMPACT) " estimates the global cost of corrosion in 2013 as $2.5 trillion which is about 3.4% of the gross domestic product (GDP) [7]. The data provided by NACE for the global cost of corrosion is shown in Figure 1.1
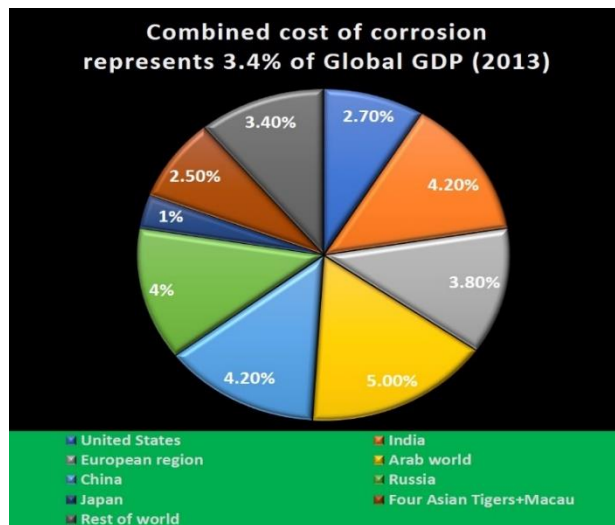
Figure 1.1. Global GDP by economic region

Loss of metal by corrosion causes waste of metal, energy, and human effort to fabricate the metal structure. Moreover, rebuilding the corroded structure needs a further investment of metal, energy, and human efforts. It is essential to implement and practice effective strategies to control corrosion and associated issues.

Corrosion costs could be of direct or indirect losses. Direct losses are those associated with the maintenance, prevention, replacement of corroded structures and machinery, or their components. The total direct cost of corrosion is estimated at $276 billion; 3.1 % of the GDP. Indirect losses are more difficult to evaluate precisely and cannot be replaced by money[8, 9]. For example

- *loss of valuable product*: water, oil, or gas may be leak out through the corroded system, leakage of antifreeze liquid through a corroded radiator may cause a serious accident

- *The shutdown of equipment* due to corrosion failure may cost a huge amount of money due to production loss

- *Loss of efficiency*: decreased heat transfer rate in heat exchangers through corrosion products, or internal combustion of an automobile engine, clogging of the pipeline for water supply by the deposition of rust demanding increased pumping capacity.

- *Contamination of the product*: The corroded product does not have enough mechanical strength. So, the possibility of contamination of the product with the substance is very high, demanding clean up, and this can be expensive

- *Overdesign*: In the expensive overdesigning of underground pipeline, reaction vessel, boiler, marine structure, etc suffers a huge amount of economic losses.

To achieve corrosion control, it is necessary to understand the mechanism of corrosion, classification of corrosion, methods to prevent corrosion and corrosion monitoring techniques

1.3. Mechanism of Corrosion

The basic mechanism of corrosion is the movement of ions at the metal electrolyte interface. The most acceptable electrochemical theory of corrosion is given by Whitney [10-12]. During the aqueous corrosion process, anodic oxidation of the metal and cathodic reduction in the environment creates two interrelated half-cell reactions[13]. For any metal (M) the oxidation reaction at the anodic site is given by

$$M \rightarrow M^{n+} + ne^- \qquad (1.1)$$
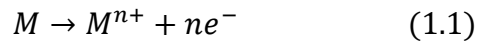
At the cathodic site, the produced electrons react with some reducible components of electrolyte through the following equations

1. Hydrogen evolution

In acid environment $\qquad 2H^+ + 2e^- \rightarrow H_2 \qquad (1.2)$
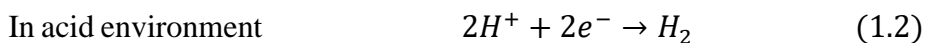
In an alkaline or neutral environment

$$2H_2O + 2e^- \rightarrow H_2 + 2OH^- \quad (1.3)$$

2. Oxygen reduction

In acid environment $$O_2 + 4H^+ + 4e^- \rightarrow 2H_2O \qquad (1.4)$$
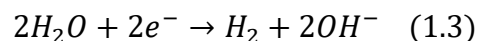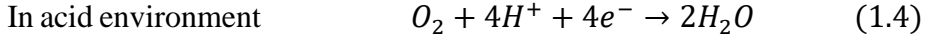
In alkaline and neutral solution

$$2H_2O + O_2 + 4e^- \rightarrow 4OH^- \qquad (1.5)$$

3. Metal deposition $$M^{n+} + ne^- \rightarrow M \qquad (1.6)$$

4. Metal ion reduction $$M^{n+} + e^- \rightarrow M^{(n-1)+} \qquad (1.7)$$
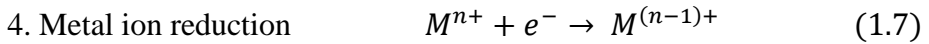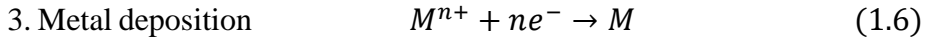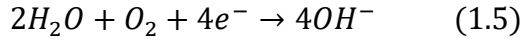
According to Faraday's law, the total flow of electrons from the anodic to the cathodic region during the corrosion process generates corrosion current (i_{corr}) and is a measure of the corrosion rate of the metal. A pictorial representation of the mechanism of corrosion is given in Figure 1.2
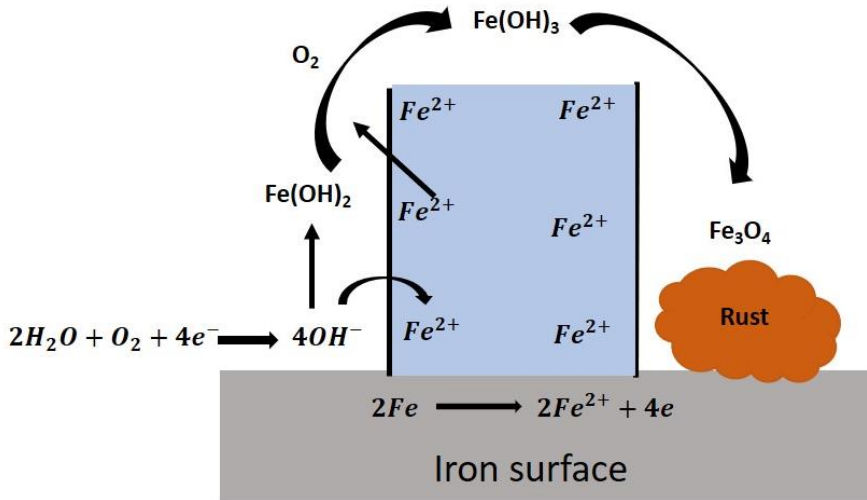
Figure 1.2. A schematic of electrochemical mechanism of iron corrosion

1.4. Classification of corrosion

Corrosion manifests in different forms. It is desirable to know the form of corrosion as it can help in the identification of the cause of corrosion and choosing the effective method of prevention. In most corrosion failure analysis, it is necessary to know the type of corrosion, which has been responsible for the failure. Corrosion can be classified in several ways like dry corrosion, wet corrosion, low temperature corrosion, high temperature corrosion etc. Based on the appearance of the corroded metals identified either through visual inspection or using modern spectroscopy there are eight forms of corrosion [14, 15] which are summarized in Figure 1.3 and 1.4
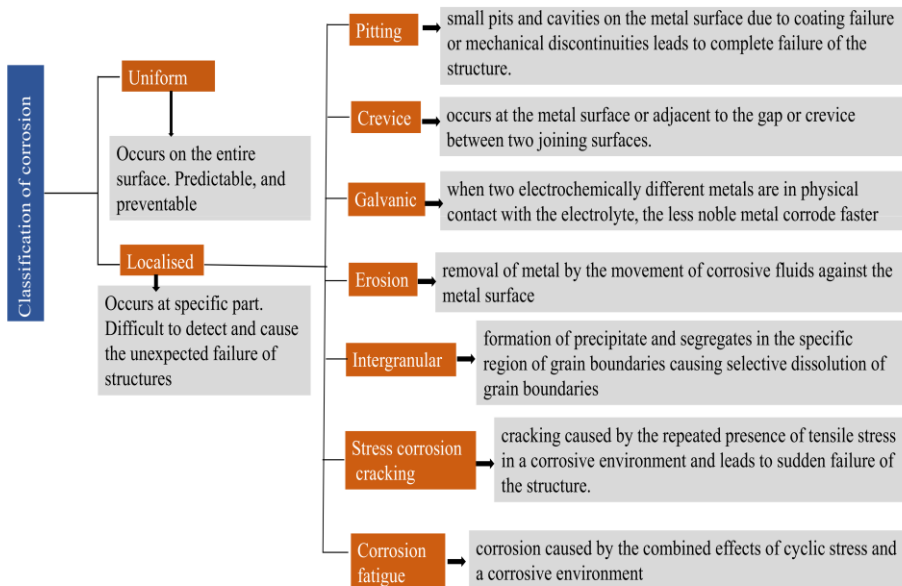
Figure 1.3. Classification of corrosion
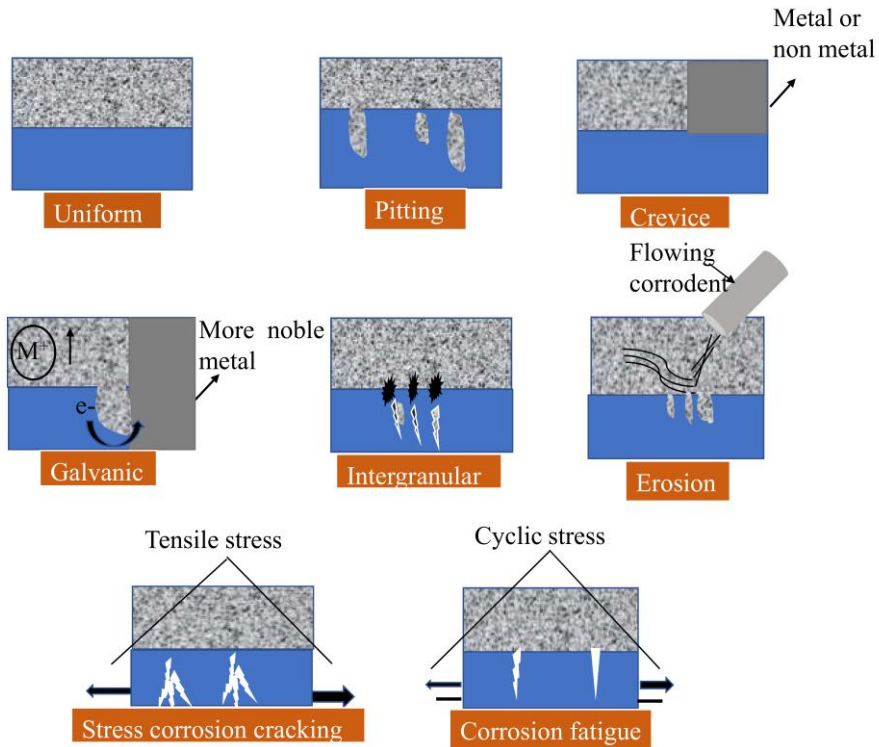
Figure 1.4. Pictorial representation of various types of corrosion

1.5. Corrosion prevention

Corrosion has been the subject of scientific study for more than 150 years. Humans have been trying to understand, control, and prevent corrosion for as long as they have been using metal objects. Corrosion never stops but its severity can be controlled by various methods either by isolating the metal from the aggressive environment or elimination of any one of the components of electrochemical cells which accelerates the corrosion process. The general classification of various corrosion prevention methods is summarized in Figure 1.5
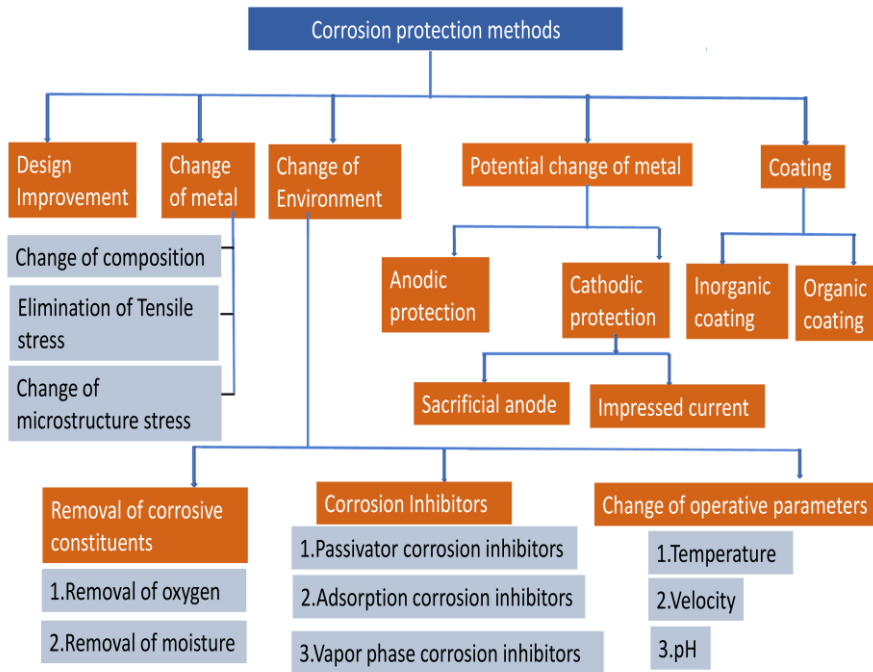
Figure 1.5 Corrosion prevention methods

1.5.1. Corrosion Inhibitors

Changing the environment by adding corrosion inhibitors (CI) is considered as an efficient corrosion management method [16-18]. A corrosion inhibitor is a chemical substance which when added in a small concentration to the corrosive environment results in a significant reduction in the corrosion rate either by reducing the rate of attack or by reducing the probability of its occurrence or by both[19]. An efficient inhibitor should be economical, environment friendly, and inhibit the corrosion process when present in a small concentration. Corrosion prevention using inhibitors has some noticeable advantages such as low

cost, simple control and operation, and non-requirement of special instruments[20]. Corrosion inhibition is achieved in two ways. In some cases, the inhibitor interacts with the metal surface and forms an inhibitive surface film at the metal/electrolyte interface. In other cases, the inhibitor can alter the corrosive environment into a less corrosive or noncorrosive environment, e.g. by chemically neutralizing dissolved acidic gases, chemically scavenging dissolved oxygen, etc. Thus, based on the mode of interaction a qualitative classification of CI is presented in Figure 1.6 [21, 22].
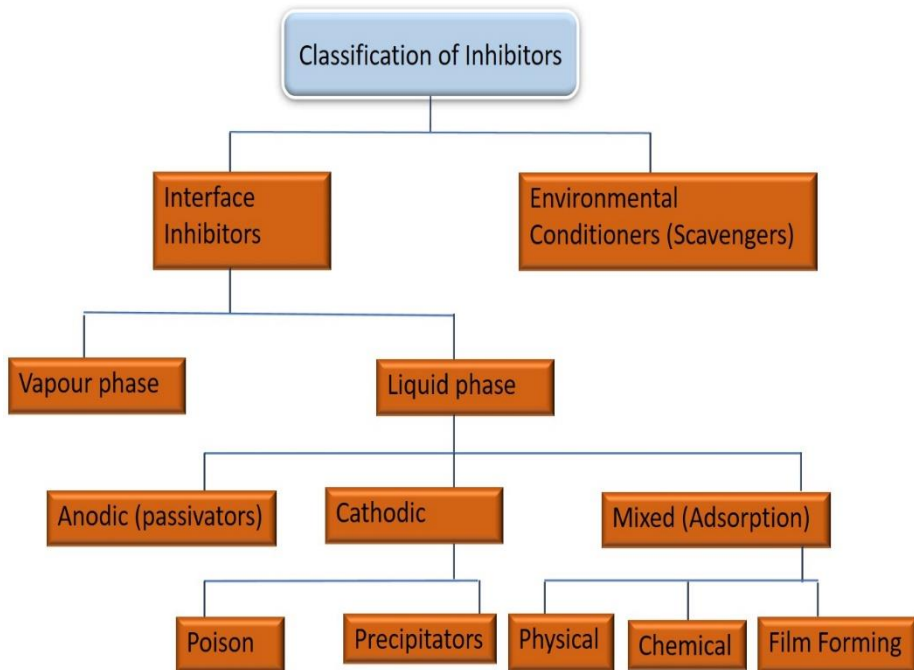
Figure 1.6. Classification of corrosion inhibitors

Environmental conditioners or scavengers control the corrosion process by decreasing the corrosivity of the medium through scavenging the

aggressive substances. In near neutral and alkaline solutions, the cathodic oxygen reduction can be controlled by decreasing the oxygen content using scavengers [23]. In a boiler system, hydrazine is used as a scavenger to remove traces of oxygen [24]. Interphase inhibitors prevent the corrosion process by forming a film at metal/environment interphase. Substances having low vapour pressure with corrosion inhibiting capacity are used as vapour phase inhibitors (VPI) against atmospheric corrosion, especially in a closed environment. In boilers, VPIs prevent corrosion in condenser tubes by neutralising the acidic CO_2. Volatile inhibitors of this type transported to the corrosion site and inhibit the corrosion process by maintaining the atmosphere alkaline [25].

LPIs are classified as cathodic, anodic, or mixed type inhibitors, based on whether they inhibit the anodic, cathodic, or both the electrochemical corrosion process. Anodic inhibitors develop a protective oxide film on the surface of the metal and causing a large anodic corrosion potential shift and thereby force the metal surface into the passivation region and hence commonly referred to as passivators. If the concentration of anodic inhibitors is not enough to block off all the anodic sites, the oxidising nature of the inhibitor encourages the anodic reaction and results in pitting corrosion. So, they are classified as 'dangerous inhibitors' and chromates, tungstate, molybdates, nitrates, etc are belonging to this category.

Cathodic inhibitors inhibit the corrosion process by either decreasing the cathodic reduction rate or by selectively precipitating an insoluble

species onto the cathodic sites to limit the diffusion of reducing species to the metal surface. They are belonging to safe inhibitors because they do not cause localised corrosion. Zinc ions are used as a cathodic inhibitor by precipitating $Zn(OH)_2$ at the cathodic site in the cathodic oxygen reduction process.

Mixed (adsorption) inhibitors work by reducing the anodic and cathodic corrosion reactions. Many inhibitors work by adsorption on the metal surface. Adsorption depends on the surface charge of the metal atom, structure of the inhibitor, and type of the electrolyte. Adsorption inhibitors offer corrosion inhibition via physisorption, chemisorption, and film formation. Physisorption by the electrostatic interaction between the metal atom and the inhibitor is removed from the surface of the metal on increasing the temperature. Chemisorption due to charge sharing or charge transfer between the metal and inhibitor molecules is more effective and not completely reversible [26]. The adsorption can be represented as

$$org_{soln} + XH_2O(ads) \rightarrow org_{ads} + XH_2O(soln) \qquad (1.8)$$

The extent of adsorption depends on the nature of the metal, the chemical structure of the inhibitor, the mode of adsorption, and the type of corrosive medium. The exact nature of adsorption can be verified from adsorption isotherms which describe the surface coverage (θ) by the inhibitor on the metal surface and the concentration of the inhibitor. Various adsorption isotherms which describe the surface coverage (θ) by the inhibitor and the concentration of the inhibitor (C) are used to know the exact nature of adsorption and are given below.

11

Table 1.1. Various adsorption isotherms

Adsorption isotherms	Equation	Verification plot
Langmuir	$$\frac{C}{\theta} = \frac{1}{k} + C$$	$\frac{C}{\theta}$ Vs C
Temkin	$lnkC = a\theta$	θ Vs lnC
Frumkin	$$\frac{\theta}{1-\theta}e^{-2a\theta} = kC$$	Log C($\frac{\theta}{1-\theta}$) Vs θ
Flory Huggins isotherm	$$log\frac{\theta}{C} = logk + xlog(1-\theta)$$	log(θ/C) Vs log(1-θ)

1.5.2. Synergism and corrosion inhibition

Synergism is considered to be an adequate method for enhancing the corrosion inhibition performance of an inhibitor especially at elevated temperatures. It can be defined as the marked augmentation of the corrosion inhibition performance of one inhibitor by adding a small amount of another inhibitor, even though the second inhibitor is less effective when used separately. Co-adsorption of two or more molecules onto the metal surface provide better inhibition than either of the individual components. Speller et al reported that the corrosion inhibition performance by phosphate-chromate mixtures is found to be more effective than their individual performance. The method of using two or more inhibitors together via synergistic interaction, is an effective method of enhancing the corrosion inhibition. Here the quantity of the inhibitors can be considerably reduced without compromising efficiency of inhibition.

1.5.3. Corrosion resistant coatings

Corrosion protection by coating has attracted much attention due to its high efficiency and durability in various aggressive environments [27, 28]. The durability and performance of corrosion resistant coatings depend on many factors such as type of metallic substrate, pre-treatment of metal, curing, adhesion between the metal and the coating, the thickness of the coating, etc[29, 30]. An effective coating must have intrinsic durability, adhesion with the metal substrate, toughness to survive cracking and keep its appearance when subjected to stress, swell, or weathering[31]. An anti-corrosive system for a highly corrosive environment usually consists of a primer, one or several intermediate coats, and a topcoat[32]. The primer ensures good adhesion to the metallic substrate and protects the metal from corrosion. The function of the intermediate coat is to build up the thickness of the coating system, resist transport of aggressive ions from electrolyte to the metal substrate, and also ensure good adhesion between the primer and the topcoat. The topcoat is exposed to the environment and must offer the metallic surface with the required colour, gloss, and resistance to ultraviolet radiation[33, 34]. Coatings can be classified into noble coatings and sacrificial coatings. Noble coatings provide barrier protection. Whereas in addition to barrier protection sacrificial coatings also provide cathodic protection. Coatings can be further classified into metallic, inorganic, and organic coatings.

- Metallic coating: metals or their alloys are applied to other metals via electroplating, hot dipping, thermal spraying, vapor deposition, etc can function as either noble coating or sacrificial coating.

- Inorganic coating: Non-metallic inorganic coating includes ceramic coating, cement, silicate, ceramics, conversion coating, and sol-gel coatings. The inorganic material in the sol- gel coating act as a good barrier against the diffusion of corrosive ions. Phosphate coating and chromate conversion coating are two usually used inorganic conversion coatings. Chromate conversion coatings (CCCs) are produced on the metal surface by chemical or electrochemical treatment of the metal or metallic coating in solutions containing Cr(VI) and other components. The porosity and stress-induced cracking developed in inorganic coatings limit their use as efficient coatings as the corrosive species diffuse through the coating to the underlying metal[35, 36]

- Organic coating: Such as epoxy, plastics, enamel, oils, greases, and paints. In organic coatings, many different types of fillers and corrosive pigments are used, but the lack of thermal resistance, flexibility, and relatively less adhesion to metallic surfaces of organic coatings limit their long-term stability.

- Organic-inorganic hybrids (OIHs): OIHs offer an effective coating on the metal substrate by linking both inorganic and organic phases covalently on the molecular scale. In OIHs the capacity of inorganic phase to bond covalently with the metal increases leading to highly adherent coatings, which impedes the diffusion of aggressive ions from the electrolyte. The inorganic compound offer scratch resistance, durability, and adhesion to the metallic substrate. The organic part improves the flexibility and functional compatibility

with the polymer system [37, 38]. OIHs coating developed via the sol-gel process is considered as an effective alternative to CCCs for the metallic substrate.

1.5.3.1. Mechanism of protection

Corrosion control using the application of coatings is demonstrated by three mechanisms. Barrier protection, sacrificial protection (galvanic effect), and passivation of the substrate surface (inhibitive effect).

- Barrier protection is attained by preventing the contact between the metallic surface and the corrosive medium and impeding the movement of aggressive ions. The barrier coating may be used as primer, intermediate, or topcoat. The thickness of the coating system and nature of the binder system affects the degree of protection offered by the barrier coating. According to NACE, a barrier coating should exhibit chemical resistance, vibration resistance, and strong adhesion. The corrosion current density between the anode and cathode is decreased due to very high electrical resistance at the metal coating interface developed as the barrier coating is non-permeable [39]. At very high temperatures, thermal barrier coating protects the metal substrate from moisture and prevents the corrosion process. The inhibitive barrier coating is made up of pigments actively prevent chemical reactions by interfering with the electrolytes at the metal electrolyte interface.

- Sacrificial coating means protecting metal or material by coating with more electrochemically active metal or alloy. For protecting steel

from corrosion, metallic zinc powder has been extensively used for several decades. In that case, the direction of the galvanic current through the electrolyte is from coating to the base metal, and hence the base metal is cathodically protected. Sacrificial coatings are effective only when the coating is in direct contact with the metal substrate, and hence they are only applied as primers[40].

- Inhibitive coatings are mainly applied in the primer portion of the coating and contain pigments that resist the chemical reactions by interfering with the electrolyte and protect the metal from corrosion. Passivation of the metal substrate and formation of a protective layer with insoluble metallic complexes impedes the diffusion of aggressive ions and is believed to be the mechanism of the coating. The commonly used inhibitive inorganic pigments are chromate, phosphate, molybdate, nitrate, etc. These pigments are partially dissolved by the permeated moisture through the coating and react with the metal substrate and form a reaction product that passivates the metal surface. An effective coating should have barrier property against corrosive ions and at the same time release an adequate amount of inhibitor on demand. However, the use of hazardous compounds like chromate-based chemical conversion coatings (CCCs), hazardous air pollutants, and volatile organic compounds (VOCs) has been restricted due to environmental and health issues.

1.6. Corrosion monitoring techniques

The corrosion of a metal or material is quantitatively expressed in terms of corrosion rate (CR). It can be expressed in different ways such as mils

per year (mpy), mg/dm^2/day (mdd), and g/inch^2/hour, etc. Corrosion rate can be determined by the non- electrochemical (weight loss) and electrochemical methods[41].

1.6.1. Weight loss studies in corrosion analysis

It is the simplest and most reliable method of all corrosion monitoring techniques. The weight loss of a metal due to corrosion is measured by exposing the specimen with a known area to the corrosive media for a particular period of time and from the difference in weight before and after the exposure, CR and percentage inhibition efficiencies (IE) are calculated using the following equations

$$CR \ in \ mgcm^{-2}h^{-1} = \frac{weight \ loss \ in \ mg}{Area \ in \ cm^2 \times time \ in \ hours} \qquad (1.9)$$

$$CR \ in \ mpy = \frac{weight \ loss \ in \ mg \times 534}{Density \ in \ g/cm^3 \times Area \ in \ cm^2 \times time \ in \ hours} \qquad (1.10)$$

Industries make their material selection for construction purposes based on their CR values in mpy. If CR is <5mpy indicates satisfactory service, 5 – 50 mpy have moderate corrosion inhibition and > 50 mpy are considered as not suitable for service[42].

$$IE = \frac{W_o - W}{W_o} \times 100 \qquad (1.11)$$

where W_o and W are the weight loss of metal in the absence and presence of inhibitor respectively. Even though it is a cheap and simple method in corrosion analysis, it requires long term exposure to corrosive medium to get reliable result.

1.6.2. Electrochemical methods for corrosion analysis

Electrochemical methods are the most widely used methods for corrosion monitoring owing to their correct theoretical understanding and rapidity. The kinetics and mechanism of the corrosion processes can be deduced using this technique.

1.6.2.1. Polarization studies

During the electrochemical corrosion process, the anode and cathode shifted from their equilibrium potential at the surface of the metal. This deviation from the equilibrium potential is called polarization. The deviation from the equilibrium causes an electrical potential difference between the unpolarized (equilibrium) and polarized electrode potential is referred to as over voltage η[14].

$$\eta = E - E_0 \qquad\qquad (1.12)$$

where E and E_0 are electrode potential with and without current flow. E_0 is also called corrosion potential or open circuit potential or rest potential.

The polarization can occur by a slow electrode reaction (activation polarization), concentration gradient adjacent to the electrode surface (concentration polarization), or by an ohmic potential drop in solution or metal-reaction product film on the metal surface (resistance polarization or ohmic polarization)[15]. The common procedure in all electrochemical techniques involves polarization of the working electrode by altering the potential of the electrode and measuring the resultant current response which has a time or potential domain.

1.6.2.2. Potentiodynamic polarization (PDP) studies

In this method potential of an electrode is varied at a particular range by applying a current through the electrolyte. It involves first sweeping the potential in a positive direction until a predominant value of current or potential is attained and the scan is reversed to negative value until the original potential value is attained. The potential attained when a metal is in contact with a corrosive medium and is not associated with any instrumentation is called corrosion potential (E_{corr}). At E_{corr}, both anodic and cathodic current densities are equal in magnitude, and hence no net current to be measured. If the metal is polarized more positive than E_{corr}, the anodic current becomes predominant and if it is polarised in the negative direction the cathodic current becomes predominant.

1.6.2.3. Tafel Extrapolation

It is an effective electrochemical method to measure the instantaneous corrosion rate and was developed by Wagner and Traud to confirm mixed potential theory [43]. Figure 1.7 represents a schematic representation of the polarization curve by the Tafel extrapolation method. Corrosion rate can be determined by the extrapolation of the Tafel region to the corrosion potential. Using the Stern-Geary equation, the icorr can be determined from the slope ($\Delta E/\Delta i$) of potential Vs log i_{corr} or i_{corr} curve [44]

$$i_{corr} = \frac{\beta_a \beta_c}{2.303(\beta_a + \beta_c)} \frac{\Delta E}{\Delta i} \qquad (1.13)$$

where βa and βc are anodic and cathodic Tafel constants. The corrosion rate in mpy is related to i_{corr} by the equation

$$CR = \frac{0.13 i_{corr}(EW)}{d} \tag{1.14}$$

where i_{corr} is the corrosion current density in $\mu A/cm^2$, (EW) is the equivalent weight of the electroactive element, and 'd' the density of corroding species.

The anodic and cathodic Tafel plots are defined by the Tafel equation,

$$\eta = \beta(log i - log i_{corr}) \tag{1.15}$$

where η is overvoltage, i is the current density at over volage in $\mu A/cm^2$, and β Tafel constant. A plot of η Vs logi is a straight line with slope β. When $\eta=0$, E_{corr}, $log(i/i_{corr}) =0$ or $i = i_{corr}$. Tafel constant β is designated as anodic and cathodic Tafel slopes (β_a and β_c).
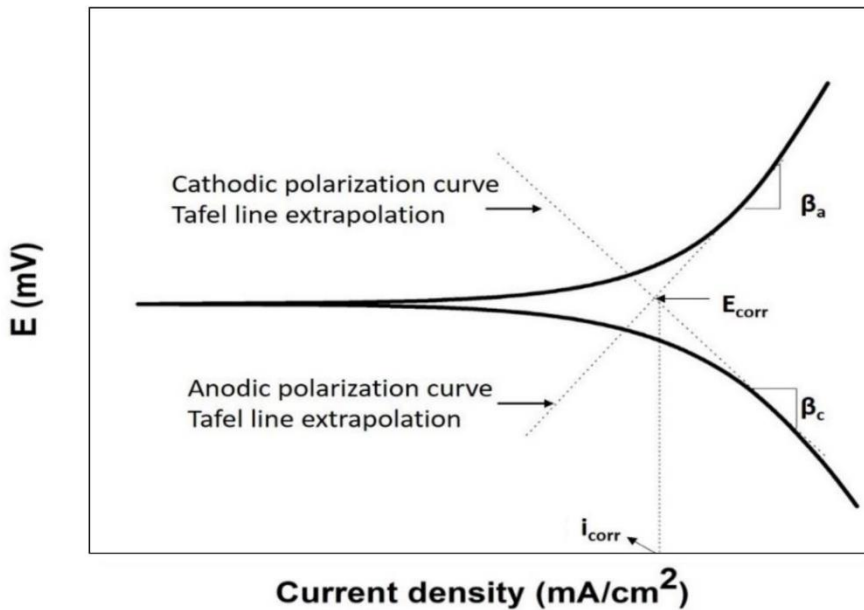
Figure 1.7. Schematic representation of polarization curve showing Tafel extrapolation

1.6.2.4. Electrochemical Impedance Spectroscopy (EIS)

EIS is a non-destructive and powerful technique for monitoring metal corrosion [45]. For the system with high electrolyte resistance, the impedance technique has been proven to be an effective method for corrosion analysis than PDP and it provides kinetic and mechanistic information of the electrochemical system. Like resistance in Ohm's law, impedance is a measure of the ability of a circuit to resist the flow of electrical current, but impedance is frequency-dependent, the AC current and voltage signals through a resistor are out of phase with each other, and doesn't follow Ohm's law at all current and voltage level. The electrochemical impedance method consists of measuring the response of a working electrode to a sinusoidal potential modulation at different frequencies and the mathematical approach of electrochemical impedance data is based on Ohm's law. The impedance measurements are achieved under sinusoidal potential modulation with a small amplitude (5-10 mV) to overcome the non-linearity of current and voltage [46]. The sinusoidal perturbation of potential ($E(\omega t)$) generates a sinusoidal current ($I(\omega t)$) of the same frequency (ω) superimposed onto the steady-state current and cause a phase shift (Φ) between applied potential and current response. The applied sinusoidal potential perturbation $E(\omega t)$ as a function of time and frequency can be expressed as

$$E(\omega t) = E_0 \sin(\omega t) \qquad (1.16)$$

where E_0 is the amplitude of the signal and ω is the radial frequency in rad/s. ω is related to angular frequency by $\omega = 2\pi f$, where f is the signal

frequency (Hz). The linear or pseudo linear current response I(ωt) for the potential perturbation E(ωt) with a phase shift (Φ) is given by

$$I(\omega t) = I_0 \, \sin(\omega t + \Phi) \tag{1.17}$$

The mathematical expression of impedance can be expressed based on Ohm's law by[47]

$$Z(\omega) = \frac{E(\omega t)}{I(\omega t)} = \frac{E_0 \sin(\omega t)}{I_0 \, \sin(\omega t + \Phi)} = Z_0 \frac{\sin(\omega t)}{\sin(\omega t + \Phi)}$$
$$= Z'(\omega) + Z''(\omega) \tag{1.18}$$

where $Z'(\omega)$ and $Z''(\omega)$ are the real and imaginary parts of the impedance vector. Using the theory of complex functions the modulus of impedance and phase shift (Φ) can be represented as

$$|Z(\omega)| = \sqrt{Z'(\omega)^2 + Z''(\omega)^2} \tag{1.19}$$

$$\Phi = \tan^{-1} \left| \frac{Z'(\omega)}{Z''(\omega)} \right| \tag{1.20}$$

The impedance data can plot in different formats

A) The Nyquist plots

Also known as Cole-Cole plot or a complex impedance plain diagram. In this plot, the imaginary part of the impedance vector is plotted against the real impedance component (Z'' Vs Z') at each excitation frequency. The advantages of the Nyquist plot are the ohmic resistance can be easily determined by extrapolating down to the x-axis at high frequency region and it emphasizes the circuit parameters that are in series. The

disadvantages of Nyquist plots are frequency does not appear evidently and even if the ohmic resistance and charge transfer resistance can be easily get from the plot, the capacitance of the working electrode can be calculated only after knowing the frequency information. A typical Nyquist plot is depicted in Figure 1.8A.
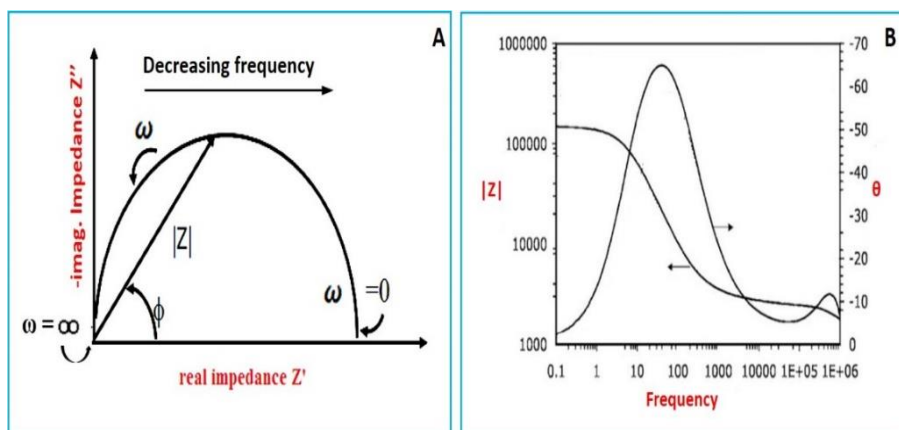
Figure 1.8 A) EIS and B) Bode plot

B) Bode plot

Bode plot is another format for evaluating the impedance data and plot log |Z| and Φ against log ω (Figure 1.8B). In the Bode plot since frequency comes as one of the axes, it is easy to determine the dependence of impedance on frequency. So, it is an alternative to the Nyquist plot. Also, the longer measurement time to determine the charge transfer resistance at low frequency region can be avoided by extrapolating the data from higher frequencies. Since impedance is resistive in nature at highest and lowest frequencies, the Bode plot will be flat with phase angle 0° and at intermediate frequencies, the phase angle is approximately 90° [48].

The physicochemical process taking place at the metal electrolyte interface can be revealed with the help of electrochemical equivalent circuits. The data from the Nyquist plots built upon equivalent circuits with electrochemical parameters connected in a particular sequence. They comprise a similar process such as the formation of ohmic resistance, charge transfer resistance of electrochemical reaction, the formation of electrical double layer, adsorbed layers formed on the metal surface by a protective coating, organic or polymeric films, etc. In equivalent circuits, the reactions occurring simultaneously are modelling by components or circuits connected in parallel, while consequently occurring reactions are modelling by components or circuits connected in series. A simple system for charge transfer controlled with one time constant could be represented by Randel's circuit shown in Figure 1.9. The elements in Randel's circuit comprised of solution resistance between the working electrode and the reference electrode (R_s), charge transfer resistance at metal/electrolyte interface (R_{ct}), and double-layer capacitance arising from the charge accumulation at the metal/electrolyte interface (C_{dl}).
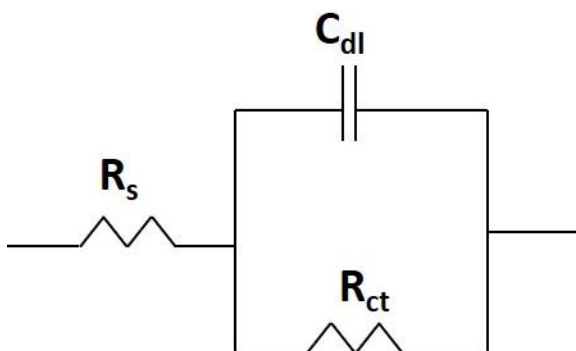
Figure 1.9. Randel's circuit

1.7. A brief survey of carbohydrate polymer as corrosion resistant material

The increased awareness of the toxicity and harmful effects of raw materials to the human and environment has demanded the development of cost-effective and benign raw material for corrosion formulations (inhibitor and coating). Several naturally occurring, chemically stable, cost-effective, and eco-friendly macromolecules like carbohydrate polymers and their derivatives are being used for several applications like catalysis, drug delivery, adsorption, anti-microbial activity, corrosion inhibitors, corrosion resistant coating, etc. In corrosion formulations, carbohydrate polymers protect the metal from the corrosion process owing to their large molecular weight, availability of lone pair and bond pair electrons to metal chelation, adhesion among the metal substrate, and coating. Chitosan, a natural linear polysaccharide derived from chitin by the alkaline deacetylation can be used as an eco-friendly candidate for corrosion formulations because of its non-toxic nature, film-forming capability, and chelation with metal ion [49]. Guar Gum, a galactomannan polysaccharide can be employed in corrosion formulations owing to its biodegradability, non-toxic nature, low cost, and presence of a considerable number of hydroxyl groups [50]. Pectin, a heteropolysaccharide originates from plants has attracted a suitable candidate in corrosion formulations because of its biodegradability, non-toxicity, and suitable molecular structure with carboxylic and carboxymethyl functional group [51]. Because of these properties in recent years, carbohydrate polymers like chitosan, guar gum, and pectin have gained considerable attention as corrosion protectives for metals

and alloys in different aggressive media. A review of the same is presented below in the context of the present study.

1.7.1. Chitosan based corrosion monitoring studies

In the 21st century, researchers working in corrosion monitoring are aimed to develop eco-friendly corrosion inhibitors and corrosion resistant coatings for metals and alloys in various corrosive media. Chitosan and its derivates have got significant attention in corrosion research because of its versatile properties. Owing to its biodegradability, biocompatibility, availability, and high solubility in polar media, chitosan and its derivatives can be considered as one of the green and environmentally viable and liable alternative materials as corrosion inhibitors [51]. Previously, several authors reported the corrosion prevention capability of chitosan as inhibitors and corrosion resistant coatings.

A. Chitosan as an inhibitor

Chemical adsorption of chitosan on mild steel surface in 0.5M HCl was considered as the cause of corrosion inhibition and confirmed using weight loss, electroanalytical, and surface studies [51]. Using EIS, PDP, EFM (electrochemical frequency modulation), surface studies, and quantum chemical calculations, El Haddad reported copper corrosion inhibition in 0.5M HCl [52]. According to Ubong et.al chitosan from shrimp shells acted as a mixed type inhibitor for mild steel (MS) in 0.5M H_2SO_4 and tested using electrochemical and surface analytical techniques [53]. Corrosion of mild steel in 3.65% NaCl medium was

inhibited using water soluble chitosan [54]. Copper corrosion inhibition in 3.5% NaCl using chitosan was also reported by Oukhrib et. al. DFT and MD simulation were employed to justify the experimental observations [55]. Recently Harmami et. al studied chitosan from shrimp and mussel shells used as corrosion inhibitor for tin plate in 2.0% NaCl by weight loss and PDP studies [56].

The functionalisation of both amino and hydroxyl groups on the chitosan skeleton with polar functional groups could improve the adsorption of chitosan on the metal surface. Various chitosan derivatives were synthesised and used as corrosion resistant coatings and inhibitors. Salicylaldehyde chitosan Schiff's base was synthesised and its corrosion inhibition for MS [57], Q2345 steel [58] in 1.0 M HCl, and J55 steel in CO_2 saturated 3.5% NaCl at 65°C for oil-gas industries[59] were reported. Water soluble carboxymethyl chitosan could inhibit the carbon steel (CS) corrosion in 3.5% NaCl [60]. The carbon steel corrosion in 2.0M HCl was inhibited by interacting the pendant group in the water soluble sulfonated chitosan with the carbon surface [61]. Rbaa et. al reported 5-chloromethyl-8-hydroxyquinoline derivative of C and D-glucose grafted chitosan as corrosion inhibitor for MS in acidic medium. DFT calculation and molecular dynamic simulation studies were carried out to corroborate the experimental result [62, 63]. Thiocarbohydrazide-cross linked chitosan offered corrosion protection for stainless steel (SS) in 3.5% NaCl and was monitored using EIS, PDP, and cyclic voltammetry by Khadija et. al [64]. Corrosion inhibition of polyaniline/chitosan composite for MS in acidic medium was tested by electrochemical, morphological, and quantum chemical calculations

[65]. In a CO_2 saturated chloride solution, N-propyl chitosan oligosaccharide quaternary ammonium salt and N-benzyl chitosan oligosaccharide quaternary ammonium salt could inhibit the corrosion of P110 steel [66]. Water-soluble poly (*N*-vinyl imidazole) grafted carboxymethyl chitosan composite has been synthesized by Ubong et.al and deployed as corrosion inhibitor for APIX70 steel in 1M HCl [67]. Ubong et. al grafted chitosan with glucosyloxyethyl acrylate via Michael addition reaction and applied as corrosion inhibitor for pipeline steel in 1 M HCl [68].

B. Chitosan based coatings

Chitosan is a promising candidate for corrosion resistant coating owing to its properties like film-forming nature, good adhesion to the metallic substrate, and easiness of chemical functionalization. The information on the chitosan-based corrosion resistant coating for different metals are given in Table. 1.2

Table 1.2. Chitosan-based corrosion resistant coating. (SBF, DMEM, SKP stand for simulated body fluid, Dulbecco's modified Eagle's medium, Scanning Kelvin probe).

Coating	Metal	Corrosive medium	Corrosion monitoring techniques	Reference
Chitosan	304SS	SBF	EIS, PDP, OCP	[69]
Chitosan	AISI 316 L	SBF	EIS, PDP	[70]
Chitosan/polyvinyl alcohol	MS	0.1M HCl	EIS, PDP	[71]
Chitosan/polyvinyl butyral	CS	0.3M salt	EIS, PDP	[72]
Chitosan/polypyrrole/carbon nanotube	St-12	3.5% NaCl	EIS, PDP, OCP	[73]

Chitosan/polypyrrole/SiO$_2$	MS	3.5% NaCl	EIS, PDP, OCP	[74]
Chitosan/poly(aniline-anisidine)/SiO$_2$	MS	3.5% NaCl	EIS, PDP, Salt spray test	[75]
Chitosan/hexagonal boron nitride/TiO$_2$	316L	DMEM	PDP	[76]
Chitosan/epoxy silane	Zn	1.0 M KCl	EIS, PDP, LPR, SKP	[77]
Chitosan/bioactive glass	316L	Artificial saliva	PDP	[78]
Chitosan/Au/Ni	316L	2MH_2SO_4+2M H_3PO_4	EIS, PDP, OCP	[79]
Oleic acid modified Chitosan/Graphene oxide	CS	3.5% NaCl	EIS, PDP	[80]
Chitosan/ZnO	MS	0.1M HCl	EIS, PDP, LPR	[81]
Chitosan/ZnO	CS	3.5% NaCl	PDP	[82]
Chitosan/TiO$_2$	MS	0.1M HCl	EIS, PDP	[83]
Chitosan/(SiO$_2$-CaO-MgO)	Ti-6Al-4V alloy	SBF	EIS, PDP	[84]
Chitosan/ Nd$_2$Ti$_2$O$_7$	CS	3.5% NaCl	EIS, PDP, OCP, LPR	[85]
Chitosan/indigo carmine	Zn	Na$_2$SO$_4$/[Fe(CN)$_4$]$^{2-}$+[Fe(CN)$_6$]$^{3-}$	EIS, PDP	[86]
Chitosan-poly(ethylene-alt-maleic anhydride)/ 2-mercaptobenzothiazole and chitosan-poly(maleic anhydride-alt-1-octadecene)/2-mercaptobenzothiazole	AA2024	50 mM NaCl	EIS	[87]
Chitosan cross linked with genipin	Mgalloy AZ31	SBF	EIS, PDP	[88]
Carboxymethyl chitosan-graphene oxide/water born epoxy	Steel	3.5% NaCl	EIS	[89]

1.7.2. *Natural gum as a corrosion inhibitor*

Gums gained from plants are solids comprising of polysaccharides which are either water soluble or forming a gel by absorbing water. The

natural gum obtained from different plants has been reported as good corrosion inhibitors for different metals. According to Eddy et. al, non-toxic, eco-friendly, flexible functional group with oxygen and nitrogen atom and large molecular weight of natural gum causes metal-gum complex formation and blanket the metal surface from the diffusion of aggressive ions [90]. Gum Arabic is used as a green corrosion inhibitor for aluminium and MS in acidic and alkaline medium [91-93]. Exudate gums are generally viscous and sticky when wet and harden when they dry. So they are used as binders and adhesive in oil gas industry [94]. Exudate gum extracted from Fenugreek Gum, a galactomannan polysaccharide from the endosperm of the seeds of fenugreek, used as corrosion inhibitor for MS in acidic medium and the interaction with the steel surface in 1.0 M HCl were confirmed using chemical, electrochemical and surface studies combined with DFT, MD, RDF (radial distribution function) and MSD (mean square displacement) studies [95]. Exudate gum extracted from acacia tree, Daniella olliverri, Ferula assafoetida, Dorema ammoniacum, Ficus benjamina and Ficus glumosa were reported as corrosion inhibitors for different metal atoms [90, 96-98]. Guar gum (GG) or guaran, from guar been seed endosperm, is another class of natural gum as corrosion resistant material. The corrosion inhibition property of GG for CS in 1M H_2SO_4 using weight loss and PDP technique was first identified by Abdella et. al and the adsorption of GG on the steel surface followed Langmuir adsorption isotherm[99]. Messali et. al also reported CS corrosion inhibition in phosphoric acid medium using electrochemical, surface studies, and basic theoretical calculations [100]. Aluminium corrosion in 1.0 M HCl

was also inhibited by GG. The inhibition efficiency was calculated using gravimetric and electrochemical methods and adsorption follows Temkin adsorption pattern [101]. The effect of percentage grafting on the corrosion inhibition efficiency of polyacrylamide grafted GG towards mild steel corrosion in 1M HCl was studied by Roy et. al. The maximum inhibition efficiency obtained at 86% grafting and thereafter it gets decreased [102].

1.7.3. Pectin as a corrosion inhibitor

Many fruits like citrus fruits, apple, grapes, banana, apricot, cherries, and jackfruit are very good sources of pectin. Commercially it is used as a gelling agent and stabilizer in food industry. The properties of pectin like non-toxicity, low production cost, biodegradability, and polyfunctionality made it as a promising corrosion inhibitor for various metals. Umoren et. al reported corrosion inhibition for X60 steel in 0.5M HCl using commercial pectin from apple and tested using electrochemical, morphological, and quantum chemical calculations [103]. The addition of CeO_2 nanoparticle could increase the inhibition efficiency of apple pectin by synergistic effect at a higher concentration of CeO_2 and longer immersion time in the acidic medium [104]. Pectin extracted from citrus peel could inhibit mild steel and aluminium corrosion in an acidic environment by chemically adsorbing on the metal surface [105, 106]. Pectin extracted from tomato waste was used as an efficient inhibitor for tin corrosion in sodium chloride/acetic acid medium and in a mixture of 2% NaCl, 1% acetic acid, and 0.5% citric acid corrosive media[107, 108]. The corrosion inhibition of pectin

extracted from Opuntia Ficus Indica cladode on MS in HCl using weight loss and the electrochemical method was studied by Saidi et. al [109]. Pectin grafted poly-acrylic acid and pectin grafted poly-acrylamide was synthesised and their corrosion inhibition for MS in 3.5% NaCl were studied using electrochemical techniques [110]. Xuemei et. al extracted pectin with different molecular weight from sunflower head by enzyme assisted extraction and offered corrosion inhibition for MS in 1.0M HCl at its optimum concentration 2.0 g/L. In addition to electrochemical studies, theoretical studies using DFT and MD simulation also revealed the mechanism of corrosion inhibition [111].

1.8. Present investigation

Corrosion is a destructive phenomenon predominant in industries, costs heavily on governments and individuals. Every year almost all country in the world faces a large amount of economic loss due to corrosion. Owing to global interest in human and environmental safety, the use of toxic chemicals as corrosion formulation is gradually substituted by greener substances. Generally, green or eco-friendly corrosion formulations are those chemicals without direct or indirect negative impacts on health and the environment. The recommended corrosion resistant coating is expected to be green with a very low volatile organic compound (VOC). While choosing an inhibitor for corrosion inhibition, in addition to its availability and inhibition efficiency environmental liability is a major consideration. However, most of the compounds used as corrosion formulation are toxic and hazardous to human and environment and needs to be replaced with eco-friendly and non-toxic

chemicals. From the literature, it is known that carbohydrate polymers and their derivatives have been extensively used as corrosion formulations owing to its properties like non-toxic nature, biodegradability, cost-effectiveness, large molecular weight, availability of lone pair electrons to metal complex formation, etc. Hence the present study focused on the development of eco-friendly substitute for corrosion control using carbohydrate polymers like chitosan, guar gum, and pectin.

Mild steel is extensively used as construction and engineering material in a variety of chemical and petrochemical industries owing to its excellent mechanical properties, cost-effectiveness, and easy fabrication. During applications, it is very much exposed to aggressive acid solutions and corrodes heavily. Therefore, more attention was made to corrosion prevention of mild steel in the present study.

References

[1]   J.R. Davis, Corrosion: Understanding the basics, Asm International, 2000.

[2]   H.H. Hassan, E. Abdelghani, M.A. Amin, Inhibition of mild steel corrosion in hydrochloric acid solution by triazole derivatives: Part I. Polarization and EIS studies, Electrochimica Acta, 52 (2007) 6359-6366.

[3]   M.G. Fontana, N.D. Greene, Corrosion engineering, McGraw-hill, 2018.

[4]   M. Yamashita, H. Uchida, Recent research and development in solving atmospheric corrosion problems of steel industries in Japan, in: Industrial Applications of the Mössbauer Effect, Springer, 2002, pp. 153-166.

[5]   H. Mohebbi, C. Li, Experimental investigation on corrosion of cast iron pipes, International Journal of Corrosion, 2011 (2011).

[6]   R. Walker, Triazole, benzotriazole and naphthotriazole as corrosion inhibitors for copper, Corrosion, 31 (1975) 97-100.

[7]   V.S. Saji, S.A. Umoren, Corrosion Inhibitors in the Oil and Gas Industry, Wiley Online Library, 2020.

[8]   M. Fajobi, R.T. Loto, O. Oluwole, Corrosion in crude distillation overhead system: A review, Journal of Bio-and Tribo-Corrosion, 5 (2019) 67.

[9]   L.K.M. Goni, M.A. Mazumder, Green Corrosion Inhibitors, in: Corrosion Inhibitors, IntechOpen, 2019.

[10]   N. Sato, 1989 Whitney Award Lecture: toward a more fundamental understanding of corrosion processes, Corrosion, 45 (1989) 354-368.

[11]   W. Whitney, The Corrosion of Iron, Corrosion, 3 (1947) 331-340.

[12]   O.P. Watts, The electrochemical theory of corrosion, Transactions of the Electrochemical Society, 64 (1933) 125.

[13]   E. Bardal, Corrosion and protection, Springer Science & Business Media, 2007.

[14]   M.G. Fontana, Corrosion engineering, Tata McGraw-Hill Education, 2005.

[15]   N. Perez, Electrochemistry and corrosion science, Springer, 2004.

[16]   S.A. Umoren, M.M. Solomon, I.B. Obot, R.K. Suleiman, A critical review on the recent studies on plant biomaterials as corrosion inhibitors for industrial metals, Journal of Industrial and Engineering Chemistry, 76 (2019) 91-115.

[17]   M. Al-Otaibi, A. Al-Mayouf, M. Khan, A. Mousa, S. Al-Mazroa, H. Alkhathlan, Corrosion inhibitory action of some plant extracts on the corrosion of mild steel in acidic media, Arabian Journal of Chemistry, 7 (2014) 340-346.

[18]   R.Y. Khaled, A. Abdel-Gaber, H. Holail, Electrochemical studies of the inhibition effect of 4, 6-dichloro-2-(methylthio) pyrimidine on the corrosion of AISI type 321 stainless steel in 1.0 M hydrochloric acid, Int. J. Electrochem. Sci, 11 (2016) 2790-2798.

[19]   P.B. Raja, M.G. Sethuraman, Natural products as corrosion inhibitor for metals in corrosive media—a review, Materials letters, 62 (2008) 113-116.

[20]   J.M. Gaidis, Chemistry of corrosion inhibitors, Cement and Concrete Composites, 26 (2004) 181-189.

[21]   V.S. Sastri, Green corrosion inhibitors: theory and practice, John Wiley & Sons, 2012.

[22]   A. Rostami, Review and evaluation of corrosion inhibitors used in well stimulation, in: SPE International Symposium on Oilfield Chemistry, Society of Petroleum Engineers, 2009.

[23]   E. Lyublinski, P. Lynch, I. Roytman, T. Yakubovskaya, Application experience and new approaches for volatile corrosion inhibitors, International Journal of Corrosion and Scale Inhibition, 4 (2015) 176-192.

[24]   S.T.M. TAKADA, H. GOTOU, K. MAWATARI, N. ISHIHARA, R. KAI, Alternatives to hydrazine in water treatment at thermal power plants, Mitsubishi Heavy Industries Technical Review, 46 (2009) 43.

[25]   A. Leng, M. Stratmann, The inhibition of the atmospheric corrosion of iron by vapour-phase-inhibitors, Corrosion science, 34 (1993) 1657-1683.

[26]   E. Gutiérrez, J.A. Rodríguez, J. Cruz-Borbolla, J.G. Alvarado-Rodríguez, P. Thangarasu, Development of a predictive model for corrosion inhibition of carbon steel by imidazole and benzimidazole derivatives, Corrosion Science, 108 (2016) 23-35.

[27]   Y. Qian, Y. Li, S. Jungwirth, N. Seely, Y. Fang, X. Shi, The Application of Anti-Corrosion Coating for Preserving the Value of Equipment Asset in Chloride-Laden Environments: A, Int. J. Electrochem. Sci, 10 (2015) 10756-10780.

[28]   F. Presuel-Moreno, M. Jakab, N. Tailleart, M. Goldman, J. Scully, Corrosion-resistant metallic coatings, Materials today, 11 (2008) 14-23.

[29]   M. Dabral, L. Francis, L. Scriven, Drying process paths of ternary polymer solution coating, AIChE journal, 48 (2002) 25-37.

[30]   E. Almeida, Surface treatments and coatings for metals. A general overview. 1. Surface treatments, surface preparation, and the nature of coatings, Industrial & engineering chemistry research, 40 (2001) 3-14.

[31]   P.A. Sørensen, S. Kiil, K. Dam-Johansen, C.E. Weinell, Anticorrosive coatings: a review, Journal of Coatings Technology and Research, 6 (2009) 135-176.

[32]   D. Kjernsmo, K. Kleven, J. Scheie, Corrosion protection, Bording A/S, Copenhagen, (2003).

[33]   R. Zhang, H. Chen, H. Cao, C.M. Huang, P. Mallon, Y. Li, Y. He, T. Sandreczki, Y. Jean, R. Suzuki, Degradation of polymer coating systems studied by positron annihilation spectroscopy. IV. Oxygen effect of UV irradiation, Journal of Polymer Science Part B: Polymer Physics, 39 (2001) 2035-2047.

[34]   J. Pospı̈šil, S. Nešpurek, Photostabilization of coatings. Mechanisms and performance, Progress in Polymer Science, 25 (2000) 1261-1335.

[35]   M. Norouzi, A.A. Garekani, Corrosion protection by zirconia-based thin films deposited by a sol–gel spin coating method, Ceramics International, 40 (2014) 2857-2861.

[36]   J. Quinson, C. Chino, A. De Becdelievre, C. Guizard, M. Brunel, Deformation capability and protective role of zirconia coatings on stainless steel, Journal of materials science, 31 (1996) 5179-5184.

[37]   C. Jackson, B. Bauer, A. Nakatani, J. Barnes, Synthesis of hybrid organic−inorganic materials from interpenetrating polymer network chemistry, Chemistry of materials, 8 (1996) 727-733.

[38]   T.L. Metroke, R.L. Parkhill, E.T. Knobbe, Passivation of metal alloys using sol–gel-derived materials—a review, Progress in Organic Coatings, 41 (2001) 233-238.

[39]   N.S. Sangaj, V. Malshe, Permeability of polymers in protective organic coatings, Progress in Organic coatings, 50 (2004) 28-39.

[40]   C.H. Hare, Zinc Loadings, Cathodic Protection, and Post-Cathodic Protective Mechanisms in Organic Zin-Rich Metal Primers, JPCL, 18 (2001) 54.

[41]   A. Mercer, Test methods for corrosion inhibitors: report prepared for the European Federation of Corrosion Working Party on inhibitors, British corrosion journal, 20 (1985) 61-70.

[42]   H. de Wit, T. Fransen, Corrosion studies, in: Handbook of Solid State Electrochemistry, CRC Press, 2019, pp. 555-585.

[43]   F. Mansfeld, The polarization resistance technique for measuring corrosion currents, in: Advances in corrosion science and technology, Springer, 1976, pp. 163-262.

[44]   S. Evans, E. Koehler, Use of polarization methods in the determination of the rate of corrosion of aluminum alloys in anaerobic media, Journal of the Electrochemical Society, 108 (1961) 509.

[45]   S.L. Zelinka, L. Ortiz-Candelaria, D.S. Stone, D.R. Rammer, Electrochemical impedance spectroscopy (EIS) as a tool for measuring corrosion of polymer-

coated fasteners used in treated wood, Forest products journal. Vol. 59, nos. 1/2 (Jan./Feb. 2009): Pages 77-82., (2009).

[46]   H. Cesiulis, N. Tsyntsaru, A. Ramanavicius, G. Ragoisha, The study of thin films by electrochemical impedance spectroscopy, in: Nanostructures and thin films for multifunctional applications, Springer, 2016, pp. 3-42.

[47]   D. Landolt, Corrosion and surface chemistry of metals, CRC press, 2007.

[48]   T. Abbaz, A. Bendjeddou, D. Villemin, Structure, electronic properties, NBO, NLO and chemi-cal reactivity of bis (1, 4-dithiafulvalene) derivatives: functional density theory study, International Journal of Advanced Chemistry, 6 (2017) 18-25.

[49]   Q. Li, E. Dunn, E. Grandmaison, M.F. Goosen, Applications and properties of chitosan, Journal of Bioactive and Compatible Polymers, 7 (1992) 370-397.

[50]   V.D. Prajapati, G.K. Jani, N.G. Moradiya, N.P. Randeria, B.J. Nagar, N.N. Naikwadi, B.C. Variya, Galactomannan: a versatile biodegradable seed polysaccharide, International journal of biological macromolecules, 60 (2013) 83-92.

[51]   S.A. Umoren, U.M. Eduok, Application of carbohydrate polymers as corrosion inhibitors for metal substrates in different media: a review, Carbohydrate polymers, 140 (2016) 314-341.

[52]   M.N. El-Haddad, Chitosan as a green inhibitor for copper corrosion in acidic medium, International journal of biological macromolecules, 55 (2013) 142-149.

[53]   U.M. Eduok, M.M. Khaled, RETRACTION: Corrosion protection of steel sheets by chitosan from shrimp shells at acid pH, (2014).

[54]   O. Fayomi, I. Akande, O. Oluwole, D. Daramola, Effect of water-soluble chitosan on the electrochemical corrosion behaviour of mild steel, Chemical Data Collections, 17 (2018) 321-326.

[55]   R. Oukhrib, B. El Ibrahimi, H. Bourzi, K. El Mouaden, A. Jmiai, S. El Issami, L. Bammou, L. Bazzi, Quantum chemical calculations and corrosion inhibition efficiency of biopolymer "chitosan" on copper surface in 3% NaCl, J. Mater. Environ. Sci, 8 (2017) 195-208.

[56]   H. Harmami, I. Ulfin, A.H. Sakinah, Y.L. Ni'mah, Water-soluble chitosan from shrimp and mussel shells as corrosion inhibitor on tinplate in 2% NaCl, Malaysian Journal of Fundamental and Applied Sciences, 15 (2019) 212-217.

[57]   R. Menaka, S. Subhashini, Chitosan Schiff base as eco-friendly inhibitor for mild steel corrosion in 1 M HCl, Journal of adhesion science and Technology, 30 (2016) 1622-1640.

[58]   N. Chen, P. Kong, H. Feng, Y. Wang, D. Bai, Corrosion Mitigation of Chitosan Schiff Base for Q235 Steel in 1.0 M HCl, Journal of Bio-and Tribo-Corrosion, 5 (2019) 27.

[59]   K. Ansari, D.S. Chauhan, M. Quraishi, M.A. Mazumder, A. Singh, Chitosan Schiff base: an environmentally benign biological macromolecule as a new corrosion inhibitor for oil & gas industries, International Journal of Biological Macromolecules, 144 (2020) 305-315.

[60]   R.G.M. de Araújo Macedo, N. do Nascimento Marques, J. Tonholo, R. de Carvalho Balaban, Water-soluble carboxymethylchitosan used as corrosion inhibitor for carbon steel in saline medium, Carbohydrate polymers, 205 (2019) 371-376.

[61]   A. Farhadian, M.A. Varfolomeev, A. Shaabani, S. Nasiri, I. Vakhitov, Y.F. Zaripova, V.V. Yarkovoi, A.V. Sukhov, Sulfonated chitosan as green and high cloud point kinetic methane hydrate and corrosion inhibitor: Experimental and theoretical studies, Carbohydrate Polymers, 236 (2020) 116035.

[62]   M. Rbaa, F. Benhiba, R. Hssisou, Y. Lakhrissi, B. Lakhrissi, M.E. Touhami, I. Warad, A. Zarrouk, Green synthesis of novel carbohydrate polymer chitosan oligosaccharide grafted on d-glucose derivative as bio-based corrosion inhibitor, Journal of Molecular Liquids, (2020) 114549.

[63]   M. Rbaa, M. Fardioui, C. Verma, A.S. Abousalem, M. Galai, E. Ebenso, T. Guedira, B. Lakhrissi, I. Warad, A. Zarrouk, 8-Hydroxyquinoline based chitosan derived carbohydrate polymer as biodegradable and sustainable acid corrosion inhibitor for mild steel: Experimental and computational analyses, International Journal of Biological Macromolecules, (2020).

[64]   K.E. Mouaden, D. Chauhan, M. Quraishi, L. Bazzi, Thiocarbohydrazide-crosslinked chitosan as a bioinspired corrosion inhibitor for protection of stainless steel in 3.5% NaCl, Sustainable Chemistry and Pharmacy, 15 (2020) 100213.

[65]   P. Kong, H. Feng, N. Chen, Y. Lu, S. Li, P. Wang, Polyaniline/chitosan as a corrosion inhibitor for mild steel in acidic medium, RSC advances, 9 (2019) 9211-9217.

[66]   G. Cui, J. Guo, Y. Zhang, Q. Zhao, S. Fu, T. Han, S. Zhang, Y. Wu, Chitosan oligosaccharide derivatives as green corrosion inhibitors for P110 steel in a carbon-dioxide-saturated chloride solution, Carbohydrate polymers, 203 (2019) 386-395.

[67]   U. Eduok, E. Ohaeri, J. Szpunar, Electrochemical and surface analyses of X70 steel corrosion in simulated acid pickling medium: Effect of poly (N-vinyl imidazole) grafted carboxymethyl chitosan additive, Electrochimica Acta, 278 (2018) 302-312.

[68] U. Eduok, E. Ohaeri, J. Szpunar, I. Akpan, Synthesis, characterization and application of glucosyloxyethyl acrylate graft chitosan against pipeline steel corrosion, Journal of Molecular Liquids, 315 (2020) 113772.

[69] G. Blanda, V. Brucato, F. Carfì, G. Conoscenti, V. La Carrubba, S. Piazza, C. Sunseri, R. Inguanta, Chitosan-coating deposition via galvanic coupling, ACS Biomaterials Science & Engineering, 5 (2019) 1715-1724.

[70] F. Gebhardt, S. Seuss, M.C. Turhan, H. Hornberger, S. Virtanen, A.R. Boccaccini, Characterization of electrophoretic chitosan coatings on stainless steel, Materials letters, 66 (2012) 302-304.

[71] S. John, A. Joseph, M. Kuruvilla, T. Sajini, Inhibition of mild steel corrosion using Chitosan–Polyvinyl Alcohol nanocomposite films by Sol–Gel method: An environmentally friendly approach, Journal of Bio-and Tribo-Corrosion, 3 (2017) 3.

[72] G.E. Luckachan, V. Mittal, Anti-corrosion behavior of layer by layer coatings of cross-linked chitosan and poly (vinyl butyral) on carbon steel, Cellulose, 22 (2015) 3275-3290.

[73] H. Ashassi-Sorkhabi, R. Bagheri, B. Rezaei-moghadam, Sonoelectro chemical synthesis of ppy-MWCNTs-chitosan nanocomposite coatings: Characterization and corrosion behavior, Journal of Materials Engineering and Performance, 24 (2015) 385-392.

[74] G. Ruhi, O. Modi, S. Dhawan, Chitosan-polypyrrole-SiO2 composite coatings with advanced anticorrosive properties, Synthetic Metals, 200 (2015) 24-39.

[75] P. Sambyal, G. Ruhi, S. Dhawan, B. Bisht, S. Gairola, Enhanced anticorrosive properties of tailored poly (aniline-anisidine)/chitosan/SiO2 composite for protection of mild steel in aggressive marine conditions, Progress in Organic Coatings, 119 (2018) 203-213.

[76] N.S. Raddaha, L. Cordero-Arias, S. Cabanas-Polo, S. Virtanen, J.A. Roether, A.R. Boccaccini, Electrophoretic deposition of chitosan/h-BN and chitosan/h-BN/TiO2 composite coatings on stainless steel (316L) substrates, Materials, 7 (2014) 1814-1829.

[77] C. Fernandez-Solis, A. Erbe, Waterborne chitosan–epoxysilane hybrid pretreatments for corrosion protection of zinc, Biointerphases, 11 (2016) 021001.

[78] M. Mehdipour, A. Afshar, A study of the electrophoretic deposition of bioactive glass–chitosan composite coating, Ceramics international, 38 (2012) 471-476.

[79] R.H. Tammam, A.M. Fekry, Corrosion Behavior of 316L Stainless Steel Coated by Chitosan/Gold/Nickel Nanoparticles in Mixed Acid Mixture Containing Inorganic Anions, Int. J. Electrochem. Sci, 12 (2017) 8991-9006.

[80]   E.M. Fayyad, K.K. Sadasivuni, D. Ponnamma, M.A.A. Al-Maadeed, Oleic acid-grafted chitosan/graphene oxide composite coating for corrosion protection of carbon steel, Carbohydrate polymers, 151 (2016) 871-878.

[81]   S. John, A. Joseph, A.J. Jose, B. Narayana, Enhancement of corrosion protection of mild steel by chitosan/ZnO nanoparticle composite membranes, Progress in Organic Coatings, 84 (2015) 28-34.

[82]   Z.F. Lin, P. Wang, D. Zhang, Y. Wang, A ZnO/Chitosan composite film: fabrication and anticorrosion characterization, in: Advanced Materials Research, Trans Tech Publ, 2011, pp. 1199-1202.

[83]   S. John, A. Salam, A.M. Baby, A. Joseph, Corrosion inhibition of mild steel using chitosan/TiO2 nanocomposite coatings, Progress in Organic Coatings, 129 (2019) 254-259.

[84]   S. Rastegari, E. Salahinejad, Surface modification of Ti-6Al-4V alloy for osseointegration by alkaline treatment and chitosan-matrix glass-reinforced nanocomposite coating, Carbohydrate polymers, 205 (2019) 302-311.

[85]   M. Martinez-Gomez, A. Quinto-Hernandez, N. Flores-Garcia, J. Mayén, M. Dominguez-Diaz, H. Martinez, J. Porcayo-Calderon, J. Gonzalez-Rodriguez, L. Martinez-Gomez, Electrophoretic deposition of chitosan films doped with Nd2Ti2O7 nanoparticles as protective coatings against corrosion in saline solutions, International Journal of Polymer Science, 2019 (2019).

[86]   Á.F. Szőke, G.S. Szabó, Z. Hórvölgyi, E. Albert, L. Gaina, L.M. Muresan, Eco-friendly indigo carmine-loaded chitosan coatings for improved anti-corrosion protection of zinc substrates, Carbohydrate polymers, 215 (2019) 63-72.

[87]   J. Carneiro, J. Tedim, S.C. Fernandes, C. Freire, A. Gandini, M. Ferreira, M. Zheludkevich, Functionalized chitosan-based coatings for active corrosion protection, Surface and Coatings Technology, 226 (2013) 51-59.

[88]   L.d.Y. Pozzo, T.F. da Conceição, A. Spinelli, N. Scharnagl, A.T.N. Pires, The influence of the crosslinking degree on the corrosion protection properties of chitosan coatings in simulated body fluid, Progress in Organic Coatings, 137 (2019) 105328.

[89]   H. Shi, W. Liu, Y. Xie, M. Yang, C. Liu, F. Zhang, S. Wang, L. Liang, K. Pi, Synthesis of carboxymethyl chitosan-functionalized graphene nanomaterial for anticorrosive reinforcement of waterborne epoxy coating, Carbohydrate Polymers, (2020) 117249.

[90]   N.O. Eddy, P. Ameh, C.E. Gimba, E.E. Ebenso, GCMS studies on Anogessus leocarpus (Al) gum and their corrosion inhibition potential for mild steel in 0.1 M HCl, Int J Electrochem Sci, 6 (2011) 5815-5829.

[91]   S. Umoren, I. Obot, E. Ebenso, P. Okafor, O. Ogbobe, E. Oguzie, Gum arabic as a potential corrosion inhibitor for aluminium in alkaline medium and its adsorption characteristics, Anti-corrosion methods and materials, (2006).

[92]   K. Azzaoui, E. Mejdoubi, S. Jodeh, A. Lamhamdi, E. Rodriguez-Castellón, M. Algarra, A. Zarrouk, A. Errich, R. Salghi, H. Lgaz, Eco friendly green inhibitor Gum Arabic (GA) for the corrosion control of mild steel in hydrochloric acid medium, Corrosion Science, 129 (2017) 70-81.

[93]   S. Umoren, Inhibition of aluminium and mild steel corrosion in acidic medium using Gum Arabic, Cellulose, 15 (2008) 751.

[94]   L. Chaires-Martínez, J. Salazar-Montoya, E. Ramos-Ramírez, Physicochemical and functional characterization of the galactomannan obtained from mesquite seeds (Prosopis pallida), European Food Research and Technology, 227 (2008) 1669.

[95]   H. Lgaz, I.-M. Chung, R. Salghi, I.H. Ali, A. Chaouiki, Y. El Aoufir, M.I. Khan, On the understanding of the adsorption of Fenugreek gum on mild steel in an acidic medium: Insights from experimental and computational studies, Applied Surface Science, 463 (2019) 647-658.

[96]   M. Abu-Dalo, A. Othman, N. Al-Rawashdeh, Exudate gum from acacia trees as green corrosion inhibitor for mild steel in acidic media, Int. J. Electrochem. Sci, 7 (2012) 9303-9324.

[97]   M. Behpour, S. Ghoreishi, M. Khayatkashani, N. Soltani, The effect of two oleo-gum resin exudate from Ferula assa-foetida and Dorema ammoniacum on mild steel corrosion in acidic media, Corrosion science, 53 (2011) 2489-2501.

[98]   P.O. Ameh, L. Magaji, T. Salihu, Corrosion inhibition and adsorption behaviour for mild steel by Ficus glumosa gum in H2SO4 solution, African Journal of Pure and Applied Chemistry, 6 (2012) 100-106.

[99]   M. Abdallah, Guar gum as corrosion inhibitor for carbon steel in sulfuric acid solutions, Portugaliae Electrochimica Acta, 22 (2004) 161-175.

[100]   M. Messali, H. Lgaz, R. Dassanayake, R. Salghi, S. Jodeh, N. Abidi, O. Hamed, Guar gum as efficient non-toxic inhibitor of carbon steel corrosion in phosphoric acid medium: electrochemical, surface, DFT and MD simulations studies, Journal of Molecular Structure, 1145 (2017) 43-54.

[101]   G. Palumbo, K. Berent, E. Proniewicz, J. Banaś, Guar gum as an eco-friendly corrosion inhibitor for pure aluminium in 1-M HCl solution, Materials, 12 (2019) 2620.

[102]   P. Roy, P. Karfa, U. Adhikari, D. Sukul, Corrosion inhibition of mild steel in acidic medium by polyacrylamide grafted Guar gum with various grafting percentage: Effect of intramolecular synergism, Corrosion Science, 88 (2014) 246-253.

[103] S.A. Umoren, I.B. Obot, A. Madhankumar, Z.M. Gasem, Performance evaluation of pectin as ecofriendly corrosion inhibitor for X60 pipeline steel in acid medium: Experimental and theoretical approaches, Carbohydrate polymers, 124 (2015) 280-291.

[104] S.A. Umoren, A. Madhankumar, Effect of addition of CeO2 nanoparticles to pectin as inhibitor of X60 steel corrosion in HCl medium, Journal of Molecular Liquids, 224 (2016) 72-82.

[105] M.V. Fiori-Bimbi, P.E. Alvarez, H. Vaca, C.A. Gervasi, Corrosion inhibition of mild steel in HCL solution by pectin, Corrosion science, 92 (2015) 192-199.

[106] M.M. Fares, A. Maayta, M.M. Al-Qudah, Pectin as promising green corrosion inhibitor of aluminum in hydrochloric acid solution, Corrosion Science, 60 (2012) 112-117.

[107] A.N. Grassino, J. Halambek, S. Djaković, S.R. Brnčić, M. Dent, Z. Grabarić, Utilization of tomato peel waste from canning factory as a potential source for pectin production and application as tin corrosion inhibitor, Food hydrocolloids, 52 (2016) 265-274.

[108] J. Halambek, I. Cindrić, A.N. Grassino, Evaluation of pectin isolated from tomato peel waste as natural tin corrosion inhibitor in sodium chloride/acetic acid solution, Carbohydrate Polymers, 234 (2020) 115940.

[109] N. Saidi, H. Elmsellem, M. Ramdani, A. Chetouani, K. Azzaoui, F. Yousfi, A. Aouniti, B. Hammouti, Using pectin extract as eco-friendly inhibitor for steel corrosion in 1 M HCl media, Der Pharma Chemica, 7 (2015) 87-94.

[110] R. Geethanjali, A. Sabirneeza, S. Subhashini, Water-soluble and biodegradable pectin-grafted polyacrylamide and pectin-grafted polyacrylic acid: electrochemical investigation of corrosion-inhibition behaviour on mild steel in 3.5% NaCl media, Indian Journal of Materials Science, 2014 (2014).

[111] X. Ma, J. Wang, J. Xu, J. Jing, J. Li, H. Zhu, S. Yu, Z. Hu, Sunflower Head Pectin with Different Molecular Weights as Promising Green Corrosion Inhibitors of Carbon Steel in Hydrochloric Acid Solution, ACS omega, 4 (2019) 21148-21160.

Materials and Methods
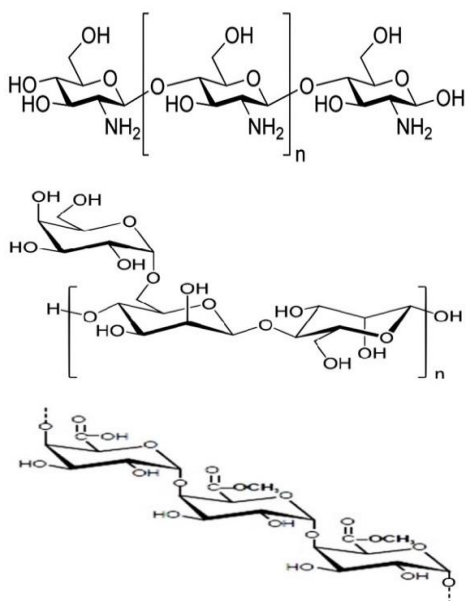
Chapter 2

This chapter describes the details of materials used in this study and the structure of the carbohydrate polymer used for corrosion studies. The synthetic routes for the development of various corrosion resistant coating and inhibitors used in this study are also given in this session. Various characterization methods and corrosion monitoring techniques used in the whole work are also mentioned in this chapter. The details of the theoretical calculations including NBO analysis and Monte Carlo simulation performed in this study are also discussed in this section.

CONTENTS

2.1 Carbohydrate polymers and other chemical used for this study

2.2. Metal

2.3. Medium

2.4. Synthesis and functionalization 2.5. Development of chitosan-based coating on MS

2.6. Characterization techniques

2.7. Corrosion monitoring strategies

2.8. Quantum chemical studies

2.1. Carbohydrate polymers and other chemical used for this study

Chitosan oligosaccharide with a molecular weight of 5kDa and guar gum were commercially obtained and used as received. Pectin is isolated from jackfruit peel waste by acid extraction. The other chemicals and reagents, used throughout the study were all A.R. grade. The name, chemical formula, and suppliers of the chemicals are listed in Table 2.1

Table 2.1. List of chemicals and carbohydrate polymers used in the study.

S. No	Name	Chemical formula	Make
1	Hydrochloric acid	HCl	Merck
2	Sodium chloride	NaCl	Himedia
3	Acetone	C_3H_6O	Merck
4	Ethanol	C_2H_5OH	Merck
5	Oxalic acid	$C_2H_2O_4$	Merck
6	Chitosan oligosaccharide	-	Sigma Aldrich
7	Guar Gum	-	Himedia
8	Jackfruit peel waste	-	-
9	Stearic acid	$C_{18}H_{36}O_2$	Sigma Aldrich
10	1-ethyl-3-(3-dimethylaminopropyl) carbodiimide-HCl (EDC-HCl)	$C_8H_{17}N_3.HCl$	Spectrochem
11	Tetra ethyl orthosilicate	$SiC_8H_{20}O_4$	Sigma Aldrich
12	Hexa methyl disilazane	$C_6H_{19}NSi_2$	Avra
15	Triton X 100	$C_{14}H_{22}O(C_2H_4O)n$ (n = 9-10)	Alfa Aesar
16	Tween-80	$C_{64}H_{124}O_{26}$	Merck

The chemical structure of the carbohydrate polymers used in the investigations are shown in Figure 2.1
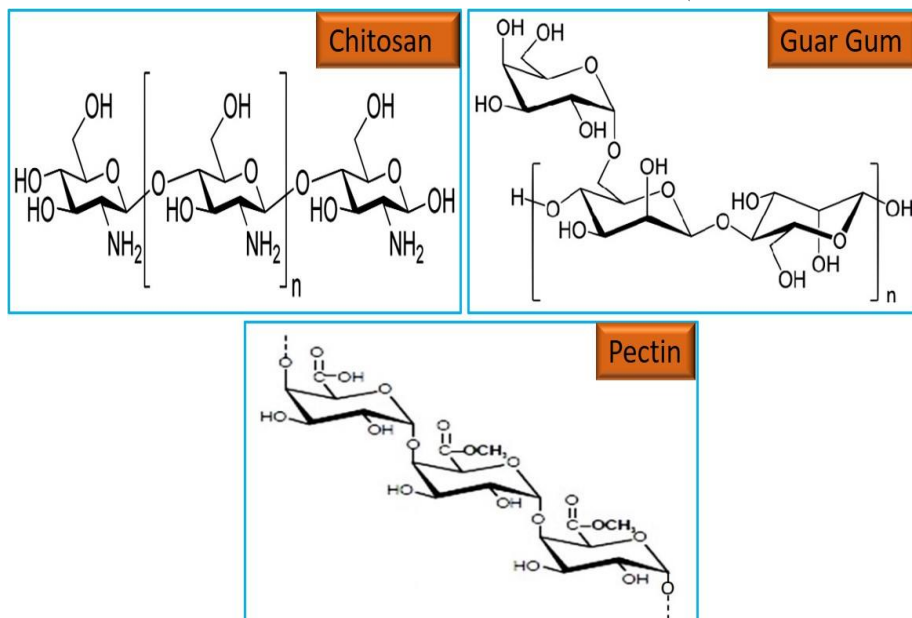
Figure 2.1. Molecular structure of carbohydrate polymers used in this study

2.2. Metal

The corrosion inhibition behaviour of the studied carbohydrates was performed using mild steel (MS) with the chemical composition, as analysed using EDX spectral method, (in atom %): $C \approx 0.2\%$; $Mn \approx 1\%$; P 0.03%; $S \approx 0.02\%$; $Fe \approx 98.75\%$. The metal coupons used for weight loss methods were cut into $2 \times 1.8 \ cm^2$ in area. For electrochemical studies, MS coupons with an exposed area of $1 cm^2$ were used in each measurement.

2.2.1. Pre-treatment of metal coupons

Before each test, various grades of emery papers were used for the surface cleaning and finishing of metal coupons. After surface finishing,

the MS coupons were cleaned with ethanol, acetone, and subsequently with distilled water and dried at room temperature before each measurement as proposed by ASTM standard G-1-72.

2.3. Medium

Corrosion studies were performed in the acidic and saline medium. The acidic corrosive medium, 0.5M HCl was prepared by diluting reagent grade 37% HCl with distilled water. The saline medium 3.5% NaCl was prepared from the analytical grade NaCl. All the studies were conducted in an aerated medium at atmospheric pressure and room temperature. The corrosion inhibition studies were carried out by dissolving various concentrations of inhibitor in aerated, unstirred, uninhibited and inhibited acid solution at different temperatures.

2.4. Synthesis and functionalization

Owing to the excellent mechanical strength and low cost, MS has been extensively used in industries, and constructions. However, as the passive oxide layer is highly porous in the case of MS the electrolyte penetrates through the metal surface and further corrosion occurs beneath the passive oxide layer. So, the MS can be protected by stabilizing the passive oxide layer. Corrosion prevention of MS using three carbohydrate polymers were investigated in the acidic and saline medium. Chitosan-based coating is a promising candidate for metal protection in different aggressive media. So, we have functionalised chitosan with stearic acid to improve its barrier property. The influence of different loadings of hydrophobic mesoporous silica nanoparticles on

the anticorrosion performance of chitosan polymer matrix and stearic acid grafted chitosan film were investigated. Two natural carbohydrate polymer, guar gum and pectin (isolated from jackfruit peel waste) used as inhibitors for MS corrosion.

2.4.1. Functionalization of chitosan with stearic acid

Stearic acid grafted chitosan (CS-g-SA) film was synthesized via a coupling reaction of the amino group of chitosan (CS) with the carboxyl group of stearic acid (SA) in the presence of a water-soluble carbodiimide coupling reagent EDC.HCl (1-ethyl-3-(3-dimethylaminopropyl) carbodiimide). Chitosan oligosaccharide (1.5g) was dissolved in 50 mL of distilled water and heated to 60°C. EDC.HCl-1.4 g and SA-0.4 g with a molar ratio of 5:1 was dissolved in a solution of 35 mL acetone and 15 mL ethanol. After stirring for 30 minutes at 400 rpm (maintained at 60°C), the solution was added to the CS solution and stirred for 24 hours. For the formation of self-assembled monolayer and for removing isourea as a by-product, the sample was purified by using MWCO: 7kDa dialysis membrane against distilled water for 48 hours, and the reaction content lyophilized. The unreacted SA in the lyophilized product was further removed by washing with ethanol [1-3]. EDC catalyst reacts with the acid group of SA to form an active ester intermediate. Subsequently, this intermediate reacts with the amino group of CS forming an amide bond. The mechanism of the reaction is illustrated in scheme. 2.1. The CS and CS-g-SA films were made by drying 10 ml of the solution at 70°C and neutralized using NaOH [4]. Corrosion protection by CS-g-SA in the saline medium was

carried out by dispersing in epoxy resin by ultrasonication before coating. Epoxy resin (Bisphenol A) and polyamide hardener in the ratio 2:1 was used to prepare epoxy coatings.
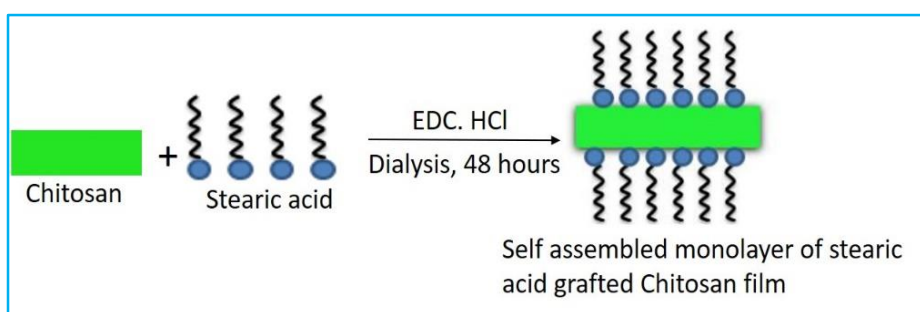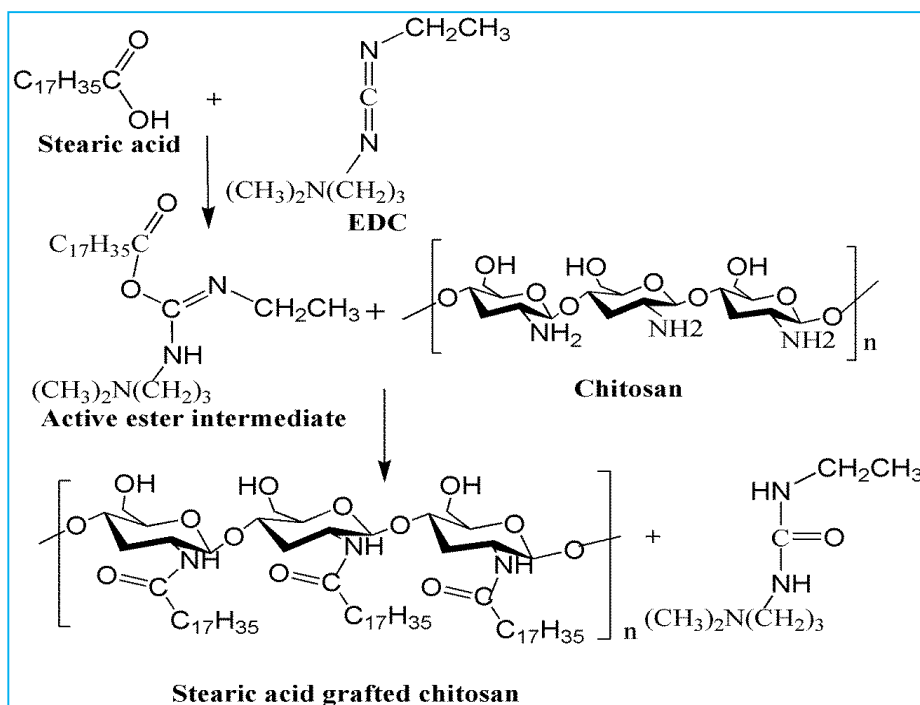
Scheme 2.1. Mechanism of formation stearic acid grafted chitosan film and its Schematic representation

2.4.2. Synthesis of Chitosan/SiH film grafted with SA (CSiHS)

SiO$_2$ particle was synthesized using tetra ethyl orthosilicate, acetic acid, and water in the molar ratio 1:6.93:4.11 and aged for 6 hours, and the resulting sol was centrifuged and washed with alcohol and the precipitate was dried at 60°C and calcined at 600°C [5]. The hydrophilic Si rendered more hydrophobic using a commonly used silylating agent hexa methyl disilazane (HMDS). 1 gram of SiO$_2$ was dispersed in water. Hexa methyl disilazane (HMDS) in ethanol at a 1:8 wt/wt ratio was added into the silica sol and the mixture was transferred into an autoclave and kept at 180°C for 24 hours. The obtained gel was washed with ethyl alcohol to remove excess HMDS. Finally, the product (SiH) was washed several times and dried at 110°C for 4 hours[6, 7]. To the chitosan solution, different weight percentages (1.0, 3.0, and 5.0 wt %) of SiH were added and stirred for 2 hours. SA and EDC. HCl (1:5 mol/mol) in ethanol- acetone mixture was added into the CSiH solution and stirred for 24 hours. The resulting solution is dialyzed to remove the bye product and lyophilized for 12 hours[8]. Corrosion protection in the saline medium was carried out by dispersing in bisphenol A based epoxy resin.

2.4.3. Corrosion inhibition by natural carbohydrate polymers

2.4.3.1. Guar Gum as a corrosion inhibitor

GG with a concentration of 200-800ppm and 5ppm of surfactants (Tween-80, Triton-X) were prepared using double distilled water.

2.4.3.2. Extraction of Pectin from jackfruit peel waste

Jack fruit peel waste with conical carpel apices was manually peeled off and washed thoroughly to remove any adhesive waste on the surface. Then the peels were finely chopped, washed, blanched at 80ºC for 15 min, and dried in a hot air oven at 60°C until it reaches the stable weight. The dried peels were pulverized using a grinder and passed through a 40-mesh sieve and powdered samples were kept in polyethylene bags and stored at room temperature. According to Sundarraj et al among the different mineral acid extraction, oxalic acid was the best acid for the extraction of pectin from jack fruit peel waste with high yield[9]. Briefly, 25g of the ground jackfruit peel powder was added into a beaker containing 250 mL of distilled water and acidified with 0.05N oxalic acid. Then the mixture was stirred in a water bath for 60 minutes at 90ºC. The oxalic acid extract was filtered through a muslin cloth. The filtrate was cooled to room temperature. Then 95% of ethanol was added to the cold solution and allowed to precipitate pectin. The precipitate was collected and dried at 50ºC for 24 hours. The pectin yield was calculated using the following equation[10]

$$yield \ (\%) = 100 \times \lfloor P/_{Bi} \rfloor \qquad (2.1)$$

where P is the weight of extracted pectin in gram and Bi is the initial amount of jackfruit peel powder (25g). 250-1000ppm of the extracted pectin was introduced to the corrosive medium.

2.5. Development of Chitosan-based coating on MS

CS-based systems were deposited on the MS surface using SPEKTON dip coater at a constant speed of 60mm per minute. Cleaned and dried MS coupons were immersed into the solution for 20 seconds and withdrawn from it at a constant movement rate of 60mm/min. After triplicate dip coating the substrates were dried at room temperature for 24 hours in the fume hood before corrosion study.

2.6. Characterization techniques

The corrosion formulations were characterized using various techniques. The elemental analysis was carried out using CHNSO analyser and Energy dispersive X-ray analysis (EDX) technique. The hydrophobicity was measured with a Digi drop goniometer. A JASCO FT/IR-4600 was used for IR spectroscopy. NMR spectra was taken with Bruker 400 Avance III 400 MHz NMR. Fluorescence measurements were done using a Cary Eclipse Fluorescence Spectrophotometer. Thermogravimetric analysis was performed with Perkin Elmer STA 8000 Thermal Analyzer under the nitrogen atmosphere. The pore characteristics of silica particles were done using Belsorp Max surface area analyser. XPS was carried out using PHI 5000 Versa Probe II, ULVAC-PHI Inc. A CARL ZEISS Field Emission Scanning Electron Microscope associated with Energy dispersive X-ray analysis system was used for FESEM and EDX. AFM topography of inhibitors were carried out using NTEGRA PRIMA Atomic Force Microscope with silicone intrude cantilever. Carl Zeiss Stemi 508 was used to monitor stereomicroscopic images of coating. HRTEM micrograph of silica was

done with Jeol/JEM 2100. Electrochemical corrosion monitoring was done using Gill AC electrochemical work station (ACM instrument, model No: 1475). Quantum chemical studies were performed via DFT/B3LYP/6-311G (d, p) method using Gaussian 09 package. BIOVIA material studio programme was used for molecular simulation studies.

2.6.1. Elemental analysis

Carbon, hydrogen, and oxygen percentage in chitosan and stearic acid grafted chitosan were determined using a CHNSO analyser (Thermo Scientific FLASH 2000 HT Elemental Analyser). The basic principle of quantitative CHNSO analysis is the combustion of organic and inorganic solids and liquids into their oxide and separated into their various components and percentage of elements were analysed with a suitable detector [11]

2.6.2. Contact angle Measurements

Water contact angle measurements were used to assign the wettability of the solid surface based on the degree of wetting where solid and liquid interface encounters on a solid surface. Water contact angles were assessed with a Digi drop goniometer equipped with a special optical system and a CCD camera at room temperature. The goniometer measured the contact angle by taking water in a micro syringe and a drop of liquid (5 μl) was placed on the coated substrate placed on a quartz plate and after the stabilization of the contact between the water droplet

and coated substrate, the measurements were done and performed five times for each sample.

2.6.3. Fourier Transform Infra-Red Spectroscopy (FTIR)

The IR spectra of corrosion resistant formulations (inhibitor and coating) were carried out by the KBr pellet method on JASCO FT/IR-4600 instrument in the absorption range of 4000-400cm^{-1}. The variation in the various stretching frequency of studied inhibitor before and after corrosion study can be effectively used to predict metal-inhibitor complex formation as well as to confirm the chemical functionalisation of the chitosan-based coating. The FTIR spectra of inhibitor after corrosion was taken by immersing the metal sample in 0.5M HCl solution containing an optimum concentration of inhibitor. After 24 hours of immersion, the metal coupons were removed, rinsed with water, and dried at room temperature. The adsorbed inhibitor on the metal surface was scraped out and pelletized with KBr and subjected to FTIR spectroscopy.

2.6.4. Nuclear Magnetic Resonance Spectroscopy (^{1}HNMR and ^{13}C NMR)

NMR spectra were taken to confirm the grafting of chitosan with stearic acid. The ^{1}HNMR and ^{13}C NMR spectra of chitosan (in D_2O) and stearic acid grafted chitosan (in DMSO-D_6) were taken using a Bruker 400 Avance III 400 MHz NMR instrument. TMS (tetramethylsilane) was used as the internal reference.

2.6.5. Fluorescence measurements

The fluorescence measurements were carried out to determine critical micelle concentration (CMC) of stearic acid grafted chitosan (CS-g-SA) using pyrene as a fluorescent probe. A solution of CS-g-SA with concentration 2×10^{-3} to 1.0 mg/ml and 6×10^{-7}M of pyrene was prepared and the fluorescence spectrum was taken by using a Cary Eclipse Fluorescence Spectrophotometer. The excitation wavelength (λ_{ex}) was 334nm and the slit opening was set at 5nm (excitation) and 5 nm (emission). Then the fluorescence intensity ratio of the first (372nm) and the third (392nm) highest energy bands were determined from the pyrene emission spectra [12-14].

2.6.6. Thermogravimetric Analysis

TGA has been used to estimate the thermal behaviour of materials and to demonstrate the mechanism by which a material loses its weight as a result of controlled heating. The quantitative variation of weight loss is examined with respect to time or temperature in a thermal or scanning mode. Thermal analysis (TGA and DTG) of the compound were conducted with Perkin Elmer STA 8000 Thermal Analyzer under the nitrogen atmosphere from 30-600°C at a heating rate of 10°C/min.

2.6.7. X-ray photoelectron spectroscopy (XPS)

XPS can provide insight in to the electronic state of the elements within a material, elemental composition, and chemical bonds in a molecule. The MS sample was immersed in 0.5M HCl solution containing an optimum concentration of inhibitor for 24 hours, rinsed with water, and

dried at room temperature. The surface chemistry of the studied inhibitors on MS surface was analysed using X-ray photoelectron spectroscopy (XPS, PHI 5000 Versa Probe II, ULVAC-PHI Inc., USA) equipped with micro focused (200 μm, 15 KV) monochromatic Al-Kα X-Ray source (hν = 1486.6 eV). Both survey spectra and narrow scan (high-resolution spectra) were recorded. Survey scans were recorded with an X-ray source power of 50W and pass energy of 187.85 eV. High-resolution spectra of the major elements were recorded at 46.95 eV pass energy.

2.6.8. Nitrogen Adsorption/Desorption

The pore characteristics of the SiO_2 and surface modified SiO_2 particles were monitored by determining the nitrogen sorption behaviour using a surface area and pore size analyser (Belsorp Max surface area analyzer). The Si particles were first degassed for 6 hours at 100^oC. The BET and Barrett–Joyner–Halenda procedures were used to characterize the pore of Si particles from the adsorption branches of the isotherms.

2.6.9. FESEM and EDX

Field emission Scanning Electron Microscopy (FESEM) is an analytical technique used to examine the surface of objects by scanning with a high-energy beam of electrons in a raster scan pattern. When an electron beam is irradiated on the sample surface, the electrons interact with atoms of the sample and produces various signals that comprise the information about the surface topography and sample surface compositions. The variation in the surface morphology of coated and

inhibited MS samples after different immersion time in the corrosive media was carried out by A CARL ZEISS Field Emission Scanning Electron Microscope associated with Energy dispersive X-ray analysis (EDX) system. The surface morphology of coated and inhibited MS samples was obtained using SE2 detector at an electron accelerating voltage of 20 kV at different magnifications. EDX analysis was performed using Nano XFlash Detector, Bruker.

2.6.10. Atomic force microscopy

Atomic force microscopy (AFM) is a high-resolution scanning probe microscope used for micro and nanostructured surface studies. AFM of the uninhibited and inhibited MS samples was taken after 24 hours of immersion in 0.5M HCl and then cleaned with distilled water, dried at room temperature, and then used for AFM topography using NTEGRA PRIMA Atomic Force Microscope with silicone intrude cantilever in semi-contact mode to evaluate the surface roughness. AFM topography of Chitosan-based coating on MS sample was analysed using Bruker multimode nanoscope version 8 with high-speed Scan Asyst Mode and Tapping Mode.

2.6.11. Transmission Electron Microscopy (TEM)

HRTEM (High resolution transmission electron microscopy) micrograph was employed to characterize the size, porous structure, pore diameter, and morphology of mesoporous SiO_2 and hydrophobically modified mesoporous SiO_2 with HRTEM: Jeol/JEM

2100. The TEM micrographs of the samples were attained with an accelerating voltage of 200 kV.

2.7. Corrosion monitoring strategies

The corrosion protection performance of the studied carbohydrate polymer-based coatings and inhibitors was monitored via non-electrochemical (weight loss) and electrochemical (electrochemical impedance spectroscopy, EIS and potentiodynamic polarization) methods

2.7.1. Non-Electrochemical (Weight loss) method

The MS coupons with an area of 2×1.8 cm^2 were cleaned according to ASTM standard G-1-72 and dipped in the corrosive medium with and without inhibitor or coating for specific immersion time at room temperature. The coupons were released, rinsed with water, and acetone and dried in an air oven. From the initial and after test weights of the metal specimen weight loss was determined. From the weight loss, the corrosion rate and percentage inhibition efficiency were calculated. The surface coverage (θ) was calculated to realize the adsorption of inhibitor on MS surface by replacing the pre-adsorbed water molecule using the following equation

$$\theta = \frac{IE}{100}$$ (2.2)

2.7.2. Electroanalytical techniques

Electrochemical impedance spectroscopy (EIS) and potentiodynamic polarization (PDP) measurements were carried out using a three-

electrode setup in one compartment cell and Gill AC electrochemical work station (ACM instrument, model No: 1475) (Figure 2.2).

Figure 2.2. Electrochemical workstation with dip coater

The working electrode was a MS specimen with $1cm^2$ exposed area, a saturated calomel electrode as the reference electrode with a Luggin capillary to minimize the IR drop at the working electrode, and a platinum counter electrode. The MS working electrode was vertically immersed in the corrosive medium in the absence and presence of inhibitor or coating for 1 hour and OCP (open circuit potential) was evaluated from the time vs potential curve. When potential became nearly constant (<5mV) to time, electrochemical measurements were carried out. Each electrochemical experiment was repeated at least thrice to check the reproducibility of results.

2.7.2.1. Electrochemical impedance spectroscopy (EIS)

Impedance analysis was performed with a minimum amplitude of 10 mV at a frequency domain from 0.1 Hz to 10 kHz. The data from the

EIS plot were fitted with a suitable equivalent circuit via Z simp win software. Charge transfer resistance (R_{ct}) obtained from the EIS plot was used to calculate the inhibition efficiency (IE) using the following equation

$$IE = \frac{R_{ct}^* - R_{ct}}{R_{ct}^*} \qquad (2.3)$$

where R_{ct}^* and R_{ct} are charge transfer resistance of acid solution without and with inhibitor

2.7.2.2. Potentiodynamic polarization studies (PDP)

The PDP curves were recorded by polarizing the electrode cathodically by −250mV and +250 mV anodically concerning the OCP at a scan rate of 60 mV/minute. The PDP parameters, such as I_{corr} (corrosion current density), E_{corr} (corrosion potential), R_p (polarization resistance), CR (corrosion rate), and βa and βc (anodic and cathodic Tafel constants) were determined from the Tafel extrapolation method of anodic and cathodic Tafel plots of PDP curve. Corrosion current density (I_{corr}) from the intercept of extrapolated anodic and cathodic Tafel lines at the corrosion potential (E_{corr}) were used to estimate the IE by using the following expression.

$$IE = \frac{I_{corr}^* - I_{corr}}{I_{corr}^*} \qquad (2.4)$$

where I_{corr}^* and I_{corr} are corrosion current density of MS samples without and with inhibitor.

2.7.3. Scotch tape Adhesion test

According to ASTM D-3359 test method B-cross cut tape test, the adhesion strength of CS-based coating on MS was investigated using Scotch tape (fabricated by 3M). The coated surface was cut by a razor blade at a distance of 1 mm each other to make the grid lines. After making all cross cuts on the coated MS surface, the Scotch tape was firmly applied on the grid area of coated surface followed by peeling it off [15]. Three samples were examined for each test and the adhesion test results were evaluated. The adhesion strength of the coatings on the metal surface can be evaluated by counting the number of squares peeled off compare to the total number of squares. Carl Zeiss Stemi 508 was used to monitor stereomicroscopic images of the grid area of the coated samples. After the test, the coated samples were classified on a 0B to 5B scale, 5B corresponding to perfect adhesion of coating and 0B corresponding to flaking of the coating.

2.8. Quantum chemical studies

2.8.1. Density Functional Theory Method

The theoretical calculations were achieved employing Gaussian 09 package. The geometry optimization and single point energy calculations of the studied inhibitors in the gas and water phase were performed by DFT/B3LYP/6-311G (d, p) method. E_{HOMO} (energy of highest occupied molecular orbital), E_{LUMO} (energy of lowest unoccupied molecular orbital), ΔE (energy gap between the LUMO and HOMO), μ (dipole moment) and the global descriptive parameters η

(hardness), χ (electronegativity), and S (softness) are calculated by Koopmann's theorem by applying the following equations[16]

$$Ionization\ potential\ (IP) = -E_{HOMO} \qquad (2.5)$$

$$Electron\ affinity\ (EA) = -E_{LUMO} \qquad (2.6)$$

$$Absolute\ Hardness\ (\eta) = \frac{IP - EA}{2} \qquad (2.7)$$

$$Absolute\ Electronegativity\ (\chi) = \frac{IP + EA}{2} \qquad (2.8)$$

By Pearson's method, the tendency of an inhibitor for transferring electron density to the specimen can be evaluated by obtaining the number of the transferred electron using the equation given below[17].

$$\Delta N = \frac{\Phi - \chi_{inh}}{2(\eta_{Fe} + \eta_{inh})} \qquad (2.9)$$

where Φ is the work function, χ_{inh} is the electronegativity of inhibitor, η_{Fe}, and η_{inh} are the absolute hardness of Fe metal and the inhibitor. Since the IP and EA of bulk metal atoms are the same, the theoretical value of η_{Fe} is frequently used as zero and the value of Φ is 4.82[18, 19].

2.8.1.1. NBO analysis

The natural bonding orbital (NBO) analysis in the gas and water phase was accomplished using NBO 3.1 as enabled in the Gaussian 09 at the DFT/B3LYP/6-311G(d,p) level to acquire intra and intermolecular interaction between guar gum and surfactants [20, 21]. To study the

better inhibition of guar gum-tween 80 synergistic pair over guar gum-triton-X pair the inter and intramolecular interaction between GG and surfactants was carried out via NBO analysis using the second-order interaction energy(E2). The second-order Fock- matrix was implemented to assess the donor-acceptor interactions on the NBO basis. E2 describes the intensity of each electron donor between the Lewis donor (*i*) and non-Lewis acceptor NBO (*j*). E2 associated with i→j delocalization can be determined as[20, 22, 23]

$$E(2) = q_i \frac{{F_{(i,j)}}^2}{\mathcal{E}_j - \mathcal{E}_i} \qquad (2.10)$$

where q_i is the donor orbital occupancy, $\mathcal{E}i$ and $\mathcal{E}j$ are diagonal elements and F(i,j) is the off-diagonal NBO Fock matrix element.

Inhibitor molecule adsorbs on the MS surface by donating an electron to the metal and back donation of electron to the inhibitor. To interpret both electrophilic and nucleophilic reactive centres on the inhibitor, we have used condensed Fukui function via finite difference approximation from natural population analysis and Mullikan population analysis using Dmol3 calculation via Material studio. The Fukui functions were determined as follows [24-27]

$$f_k^+ = qk(N + 1) - qk(N) \qquad (2.11)$$

$$f_k^- = qk(N) - qk(N - 1) \qquad (2.12)$$

where qk(N), qk(N-1), and qk(N+1) are the atomic charges of the system with N, N-1 and N+1 electron.

2.8.2. Monte Carlo simulation studies

The adsorption model for inhibitors on the (1 1 0) plane of Fe was generated using the BIOVIA material studio programme. The crystal structure of Fe was constructed by using the builder module of the Material studio. The Fe crystals were cleaved along (110) plane. The Fe surface was then enlarged to 10×10 supercells (in guar gum) and 15×15 supercells (in guar gum-surfactant synergistic pair) designed for providing maximum surface interaction of inhibitor and water with Fe surface. A vacuum slab with $10A^{o}$ thickness was built. The Fe (1 1 0) surface was relaxed by minimizing energy using the COMPASS (Condensed phase Optimized Molecular Potentials for Atomistic Simulation Studies) Force field[28]. A single molecule of an optimized inhibitor was introduced onto the Fe (110) surface in the gas phase and inhibitor along with 200 water molecules were introduced via the adsorption locator module.

References

[1]   F.-Q. Hu, M.-D. Zhao, H. Yuan, J. You, Y.-Z. Du, S. Zeng, A novel chitosan oligosaccharide–stearic acid micelles for gene delivery: Properties and in vitro transfection studies, International journal of pharmaceutics, 315 (2006) 158-166.

[2]   H. Yuan, X. Bao, Y.-Z. Du, J. You, F.-Q. Hu, Preparation and evaluation of SiO2-deposited stearic acid-g-chitosan nanoparticles for doxorubicin delivery, International journal of nanomedicine, 7 (2012) 5119.

[3]   F.-Q. Hu, X.-l. Wu, Y.-Z. Du, J. You, H. Yuan, Cellular uptake and cytotoxicity of shell crosslinked stearic acid-grafted chitosan oligosaccharide micelles encapsulating doxorubicin, European Journal of Pharmaceutics and Biopharmaceutics, 69 (2008) 117-125.

[4]   E.M. Fayyad, K.K. Sadasivuni, D. Ponnamma, M.A.A. Al-Maadeed, Oleic acid-grafted chitosan/graphene oxide composite coating for corrosion protection of carbon steel, Carbohydr. Polym., 151 (2016) 871-878.

[5]   R. Dubey, Y. Rajesh, M. More, Synthesis and characterization of SiO2 nanoparticles via sol-gel method for industrial applications, Materials Today: Proceedings, 2 (2015) 3575-3579.

[6]   A.M. Kartal, C. Erkey, Surface modification of silica aerogels by hexamethyldisilazane–carbon dioxide mixtures and their phase behavior, The Journal of Supercritical Fluids, 53 (2010) 115-120.

[7]   P. Jaseela, K. Shamsheera, A. Joseph, HMDS–GPTMS Modified Titania Silica Nanocomposite: A New Material for Oil–Water Separation, Journal of Inorganic and Organometallic Polymers and Materials, (2019) 1-8.

[8]   S. KO, A.R. Prasad, J. Garvasis, S.M. Basheer, A. Joseph, Stearic acid grafted chitosan/epoxy blend surface coating for prolonged protection of mild steel in saline environment, Journal of Adhesion Science and Technology, 33 (2019) 2250-2264.

[9]   A.A. Sundarraj, R.T. Vasudevan, G. Sriramulu, Optimized extraction and characterization of pectin from jackfruit (Artocarpus integer) wastes using response surface methodology, International journal of biological macromolecules, 106 (2018) 698-703.

[10]   S. Ranganna, Handbook of analysis and quality control for fruit and vegetable products, Tata McGraw-Hill Education, 1986.

[11]   F. Aşçi, M. Uçar, Ş. Kabak, M. Özkan, Assessment of the Phylogenetic Affiliation Levels of Water Mite (Acari, Hydrachnidia) Species with the Elemental Analysis Method, Advances in Bioscience and Biotechnology, 6 (2015) 427.

[12]   X. Li, J. You, F. Cui, Y. Du, H. Yuan, F. Hu, Preparation and characteristics of stearic acid grafted chitosan oligosaccharide polymeric micelle containing 10-hydroxycamptothecin, Asian J Pharm Sci, 3 (2008) 80-87.

[13]   S.-T. Huang, Y.-Z. Du, H. Yuan, X.-G. Zhang, J. Miao, F.-D. Cui, F.-Q. Hu, Synthesis and anti-hepatitis B virus activity of acyclovir conjugated stearic acid-g-chitosan oligosaccharide micelle, Carbohydrate polymers, 83 (2011) 1715-1722.

[14]   E. Moazeni, K. Gilani, A.R. Najafabadi, M. reza Rouini, N. Mohajel, M. Amini, M.A. Barghi, Preparation and evaluation of inhalable itraconazole chitosan based polymeric micelles, DARU Journal of Pharmaceutical Sciences, 20 (2012) 85.

[15]   Y. Wei, J.-M. Yeh, D. Jin, X. Jia, J. Wang, G.-W. Jang, C. Chen, R.W. Gumbs, Composites of electronically conductive polyaniline with polyacrylate-silica hybrid sol-gel materials, Chemistry of materials, 7 (1995) 969-974.

[16]   V.K. Rajan, C. Hasna, K. Muraleedharan, The natural food colorant Peonidin from cranberries as a potential radical scavenger–A DFT based mechanistic analysis, Food chemistry, 262 (2018) 184-190.

[17]   S. Martinez, Inhibitory mechanism of mimosa tannin using molecular modeling and substitutional adsorption isotherms, Materials Chemistry and Physics, 77 (2003) 97-102.

[18]   A. Kokalj, On the HSAB based estimate of charge transfer between adsorbates and metal surfaces, Chemical Physics, 393 (2012) 1-12.

[19]   H. Lgaz, I.-M. Chung, R. Salghi, I.H. Ali, A. Chaouiki, Y. El Aoufir, M.I. Khan, On the understanding of the adsorption of Fenugreek gum on mild steel in an acidic medium: Insights from experimental and computational studies, Applied Surface Science, 463 (2019) 647-658.

[20]   R. Raju, C.Y. Panicker, P.S. Nayak, B. Narayana, B. Sarojini, C. Van Alsenoy, A.A. Al-Saadi, FT-IR, molecular structure, first order hyperpolarizability, MEP, HOMO and LUMO analysis and NBO analysis of 4-[(3-acetylphenyl)   amino]-2-methylidene-4-oxobutanoic   acid, Spectrochimica Acta Part A: Molecular and Biomolecular Spectroscopy, 134 (2015) 63-72.

[21]   E. Glendening, A. Reed, J. Carpenter, F. Weinhold, NBO 3.0 program manual, Theoretical Chemistry Institute, University of Wisconsin, Madison, WI, (1990).

[22]   T. Polat, F. Bulut, I. Arıcan, F. Kandemirli, G. Yildirim, Vibrational assignments, spectroscopic investigation (FT-IR and FT-Raman), NBO, MEP, HOMO–LUMO analysis and intermolecular hydrogen bonding interactions of 7-fluoroisatin, 7-bromoisatin and 1-methylisatin–A comparative study, Journal of Molecular Structure, 1101 (2015) 189-211.

[23]   M. Khalid, A. Ali, S. Asim, M.N. Tahir, M.U. Khan, L.C.C. Vieira, F. Alexander, M. Usman, Persistent prevalence of supramolecular architectures of novel ultrasonically synthesized hydrazones due to hydrogen bonding [X–H··· O; X= N]: Experimental and density functional theory analyses, Journal of Physics and Chemistry of Solids, (2020) 109679.

[24]   K. Akhtari, K. Hassanzadeh, B. Fakhraei, N. Fakhraei, H. Hassanzadeh, S.A. Zarei, A density functional theory study of the reactivity descriptors and antioxidant behavior of Crocin, Computational and Theoretical Chemistry, 1013 (2013) 123-129.

[25]   J. Sánchez-Márquez, D. Zorrilla, A. Sánchez-Coronilla, M. Desireé, J. Navas, C. Fernández-Lorenzo, R. Alcántara, J. Martín-Calleja, Introducing "UCA-FUKUI" software: reactivity-index calculations, Journal of molecular modeling, 20 (2014) 2492.

[26]   S.K. Saha, P. Ghosh, A. Hens, N.C. Murmu, P. Banerjee, Density functional theory and molecular dynamics simulation study on corrosion inhibition performance of mild steel by mercapto-quinoline Schiff base corrosion inhibitor, Physica E: Low-dimensional systems and nanostructures, 66 (2015) 332-341.

[27]   D. Villemin, T. Abbaz, A. Bendjeddou, Structure, electronic properties, NBO, NLO andi chemi-cal reactivity of bis (1, 4-dithiafulvalene) derivatives: functional density theory study, (2017).

[28]   H. Sun, COMPASS: an ab initio force-field optimized for condensed-phase applications overview with details on alkane and benzene compounds, The Journal of Physical Chemistry B, 102 (1998) 7338-7364.

Protection of Mild Steel in Aggressive Environments using Stearic Acid Grafted Chitosan

Chapter 3
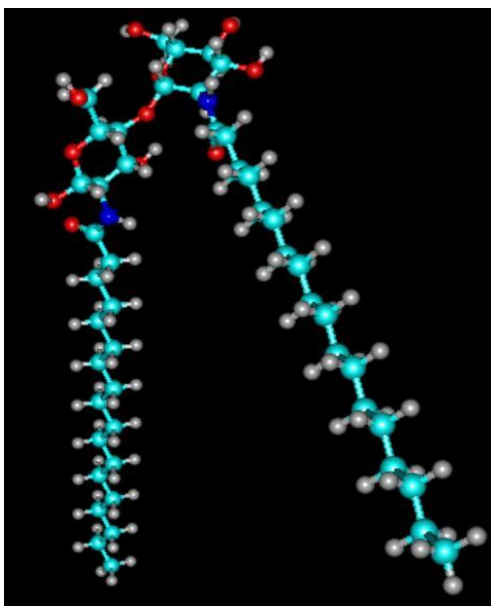
This chapter illustrates the corrosion resistance property of chitosan film which is modified by grafting with stearic acid via a water-soluble coupling agent, EDC. HCl. The interaction between chitosan and stearic acid was experimentally evident from FTIR-ATR, NMR, TGA, water contact angle measurements, and CHNSO analysis and the results are theoretically compared by using Gaussian 09 package. Corrosion protection studies was evaluated by non-electrochemical and electrochemical strategies. Surface morphological studies were carried out using FESEM, AFM, and stereomicroscopic techniques.

CONTENTS

3.1. Introduction

The development of corrosion-resistant coating is an effective way to protect mild steel from corrosion. The primary purpose of organic coating in corrosion protection is to isolate the material from the corrosive agents such as water, oxygen, and other aggressive ions. Chitosan (CS) based green coatings are promising candidates for the replacement of eco-harmful hexavalent chromate conversion coating because of its low cost, non-toxic nature, superior film forming capability, and complexation with the metal ions. To improve the adhesiveness of CS on the metal surface, it is necessary to functionalize the CS skeleton through the hydroxyl and amino groups. Here a novel corrosion resistant film made of stearic acid grafted chitosan (CS-g-SA) was used to protect the MS in acidic (0.5M HCl) and saline (3.5% NaCl) medium. The synthesis as well as various characterization methods of CS-g-SA film are given in chapter 2 (sec. 2.4.1 and 2.6). The development of CS-g-SA coating on the MS surface is described in sec. 2.5. For corrosion studies in HCl medium, the different CS-based systems were applied to MS. To enhance the adhesion and durability of the coating on MS in saline environment, CS-g-SA dispersed in Bisphenol A based epoxy resin was used. Epoxy resin (Bisphenol A) and polyamide hardener in the ratio 2:1 was used to prepare epoxy coatings.

3.2. Result and Discussion

3.2.1. Elemental analysis

The elemental composition of CS gets increased upon grafting with SA. CHN percentage is presented in the Table 3.1 indicated successful grafting of SA into the CS film.

Table 3.1. CHNS analyses on CS and CS-g-SA as weight %

Sample name	C	H	N
CS	30.433	5.3373	1.1316
CS-g-SA	45.895	7.6588	1.1501

3.2.2. Hydrophobic nature of the CS-based coatings

The hydrophobicity of the coatings was characterized by water contact angle measurements which are shown in Figure 3.1. The water contact angle of 89° got for CS film designates hydrophilic nature arising due to the free –OH and –NH_2 functional groups [1-3]. Hence it needs to impart hydrophobicity for protective applications. Upon grafting the CS matrix with SA water contact angle increased to 118°, which indicates that the hydrophilic CS film is modified to hydrophobic CS-g-SA film. The higher values of contact angles are attributed to the surface modification by the large alkyl chain of SA which imparts high hydrophobicity [4]
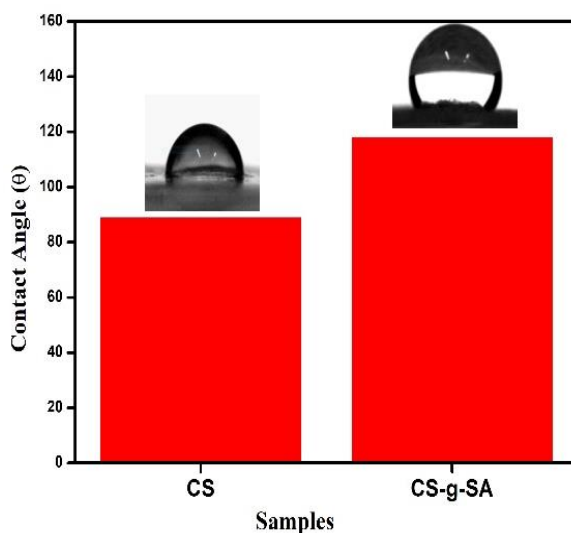
Figure 3.1. Water contact angle of CS and CS-g-SA

3.2.3. FTIR-ATR analysis

Figure 3.2 represents the ATR spectra of CS and CS-g-SA films. The spectra of CS shows an intense and broad band between 3500 and 3150 cm^{-1}, correlated with the axial stretching vibrations of the O-H and N-H bonds, a band at $2924cm^{-1}$, corresponding to the symmetric or asymmetric C-H (of the pyranose ring) stretching vibration and bands located at 1646, 1548 and 1423 cm^{-1} are assigned to amide I, amide II, and amide III vibrations respectively. A band obtained at $1057cm^{-1}$ is corresponding to the C-O stretching vibration. The peaks at 1147, 1062, and 1023 cm^{-1} correspond to the stretching vibration of C-O-C linkage in the glucosamine rings[5, 6]. The binding between SA carboxylic group and the CS amino group accounts for the spectral changes observed in the CS-g-SA ATR spectrum. The increase of the C-H absorption at $2924 \, cm^{-1}$ showed the presence of SA. CS-g-SA film showed absorption at $1639 \, cm^{-1}$ that ascribed to the carbonyl region

which related to the amide bond formation via chemical binding of SA and CS.
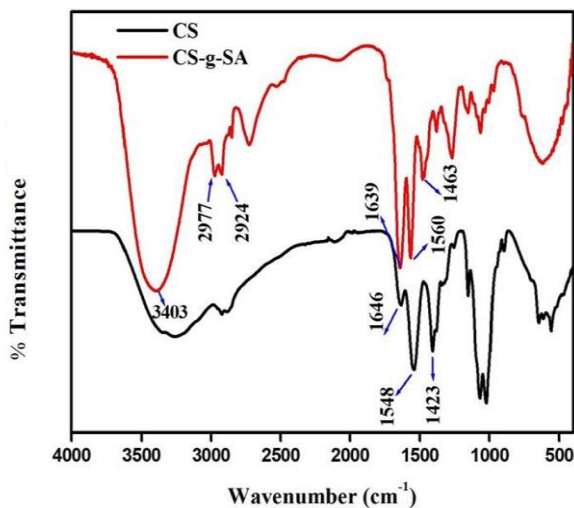
Figure 3.2. FTIR-ATR spectra of CS and CS-g-SA film

3.2.4. NMR analysis

The chemical structure of CS and CS-g-SA was confirmed by ^{1}H NMR spectra (Figure 3.3). In the NMR spectra of CS, the peak at 1.32ppm was attributed to the methyl proton of the N-alkylated glucosamine residue. Multiplet between 3-4 ppm is attributed to the methine proton of glucosamine and N-acetylated glucosamine. In CS-g-SA NMR spectra, the peaks for CH_3 and CH_2 protons of SA appeared in the spectrum. The peak at 0.85 and 1.09ppm was attributed to the terminal methyl and methylene proton of the stearate group of CS-g-SA. The peak at 2.18 ppm is attributed to the methylene proton of SA linked with the carbonyl group. The peak at 6.04 ppm was attributed to the amide proton of CS-g-SA. This indicated that SA was successfully grafted to the CS film via amide bond formation[7-9]. The formation of CS-g-SA

was again confirmed by ^{13}C NMR spectrum (Figure 3.4). The peak at 174 ppm was attributed to the carbonyl carbon of the stearate group of CS-g-SA, while no such peaks were observed in ^{13}C NMR spectrum of CS confirmed effective grafting. These results demonstrated that the SA was successfully grafted onto the CS film.

Figure 3.3. NMR spectra of CS and CS-g-SA.
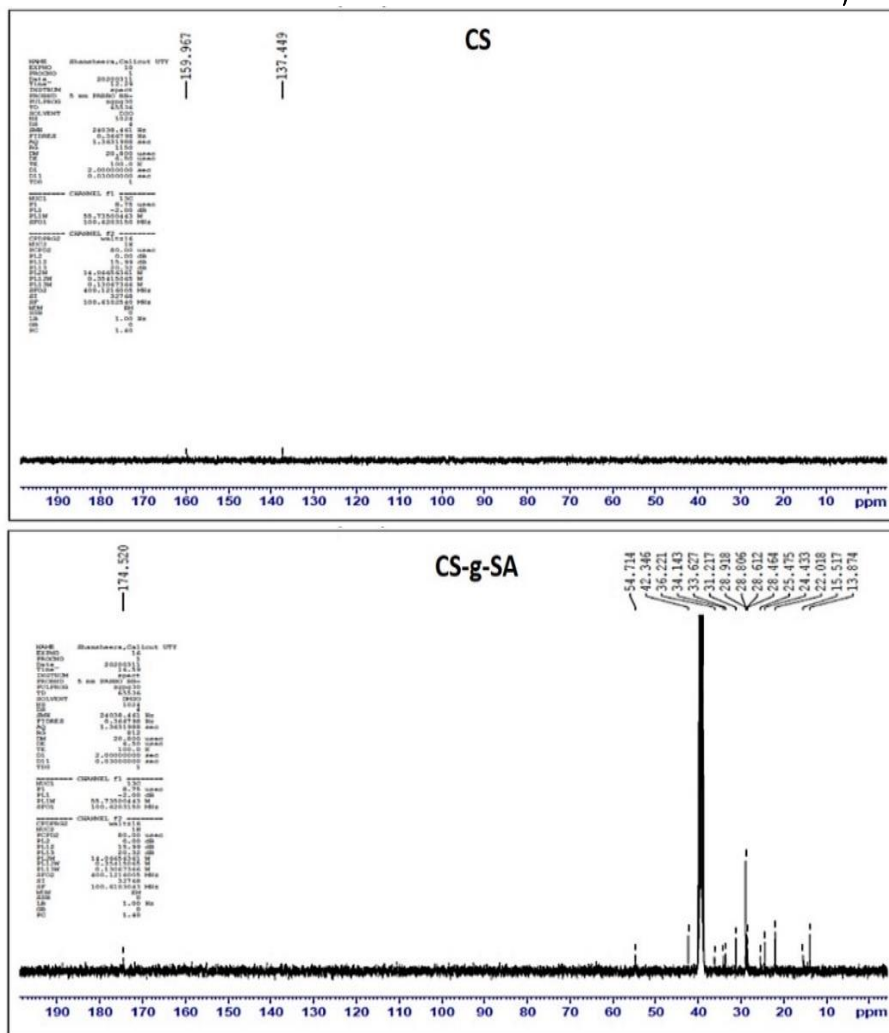
Figure 3.4. ^{13}C NMR of CS and CS-g-SA

3.2.5. Critical micelle concentration measurement

Pyrene has been used as a fluorescent probe for heterogeneous systems like polymers, micelles, biological membranes, etc owing to the long-life time of pyrene monomer and its ability to form excimer. The fluorescence emission spectrum of pyrene is characterized by five major

vibronic bands. Band III is highly sensitive to the polarity of the probe's environment. It shows increased fluorescence emission intensity in comparison to that of band I in hydrophobic environments. In contrast, the intensity of band I will be higher than that of band III in polar environments and then the ratio of I_1/I_3 is calculated. Generally, the critical micelle concentration (CMC) value of polymeric micelles is low compared to low molecular weight surfactant micelle. The grafted CS-g-SA was self-assembled to form micelles in aqueous solution. The CMC value of the grafted CS polymer was determined from the changes in the fluorescence intensity ratio of I_1/I_3. The plot of the fluorescence intensity ratio of I_1/I_3 versus the logarithm concentration of CS-g-SA was displayed in Figure 3.5. The interception of the two straight lines was regarded as the CMC value of the grafted polymer and that was determined 66 μg/mL, which showed the self-assembling ability of CS-g-SA micelles [8].
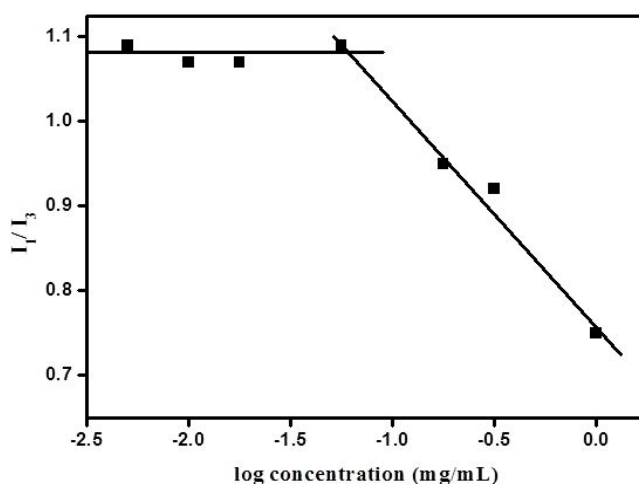
Figure 3.5. Variations in fluorescence intensity ratio of I_1/I_3 with logarithm concentration of CS-g-SA.

3.2.6. Thermogravimetric analysis (TGA)

The thermal stability of CS and CS-g-SA films was studied by thermogravimetric analysis (Figure 3.6). The total degradation of CS and CS-g-SA was observed in two stage decomposition from 30-600°C. Both CS and CS-g-SA exhibited first thermal degradation below 80°C with a weight loss of 9% for CS and 5% for CS-g-SA. Since CS-g-SA is hydrophobic in nature, the bounded water molecules by amino and hydroxyl groups are less. So, a relatively low weight loss was observed in the TGA of grafted film. The second degradation from 160-360°C with 68% for CS and 72% for CS-g-SA refers to a complex process including depolymerisation and dehydration from saccharide ring. The relatively higher weight loss for the grafted polymer is attributed to the overlapping of the decomposition process of the stearate group with the decomposition of N-acetylated unit [1, 10, 11].
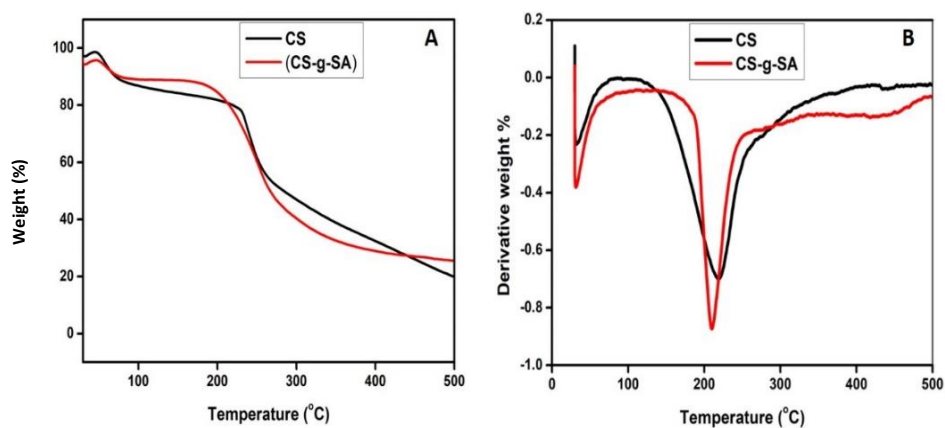
Figure 3.6. TGA and DTG of CS and CS-g-SA film

3.2.7. Computational study

The EDC catalyst activates the carboxylic groups of SA to react with a nucleophile. Chitosan is a polynucleophilic polymer, both amino and

hydroxyl groups of CS can act as nucleophilic groups[12]. However, since –NH$_2$ groups are stronger nucleophiles than –OH groups, without blocking amino group ester bond formation is almost impossible. Theoretically, we have proved that the amide bond formation is preferred rather than an ester bond. Here the geometries of CS monomer molecule and SA are first optimized and the optimized geometry and total energy of the two possible structures (CS-NH-SA and CS-O-SA) were calculated using DFT [13-15]. The higher negative value of energy for CS-NH-SA denotes thermodynamically favourable complex. The optimized geometry of monomer, HOMO, and LUMO of CS-g-SA monomer and dimer are exhibited in Figure 3.7.
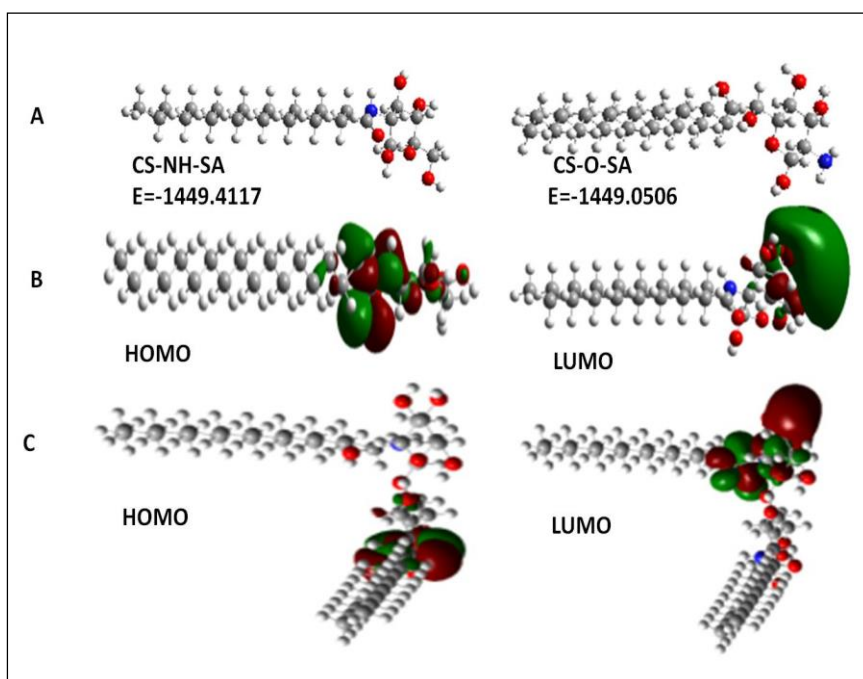
Figure 3.7. A) Optimised geometry of CS-NH-SA (CS-g-SA) and CS-O-SA B) & C) HOMO and LUMO of CS-g-SA monomer and dimer.

E_{HOMO}, E_{LUMO}, ΔE (energy gap between the LUMO and HOMO), μ (dipole moment) and the global descriptive parameters like η (hardness), χ (electronegativity), and S (softness) calculated by Koopmann's theorem [16] are tabulated in Table. 3.2. The lower ΔE value and higher dipole moment of CS-g-SA compared to CS indicates that the grafted film is adsorbed more firmly on the mild steel surface [17].

Table 3.2. Quantum chemical parameters of CS and CS-g-SA

Properties	CS	CS-g-SA monomer)	CS-g-SA (dimer)
E_{HOMO} (eV)	-6.8733	-6.5868	-6.4611
E_{LUMO} (eV)	-0.1858	0.0321	0.3273
ΔE (eV)	6.6875	6.6189	6.7884
Dipole moment, μ (Debye)	0.8820	5.2895	4.1762
Ionization potential, IP (eV)	6.8733	6.5868	6.4611
Electron affinity, EA (eV)	0.1858	-0.0321	-0.3273
Electronegativity, χ (eV)	3.5296	3.2773	3.0669
Hardness, η (eV)	3.3437	3.3094	3.3942
Softness, S (eV^{-1})	0.1495	0.1511	0.1473

3.2.8. Corrosion protection studies of coatings

The corrosion protection of developed CS-based coatings was evaluated by weight loss method and electrochemical (EIS and PDP) techniques.

3.2.8.1. Weight loss measurements

The MS corrosion of CS-g-SA coated and bare samples in 0.5M HCl and 3.5% NaCl was subjected to non-electrochemical technique. During metal immersion in acid solution, anodic metal dissolution and cathodic

hydrogen evolution lead to weight loss. The corrosion rate (CR in mg cm^{-2} day^{-1}) and corrosion protection efficiency (ɳ) was calculated as follows[18]

$$CR = \frac{W}{A \times t} \qquad (3.1)$$

$$ɳ = \frac{W_o - W_c}{W_o} \qquad (3.2)$$

where W denotes the weight loss accompanied, W_o and W_c are the weight loss of the bare and coated MS sample. A is the area of dipped metal coupon and 't' is the time in days. It was found that the weight loss and corrosion rate of the CS-g-SA coated steel samples are very low compared to bare MS with duration as shown in Figure 3.8 and Table 3.3.

Table 3.3. Weight loss data for bare and CS-g-SA coated MS in 0.5M HCl and 3.5% NaCl at room temperature.

No. of days	Electrolyte	Weight loss (g)		Corrosion rate (mg cm^{-2} day^{-1})		Protection efficiency (ɳ)
		Bare MS	CS-g-SA coated MS	Bare MS	CS-g-SA coated MS	
5	0.5M HCl	1.153	1.2×10^{-1}	64.05	6.550	89.78
10	0.5M HCl	1.173	1.4×10^{-1}	32.58	3.975	87.80
15	0.5M HCl	1.323	1.7×10^{-1}	24.50	3.218	86.87
20	0.5M HCl	1.339	2.2×10^{-1}	18.59	3.106	83.29
5	3.5%NaCl	2.6×10^{-2}	1.2×10^{-3}	1.466	6.6×10^{-2}	96.45
10	3.5%NaCl	6.2×10^{-2}	3.2×10^{-3}	1.708	8.8×10^{-2}	94.79
15	3.5%NaCl	2.1×10^{-1}	1.6×10^{-2}	3.885	2.8×10^{-1}	92.56
20	3.5%NaCl	5.9×10^{-1}	6.6×10^{-2}	8.191	9.2×10^{-1}	88.77
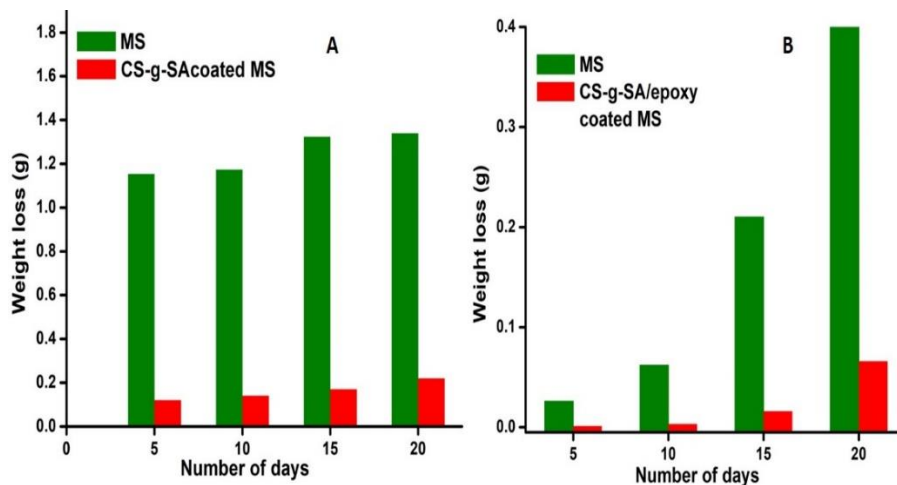
Figure 3.8. Variation of weight loss with the number of days for bare and CS-g-SA coated MS in A) 0.5M HCl and B) 3.5% NaCl at room temperature.

3.2.8.2. EIS measurements

EIS is a non-destructive technique in which response of the working electrode with bare and coated MS in 0.5M HCl and 3.5 % NaCl to an AC excitation with a wide range of frequencies from 0.1 Hz to 10,000 Hz with small AC amplitude was noticed. In modelling an electrochemical system, a potential is applied across the circuit, and the resulting current response to the frequency signal was generated. Figure 3.9A & B depicts the Nyquist plots obtained for bare and coated MS samples in the acidic and saline medium. Suitable equivalent circuits (Figure 3.10A & B) via Z simp win software were used to model the response of the working electrode to the AC sine wave and different parameters related to impedance analysis are summarised in Table 3.4. The components present in these circuits for viz, R_s is the uncompensated electrolyte resistance, R_{ct} is the charge transfer

78

resistance at MS/electrolyte interface and Q_{dl} is the double layer capacitance arising from the charge accumulation at the MS/electrolyte interface. In coated samples, two sub-interfaces are present namely, electrolyte/coating and MS/electrolyte interfaces. Therefore, the equivalent circuit used to fit the Nyquist plot for coated systems consists of two time constants. R_c is the coating resistance at electrolyte/coating interface and Q_c is the coating capacitance at electrolyte/coating interface, which is related to the water uptake capacity of the coating [19-23]. Coating resistance R_c and charge transfer resistance R_{ct} can evidently replicate the change of protective action of coated MS. Compared to bare MS, corrosion protection efficiency of CS-film coated MS in the acidic and saline medium offered good protection efficiency. The enhanced hydrophobicity of CS-g-SA coated substrates in 0.5M HCl amplified the impedance at low frequency. Compared to CS coated MS, CS-g-SA/epoxy coated MS in the saline medium exhibited good corrosion protection which almost covered the steel surface and hinders the diffusion of the chloride ions and water molecules from the electrolyte. The R_c increased significantly for CS-g-SA/epoxy coated MS indicates the superior barrier property in NaCl solution. For CS coated MS the relatively high Q_c value is due to the presence of free –OH and –NH_2 group which absorbs water from the aggressive media. Whereas in hydrophobic CS-g-SA coated MS the diffusion of electrolyte is reduced by the long alkyl chain present on the SA. This could be the reason for the low Q_c and high R_c value obtained for the grafted film on MS. For MS with CS-g-SA/epoxy coating, the impedance at low frequency enhanced due to the improved hydrophobicity of the modified film. The Q_{dl} value of the hydrophobic CS-g-SA coated MS sample is lower than that of the bare which

indicates the grafted CS coating impedes movement of corrosive ions from the electrolyte. The lower Q_{dl} value of CS-g-SA/epoxy coated MS compared to bare epoxy coated MS is due to the better adhesion properties of epoxy resin to the MS substrate and hydrophobic nature of CS-g-SA. R_{ct} values are used for calculating corrosion

protection efficiency (ɳ) by using the following equation.

$$\eta = \frac{R_{ct}^* - R_{ct}}{R_{ct}^*} \tag{3.3}$$

where R_{ct}^* and R_{ct} is the charge transfer resistance of the coated and bare MS sample. A higher R_{ct} value for the grafted film indicated that the CS-g-SA film suppressed the capability of the electrolyte to carry ions to the corrosive site.
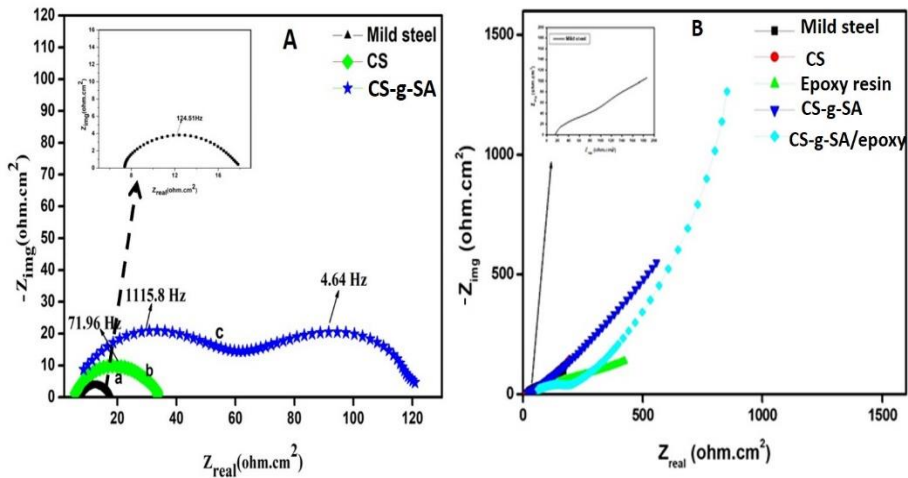
Figure 3.9. EIS plot of bare and coated MS in A) 0.5M HCl and B) 3.5% NaCl at room temperature

Table 3.4. Impedance parameters in 0.5M HCl and 3.5% NaCl for bare and coated MS.

Sample name	Electrolyte	R_s (Ωcm^2)	Q_c (F.cm^2)	n_1	R_c (Ωcm^2)	Q_{dl} (F.cm^2)	n_2	R_{ct} ($\Omega c m^2$)	Protection Efficiency(η)	Fitted circuit	$\chi 2$ value
MS	0.5M HCl	7.21	-	-	-	4.87×10^{-4}	0.80	10.34	-	A	1×10^{-3}
CS	0.5M HCl	4.93	3.39×10^{-3}	0.82	13.53	4.44×10^{-4}	0.80	29.48	64.92	B	4×10^{-3}
CS-g-SA	0.5M HCl	3.030	9.50×10^{-4}	0.81	58.12	1.184×10^{-5}	0.81	121.9	91.52	B	9×10^{-3}
MS	3.5% NaCl	11.92	-	-	-	2.78×10^{-5}	0.80	185.1	-	A	2.4×10^{-2}
CS	3.5% NaCl	12.30	8.09×10^{-3}	0.71	58.47	1.012×10^{-5}	0.90	328.7	43.68	B	3.7×10^{-2}
CS-g-SA	3.5% NaCl	14.55	2.56×10^{-3}	0.78	102.4	1.001×10^{-6}	0.79	749.7	75.31	B	8.4×0^{-2}
Epoxy resin	3.5% NaCl	22.68	6.6×10^{-3}	0.58	197.2	1.072×10^{-6}	0.80	407.8	54.61	B	6.3×10^{-2}
CS-g-SA/epoxy	3.5% NaCl	37.44	1.22×10^{-4}	0.67	1175	6.934×10^{-7}	0.80	3422	94.59	B	9.4×0^{-2}
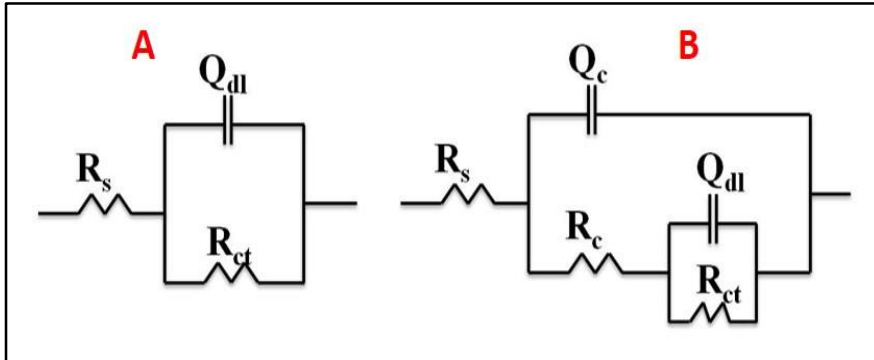
Figure 3.10. The equivalent circuits used to fit EIS data

The enhanced charge transfer resistance for the CS-g-SA coating on MS in the acidic and saline medium is further investigated from the Bode plot (Figure 3.11). The phase angle is a sensitive parameter for indicating the presence of additional time constant in the impedance spectra. Compared to bare MS, two phase maxima could be seen for the CS-g-SA coated MS at relatively low and high frequencies. The high frequency time constant is related to the hydrophobic nature of stearic acid and the barrier properties of chitosan. From the Bode impedance plot of bare and CS coated MS the lower impedance at lower and higher frequencies arises due to the presence of pores on the MS surface. So the diffusion of chloride ions through the pores and pinholes occurs and hence the corrosion damage at MS/electrolyte interfaces. However, for CS-g-SA/epoxy coated MS the high bode impedance exhibited at higher frequencies arises due to better adhesion and barrier properties of the modified film.
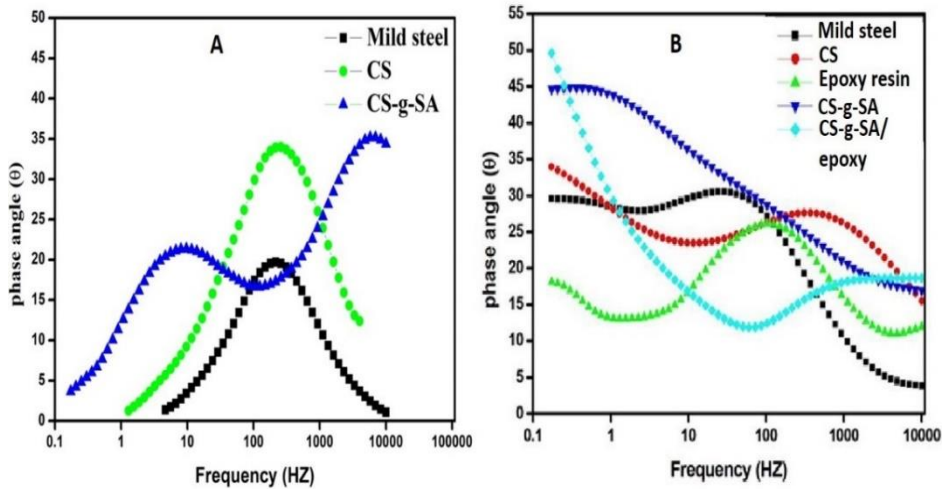
Figure 3.11. Bode phase angle plot for bare and coated MS in A) 0.5M HCl and B) 3.5% NaCl at room temperature

3.2.8.3. Potentiodynamic polarization plot

To evaluate the kinetics of anodic and cathodic reaction the potentiodynamic polarization studies were carried out on the coated and bare MS samples and the results are shown in Figure 3.12 and the electrochemical parameters such as I_{corr}(corrosion current density), E_{corr}(corrosion potential), β_a and β_c(anodic and cathodic Tafel slop) derived from the PDP plot of bare and coated MS samples are tabulated in Table 3.5. The corrosion potential (E_{corr}) of the bare MS in the saline medium was measured -699.76mV. E_{corr} value of CS-g-SA/epoxy coated MS is shifted to the more positive values (-304.95mV) compared to bare MS. This significant shift in the corrosion potential of coated samples could be attributed to an improvement in the protective nature of CS-g-SA films on MS. The PDP plot in the acidic and saline medium indicates that the hydrophobic CS-g-SA film has the lowest I_{corr} and corrosion

rate. The I_{corr} value was used to evaluate the corrosion protection efficiency (η) as follows[24]

$$\eta = \frac{I_{corr}^* - I_{corr}}{I_{corr}^*} \tag{3.4}$$

where I_{corr}^* and I_{corr} represent the corrosion current densities of bare and coated MS. As compared to bare MS, I_{corr} value of CS-g-SA coated MS decreased by one order of magnitude.
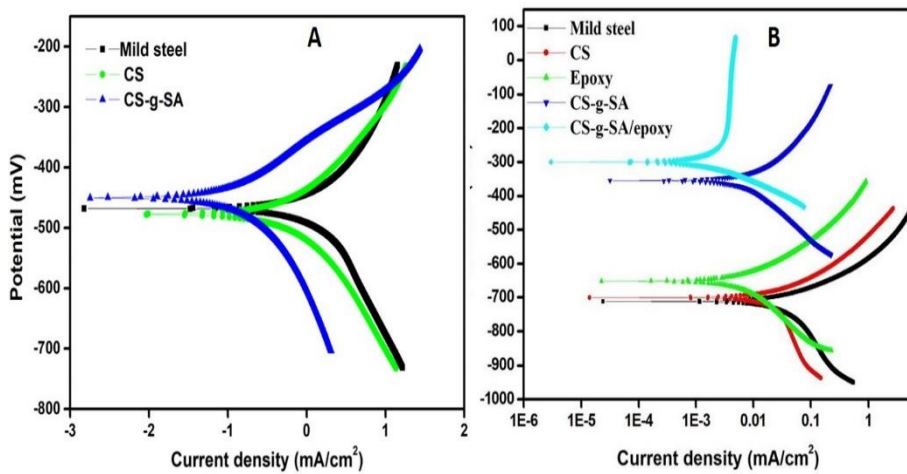
Figure 3.12. PDP plot of bare and coated MS in A)0.5M HCl and B)3.5% NaCl at room temperature.

The R_p (polarization resistance) were calculated from the Tafel extrapolation method by applying the Stern-Geary equation[25]

$$R_p = \frac{\beta_a \beta_c}{2.303(\beta_a + \beta_c)I_{corr}} \tag{3.5}$$

The lower R_p values for bare MS in 0.5M HCl and 3.5% NaCl were obtained due to the diffusion of electrolyte into the active site which

follows corrosion to MS. The lower R_p (59.85 Ω cm^2 in 0.5M HCl and 1.7 KΩ cm^2 in 3.5% NaCl) value for pure CS based coatings attributed due to the porous nature of CS which permits the corrosives to penetrate easily to the MS surface. The grafted CS film has increased R_p value, 415.8 Ω cm^2 in the acidic medium and 15 KΩ cm^2 in the saline medium indicated better surface protection.

Figure 3.13 displays the PDP plot of CS-g-SA coated MS after different immersion time in the acidic and saline medium. With an increase in immersion time, the E_{corr} value of coated MS in the saline medium is negatively shifted and an increase in I_{corr} value is observed due to the diffusion of electrolyte to the metal and its I_{corr} value (6µA/cm^2 in 3.5% NaCl and 234.3 µA/cm^2 in 0.5M HCl) is still lower than that of bare MS (31.66µA/cm^2 in 3.5% NaCl and 1290 µA/cm^2 in 0.5M HCl) after 20 days of immersion (Table 3.6).
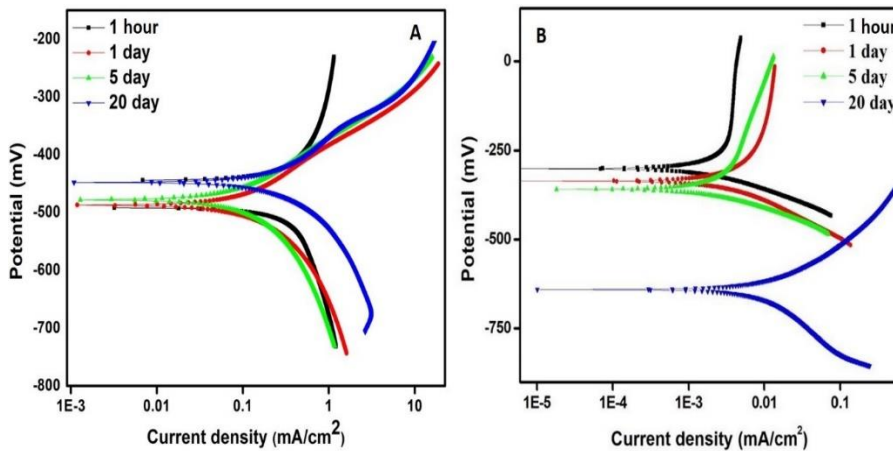
Figure 3.13. PDP plot of CS-g-SA coated MS after different immersion time in A)0.5M HCl and B) 3.5% NaCl at room temperature.

The porosity of the different coating on MS was also determined from the PDP measurements by the following relationship

$$P = \frac{R_p{}^*}{R_p} \times 10^{-(\Delta E_{corr}/\beta_a)} \tag{3.6}$$

where p is the total porosity of coating, $R_p{}^*$ and R_p are the polarization resistance of the bare and coated MS, ΔE_{corr} is the corrosion potential difference between bare and coated MS and β_a is the anodic Tafel slope [26, 27]. The porosity of CS-g-SA was found to be 0.008% when the grafted film is blended with epoxy resin and the percentage porosity decreased to 4.74×10^{-5} % imparting high polarization resistance and protection ability. With an increase in dipping time, due to the increase in percentage porosity the electrolyte diffused into the MS substrate through the pin holes on the coating.

Table 3.5. PDP parameters in 0.5M HCl and 3.5% NaCl for bare and coated MS at room temperature

Sample name	Electrolyte	$-E_{corr}$ (mV)	I_{corr} (mA/cm^2)	β_a (mV/dec)	$-\beta_c$ (mV/dec)	R_p (kΩ cm^2)	Corrosion rate(mpy)	Porosity (%)	Protection Efficiency(η)
MS	0.5M HCl	462.5	1.290	151.1	165.4	0.0265	25.95	-	-
CS	0.5M HCl	469.8	0.4588	136.1	118.1	0.0598	13.73	39.23	64.43
CS-g-SA	0.5M HCl	478.3	0.0744	144.9	140.1	0.4158	5.110	4.96	94.23
MS	3.5% NaCl	699.7	0.0316	78.22	221.3	0.7940	2.718	-	-
CS	3.5% NaCl	697.7	0.0118	70.00	138.7	1.712	1.370	43.73	62.65
CS-g-SA	3.5% NaCl	354.7	0.0062	102.4	144.9	4.204	0.1651	8.24×10^{-3}	80.37
Epoxy resin	3.5% NaCl	626.0	0.0080	104.2	201.4	3.728	0.5529	4.17	74.68
CS-g-SA/epoxy	3.5% NaCl	304.9	0.0013	202.5	66.18	15.00	0.0131	4.74×10^{-5}	95.88

Table. 3.6. PDP parameters of CS-g-SA and CS-g-SA/epoxy coated MS in the acidic and saline medium with different immersion time

Immersion time	Electrolyte	$-E_{corr}$ (mV)	I_{corr} (mA/cm^2)	β_a (mV/dec)	$-\beta_c$ (mV/dec)	R_p (kΩ cm^2)	Corrosion rate(mpy)	Porosity (%)
1 hour	0.5M HCl	478.3	0.0744	144.9	140.1	0.4158	5.110	4.96
1 day	0.5M HCl	488.4	0.0911	105.1	108.3	0.2542	7.892	5.91
5 day	0.5M HCl	477.4	0.1764	116.2	183.1	0.1749	9.755	11.27
20 day	0.5M HCl	446.7	0.2343	114.8	123.8	0.1103	13.63	32.98
1 hour	3.5% NaCl	304.9	0.0013	202.5	66.18	15.00	0.0131	4.74×10^{-5}
1 day	3.5% NaCl	337.1	0.0016	123.9	70.90	12.19	0.0138	7.71×10^{-3}
5 day	3.5% NaCl	369.3	0.0018	154.3	62.15	10.69	0.0216	5.36×10^{-2}
20 day	3.5% NaCl	639.8	0.0060	82.73	145.2	3.814	0.0705	3.93

3.2.9. Surface morphology.

FESEM images of bare and coated MS are given in Figure 3.14. Surface of bare MS sample gets highly deteriorated with deep pits and cracks under exposure to the saline and acidic medium for 20 days. CS made a uniform surface layer and SA grafting offered an efficient surface network. The lateral interaction between alkyl groups on SA changes the uniform surface morphology to a network structure which may be due to surface roughness correlated with hydrophobicity[19, 24]. This indicates that upon grafting with SA, the compactness of CS polymer and durability performance of CS-g-SA coating are enhanced[28]. After 20 days of immersion in 0.5M HCl, the network like morphology of CS-g-SA coating sustained with minor network breakages suffered from the decrease in lateral interaction between the alkyl chains but devoid of deep pits and cracks. The CS-g-SA/epoxy coated MS exhibited a uniform protective surface layer, which remains almost as such after 20 days of immersion in 3.5% NaCl.

The stereomicroscopic images (Figure 3.15) also support the effective formation of a protective coating on the MS substrate. Uniform coating devoid of material damage can be observed in the optical images of CS-g-SA and CS-g-SA/epoxy coated MS after 20 days of exposure to 0.5M HCl and 3.5%NaCl. For the bare steel samples after 20 days of immersion, the corrosion destruction is clear.
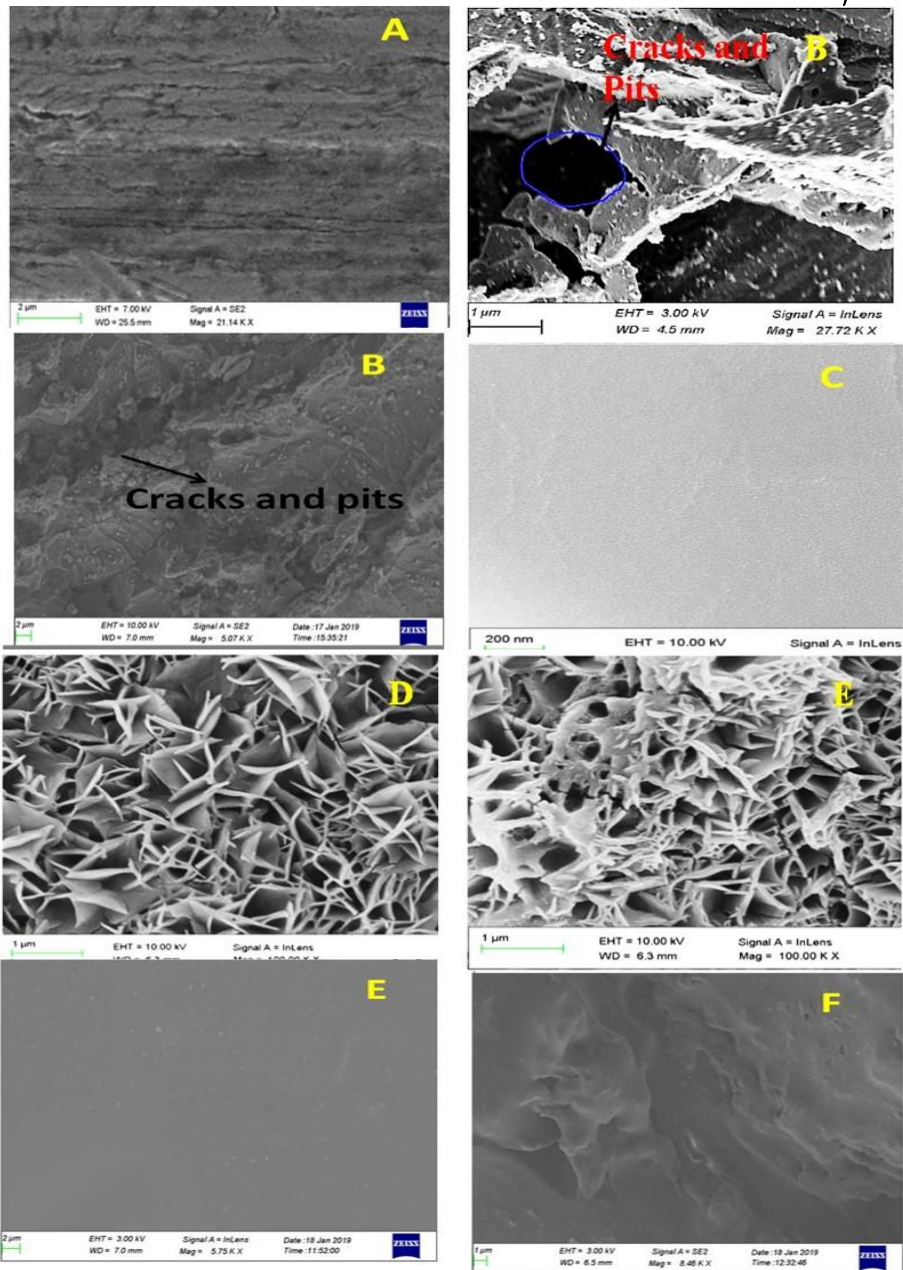
Figure 3.14. FESEM images of A) bare MS, B) and C) MS after 20 days of immersion in 0.5M HCl and 3.5% NaCl, D) CS coated MS, E) CS-g-SA coated MS, F) CS-g-SA coated MS after 20 days of immersion in 0.5M HCl, G) CS-g-SA/epoxy coated MS, and H) CS-g-SA coated MS after 20 days of immersion in 3.5% NaCl.

90
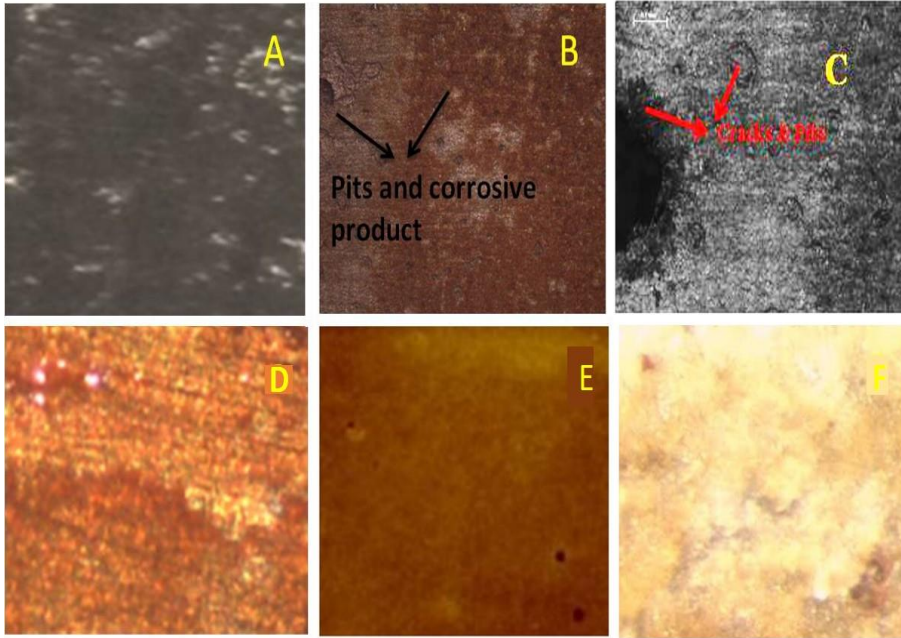
Figure 3.15. Optical images of A) MS, B) and C) MS after 20 days of immersion in 3.5 % NaCl and 0.5M HCl, D) CS-g-SA coated MS, E) CS-g-SA/epoxy coated MS, and F) Cs-g-SA/epoxy coated MS after 20 days of immersion in 3.5% NaCl.

Figure 3.16 illustrated the 2D and 3D AFM images of CS and CS-g-SA coated MS. The topography of CS-g-SA coated MS had changed compared to CS, which was consistent with the FESEM images. Even though CS can form uniform film coating on MS, various pores are observed in the 2D images. Such a porous film coating was not present in the CS-g-SA coated MS. From the topography observation, the average surface roughness of CS-g-SA coated MS get increased compared to CS coated MS. This is correlated with the enhanced hydrophobicity of the grafted film[29].
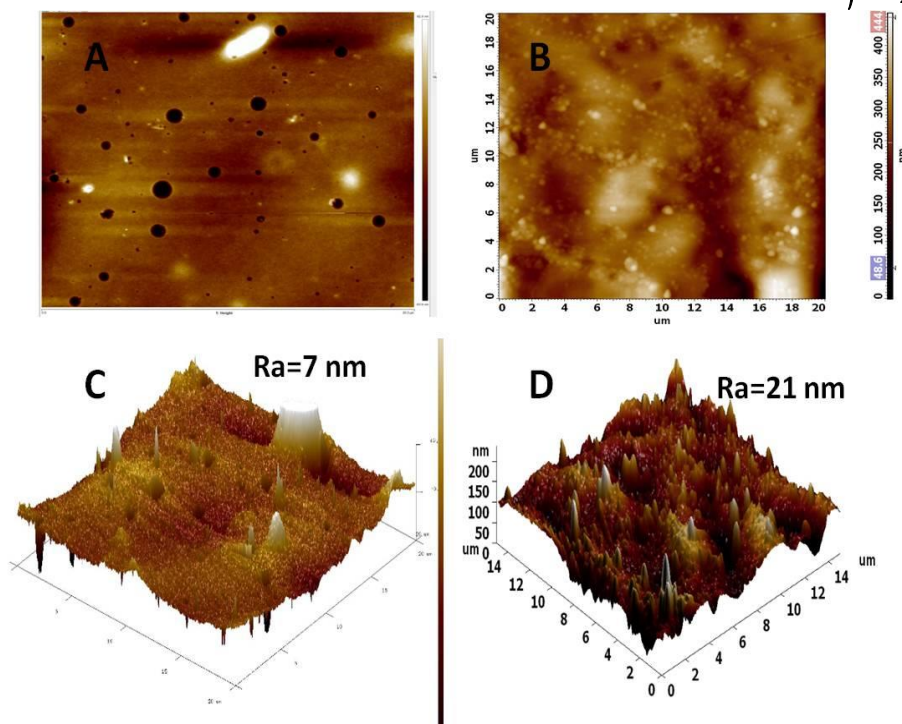
Figure 3.16. 2D and 3D AFM images of CS and CS-g-SA coated MS

3.3. Conclusions

Stearic acid grafted chitosan film has been successfully synthesized by an EDC mediated coupling reaction. FTIR, NMR, TGA, and elemental analysis confirmed the effective grafting of SA onto CS. The interaction between chitosan and stearic acid was experimentally evident and theoretically proven. Grafted chitosan film contains chemical constituents capable of forming passivation layers that prevent the passage of corrosive ions across the metal-solution interface. The corrosion protection efficiency of the bare chitosan system was limited due to the porous nature and wettability whereas CS-g-SA offers enhanced protection efficiency in 0.5M HCl and 3.5% NaCl. This

enhanced protection efficiency of the grafted system is attributed to the improved hydrophobic nature and barrier property. From weight loss data, the corrosion rate of CS-g-SA coated steel samples is very low compared to bare mild steel. EIS and PDP studies revealed that CS-g-SA film offered remarkable corrosion protection for MS in the acidic and saline medium over unmodified CS film. Surface morphological studies also revealed an effective formation of the coating on MS after exposure to the acidic and saline medium.

References

[1] C.d.T. Neto, J. Giacometti, A. Job, F. Ferreira, J. Fonseca, M. Pereira, Thermal analysis of chitosan based networks, Carbohydrate Polymers, 62 (2005) 97-103.

[2] E.A. El-Hefian, M.M. Nasef, A.H. Yahaya, Preparation and characterization of chitosan/poly (vinyl alcohol) blended films: mechanical, thermal and surface investigations, Journal of Chemistry, 8 (2011) 91-96.

[3] E.M. Fayyad, K.K. Sadasivuni, D. Ponnamma, M.A.A. Al-Maadeed, Oleic acid-grafted chitosan/graphene oxide composite coating for corrosion protection of carbon steel, Carbohydrate polymers, 151 (2016) 871-878.

[4] W. Zhang, Y. Chen, M. Chen, S. Zhao, J. Mao, A. Qu, W. Li, Y. Zhao, N. Huang, G. Wan, Strengthened corrosion control of poly (lactic acid)(PLA) and poly (ε-caprolactone)(PCL) polymer-coated magnesium by imbedded hydrophobic stearic acid (SA) thin layer, Corrosion Science, 112 (2016) 327-337.

[5] S.C. Angadi, L.S. Manjeshwar, T.M. Aminabhavi, Stearic acid-coated chitosan-based interpenetrating polymer network microspheres: controlled release characteristics, Industrial & Engineering Chemistry Research, 50 (2011) 4504-4514.

[6] G. Ruhi, O. Modi, S. Dhawan, Chitosan-polypyrrole-SiO2 composite coatings with advanced anticorrosive properties, Synthetic Metals, 200 (2015) 24-39.

[7] F.-Q. Hu, G.-F. Ren, H. Yuan, Y.-Z. Du, S. Zeng, Shell cross-linked stearic acid grafted chitosan oligosaccharide self-aggregated micelles for controlled release of paclitaxel, Colloids and Surfaces B: Biointerfaces, 50 (2006) 97-103.

[8] Y.-T. Xie, Y.-Z. Du, H. Yuan, F.-Q. Hu, Brain-targeting study of stearic acid–grafted chitosan micelle drug-delivery system, International journal of nanomedicine, 7 (2012) 3235.

[9] F.-Q. Hu, L.-N. Liu, Y.-Z. Du, H. Yuan, Synthesis and antitumor activity of doxorubicin conjugated stearic acid-g-chitosan oligosaccharide polymeric micelles, Biomaterials, 30 (2009) 6955-6963.

[10] R.K. Singh, A. Kukrety, A.K. Chatterjee, G.D. Thakre, G.M. Bahuguna, S. Saran, D.K. Adhikari, N. Atray, Use of an acylated chitosan schiff base as an ecofriendly multifunctional biolubricant additive, Industrial & Engineering Chemistry Research, 53 (2014) 18370-18379.

[11] X. Liu, W. Xia, Q. Jiang, Y. Xu, P. Yu, Synthesis, characterization, and antimicrobial activity of kojic acid grafted chitosan oligosaccharide, Journal of agricultural and food chemistry, 62 (2013) 297-303.

[12] A. Niemczyk, A. Kmieciak, M. El Fray, A. Piegat, THE INFLUENCE OF C18-FATTY ACIDS ON CHEMICAL STRUCTURE OF CHITOSAN

DERIVATIVES AND THEIR THERMAL PROPERTIES, Progress on Chemistry and Application of Chitin and its Derivatives, 21 (2016) 165-175.

[13] H. Parra-Barraza, M.G. Burboa, M. Sánchez-Vázquez, J. Juárez, F.M. Goycoolea, M.A. Valdez, Chitosan− Cholesterol and Chitosan− Stearic Acid Interactions at the Air− Water Interface, Biomacromolecules, 6 (2005) 2416-2426.

[14] S. Elsaeed, H. El Sayed, H. Ashour, E. Zaki, E. Khamis, H. El Nagy, Corrosion and hydrogen evolution rate control for X-65 carbon steel based on chitosan polymeric ionic liquids: experimental and quantum chemical studies, RSC Advances, 8 (2018) 37891-37904.

[15] K. Fink, S. Höhne, S. Spange, F. Simon, Hydrophobically functionalized chitosan particles, Journal of adhesion science and technology, 23 (2009) 297-315.

[16] V.K. Rajan, C. Hasna, K. Muraleedharan, The natural food colorant Peonidin from cranberries as a potential radical scavenger–A DFT based mechanistic analysis, Food chemistry, 262 (2018) 184-190.

[17] L. Xiong, J. Liu, M. Yu, S. Li, Improving the corrosion protection properties of PVB coating by using salicylaldehyde@ ZIF-8/graphene oxide two-dimensional nanocomposites, Corrosion Science, 146 (2019) 70-79.

[18] B. Rikhari, S.P. Mani, N. Rajendran, Electrochemical behavior of polypyrrole/chitosan composite coating on Ti metal for biomedical applications, Carbohydrate polymers, 189 (2018) 126-137.

[19] D. Zhang, L. Wang, H. Qian, X. Li, Superhydrophobic surfaces for corrosion protection: a review of recent progresses and future directions, Journal of Coatings Technology and Research, 13 (2016) 11-29.

[20] G. Boisier, A. Lamure, N. Pébère, N. Portail, M. Villatte, Corrosion protection of AA2024 sealed anodic layers using the hydrophobic properties of carboxylic acids, Surface and Coatings Technology, 203 (2009) 3420-3426.

[21] T. Ishizaki, Y. Masuda, M. Sakamoto, Corrosion resistance and durability of superhydrophobic surface formed on magnesium alloy coated with nanostructured cerium oxide film and fluoroalkylsilane molecules in corrosive NaCl aqueous solution, Langmuir, 27 (2011) 4780-4788.

[22] R.B. Vignesh, J. Balaji, M. Sethuraman, Surface modification, characterization and corrosion protection of 1, 3-diphenylthiourea doped sol-gel coating on aluminium, Progress in Organic Coatings, 111 (2017) 112-123.

[23] J. Carneiro, J. Tedim, S.C. Fernandes, C. Freire, A. Gandini, M. Ferreira, M. Zheludkevich, Functionalized chitosan-based coatings for active corrosion protection, Surface and Coatings Technology, 226 (2013) 51-59.

[24] S. KO, A.R. Prasad, J. Garvasis, S.M. Basheer, A. Joseph, Stearic acid grafted chitosan/epoxy blend surface coating for prolonged protection of mild steel

in saline environment, Journal of Adhesion Science and Technology, 33 (2019) 2250-2264.

[25] G. Badea, A. Caraban, M. Sebesan, S. Dzitac, P. Cret, A. Setel, Polarisation measurements used for corrosion rates determination, Journal of sustenable energy, 1 (2010) 1.

[26] B. Matthes, E. Broszeit, J. Aromaa, H. Ronkainen, S.-P. Hannula, A. Leyland, A. Matthews, Corrosion performance of some titanium-based hard coatings, Surface and Coatings Technology, 49 (1991) 489-495.

[27] W.-S. Jeon, J.-G. Kim, Y.-J. Kim, J.-G. Han, Electrochemical properties of TiN coatings on 316L stainless steel separator for polymer electrolyte membrane fuel cell, Thin Solid Films, 516 (2008) 3669-3672.

[28] G.H. Hamedi, A. Sahraei, M.R. Esmaeeli, Investigate the effect of using polymeric anti-stripping additives on moisture damage of hot mix asphalt, European Journal of Environmental and Civil Engineering, (2018) 1-14.

[29] J.-H. Zhi, L.-Z. Zhang, Y. Yan, J. Zhu, Mechanical durability of superhydrophobic surfaces: The role of surface modification technologies, Applied Surface Science, 392 (2017) 286-296.

Check for updates

Stearic acid grafted chitosan/epoxy blend surface coating for prolonged protection of mild steel in saline environment

Shamsheera K O, Anupama R Prasad, Julia Garvasis, Sabeel M Basheer and Abraham Joseph

Department of Chemistry, University of Calicut, Calicut, India

ABSTRACT

Chitosan (CS) is a promising candidate for green anticorrosive coating owing to its film forming nature, complexation with metals, biocompatibility, and varied surface functionalization. This paper illustrates the surface properties of chitosan film which is modified by grafting with stearic acid via a water-soluble coupling agent, 1-ethyl-3-(3-dimethylaminopropyl) carbodiimide (EDC). The interaction between chitosan and stearic acid were investigated theoretically by Gaussian 09 package. The purified co polymeric films so formed were characterized by FTIR-ATR, NMR, XRD, TGA, CHNSO, SEM, AFM and EDX techniques. Stearic acid grafted CS film was developed on mild steel surface via dip coating technique and investigated for its corrosion resistance in 3.5% NaCl via electrochemical techniques. EIS measurements and potentiodynamic polarization studies have proven that the grafted CS when blended with epoxy resin offers better corrosion protection to mild steel in saline environment. The coating offers prolonged protection for the metal surface with enhanced barrier properties and hydrophobic nature.

1. Introduction

Corrosion is a continuous material deterioration due to chemical or electrochemical reaction between the constituent phases resulting in enormous economic losses, especially in the aerospace, automotive, and petroleum industries. The destructive phenomenon is prevalent in industries, costs heavily on governments and individuals [1]. Among the strategies of corrosion protection, the chromate conversion coating is quite popular. Even though these coatings are adequate, they are proved to be environmentally unfriendly [2,3]. In the past two decades, researchers are striving for the development of non-chromate, environmentally more benign coatings for surface pretreatment. Because of the excellent mechanical strength and low cost, mild steel has

---

Data Article

Development of self-assembled monolayer of stearic acid grafted chitosan on mild steel and inhibition of corrosion in hydrochloric acid

Shamsheera KO, Anupama R. Prasad, Jaseela PK, Abraham Joseph*

Department of Chemistry, University of Calicut, Calicut University P O, Kerala, India

ARTICLE INFO

ABSTRACT

Chitosan (CS) based systems are extensively used as a green alternative for corrosion protection of mild steel (MS) possessing good film-forming properties, chelation with metal and nontoxic nature. In this study, a self-assembled monolayer of stearic acid grafted chitosan was developed via 1-ethyl-3-(3-dimethylaminopropyl) carbodiimide mediated coupling reaction and casted on the MS surface. From the fluorescence intensity of the fluorescent probe pyrene, the critical micelle concentration (66 μg/mL) of self-aggregates in aqueous solution was determined. The purified chitosan grafted films were characterized by apposite analytical techniques. The film developed was employed for corrosion protection of MS in 0.5 and 1 N HCl via electrochemical and non-electrochemical techniques. The results showed that stearic acid grafted chitosan (CSA) films do offer better corrosion protection to MS than bare CS film.

© 2020 Elsevier B.V. All rights reserved.

Specification table

Subject area	Corrosion science
Compounds	Chitosan and Stearic acid grafted Chitosan
Data Category	Spectral, Synthesised, Weight loss, Electrochemical Impedance Spectroscopy, Potentiodynamic Polarization, FESEM, EDAX
Data acquisition format	ATR, NMR, Weight loss, Electrochemical Impedance Spectroscopy, Potentiodynamic Polarization, Scanning Electron microscopy
Data type	Raw data, analyzed
Procedure	Chitosan is grafted with stearic acid and coated on mild steel via dip-coating and corrosion evaluation was carried out using non- electrochemical and electrochemical methods.
Data accessibility	Data is with this article

1. Rationale

All-natural processes tend towards the lowest possible energy state by a spontaneous reaction. Corrosion is a perpetual deterioration of metal or material owing to its reaction with different aggressive environments causing massive economic loss, primarily in the petroleum industries, and in aerospace. Corrosion research aims to discover strategies for prevent-

---

* Corresponding author
  E-mail address: abrahamjoseph@uoc.ac.in (A. Joseph).

Extended protection of mild steel in saline and acidic environment using stearic acid grafted chitosan preloaded with mesoporous hydrophobic silica

Chapter 4
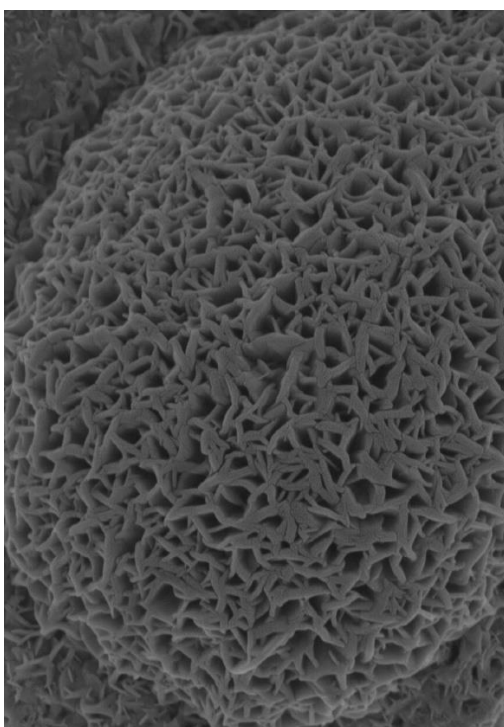
This chapter encompasses the development and corrosion protection performance of stearic acid grafted chitosan preloaded with mesoporous-hydrophobic silica. Corrosion protection studies was evaluated by non-electrochemical and electro-chemical techniques. Corrosion studies after different immersion times in acidic and saline media were carried out. Scotch tape adhesion test was also performed to ensure the effective formation of coating on the mild steel surface. Morphological studies were carried to ensure the presence of coating after exposure to corrosive media.

CONTENTS

4.1. Introduction

The incorporation of metal oxide nanoparticles can enhance the durability of the polymer coatings and provide extra protection by forming a dense barrier against the diffusion of aggressive ions [1-3]. Ruhi et al incorporated chitosan-polypyrrol-SiO_2 composite into the epoxy coating and coated on MS and the composite offered a protection efficiency of about 97% after 60 days of immersion[4]. Fayyad et al used graphene oxide as nanofiller into the Chitosan oleate matrix and offered effective protection of carbon steel in 3.5 % NaCl solution [5]. Because of the surface hydroxyl groups of SiO_2 in the form of isolated, geminal, and vicinal silanol it is unfit as a filler in the chitosan matrix. Therefore, to enhance the compatibility between the chitosan matrix and silica material, the hydrophilic surface of silica needs to be modified to hydrophobic[6-8]. Herein we silylated SiO_2 surface via HMDS, as it can scavenge the –OH group by inert methyl siloxy group[9, 10]. This work focusses on the influence of different loadings of hydrophobic silica nanoparticles in to chitosan polymer matrix and SA grafted chitosan for extended corrosion protection of mild steel in acidic and saline environment.

4.2. Result and Discussion

4.2.1. Surface characterization of Si and SiH

The N_2 adsorption−desorption isotherms for Si and SiH are displayed in Figure 4.1. The N_2 adsorption/desorption isotherms correspond to isotherms of type IV and exhibit clear hysteresis loops in the high relative pressure region, suggesting the mesoporous structure of Si and SiH[6, 11]. The Si has a total surface area of 601.37 m^2g^{-1}, a total pore volume of 0.4363 cm^3g^{-1}, and a mean pore diameter of 2.9023nm indicating its mesoporous nature. Iin SiH as the surface silanol group is

replaced by methyl siloxy group, the defect sites in the pore wall of as synthesized Si may be occupied by methyl siloxy group and decreased the adsorption site for nitrogen molecule providing a decrease in the surface area into 358.55 m^2g^{-1}, total pore volume to 0.2029 cm^3g^{-1}, and mean pore diameter into 2.2634nm[12-15].
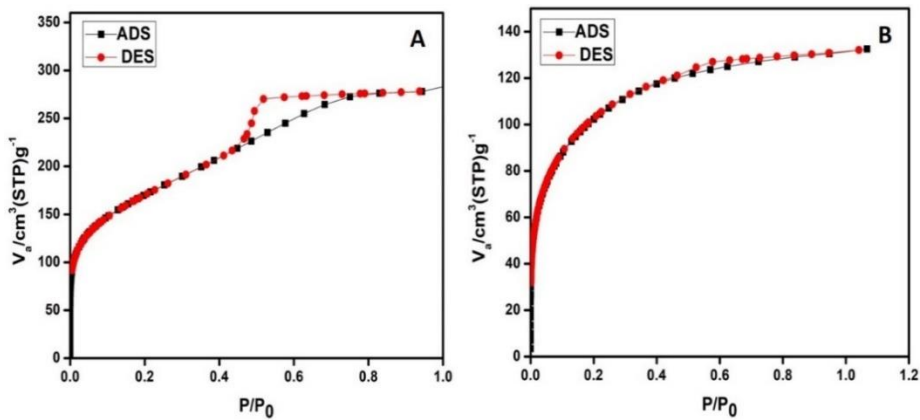
Figure 4.1. N_2 adsorption-desorption isotherm of A) Si, and B) SiH

The TEM micrograph also showed that the surface textures of Si and SiH particles have a porous structure (Figure 4.2). The pore size determined using Imagej software was almost consistent with the BET analysis. FESEM (Figure 4.3) images assembled with EDX were taken to study the morphology and composition of silica particles. The SEM micrograph of silica exhibited a relatively uniform particle. The hydrogen bond formation via surface -OH group in silica particle has probably made some aggregates as observed [16]. From EDS elemental analysis, it was observed that only Si and O were identified in the EDS profile of Si. The results indicate silica particle was free from foreign impurities. in surface-modified silica, in addition to Si and O, C was existing. The presence of carbon indicated that the silica surface is

effectively modified with HMDS. Water contact angle (WCA) measurements of silica particles revealed that the hydrophilic Si has been modified into hydrophobic SiH particle (Figure 4.4) [7, 17]
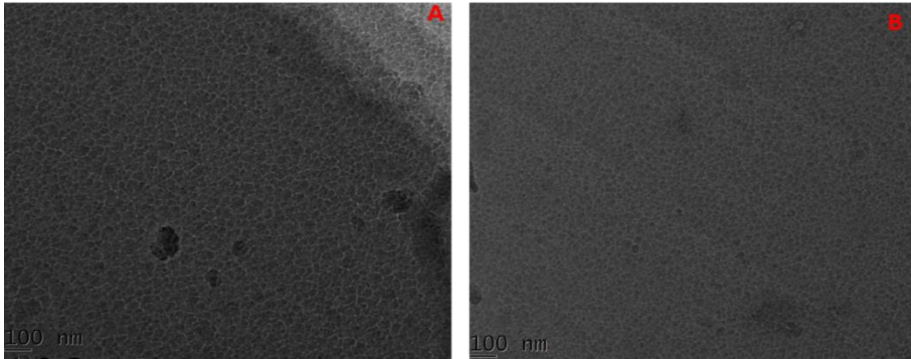
Figure 4.2. TEM micrographs of A) Si and B) SiH
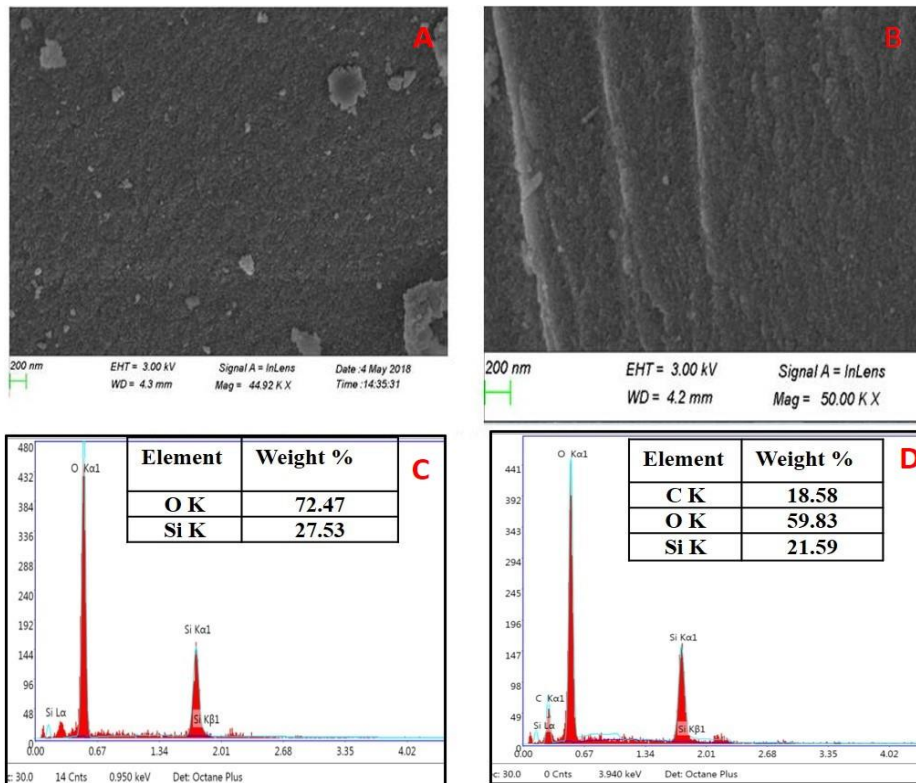
Figure 4.3. A) and B) FESEM image of Si and SiH, C) and D) EDX spectrum of Si and SiH.
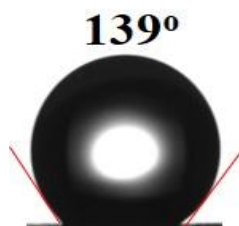
Figure 4.4. Water contact angle of SiH

4.2.2. FTIR spectrum

Figure 4.5 displays the FTIR spectra of Si and SiH powder, CS and CSiHS film. The silica particle shows a band at 3468 cm^{-1} which represents the stretching of the free O-H group. The band at 1080 cm^{-1} and 801 cm^{-1} corresponds to the asymmetric and symmetric stretching vibrations of Si-O-Si. The Si-O stretching in silanol groups shows a band at 948cm^{-1}. The band at 1646 cm^{-1} corresponds to the stretching of water molecules surrounding the silica particle. In surface-modified silica nanoparticles, as the –OH group is replaced with CH$_3$, the intensity of O-H stretching frequency is reduced compared to as-synthesized Si. The band at 2979 cm^{-1} and 2899 cm^{-1} in surface-modified silica indicated the stretching of the CH$_3$ group and which confirmed that the superficial –OH group is replaced with methyl siloxy group.[16, 18, 19]. All the characteristic peaks of chitosan were observed in the FTIR spectra of CS [20]. After filler (SiH) loading into CS matrix and further grafting with SA, the intensity of C-H stretching frequency gets increased. A distinct band at 1639 cm^{-1} which is attributed to the carbonyl region correlated to the chemical binding of filler loaded CS matrix and SA. The increase of the C-H absorption at 2924 cm^{-1}

indicates the existence of SA and the grafting of SA on CS film resulting

good dispersion of surface-modified silica into the matrix [9]
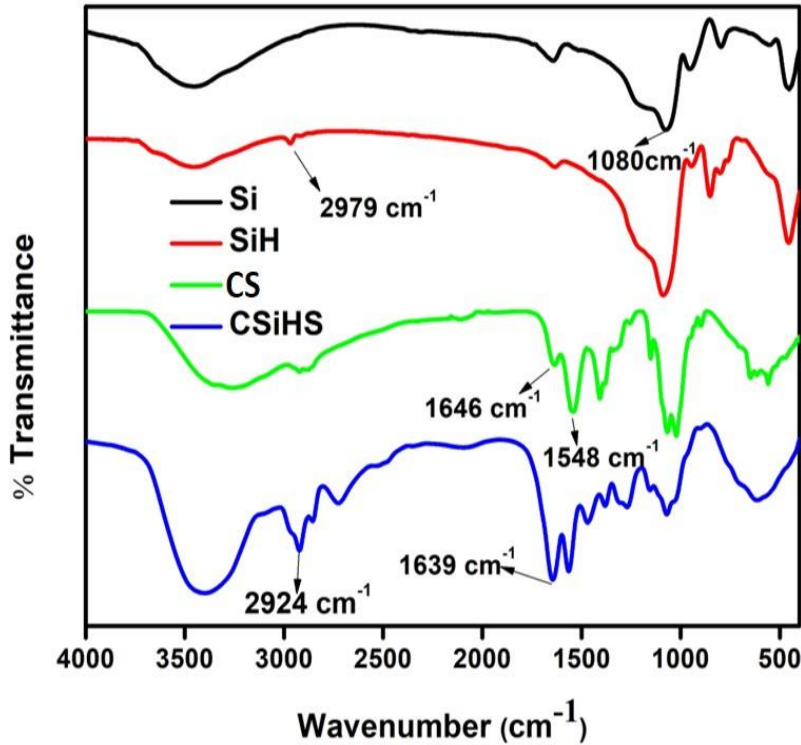
Figure 4.5. FTIR spectra of Si, SiH, CS, and CSiHS

4.2.3. Thermogravimetric analysis

TGA has been used to estimate the thermal behaviour of materials and to demonstrate the mechanism by which a material loses its weight as a result of controlled heating[21]. The thermograms (Figure 4.6) were recorded from 30-600°C with a heating rate of 10°C/minute. According to the TGA of as-synthesized silica (Si), there is a steady decline in the mass of silica within the temperature range of 55°C and 120°C. The

initial water loss is smaller in surface-modified silica compared to as-synthesized silica, which is due to the replacement of the superficial -OH group by hydrophobic methyl siloxy group $(CH_3)_3Si-O-)$[22]. Hence the superficial adsorbed water molecules are less. In the thermogram of CS and CSiHS, a two-stage decomposition could be observed. In CS the second stage weight loss was attributed to the thermal and oxidative decomposition of polysaccharide backbone. In CSiHS the second weight loss starts at 165°C, which refers to a complex process including decomposition of the stearate group of the grafted chitosan polymer, dehydration from saccharide ring, decomposition of the acetylated and deacetylated units of the chitosan matrix, etc[23-25].
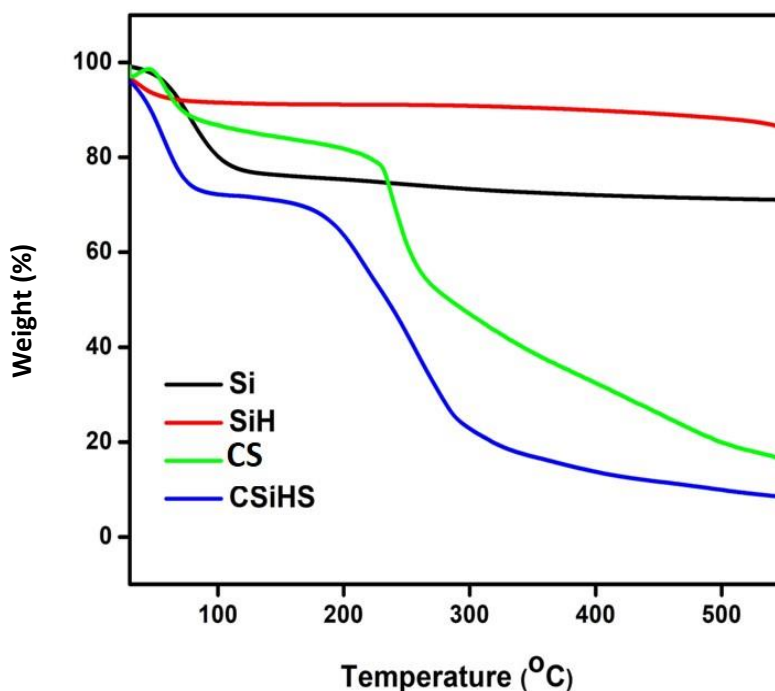
Figure 4.6. TGA of Si, SiH, C, and CSiHS

4.2.4. Corrosion protection studies

4.2.4.1. Weight loss measurements

The MS coupons of bare and CSiHS coated MS were immersed in 0.5M HCl and 3.5% NaCl solution maintained at room temperature for 20 days without stirring. After testing, the corrosion products were discarded from the sample surface, dried in the air, and weighed every 5 days. The weight loss and corrosion rate of the CSiHS coated MS coupons calculated using equation 3.1 and 3.2 are very low related to the bare samples as exhibited in Figure 4.7 and Table 4.1. After 20 days of immersion, the protection efficiency is 90.89% in 0.5M HCl and 93.77% in 3.5% NaCl for the CSiHS coated MS coupons.
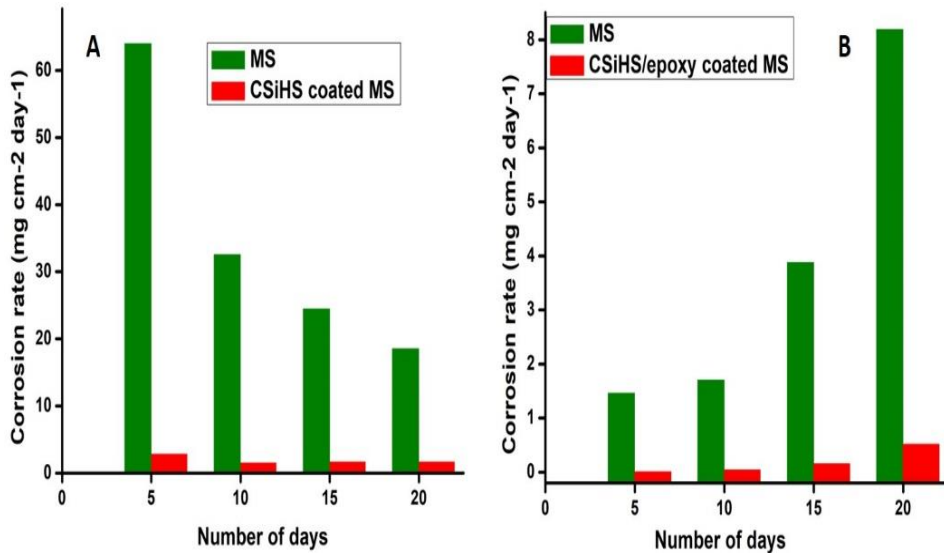
Figure 4.7. Variation of corrosion rate with the number of days for bare and CSiHS coated MS in A) 0.5M HCl and B) 3.5% NaCl at room temperature

Table 4.1. Weight loss data for bare and CSiHS coated MS in 0.5M HCl and 3.5% NaCl at room temperature

No. of days	Electrolyte	Weight loss (g)		Corrosion rate $(mg\ cm^{-2}\ day^{-1})$		Protection efficiency (η)
		Bare MS	CSiHS coated MS	Bare MS	CSiHS coated MS	
5	0.5M HCl	1.153	5.2×10^{-2}	64.05	2.873	95.52
10	0.5M HCl	1.173	5.5×10^{-2}	32.58	1.538	95.27
15	0.5M HCl	1.323	9.0×10^{-2}	24.50	1.674	93.17
20	0.5M HCl	1.339	1.2×10^{-1}	18.59	1.696	90.89
5	3.5% NaCl	2.6×10^{-2}	4.5×10^{-5}	1.466	2.5×10^{-3}	99.82
10	3.5% NaCl	6.2×10^{-2}	1.3×10^{-3}	1.708	3.6×10^{-2}	97.90
15	3.5% NaCl	2.1×10^{-1}	8.2×10^{-3}	3.885	0.1518	96.09
20	3.5% NaCl	5.9×10^{-1}	3.7×10^{-2}	8.191	0.5097	93.77

4.2.4.2. EIS measurements

EIS is a safe technique, which gives information about the mechanism of corrosion inhibition performance. Impedance measurements were carried out by immersing the bare and coated steel specimens in 0.5M HCl and 3.5% NaCl solution at OCP conditions for 1 hour at room temperature. EIS (Figure 4.8) plots were drawn for bare and coated MS in the acidic and saline media. The EIS data could be described with suitable electrochemical equivalent circuits. $R_s(Q_{dl}R_{ct})$ circuit was used to fit EIS data of bare MS, whereas $R_s(Q_c(R_c(Q_{dl}R_{ct})))$ circuit gave the best fit for CS, CSi, CSiH, and CSiHS coated MS. The single semicircle in the EIS profile for bare MS surface in acidic medium indicates the occurrence of a single charge-transfer reaction in the high-frequency region. However, EIS profile of CSiHS coated MS is slightly different

with two capacitive loops. The increase in arc length of the Nyquist diagram of CSi, CSiH indicates a protective layer is formed which enhances the charge transfer resistance. Greater R_{ct} value of MS coated with CSiH (3.0 wt%) compared to CSiH (1.0 wt%) could be attributed to the better filler and CS matrix interaction which prevent the diffusion of aggressive ions from the electrolyte. When 5.0 wt% was loaded into CS matrix R_{ct} value gets decreased, which is ascribed by the filler-filler interaction rather than filler matrix interaction. Therefore, CS with 3.0 wt% SiH could be the optimum loading of modified silica to get the desired corrosion protection efficiency.

The data presented in Table 4.2 reveals that the R_c and R_{ct} values of coating increase significantly for CSiHS coated MS, which can be explained by good dispersibility of hydrophobic SiH in CS matrix and the large alkyl group of SA in coating impedes the diffusion of aggressive ions onto MS surface. Q_{dl} and Q_c values of CSiHS coating is significantly lower compared to CS, CSi, and CSiH coating on MS, which ensured that the CSiHS coating on MS could prevent the corrosion process. Using R_{ct} values, protection efficiency was calculated using equation 3.3. The CSiHS coating on MS offered an η of 97.36% in acidic medium and 96.70% in saline medium. The result indicates that a protective layer is formed at the interface of the electrolyte solution and working electrode which resist the diffusion of corrosive ions onto the MS surface.
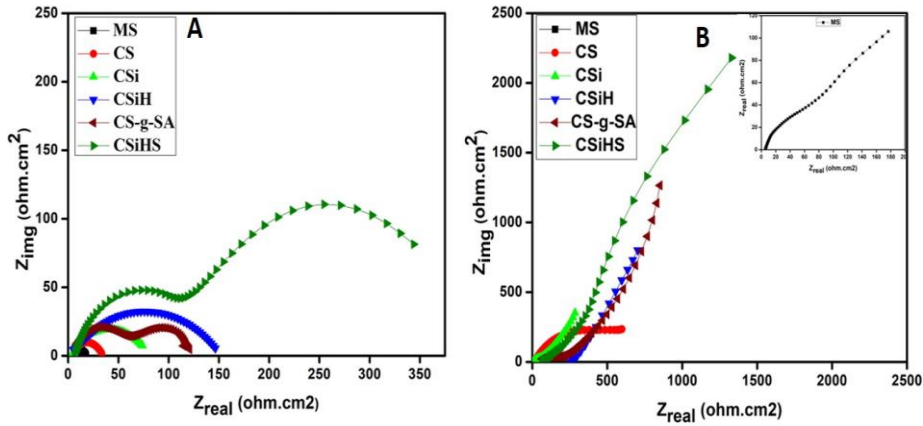
Figure 4.8. EIS plot of bare and coated MS in A) 0.5M HCl and B) 3.5% NaCl

The two-phase maxima at relatively high and low frequencies could be seen in the Bode phase angle plot (Figure 4.9) of CSiHS coating on MS. Due to the coating capacitance and charge transfer process, the Bode plots exhibits high and low-frequency regions in the graph[26]. Figure 4.10 displays the EIS plot of CSiHS coated MS after different immersion time in acidic and saline media. With extending immersion time, R_c and R_{ct} values of CSiHS coating decreases (Table 4.3), which is ascribed to electrolyte diffusion into the coating and corrosive ions reach metal coating interface; consequently, the electrochemical corrosion process takes place at metal coating interface, leading to coating delamination after 20 days of immersion. With prolonged immersion in electrolyte the Q_{dl} and Q_c values increase due to coating delamination[27].

Table 4.2. Impedance parameters for bare and coated MS in the acidic and saline media

Sample name	Electrolyte	R_s (Ωcm^2)	Q_c (F.cm^2)	n_1	R_c (Ωcm^2)	Q_{dl} (F.cm^2)	n_2	R_{ct} (Ωcm^2)	Protection Efficiency(η)
MS	0.5M HCl	7.21	-	-	-	4.876×10^{-4}	0.80	10.34	-
CS	0.5M HCl	4.93	3.391×10^{-3}	0.82	13.53	4.443×10^{-4}	0.80	29.48	64.92
CSi	0.5M HCl	1.74	1.788×10^{-3}	0.82	5.275	1.173×10^{-4}	0.87	80.42	87.14
CSiH	0.5M HCl	4.95	9.951×10^{-4}	0.80	8.792	1.149×10^{-5}	0.82	143.7	92.80
CS-g-SA	0.5M HCl	3.03	9.501×10^{-4}	0.81	58.12	1.18×10^{-5}	0.80	121.9	91.43
CSiHS	0.5M HCl	5.93	8.859×10^{-5}	0.85	132.1	1.368×10^{-6}	0.85	392.0	97.36
MS	3.5%NaCl	11.9	-	-	-	2.788×10^{-5}	0.80	185.1	-
CS	3.5%NaCl	12.3	8.092×10^{-3}	0.71	58.47	1.012×10^{-5}	0.90	328.7	43.68
CSi	3.5%NaCl	6.89	4.19×10^{-3}	0.81	64.19	4.379×10^{-6}	0.79	400.7	53.83
CSiH	3.5%NaCl	5.9	1.178×10^{-3}	0.82	220	1.023×10^{-6}	0.84	859	78.45
CS-g-SA	3.5%NaCl	11.4	1.222×10^{-4}	0.67	1175	6.934×10^{-7}	0.80	3422	94.59
CSiHS	3.5%NaCl	10.4	5.433×10^{-5}	0.78	1715	1.235×10^{-7}	0.81	5619	96.70

Figure 4.9. Bode phase angle plot of bare and coated MS in A) 0.5M HCl and B) 3.5%NaCl

Figure 4.10. EIS plot of CSiHS coated MS after different immersion time in A) 0.5M HCl and B) 3.5% NaCl

Table 4.3. Impedance parameters of CSiHS coated MS in the acidic and saline media after different immersion time

Immersion time	Electrolyte	R_s (Ωcm^2)	Q_c (F.cm^2)	n_1	R_c (Ωcm^2)	Q_{dl} (F.cm^2)	n_2	R_{ct} (Ωcm^2)
I hour	0.5M HCl	5.93	8.859×10^{-5}	0.85	132.1	1.368×10^{-6}	0.85	392.0
5 day	0.5M HCl	2.44	1.973×10^{-4}	0.80	100.3	1.773×10^{-6}	0.81	247.5
10 day	0.5M HCl	4.34	5.533×10^{-4}	0.80	59.4	1.183×10^{-5}	0.75	177.0
15 day	0.5M HCl	3.62	9.993×10^{-4}	0.80	40.02	9.621×10^{-5}	0.85	132.1
20 day	0.5M HCl	1.59	1.852×10^{-3}	0.73	25.14	1.083×10^{-4}	0.69	110.6
I hour	3.5% NaCl	10.44	5.43×10^{-5}	0.78	1715	1.235×10^{-7}	0.81	5619
5 day	3.5% NaCl	12.21	9.94×10^{-5}	0.75	1467	9.835×10^{-6}	0.67	4467
10 day	3.5% NaCl	13.54	1.698×10^{-4}	0.79	1118	6.942×10^{-6}	0.78	3894
15 day	3.5% NaCl	16.76	9.636×10^{-4}	0.71	678	2.983×10^{-6}	0.69	1537
20 day	3.5% NaCl	12.32	1.101×10^{-3}	0.79	420	1.003×10^{-6}	0.75	1089

4.2.4.3. PDP measurements

The PDP measurements for bare MS and coated MS as working electrodes in 0.5M HCl, and 3.5 wt % NaCl solutions are shown in Figure 4.11. The PDP parameters, such as I_{corr}(corrosion current density), E_{corr}(corrosion potential), R_p(polarization resistance), corrosion rate, and βa and βc (anodic and cathodic Tafel constants) in different corrosion conditions were determined from the Tafel extrapolation method of anodic and cathodic Tafel plot and are presented in Table 4.4. Interestingly, the I_{corr} for CS, CSi, CSiH, CS-g-SA, and CSiHS coatings are observed to be significantly low as compared to bare MS. When 3.0 wt % SiH is loaded into the chitosan matrix the I_{corr} value is decreased to 0.1309 mA/cm^2 in acidic medium and 1.03×10^{-2} mA/cm^2 in a saline environment. This effect may be attributed to the hydrophobic silica that could cover the pores of bare chitosan which restricts the penetration of aggressive ions to the MS substrate. When CSiH is grafted with SA, further reduction in I_{corr} value (0.0201 mA/cm^2 in 0.5M HCl and 2.4×10^{-4}in 3.5% NaCl) has been attained owing to the large alkyl group of SA which impedes the diffusion of electrolyte onto MS surface. The highest percentage protection efficiency is measured for CSiHS coating exhibiting its superior corrosion resistance property, which can isolate the MS from different corrosive ions. For bare CS coated MS, a lower polarization resistance value of (59.85 Ω cm^2) was obtained due to its porous nature in the absence of any filler. When 3.0 wt % SiH is doped into CS film, R_p value improved to 274 Ωcm^2 in acidic medium and 3.71×10^3 Ωcm^2 in saline medium, which is attributed to the hydrophobic filler interaction

with CS matrix and prevent the diffusion of corrosive ions. Further grafting CSiH with SA, R_p value increased remarkably to 1853.2 Ω cm^2 and 1.09$\times$10^5 Ω cm^2, consequently, enhanced corrosion inhibition efficiencies 98.44% in 0.5M HCl and 99.24 % in 3.5% NaCl were obtained. PDP with different immersion time in the acidic and saline environment has been exhibited in Figure 4.12 and different PDP parameters are tabulated in Table 4.5. The I_{corr} and CR of CSiHS coated MS in corrosive media for different immersion periods are found to be lower than that of the bare MS, CS, and CSi. Moreover, the η of the system remains inviolate. To ensure good barrier property, the porosity of the various coatings on MS was also determined from the PDP data. The porosity of bare CS was found to be 39.23% in HCl and 43.73% in NaCl, when 3.0 wt % SiH is doped into chitosan matrix the percentage porosity decreased to 13.38% and 5.00%, which is attributed to hydrophobic silica material fill the porous site on the CS film, and further grafting with SA porosity percentage decreased to 1.13% in acidic medium and 2.73$\times$10^{-8} % in the saline medium, imparting high polarization resistance and protection ability. The very low percentage porosity of CSiHS in the saline medium is attributed to the diffusion of chloride ions through the pinholes on the chitosan coating is again suppressed by the bisphenol-based epoxy resin. After different immersion periods, due to the increase in percentage porosity and the electrolyte get diffused to the MS substrate through the pinholes of the coating.
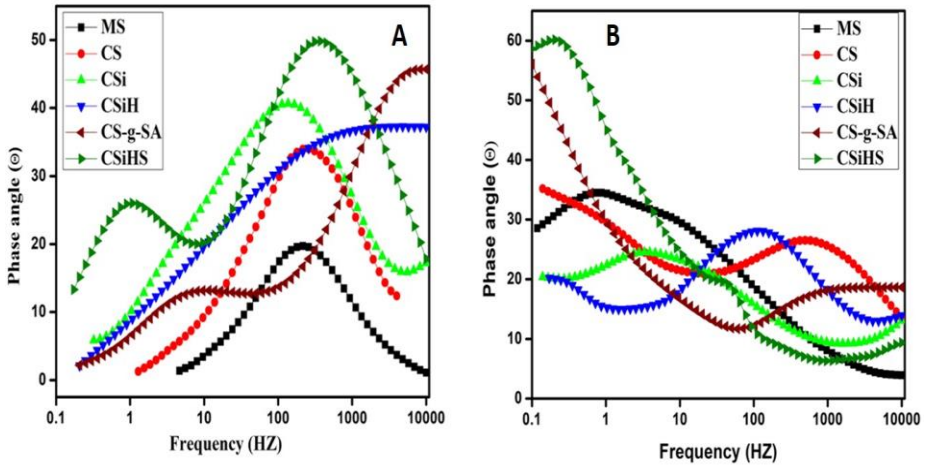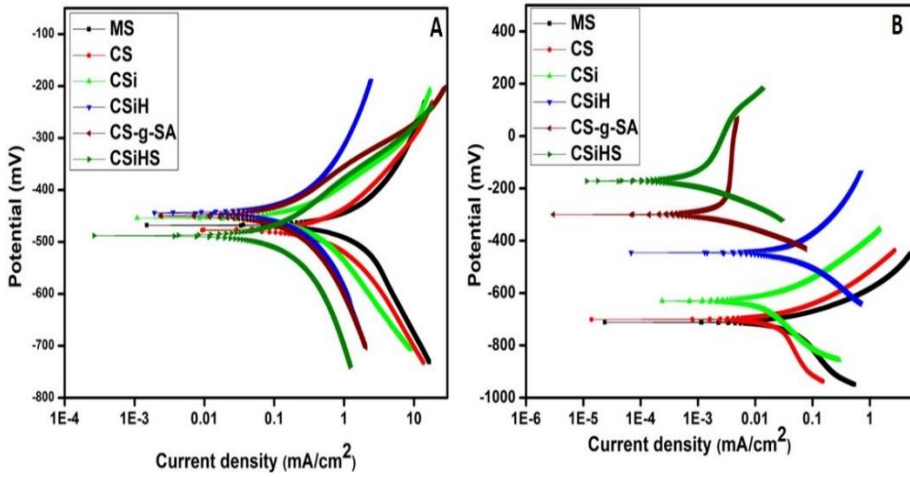
Figure 4.11. PDP plot of bare and coated MS in A)0.5M HCl and B)3.5% NaCl
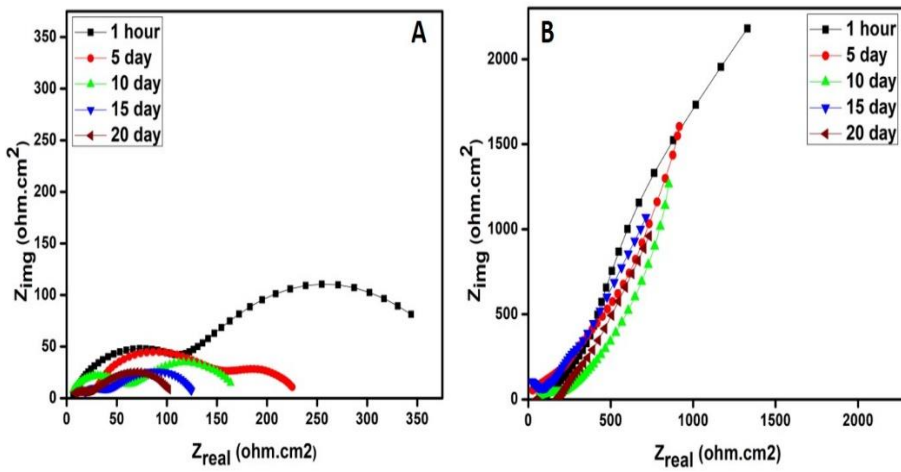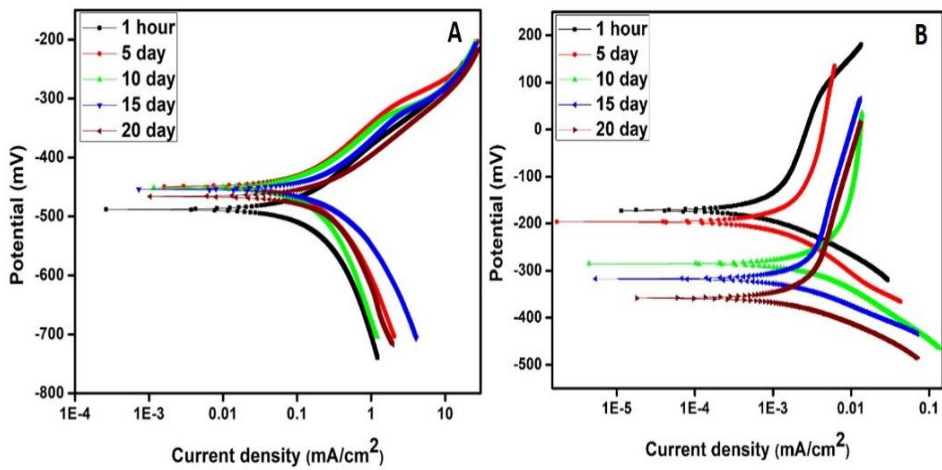

Figure 4.12. PDP plot of CSiHS coated MS after different immersion time in A) 0.5M HCl and B) 3.5% NaCl

Table 4.4. PDP parameters for bare and coated MS in the acidic and saline media

Sample name	Electrolyte	$-E_{corr}$ (mV)	I_{corr} (mA/cm^2)	β_a (mV/dec)	$-\beta_c$ (mV/dec)	R_p (kΩ cm^2)	Corrosion rate(mpy)	Porosity (%)	Protection Efficiency(η)
MS	0.5M HCl	462.5	1.290	151.1	165.4	0.0265	25.95	-	-
CS	0.5M HCl	469.8	0.4588	136.1	118.1	0.0598	13.73	39.23	64.43
CSi	0.5M HCl	454.3	0.3509	116.5	179.53	0.0874	12.75	35.68	72.80
CSiH	0.5M HCl	443.8	0.1309	131.9	221.0	0.2742	4.637	13.38	89.85
CS-g-SA	0.5M HCl	478.3	0.0744	144.9	140.1	0.4158	4.11	4.96	94.20
CSiHS	0.5M HCl	479.0	0.0201	163.4	180.6	1.853	2.213	1.13	98.44
MS	3.5% NaCl	699.7	0.0316	78.22	221.3	0.7940	2.718	-	-
CS	3.5% NaCl	697.7	0.0118	70.00	138.7	1.712	1.370	43.73	62.65
CSi	3.5% NaCl	641.2	0.0110	90.6	123.5	2.062	1.003	8.708	65.18
CSiH	3.5% NaCl	449.3	0.0103	108.2	135.4	2.535	0.8768	5.006	67.40
CS-g-SA	3.5% NaCl	304.9	0.0013	202.5	66.18	15.00	0.0131	4.74×10^{-5}	95.88
CSiHS	3.5% NaCl	173.9	0.00024	97.80	44.84	55.63	0.0033	2.73×10^{-8}	99.24

Table 4.5. PDP parameters of CSiHS coated MS in the acidic and saline media after different immersion time

Immersion time	Electrolyte	$-E_{corr}$ (mV)	I_{corr} (mA/cm^2)	β_a (mV/dec)	$-\beta_c$ (mV/dec)	R_p (kΩ cm^2)	CR (mpy)	Porosity (%)
1 hour	0.5M HCl	479.0	0.0201	163.4	180.6	1.853	2.213	1.13
5 day	0.5M HCl	450.9	0.0680	82.24	93.82	0.2798	7.659	13.13
10 day	0.5M HCl	450.42	0.0912	90.94	142.7	0.2644	9.927	13.64
15 day	0.5M HCl	458.59	0.1544	101.22	117.6	0.1529	11.41	18.97
20 day	0.5M HCl	465.45	0.2588	113.3	244.69	0.1299	13.02	19.26
1 hour	3.5% NaCl	173.9	0.00024	97.80	44.84	55.63	0.0033	2.73×10^{-8}
5 day	3.5% NaCl	202.0	0.00045	96.85	83.16	43.17	0.0089	1.33×10^{-5}
10 day	3.5% NaCl	307.9	0.0012	192.4	78.18	20.11	0.0131	3.63×10^{-2}
15 day	3.5% NaCl	320.3	0.0065	182.73	145.2	3.520	0.0705	1.89×10^{-1}
20 day	3.5% NaCl	338.1	0.0109	199.1	102.6	2.697	0.1204	4.49×10^{-1}

4.2.5. Surface morphology

To validate the role of hydrophobic silica and SA in enhancing the barrier property of CS film, morphological characterization was done using FESEM (Figure 4.13) and AFM (Figure 4.14). The dispersion of surface-modified silica into CS polymer and further grafting with SA makes the morphology into a close-packed honeycomb network structure. For bare MS after 20 days of exposure in 0.5M HCl and 3.5 % NaCl, severe cracks and pits could be observed. But CSiHS coated MS, after 20 days of exposure in 0.5M HCl, the network like morphology of coating sustained with some network breakages. However, since these network breakages are only present in the outer layer, and the dense inner layer has prevented the diffusion of electrolytes to the MS surface which is responsible for the corrosion protection efficiency of the coating after 20 days of immersion. i.e., the CSiHS coating on the MS surface does not drop adhesion with the MS and shows minimum metal deterioration. The CSiHS/epoxy coated MS showed a uniform protective surface layer, which remains almost as such in saline medium after 20 days of immersion. CSiHS can interact with epoxy to form a highly adherent, dense, and non-porous chitosan film on the MS surface. No detachment of the coating from the MS substrate after 20 days of immersion in acidic and saline medium indicating strong adhesion of CSiHS coating on MS substrate. The EDX profile was acquired on a single spot of the different materials. EDS spectra of CSiHS coated MS before and after corrosion studies confirmed good dispersion of surface-modified silica particles within the chitosan matrix. From EDS analysis also, it could be observed that the existence of silica (37.76%) in the chitosan matrix after being subjected to an acidic environment, which accounts for the high

corrosion protection efficiency of the coating. The presence of Si in the EDS of CSiHS coated MS after 20 days of exposure to the corrosive environment, indicate the hydrophobic silica material could prevent the diffusion of corrosive ions. The average surface roughness from AFM images of CSiHS coated MS gets increased compared to CS coated MS. This is correlated with the hydrophobicity of filler SiH in the CS matrix[28]. The average roughness of CS coated MS is found to be 7 nm and 35 nm for CSiHS coated MS surface. The increased roughness could be beneficial for the hindrance of the mass passage through the CSiHS film.
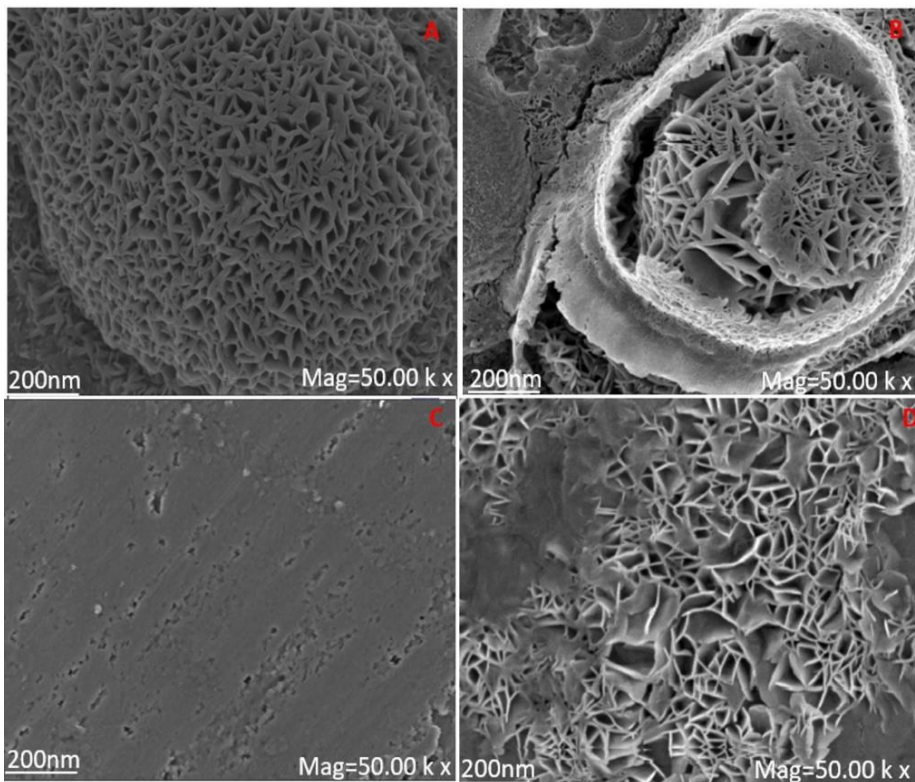
Figure 4.13. FESEM images of CSiHS coated MS before and after 20 days of immersion in 0.5M HCl (A and B) and 3.5% NaCl (C and D)
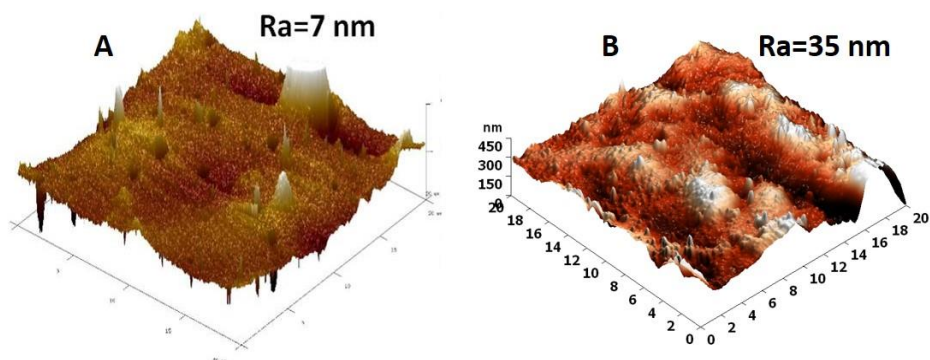
Figure 4.14. AFM topography of A) CS, B) CSiHS coated MS.

4.2.6. Scotch tape Adhesion test

Adhesion of CS-based film on the MS substrate was assessed by Scotch tape adhesion test. The adhesion strength of CSiHS on MS was found to be much higher than CS as shown by the smaller chip off areas in the stereomicroscopic images (Figure 4.15). This indicated that CSiHS has good adhesion strength on the MS surface. The results confirmed that the adhesion strength of CSiHS belongs to the 5B class, CS-g-SA belongs to the 4BClass, and that of CS is 2B.

Figure 4.15. Stereomicroscopic image of A) CS, B) CS-g-SA, and C) CSiHS after Scotch tape adhesion test

4.3. Conclusions

Hydrophobic surface modified silica particle with contact angle 139º could be synthesised using commonly used silylating agent HMDS. BET and TEM analysis revealed that both Si and SiH exhibited mesoporous structure. A new chitosan-based corrosion resistant coating was developed with the addition of 3.0 weight percentage of SiH as nano filler and further grafting with stearic acid. Non-electrochemical and electrochemical corrosion studies showed that CSiHS film offered remarkable corrosion protection for mild steel in 0.5M HCl and 3.5% NaCl. Surface morphological studies also revealed an effective formation of the coating on MS after exposure to the acidic and saline medium.

References

[1]   S. John, A. Joseph, A.J. Jose, B. Narayana, Enhancement of corrosion protection of mild steel by chitosan/ZnO nanoparticle composite membranes, Progress in Organic Coatings, 84 (2015) 28-34.

[2]   C. Zhou, X. Lu, Z. Xin, J. Liu, Y. Zhang, Polybenzoxazine/SiO2 nanocomposite coatings for corrosion protection of mild steel, Corrosion science, 80 (2014) 269-275.

[3]   A. Kumar S, H. Bhandari, C. Sharma, F. Khatoon, S.K. Dhawan, A new smart coating of polyaniline–SiO2 composite for protection of mild steel against corrosion in strong acidic medium, Polymer international, 62 (2013) 1192-1201.

[4]   G. Ruhi, O. Modi, S. Dhawan, Chitosan-polypyrrole-SiO2 composite coatings with advanced anticorrosive properties, Synthetic Metals, 200 (2015) 24-39.

[5]   E.M. Fayyad, K.K. Sadasivuni, D. Ponnamma, M.A.A. Al-Maadeed, Oleic acid-grafted chitosan/graphene oxide composite coating for corrosion protection of carbon steel, Carbohydrate polymers, 151 (2016) 871-878.

[6]   D. Borisova, H. Möhwald, D.G. Shchukin, Mesoporous silica nanoparticles for active corrosion protection, ACS nano, 5 (2011) 1939-1946.

[7]   B. Arkles, Hydrophobicity, hydrophilicity and silane surface modification, Gelest Inc, Morrisville, (2011).

[8]   N. Azizi, M.R. Saidi, Novel and efficient method for the silylation of hydroxyl groups with hexamethyldisilazane (HMDS) under solvent-free and neutral conditions, Organometallics, 23 (2004) 1457-1458.

[9]   A.M. Kartal, C. Erkey, Surface modification of silica aerogels by hexamethyldisilazane–carbon dioxide mixtures and their phase behavior, The Journal of Supercritical Fluids, 53 (2010) 115-120.

[10]   A. Kawai, J. Kawakami, Characterization of SiO2 surface treated by HMDS vapor and O2 plasma with AFM tip, Journal of Photopolymer Science and Technology, 16 (2003) 665-668.

[11]   K. Nakatsuka, K. Mori, S. Okada, S. Ikurumi, T. Kamegawa, H. Yamashita, Hydrophobic Modification of Pd/SiO2@ Single-Site Mesoporous Silicas by Triethoxyfluorosilane: Enhanced Catalytic Activity and Selectivity for One-Pot Oxidation, Chemistry–A European Journal, 20 (2014) 8348-8354.

[12]   S. Laha, P. Mukherjee, S. Sainkar, R. Kumar, Cerium containing MCM-41-type mesoporous materials and their acidic and redox catalytic properties, Journal of Catalysis, 207 (2002) 213-223.

[13]   S.M. Rafigh, A. Heydarinasab, Mesoporous chitosan–SiO2 nanoparticles: synthesis, characterization, and CO2 adsorption capacity, ACS Sustainable Chemistry & Engineering, 5 (2017) 10379-10386.

[14]   N.I. Taib, S. Endud, M.N. Katun, Functionalization of mesoporous Si-MCM-41 by grafting with trimethylchlorosilane, International Journal of Chemistry, 3 (2011) 2.

[15]   H.L. Castricum, M.C. Mittelmeijer-Hazeleger, A. Sah, E. Johan, Increasing the hydrothermal stability of mesoporous SiO2 with methylchlorosilanes—a 'structural'study, Microporous and mesoporous materials, 88 (2006) 63-71.

[16]   N.S. Nam, D.N. Khang, L.Q. Tuan, L.T. Son, Surface modification of silica nanoparticles by hexamethyldisilazane and n-butanol, Int J Env Tech Sci, 2 (2016) 31-37.

[17]   J. Philipavičius, I. Kazadojev, A. Beganskienė, A. Melninkaitis, V. Sirutkaitis, A. Kareiva, Hydrophobic antireflective silica coatings via sol–gel process, Mater. Sci, 14 (2008) 283-287.

[18]   Y. Jiang, M.A. Bourebrab, N. Sid, A. Taylor, F. Collet, S. Pretot, A. Hussain, M. Ansell, M. Lawrence, Improvement of water resistance of hemp woody substrates through deposition of functionalized silica hydrophobic coating, while retaining excellent moisture buffering properties, ACS Sustainable Chemistry & Engineering, 6 (2018) 10151-10161.

[19]   T. Siva, S. Mayavan, S. Sreejakumari, S. Sathiyanarayanan, Mesoporous silica based reservoir for the active protection of mild steel in an aggressive chloride ion environment, RSC Advances, 5 (2015) 39278-39284.

[20]   Z. Osman, A.K. Arof, FTIR studies of chitosan acetate based polymer electrolytes, Electrochimica Acta, 48 (2003) 993-999.

[21]   R.B. Prime, H.E. Bair, S. Vyazovkin, P.K. Gallagher, A. Riga, Thermogravimetric analysis (TGA), Thermal analysis of polymers: Fundamentals and applications, (2009) 241-317.

[22]   J. He, X. Li, D. Su, H. Ji, X. Zhang, W. Zhang, Super-hydrophobic hexamethyl-disilazane modified ZrO 2–SiO 2 aerogels with excellent thermal stability, Journal of Materials Chemistry A, 4 (2016) 5632-5638.

[23]   X. Liu, W. Xia, Q. Jiang, Y. Xu, P. Yu, Synthesis, characterization, and antimicrobial activity of kojic acid grafted chitosan oligosaccharide, Journal of agricultural and food chemistry, 62 (2014) 297-303.

[24]   C.d.T. Neto, J.A. Giacometti, A.E. Job, F.C. Ferreira, J.L.C. Fonseca, M.R. Pereira, Thermal analysis of chitosan based networks, Carbohydrate polymers, 62 (2005) 97-103.

[25]   A. Tozar, İ.H. Karahan, A comparative study on the effect of collagen and h-BN reinforcement of hydroxyapatite/chitosan biocomposite coatings electrophoretically deposited on Ti-6Al-4V biomedical implants, Surface and Coatings Technology, 340 (2018) 167-176.

[26]   J. Carneiro, J. Tedim, S.C. Fernandes, C. Freire, A. Silvestre, A. Gandini, M. Ferreira, M. Zheludkevich, Chitosan-based self-healing protective coatings doped with cerium nitrate for corrosion protection of aluminum alloy 2024, Progress in Organic Coatings, 75 (2012) 8-13.

[27]   X. Liu, J. Xiong, Y. Lv, Y. Zuo, Study on corrosion electrochemical behavior
         of several different coating systems by EIS, Progress in Organic Coatings, 64
         (2009) 497-503.

[28]   S. Ammar, K. Ramesh, B. Vengadaesvaran, S. Ramesh, A.K. Arof, A novel
         coating material that uses nano-sized SiO2 particles to intensify
         hydrophobicity and corrosion protection properties, Electrochimica Acta, 220
         (2016) 417-426.

Extended protection of mild steel in saline and acidic environment using stearic acid grafted chitosan preloaded with mesoporous-hydrophobic silica (mhSiO$_2$)

K.O. Shamsheera, Anupama R. Prasad, Abraham Joseph*

Department of Chemistry, University of Calicut, Calicut University P O, Kerala, India

ABSTRACT

This study produces an enhanced anti-corrosion property of chitosan-based film on mild steel (MS) in different aggressive media using surface modified SiO$_2$. Mesoporous hydrophilic SiO$_2$ is rendered hydrophobic by using silylating agent hexamethyl disilazane (HMDS). The incorporation of 3.0 weight percentage surface-modified silica into the chitosan matrix and further grafting with stearic acid (SA) through 1-ethyl-3-(3-dimethylamino-propyl) carbodiimide (EDC) mediated coupling reaction improve the anti-corrosion properties of the coating on mild steel. The resulting chitosan-based film was characterized by FTIR, TGA, AFM, FESEM, and EDX techniques. The film formed was applied for corrosion protection of mild steel in 0.5 M HCl and 3.5% NaCl and analyzed via non-electrochemical and electrochemical techniques.

1. Introduction

Mild steel is one of the most common and important industrial raw materials of daily life. Iron is sensitive to various aggressive environments like oxygen, water, and humidity. Consequently, bare steel corrodes very easily and the corrosion processes affect the mechanical properties [1,2]. One way to protect mild steel is by the application of the coatings. Among the strategies of corrosion protection, the chromate conversion coating is proved to be environmentally unfriendly. Several carbohydrate polymers and their composite are being used to develop anticorrosive coating on different metal atoms. Chitosan (C) is a promising material for coating applications because of its film-forming properties, non-toxicity, low cost, chelation by metals, and chemical functional finishing [3,4]. In our previous report, SA grafted chitosan film (CSA) contributes desirable corrosion protection for MS in 0.5 M HCl and 3.5% NaCl [5,6]. CSA acted as an effective barrier in NaCl medium when it was blended with epoxy resin. We have used electrochemical and weight loss technique to ensure the corrosion protection efficiency of CSA. We could see the protection efficiency of about 82% after 20 days of immersion when it was exposed to 3.5% NaCl and 0.5 M HCl. According to literature, the incorporation of metal oxide nanoparticles can enhance the durability of the polymer coatings and provide extra protection efficiency by forming a dense barrier against the diffusion of aggressive ions [7–9]. Ruhi et al. incorporated chitosan-polypyrrol-SiO$_2$ composite into the epoxy coating and coated

on mild steel using powder coating technique. Corrosion monitoring was carried out via salt spray test, Electrochemical impedance spectroscopy, and potentiodynamic polarization studies. The composite offered a protection efficiency of about 97% after 60 days of immersion [10]. Fayyad et al. used graphene oxide as nanofiller into the chitosan oleate matrix and the corrosion study was monitored using electrochemical impedance spectroscopy and potentiodynamic polarization studies and offered effective protection of carbon steel in 3.5% NaCl solution [11]. John et al. developed nanostructured chitosan/ZnO film on mild steel by sol-gel process and monitored anticorrosion performance via EIS and potentiodynamic polarization studies [7]. Because of the surface hydroxyl groups of SiO$_2$ in the form of isolated, geminal, and vicinal silanol it is unfit as a filler in the chitosan matrix. Therefore, to enhance the compatibility between the chitosan matrix and silica material, the hydrophilic surface of silica needs to be modified to hydrophobic [12–14]. Herein we silylated SiO$_2$ surface via HMDS, as it can scavenge the –OH group by inert methyl siloxy group [15,16]. This research investigates the influence of different loadings of hydrophobic silica nanoparticles on the anticorrosion performance of chitosan polymer matrix and SA grafted chitosan.

2. Materials used for the study

The Chitosan oligosaccharide with a degree of deacetylation of 85% was obtained from Sigma Aldrich. Stearic acid (SA), 1-ethyl-3-(3-

---

* Corresponding author.
  E-mail address: abrahamjoseph@uoc.ac.in (A. Joseph).

Inhibition of Mild Steel Corrosion in Acidic Environment Using Guar Gum as Inhibitor

Chapter 5

CONTENTS
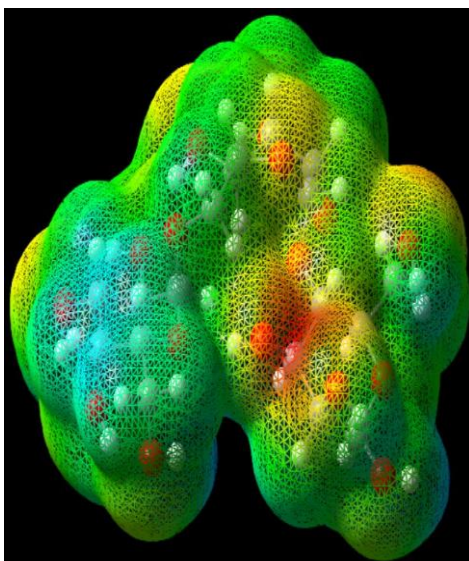
This chapter describes the corrosion inhibition performance of guar gum for mild steel in 0.5M HCl. Non electrochemical and electrochemical corrosion monitoring studies were carried out. The influence of immersion time, inhibitor concentration, and temperature on inhibition was carried out. Adsorption and kinetic studies were also conducted. Morphological studies were carried out using FESEM and AFM. DFT and MC simulation studies were performed to assess the inhibition behaviour theoretically and to account the mode of interaction between guar gum and the metal.

5.1. Introduction

In recent times, a large number of carbohydrate biopolymers and their derivatives have been successfully developed as effective corrosion inhibitors for metals in different aggressive media [1]. Owing to non-toxic nature, biodegradability, low cost, and the presence of a considerable number of flexible hydroxyl groups in the polymeric structure of Guar Gum (GG) is considered as an effective green corrosion inhibitor for different metals in aggressive environments. Corrosion inhibition of GG for carbon steel in sulphuric acid has been studied by Abdallah [2] whereas Messali et al found it in phosphoric acid media for carbon steel[3]. Herein, the corrosion inhibition of GG was studied for MS corrosion in 0.5M HCl solution via experimental and theoretical evaluations.

5.2. Result and Discussion

5.2.1. Weight loss measurement

The corrosion inhibition of MS in 0.5M HCl in the absence and presence of varying concentrations of GG ranging from 50ppm-1000ppm was studied using the weight loss method. The corrosion data obtained after 24 and 48 hours of immersion have been listed in Table 5.1. The percentage inhibition efficiency (IE) increased with an increase of GG concentration which is attributed to the inhibitor action by forming an adsorbed protective layer on the MS surface. Because of the extended life of the adsorbed inhibitor on MS, the corrosion rate decreases with time. The variation of CR and θ (surface coverage) with inhibitor

concentrations are shown in Figure 5.1. The maximum IE of 97.30% and 89.09% were observed with 800 ppm of GG after 24 and 48 hours of immersion. At this concentration, the inhibitor adsorbs by flat orientation on the surface of MS is expected such that the IE and surface coverage obtained maximum. Beyond this optimum concentration (800ppm), IE and θ were found to be decreased, due to the electrostatic repulsion between the molecules and the tendency to desorb from the metal surface.
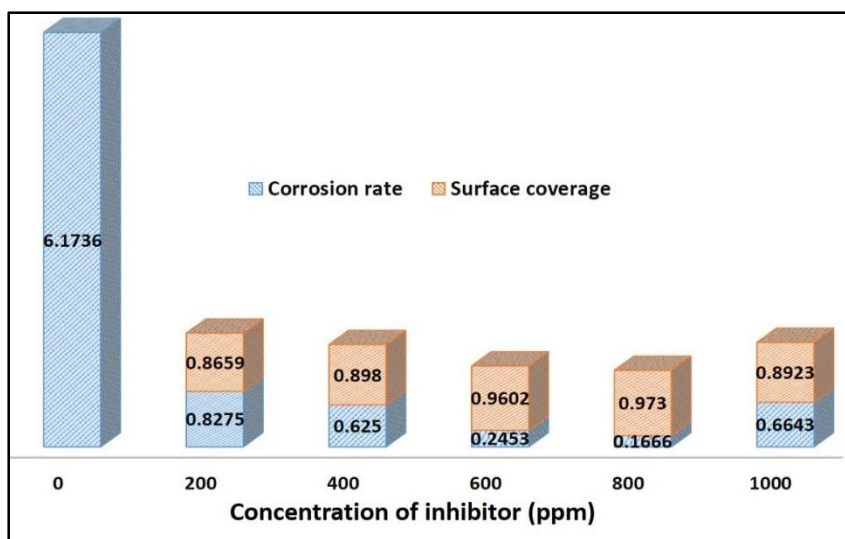
Figure 5.1. Weight loss data of MS in 0.5M HCl without and with inhibitor

Table 5.1. Weight loss data of MS in 0.5M HCl without and with GG after 24 and 48 hours of immersion

Concentration of GG	Weight loss (mg)		CR (mg cm^{-2} hr^{-1})		IE (%)		(θ)	
	24 h	48 h	24 h	48 h	24 h	48 h	24 h	48 h
Blank	533.4	624.5	6.1736	3.6140	-	-	-	-
50	178.2	265.5	2.0.625	1.536	66.59	57.48	0.6659	0.5748
100	81.10	98.93	0.9386	0.5723	84.79	84.16	0.8479	0.8416
200	71.50	95.31	0.8275	0.5515	86.59	84.73	0.8659	0.8473
300	62.42	91.14	0.7222	0.5271	88.30	85.41	0.8830	0.8541
400	54.54	83.24	0.6250	0.4814	89.80	86.67	0.8980	0.8667
500	35.27	81.24	0.4074	0.4699	93.40	86.99	0.9340	0.8699
600	21.22	79.85	0.2453	0.4618	96.02	87.22	0.9602	0.8722
700	19.35	71.93	0.2233	0.4160	96.38	88.48	0.9638	0.8848
800	14.46	68.41	0.1666	0.3940	97.30	89.09	0.9730	0.8909
900	33.63	81.26	0.3888	0.4699	93.70	86.99	0.9370	0.8699
1000	57.40	103.9	0.6643	0.6012	89.23	83.36	0.8923	0.8336

5.2.2. *Potentiodynamic polarization study*

PDP study was conducted to evaluate the kinetics of the corrosion process after executing OCP test. These polarization plots are exhibited in Figure 5.2. Corrosion current density from the intercept of extrapolated anodic and cathodic Tafel lines at the corrosion potential were used to estimate the IE using equation 2.4. The values E_{corr}, I_{corr}, β_a, β_c, and IE obtained from PDP plot are tabulated in Table 5.2. The CR and I_{corr} decline with an increase in the concentration of GG, indicating that the polymeric molecule is strongly adsorbed on the surface of MS which prevents the diffusion of corrosive ions from the aggressive media and retards the corrosion process on the MS surface. The I_{corr} values for the optimum concentration of GG were less at all studied temperatures. An inhibitor is listed as cathodic or anodic type based on the corrosion potential difference is above and below 85 mV with respect to corrosion potential of blank and if the shift is within $\pm$ 85 mV, the inhibitor is treated as mixed type. Here in GG can be considered as mixed type inhibitor. Upon increasing GG concentration, the value of polarization resistance (R_p) increases. A high value of R_p (371.02 Ω cm^2) was recorded for 800 ppm of GG indicates that the GG passivates the active site on MS surface. At elevated temperatures, lower R_p values are obtained due to the diffusion of electrolyte into the active site which follows corrosion to MS.
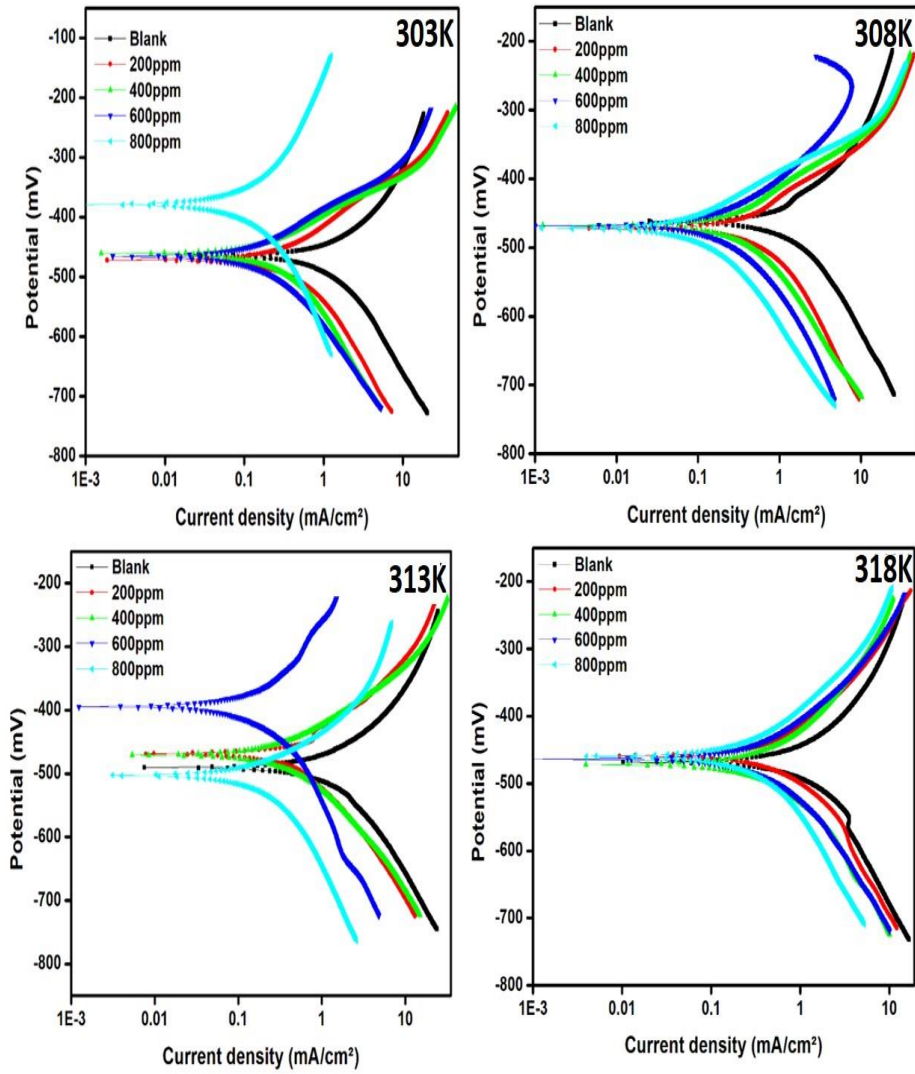
Figure 5.2. PDP plot of MS in 0.5M HCl with different concentration of GG from 303-318K

Table 5. 2. PDP parameters of MS in 0.5M HCl without and with GG at various temperatures

Temperature	Concentration of GG (ppm)	I_{corr} (mA/cm^2)	$-E_{corr}$ (mV/SCE)	β_a (mV/dec)	$-\beta_c$ (mV/dec)	R_p (Ω cm^2)	CR (mpy)	IE (%)
	Blank	1.2973	460.56	120.75	223.01	26.21	24.37	
	200	0.3172	471.66	109.51	147.75	86.09	14.59	75.54
	400	0.2274	460.80	102.19	157.61	118.29	13.09	82.47
303K	600	0.1745	466.88	103.05	149.33	151.72	6.175	86.54
	800	0.1186	377.99	200.72	204.68	371.02	2.073	90.85
	Blank	1.3627	460.25	125.67	157.19	22.25	26.04	
	200	0.3594	471.60	114.97	182.62	85.24	16.38	73.26
308K	400	0.3024	465.97	94.35	129.43	97.75	15.62	74.87
	600	0.2879	466.98	122.53	196.84	113.90	12.61	78.87
	800	0.1653	470.84	92.81	157.77	153.50	2.848	89.30
	Blank	1.4328	471.15	151.62	207.28	26.53	28.06	
	200	0.4740	468.58	117.14	184.25	65.60	20.57	66.91
313K	400	0.3839	470.23	111.54	156.41	73.64	17.71	73.20
	600	0.3281	503.58	105.16	196.01	90.57	13.45	77.06
	800	0.2046	394.27	90.64	252.51	141.55	9.383	85.72
	Blank	1.5543	467.56	185.41	213.98	27.75	32.19	
	200	0.6695	459.54	154.99	152.96	49.93	26.87	59.52
318K	400	0.6025	472.04	170.44	185.96	64.09	23.38	63.57
	600	0.4858	462.66	141.27	177.87	76.89	14.05	70.63
	800	0.3421	459.17	140.02	194.34	103.30	9.785	79.32

5.2.3. EIS measurements

The Nyquist and Bode plot of MS samples without and with GG at various temperatures are displayed in Figure 5.3 and 5.4. The IE increases with an increase in GG concentration and decreases with temperature. Also, the optimum concentration of the inhibitor at various temperatures was found to be 800 ppm. The single depressed semi-circular nature of Nyquist plots and single time constant in Bode plot designate the charge transfer mechanism at the metal electrolyte interface. The charge transfer process creates a double layer with a parallel combination of charge transfer resistance (R_{ct}) and double layer capacitance (C_{dl}). The presence of inhibitor molecules interrupts the charge transfer process by adsorption on the MS surface. Beyond 800 ppm of GG concentration, causes desorption of GG and consequently, the charge transfer process will cause a decrease of R_{ct}, and IE. EIS data were interpreted using Z simp win software. The imperfectness of the capacitive loop in the Nyquist plot is often observed at a solid electrode interface due to the surface heterogeneity and roughness of the sample surface. In such cases, the best fit could be attained by replacing capacitance with constant phase element (CPE) in the equivalent circuit [4, 5]. The CPE has the impedance function of the given form[6, 7]

$$Z_{CPE} = \frac{1}{Q(j\omega)^n} \tag{5.1}$$

where Q and n are the magnitudes of CPE and the phase shift, $j^2 = -1$ is the imaginary unit, and ω is the angular frequency. The value of n is associated with surface heterogeneity. The C_{dl} values can be estimated

using CPE parameters (Q and n) and the R_{ct} values using the following relation[8]

$$C_{dl} = \sqrt[n]{Q \times R_{ct}^{1-n}} \qquad (5.2)$$

The lower values of C_{dl} at the metal solution interface of the inhibited solution compared to the uninhibited solution arises due to decreased dielectric constant and hence better adsorption of GG on the MS surface. R_{ct} values are used to calculate the IE using equation 2.3. The different data got from the Nyquist plot are tabulated in Table 5.3
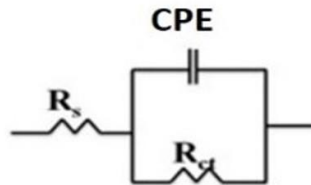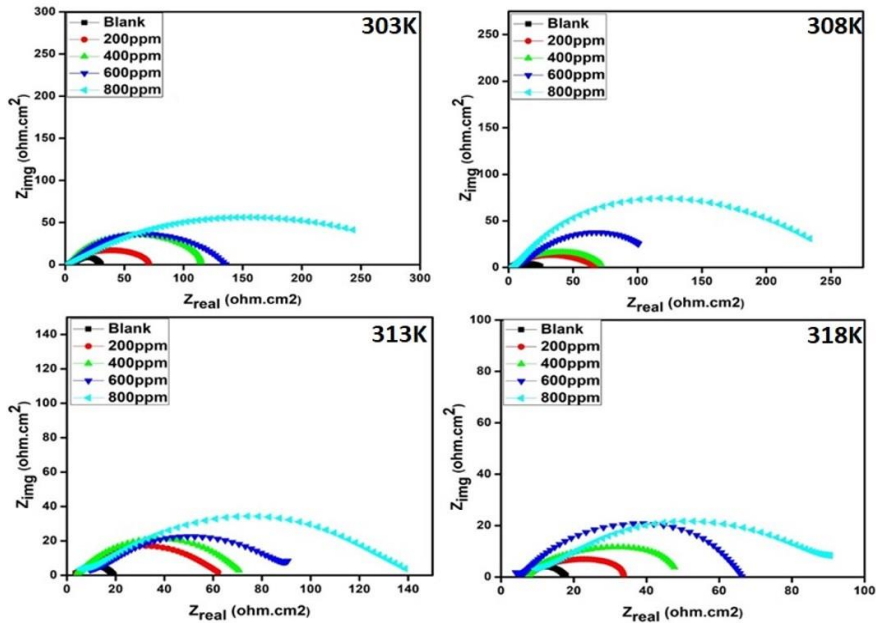
Figure 5.3. Nyquist plot of MS in 0.5M HCl with different concentrations of GG from 303-318K and the equivalent circuit used to fit.
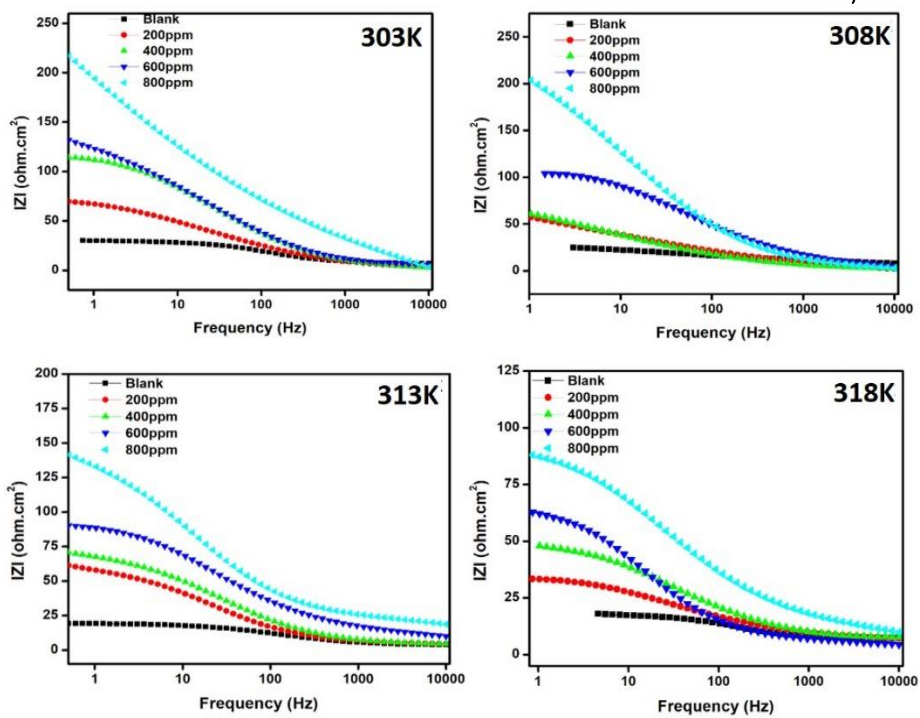
Figure 5.4. Bode impedance plot of MS without and with different concentrations of GG in 0.5M HCl from 303-318K.

Table 5.3. Parameters obtained from Nyquist plot of MS in 0.5M HCl without and with GG at various temperature

Temperature	Concentration of GG (ppm)	R_s (Ωcm^2)	R_{ct} (Ωcm^2)	n	$Q_{dl} \times 10^{-4}$ $S^n \Omega^{-1} cm^{-2}$	C_{dl} ($\mu F cm^{-2}$)	CR (mpy)	IE (%)
	Blank	7.01	22.84	0.80	10.59	417.6	13.24	
	200	2.12	79.15	0.80	6.80	327.5	5.820	71.14
	400	2.57	120.1	0.78	3.91	165.0	3.017	80.98
303K	600	4.04	129.5	0.74	3.13	101.4	1.835	82.36
	800	6.85	314.7	0.80	0.79	31.36	1.186	92.74
	Blank	5.67	20.50	0.80	14.31	592.2	14.79	
	200	1.16	68.65	0.80	8.28	404.2	6.404	70.13
308K	400	2.02	76.03	0.80	8.02	398.5	3.977	73.03
	600	2.59	105.7	0.79	7.03	352.2	2.060	80.60
	800	2.63	255	0.80	2.90	151.22	1.186	91.96
	Blank		18.91	0.80	15.4	636.1	15.99	
	200	3.44	59.41	0.78	8.65	374.4	7.089	68.1
313K	400	5.04	66.91	0.79	8.18	360.4	4.519	71.28
	600	7.32	87.16	0.79	4.32	180.6	2.969	78.30
	800	6.42	140.7	0.78	2.90	117.6	2.149	86.56
	Blank		15.92	0.8	16.25	651.5	18.99	
	200	7.34	27.71	0.80	9.70	392.7	8.91	42.54
318K	400	7.35	44.05	0.78	9.40	382.8	6.864	63.85
	600	3.03	65.47	0.77	4.30	148.0	4.018	75.68
	800	6.64	91.84	0.77	3.37	119.3	3.292	82.66

5.2.3.1. Adsorption Isotherm

To elucidate the nature of adsorption of GG and to determine the free energy involved in the process, a possible correlation between the concentration of GG and degree of surface coverage has been considered by using different adsorption isotherms[9]. Here the process of adsorption follows Langmuir isotherm and the fitted model is given in Figure 5.5.
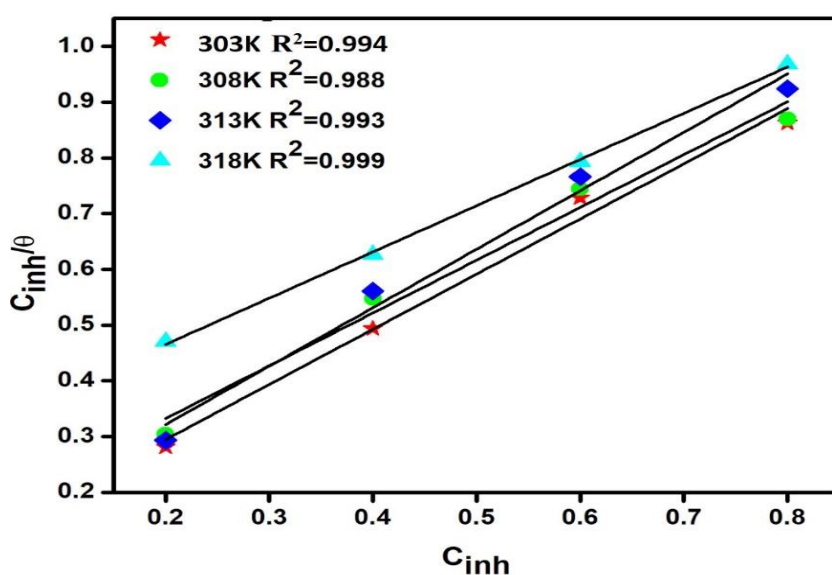
Figure 5.5. Langmuir adsorption isotherm for MS at different temperature in 0.5M HCl

Adsorption equilibrium constant (K_{ads}) was determined from the intercept of the straight lines on the C_{inh}/θ axis. The regression coefficient (R^2) values were most close to one at all studied temperatures. The high value of K_{ads} (10.33) at 303K indicates effective adsorption of GG on the MS surface and gets decreased when

temperature raised (3.33 at 318K). K_{ads} values are used for calculating the free energy of adsorption ΔG^0_{ads} using the following equation [7]

$$\Delta G^0_{ads} = -RTln(K_{ads} \times C_{solvent}) \qquad (5.3)$$

where $C_{solvent}$ is the concentration of the solvent. The negative value of ΔG^0 specifies spontaneous adsorption of GG on the MS surface. In general, the value of ΔG^0_{ads} around -20 kJ/mol or more positive are considered as physisorption, and around -40 kJ/mol or more negative are considered as chemisorption[10]. The ΔG^0 values given in Table 5.4 perceptibly support physisorption between GG and metal surface.

Table 5.4. Adsorption parameters from Langmuir adsorption isotherm for the adsorption of GG on MS at various temperature

Temperature	K_{ads}	$-\Delta G^0$
303K	10.33	23.28
308 K	8.94	23.29
313 K	8.10	23.41
318 K	3.33	21.44

5.2.3.2. Effect of temperature and activation parameters

GG probably gets adsorbed on the MS surface by the interaction between lone pair of electrons on oxygen atom and d orbital of the metal atom. At higher temperatures, some complex effects may occur on the MS surface because of etching, decomposition, and desorption of inhibitor molecules from the metal surface which cause diffusion of aggressive ions from the electrolyte to the metal side and increases the

134

CR and decreases the IE [11]. Here, the EIS measurements were employed to study the temperature effect in the range of 303-318K. The CR of MS is very low in acid media with inhibitor at all studied temperatures. The temperature effect on corrosion inhibition property of GG on MS can be further evaluated by calculating activation parameters of corrosion process using Arrhenius type relation and Transition state equation[11, 12]

$$log(CR) = \frac{-E_a}{2.303RT} + logA \qquad (5.4)$$

$$CR = \frac{RT}{Nh}\exp\left(\frac{\Delta S}{R}\right)exp\left(\frac{-\Delta H}{RT}\right) \qquad (5.5)$$

where E_a is the activation energy of metal dissolution process, R is the universal gas constant, T is the absolute temperature, A is Arrhenius pre-exponential constant, N is the Avogadro's number, h is the Planck's constant, and ΔS and ΔH are the change in activation entropy and enthalpy of the corrosion process, respectively.

The activation energy of metal dissolution without and with different concentrations of GG was derived from the slop of $-E_a/2.303R$ (Figure 5.6A). The activation parameters obtained from Arrhenius and transition state plots are presented in Table 5.5. The higher E_a observed for optimum inhibitor concentration reveals good surface coverage via strong adsorption of polymeric GG molecules and increases the energy barrier for the metal dissolution process[13, 14]. The plot of ln (CR/T) versus 1/T is exhibited in Figure 5.6B. From the slop and intercept of the plot, ΔH and ΔS values were calculated. The positive value of

enthalpy indicates the endothermic nature of metal dissolution[15] and the higher value(55.11kJ/mol) in the presence of an optimum concentration of GG reveals the retardation of the corrosion process. The higher positive value of ΔS suggests that in the rate determining step, the activated complex undergoes dissociation and disordering during its conversion from the reactants to activated complex[16].

Table 5.5. Activation parameters of MS without and with GG in 0.5M HCl

Concentration of inhibitor	Ea	ΔH	ΔS
Blank	18.28	15.71	-52.67
200	21.73	19.08	-48.52
400	41.17	38.23	9.303
600	42.95	40.39	11.86
800	61.99	55.11	56.12
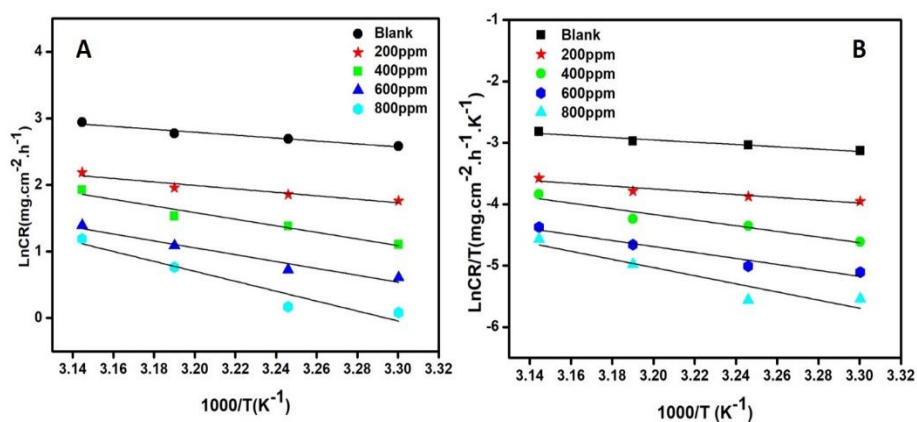
Figure 5.6. A) Arrhenius and B) Transition state plots of MS in 0.5M HCl with various concentrations of GG

5.2.4. FTIR spectroscopy

FTIR spectra of GG and GG scratched from the surface of MS after 6 hours of immersion were carried out (Figure 5.7). GG shows a broad band at 3424cm^{-1} attributed to the O-H stretching vibrations. The peak at 2917cm^{-1} is associated with C-H stretching vibrations. The O-H bending mode observed at 1654cm^{-1}. The spectra of GG scratched from the surface show a decrease in intensity of O-H stretching and bending frequency due to the association with the MS surface. The intensity of C-O(H) stretching vibration at 1163cm^{-1} gets decreased upon complex formation with metal[17-19].
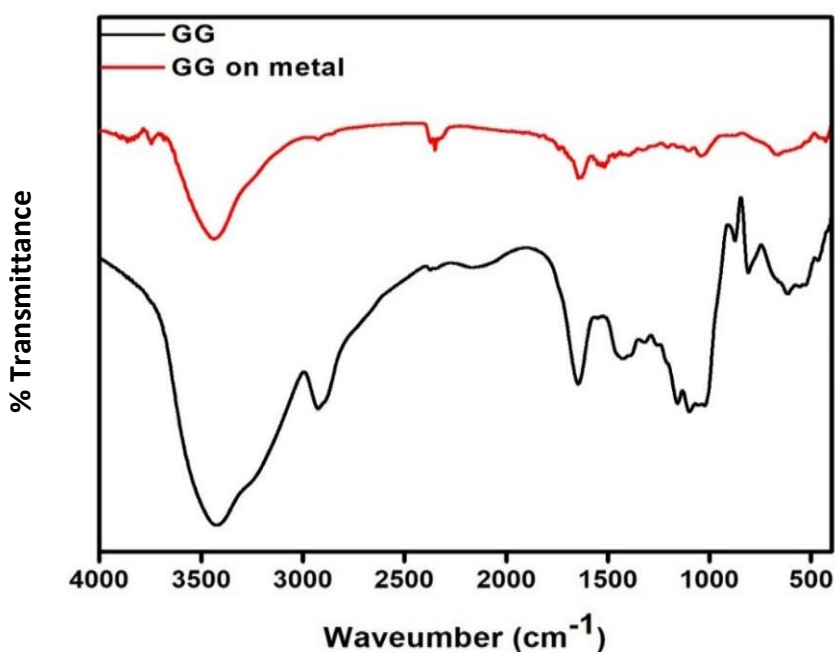
Figure 5.7. FTIR spectra of GG and GG on MS after 6 hours immersion in 0.5M HCl

5.2.5.XPS

XPS can measure the electronic state of the elements within a material, elemental composition, and chemical bond in a molecule. The survey spectrum from MS dipped in 0.5M HCl with 800 ppm of GG (Figure 5.8) encounters iron, oxygen, and carbon as the major component. To investigate the chemical environments of carbon in the GG on the MS surface, the high resolution XPS spectrum for C 1s core energy level spectrum was recorded. The spectra were corrected with C 1s at 284.8 eV. The C 1s signal can be deconvoluted into three different contributions. The peak at a binding energy of 284.63 eV was ascribed to C-C or C-H[20, 21]. The small peak at 286.20 eV was ascribed to alcohol and ether (C-O-X) group. 288.30 eV binding energy attributed to the presence of the O-C-O bond of GG. The O 1s spectra for MS in 0.5M HCl with 800 ppm of GG was deconvoluted into three components. The photoelectron peak at 528.68 eV was ascribed to the metal oxygen bond. The peak at 531.05 and 532.16 eV was attributed to the C-O bond in C-O-C and O-C-O [22-24]. Thus, GG gets strongly adsorbed on the MS surface preferably by the coordination through an oxygen atom, which ensured a strong coverage of the metal surface by GG and thus protecting MS surface from acid attack. Therefore, by assimilating the results of the adsorption isotherm and XPS analysis, we can further conclude that physisorption and chemisorption coexist.
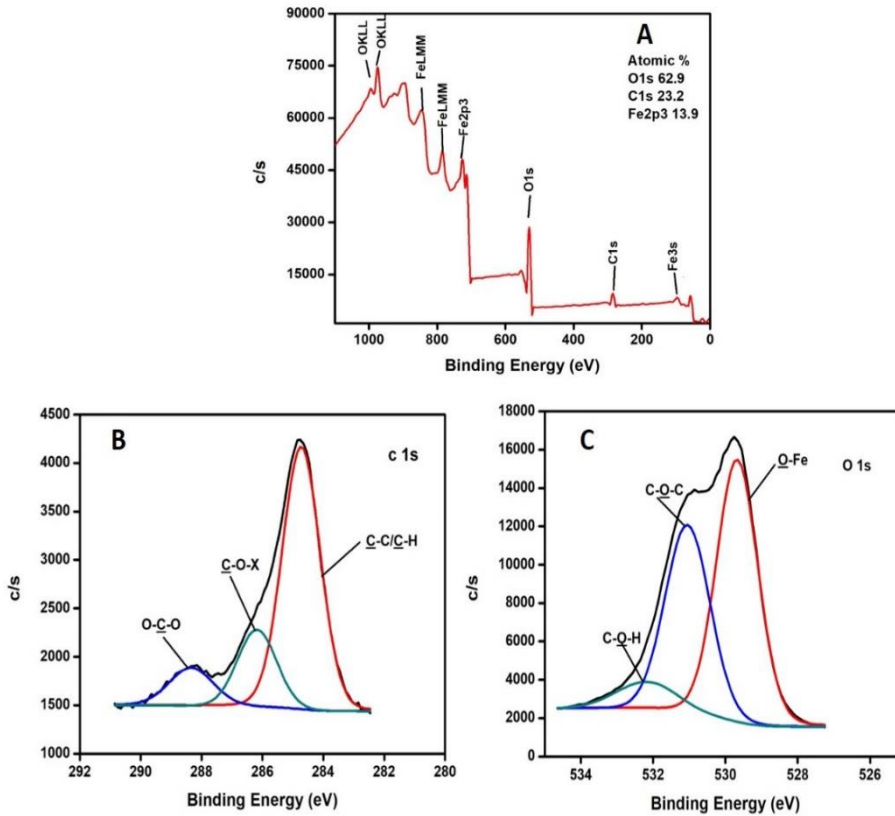
Figure 5.8. The XPS (A) survey scan spectrum and deconvoluted profiles of (B) C1s, (C) O 1s for GG treated MS after 24 hours of immersion in 0.5M HCl

5.2.6. FESEM and AFM

The morphological changes of the sample after 24 h and 48 h exposure in 0.5M HCl in the absence and presence of optimum GG concentration was monitored via FESEM micrographs (Figure 5.9). Cracks and pits were observed on the surface of MS without inhibitor due to severe corrosion whereas in the presence of GG, MS surface is protected and devoid of much damages. The network morphology of polymeric guar gum remains as such even after 48 hours of immersion. In order to

measure surface roughness of the sample without and with GG in 0.5M HCl, AFM micrographs were recorded after 24 hours of immersion.
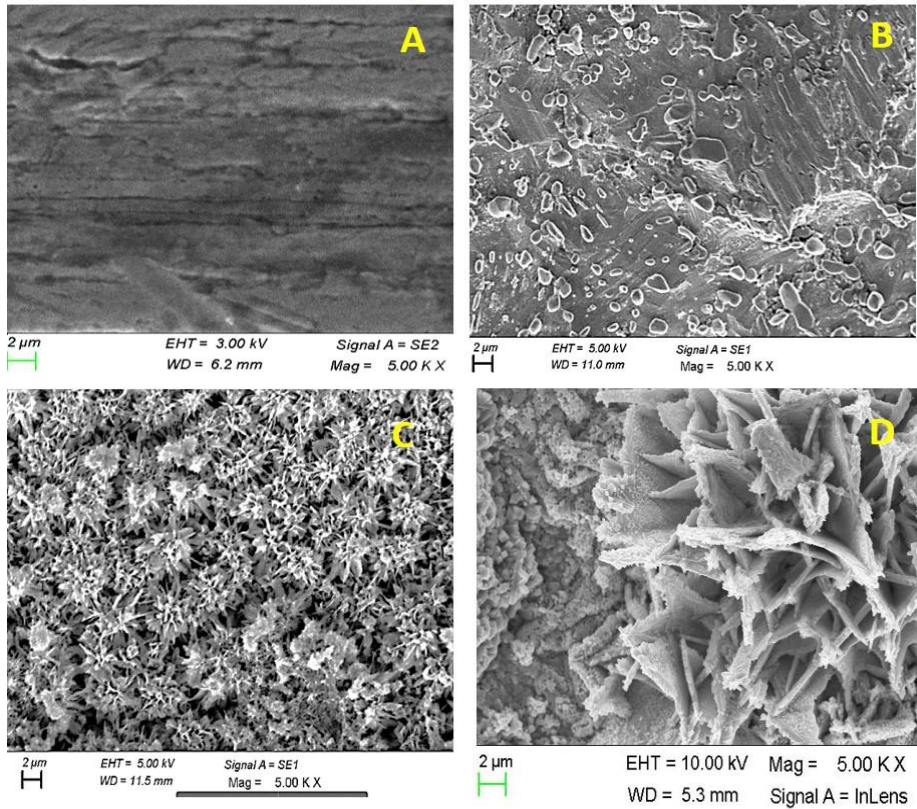
Figure 5.9. FESEM images of (A) MS (B) MS after 24 hours immersion in 0.5M HCl (C) and (D) MS in 0.5M HCl with 800ppm of GG after 24 and 48 hours of immersion

Figure 5.10 reveals the surface roughness of MS after 24 hours immersion in acid solution as 237.84 nm without GG and 29.36 nm with 800 ppm of GG. The lowering in surface roughness in the presence of the GG indicates the formation of protective film on the MS surface by replacing the pre-adsorbed water molecules.
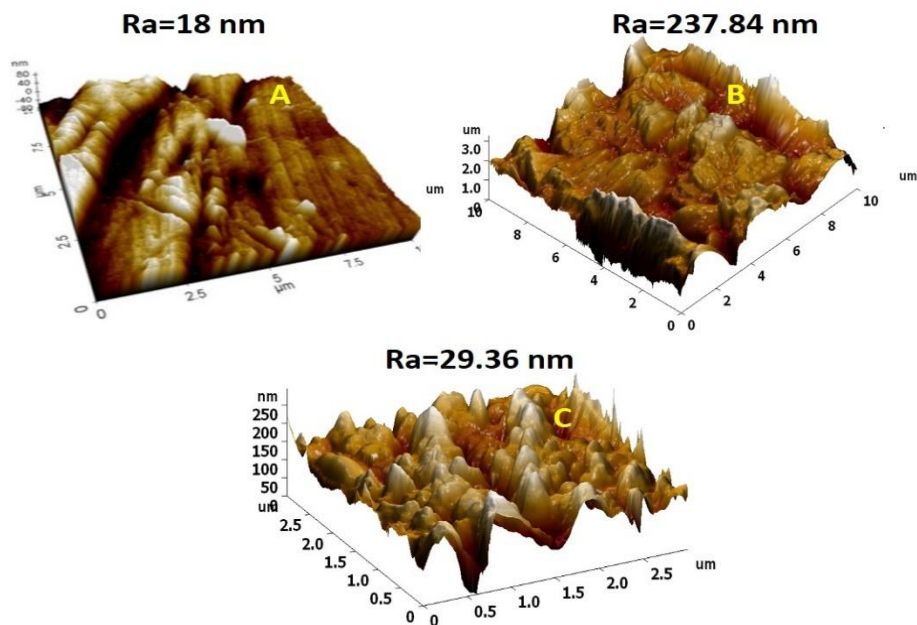
Figure 5.10. AFM images of (A) MS, (B) and (C) MS after 24 hours of immersion without and with 800ppm of GG

5.2.7. DFT calculations

The optimized geometry of GG with FMOs are exhibited in Figure 5.11. Table 5.6 contains the list of selected theoretical parameters of GG from DFT studies. The higher E_{HOMO} in the gas and water phase reveals the good electron donation tendency from the GG molecule to the d orbital of the Fe surface, while the lower E_{LUMO} suggests the better susceptibility to accept electrons by back donation. The energy gap (ΔE) between LUMO and HOMO gives an idea about the stability of the GG-metal complex. Lower ΔE value indicates that the GG can easily donate its electrons to the d orbital of metal, such that the inhibitor is adsorbed

firmly on the surface of MS[25]. The inhibitor molecule transfers its electron to the metal if it's number of transferred electron, ΔN>0 and vice versa[26]. In our study ΔN value of 0.2630 is obtained (calculated using equation 2.9) in the gas phase and 0.2557 in the water phase suggests the donation of the electron from free hydroxyl, ether group in GG molecule to the d orbital of metal. The μ of GG (4.5209 Debye) is higher as compared to μ of water (1.85 Debye) which reveals that the GG molecule has a strong tendency to adsorb on the surface of the metal by replacing pre-adsorbed water molecules.

Molecular electrostatic potential (MEP) map was used as a visual tool to understand the electron density at different regions and to determine the more reactive centres in the inhibitor molecule. In MEP map (Figure 5.11B) the red color indicates the most negative electrostatic potential region and the blue color for the most positive electrostatic potential region and the region of the zero electrostatic potential indicated by green color [27].

Table 5.6. Quantum chemical parameters of GG in gas and water phase

Inhibitor	E_{HOMO} (eV)	E_{LUMO} (eV)	ΔE (eV)	χ (eV)	η (eV)	ΔN
GG (gas phase)	-6.604	0.9252	7.529	2.839	3.765	0.2630
GG (water phase)	-6.782	1.2501	8.032	2.766	4.016	0.2557
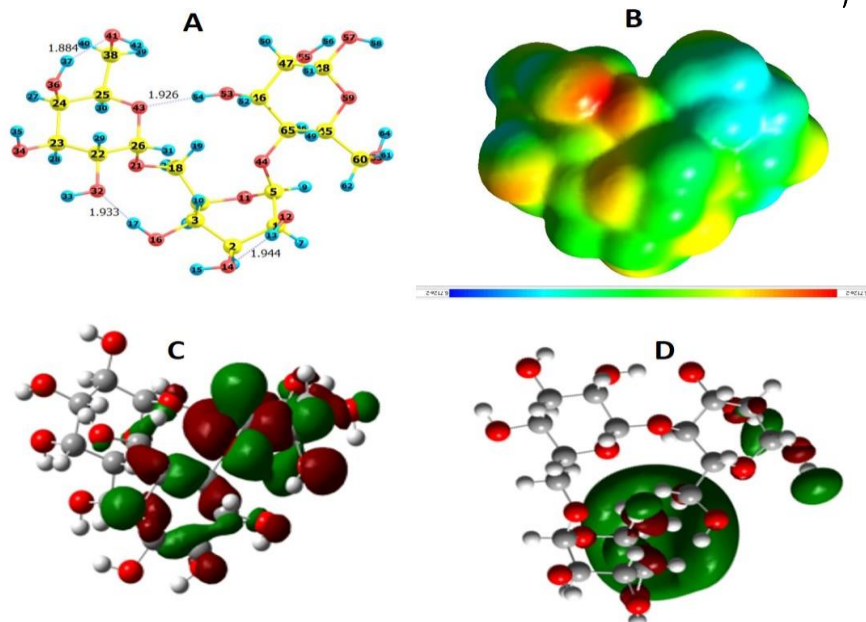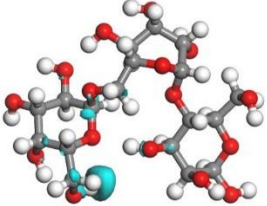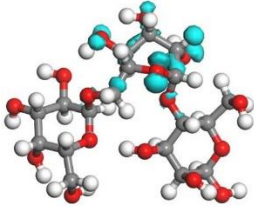
Figure 5.11. A) Optimized geometry, B) MEP map, C) and (D) FMO of GG

5.2.8. Fukui indices

Fukui calculations are useful to evaluate the reactive centres in a molecule towards electrophilic and nucleophilic attack. Electron density of the Fukui indices f_k^+ and f_k^- at 0.025 isosurfaces obtained from Mulliken population analysis along with Fukui values are shown in Table 5.7. We have also used a more precise wave function based natural population analysis by NBO to evaluate the Fukui indices of each atom on GG. The highest value of f_k^+ for oxygen indicates the high nucleophilicity of the atom and can accept an electron from the MS surface[28] and are located on O (41), O (36), and O (53) from NBO analysis and Mulliken population analysis. The highest value of f_k^- disclose the tendency of oxygen atom in GG to donate electrons to the

MS surface. Parameters of local reactivity descriptors encounter O (16), C (48), and C (5) are the more reactive site for electrophilic attack.

Table 5.7. The Fukui indices of GG calculated by NBO and DMol^3

	Fukui In atom	NBO Analysis		Mulliken population analysis	
		f^+	f	f^+	f
	C (1)	-0.0181	0.0014	-0.002	-0.027
f^+	C (2)	-0.0247	0.0211	-0.001	-0.015
	C (3)	-0.012	-0.0058	-0.01	-0.002
	C (4)	-0.008	0.0052	0.003	-0.022
	C (5)	-0.1798	**0.1853**	-0.005	**0.117**
	O (11)	0.3074	-0.4119	0.007	0.003
	O (12)	0.3907	-0.4617	-0.002	0.014
	O (14)	0.3977	-0.4465	0.011	0.052
	O (16)	-0.4028	**0.4087**	0.015	**0.074**
	C (18)	0.0853	-0.0912	-0.008	0.004
	O (21)	0.3145	-0.3417	0.011	0.021
f	C (22)	-0.0107	0.0075	0.001	-0.003
	C (23)	-0.0213	0.0218	-0.003	-0.001
	C (24)	-0.0176	0.0235	-0.014	0.001
	C (25)	0.0099	0.0007	-0.008	-0.013
	C (26)	-0.1483	0.1622	0.008	0.007
	O (32)	0.3989	-0.4132	0.01	-0.013
	O (34)	0.3935	-0.4326	0.024	0.011
	O (36)	**0.4143**	-0.447	**0.03**	0.006
	C (38)	0.1021	-0.0875	-0.017	-0.001
	O (41)	**0.4298**	-0.4266	**0.084**	0.012
	O (43)	0.3298	-0.3156	-0.07	0.004
	O (44)	0.3048	-0.3572	-0.012	0.002
	C (45)	-0.0138	0.0088	-0.006	-0.001
	C (46)	-0.0111	0.016	-0.046	-0.006
	C (47)	-0.013	0.0122	-0.008	-0.004
	C (48)	-0.1853	**0.1926**	0.003	**0.011**
	O (53)	**0.4095**	-0.4493	**0.022**	0.004
	O (55)	0.3899	-0.448	0.004	0.014
	O (57)	0.396	-0.3999	0.004	0.011
	O (59)	0.3171	-0.3553	0.014	0.01
	C (60)	0.0607	-0.0604	-0.004	0.001
	O (63)	0.3859	-0.4212	0.008	0.006
	C (65)	-0.025	0.0099	-0.001	-0.018

5.2.9. Monte Carlo Simulation

MC simulation is another efficient tool for the theoretical explanation of the adsorption tendency of the inhibitor molecule on a metallic surface. In the water phase, one monomer unit of GG accompanied with 200 water molecules was subjected to simulation on Fe(1 1 0) plane. The final adsorption configurations of GG in the gas and water phase over the metal surface is displayed in Figure 5.12. After 500,000 steps, the GG molecule moves in a parallel manner on the metal surface.
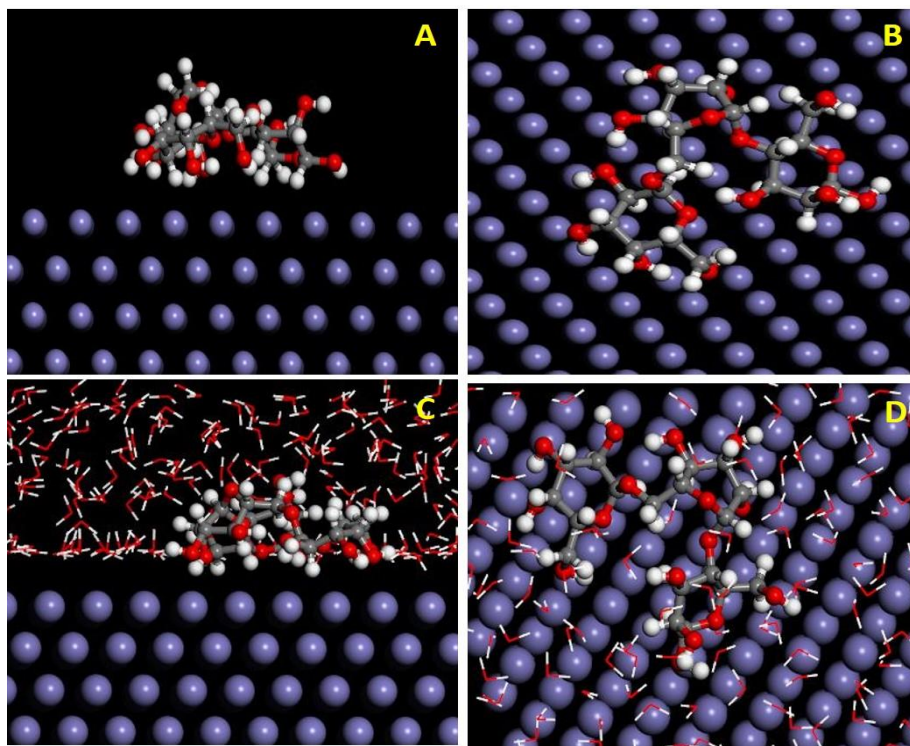
Figure 5.12. Side and top view of GG adsorption on Fe (110) surface (A-B) in gas and (C-D) in aqueous phase

The adsorption energy of GG in both phases denoted that GG gets adsorbed more firmly in the water phase. The high negative adsorption energy of GG (-288.66 kJ/mol) compared to water molecule (-33.90 kJ/mol) in the water phase indicates the stronger adsorption capacity of GG by substituting the water molecules from the MS surface leading to the formation of a stable protective layer (Table 5.8) [27]

Table 5.8. Energy parameters obtained from MC simulations for the adsorption of GG on Fe (110) surface in gas and water phase (in kJ/mol)

Phase	Total Energy (kJ/mol)	Adsorption Energy (kJ/mol)	Rigid adsorption energy (kJ/mol)	Deformatio nEnergy (kJ/mol)	Guar Gum: dEad/d Ni (kJ/mol)	Water: dEad/d Ni (kJ/mol)
Water	-2.72×10^3	-6.73×10^3	-2.99×10^3	-3.73×10^3	-282.66	-33.90
Gas	-115.56	-438.3	-217.3	-220.9	-438.2	-

5.3. Conclusions

The abundance of hydroxyl group in the GG molecule and large chain molecular structure makes an effective corrosion inhibitor in 0.5M HCl and the IE was influenced by temperature and concentration of inhibitor. Stable interaction between the MS and inhibitor are well supported by FTIR, SEM, AFM, and XPS studies. DFT studies provided a more detailed account of the mode of donor-acceptor synergy between the studied inhibitor and metal surface. MC simulation study revealed that GG adsorbed on the MS surface by their flat horizontal orientation and high negative value of interaction energy indicated that the inhibitor can act as a strong and stable adsorbate on the metal surface and hence offers good corrosion inhibition property.

References

[1]   S.A. Umoren, U.M. Eduok, Application of carbohydrate polymers as corrosion inhibitors for metal substrates in different media: a review, Carbohydrate polymers, 140 (2016) 314-341.

[2]   M. Abdallah, Guar gum as corrosion inhibitor for carbon steel in sulfuric acid solutions, Portugaliae Electrochimica Acta, 22 (2004) 161-175.

[3]   M. Messali, H. Lgaz, R. Dassanayake, R. Salghi, S. Jodeh, N. Abidi, O. Hamed, Guar gum as efficient non-toxic inhibitor of carbon steel corrosion in phosphoric acid medium: Electrochemical, surface, DFT and MD simulations studies, Journal of Molecular Structure, 1145 (2017) 43-54.

[4]   B.D. Mert, A.O. Yüce, G. Kardaş, B. Yazıcı, Inhibition effect of 2-amino-4-methylpyridine on mild steel corrosion: experimental and theoretical investigation, Corrosion science, 85 (2014) 287-295.

[5]   M. Chevalier, F. Robert, N. Amusant, M. Traisnel, C. Roos, M. Lebrini, Enhanced corrosion resistance of mild steel in 1 M hydrochloric acid solution by alkaloids extract from Aniba rosaeodora plant: Electrochemical, phytochemical and XPS studies, Electrochimica Acta, 131 (2014) 96-105.

[6]   D. Daoud, T. Douadi, H. Hamani, S. Chafaa, M. Al-Noaimi, Corrosion inhibition of mild steel by two new S-heterocyclic compounds in 1 M HCl: experimental and computational study, Corrosion Science, 94 (2015) 21-37.

[7]   Y. Tang, F. Zhang, S. Hu, Z. Cao, Z. Wu, W. Jing, Novel benzimidazole derivatives as corrosion inhibitors of mild steel in the acidic media. Part I: Gravimetric, electrochemical, SEM and XPS studies, Corrosion science, 74 (2013) 271-282.

[8]   H. Lgaz, R. Salghi, K.S. Bhat, A. Chaouiki, S. Jodeh, Correlated experimental and theoretical study on inhibition behavior of novel quinoline derivatives for the corrosion of mild steel in hydrochloric acid solution, Journal of Molecular Liquids, 244 (2017) 154-168.

[9]   S. John, A. Joseph, Electroanalytical and Theoretical Investigations of the Corrosion Inhibition Behavior of Bis-1, 2, 4-Triazole Precursors EBATTand BBATT on Mild Steel in 0.1 N HNO3, Industrial & engineering chemistry research, 51 (2012) 16633-16642.

[10]   K. Shainy, P.R. Ammal, A. Joseph, Development of passive film and enhancement of corrosion protection of mild steel in hydrochloric acid through the synergistic interaction of 2-amino-4-methyl benzothiazole (AMBT) and (E)-2-methylbenzo [d] thiazol-2-yl) imino-4-methyl) phenol (MBTP, Egyptian journal of petroleum, (2017).

[11]   P.R. Ammal, M. Prajila, A. Joseph, Effect of substitution and temperature on the corrosion inhibition properties of benzimidazole bearing 1, 3, 4-

oxadiazoles for mild steel in sulphuric acid: physicochemical and theoretical studies, Journal of environmental chemical engineering, 6 (2018) 1072-1085.

[12]   C. Verma, M. Quraishi, A. Singh, 2-Amino-5-nitro-4, 6-diarylcyclohex-1-ene-1, 3, 3-tricarbonitriles as new and effective corrosion inhibitors for mild steel in 1 M HCl: experimental and theoretical studies, Journal of Molecular Liquids, 212 (2015) 804-812.

[13]   G. Schmid, H. Huang, Spectro-electrochemical studies of the inhibition effect of 4, 7-diphenyl-1, 10-phenanthroline on the corrosion of 304 stainless steel, corrosion science, 20 (1980) 1041-1057.

[14]   J. Haque, K. Ansari, V. Srivastava, M. Quraishi, I. Obot, Pyrimidine derivatives as novel acidizing corrosion inhibitors for N80 steel useful for petroleum industry: a combined experimental and theoretical approach, Journal of Industrial and Engineering Chemistry, 49 (2017) 176-188.

[15]   M.V. Fiori-Bimbi, P.E. Alvarez, H. Vaca, C.A. Gervasi, Corrosion inhibition of mild steel in HCL solution by pectin, Corrosion Science, 92 (2015) 192-199.

[16]   F. Bentiss, M. Lebrini, M. Lagrenée, Thermodynamic characterization of metal dissolution and inhibitor adsorption processes in mild steel/2, 5-bis (n-thienyl)-1, 3, 4-thiadiazoles/hydrochloric acid system, Corrosion Science, 47 (2005) 2915-2931.

[17]   L. Dai, B. Wang, X. An, L. Zhang, A. Khan, Y. Ni, Oil/water interfaces of guar gum-based biopolymer hydrogels and application to their separation, Carbohydrate polymers, 169 (2017) 9-15.

[18]   R. Sharma, B.S. Kaith, S. Kalia, D. Pathania, A. Kumar, N. Sharma, R.M. Street, C. Schauer, Biodegradable and conducting hydrogels based on Guar gum polysaccharide for antibacterial and dye removal applications, Journal of environmental management, 162 (2015) 37-45.

[19]   N. Thombare, S. Mishra, M. Siddiqui, U. Jha, D. Singh, G.R. Mahajan, Design and development of guar gum based novel, superabsorbent and moisture retaining hydrogels for agricultural applications, Carbohydrate polymers, 185 (2018) 169-178.

[20]   N.R. Singha, A. Dutta, M. Mahapatra, M. Karmakar, H. Mondal, P.K. Chattopadhyay, D.K. Maiti, Guar gum-grafted terpolymer hydrogels for ligand-selective individual and synergistic adsorption: Effect of comonomer composition, ACS omega, 3 (2018) 472-494.

[21]   M. Herstedt, D.P. Abraham, J.B. Kerr, K. Edström, X-ray photoelectron spectroscopy of negative electrodes from high-power lithium-ion cells showing various levels of power fade, Electrochimica Acta, 49 (2004) 5097-5110.

[22]   M. Dhayal, D.M. Ratner, XPS and SPR analysis of glycoarray surface density, Langmuir, 25 (2009) 2181-2187.

[23]   J. Kovac, Surface characterization of polymers by XPS and SIMS techniques, MTAEC9, 45 (2011) 191-197.

[24]   M. Yadav, T. Sarkar, I. Obot, Carbohydrate compounds as green corrosion inhibitors: electrochemical, XPS, DFT and molecular dynamics simulation studies, RSC advances, 6 (2016) 110053-110069.

[25]   A. Suvitha, S. Periandy, S. Boomadevi, M. Govindarajan, Vibrational frequency analysis, FT-IR, FT-Raman, ab initio, HF and DFT studies, NBO, HOMO–LUMO and electronic structure calculations on pycolinaldehyde oxime, Spectrochimica Acta Part A: Molecular and Biomolecular Spectroscopy, 117 (2014) 216-224.

[26]   N. Kovačević, A. Kokalj, Analysis of molecular electronic structure of imidazole-and benzimidazole-based inhibitors: a simple recipe for qualitative estimation of chemical hardness, Corrosion Science, 53 (2011) 909-921.

[27]   S. Kaya, B. Tüzün, C. Kaya, I.B. Obot, Determination of corrosion inhibition effects of amino acids: quantum chemical and molecular dynamic simulation study, Journal of the Taiwan Institute of Chemical Engineers, 58 (2016) 528-535.

[28]   C. Verma, L.O. Olasunkanmi, E.E. Ebenso, M.A. Quraishi, I.B. Obot, Adsorption behavior of glucosamine-based, pyrimidine-fused heterocycles as green corrosion inhibitors for mild steel: experimental and theoretical studies, The Journal of Physical Chemistry C, 120 (2016) 11598-11611.

Computational simulation, surface characterization, adsorption studies and electrochemical investigation on the interaction of guar gum with mild steel in HCl environment

K.O. Shamsheera, R. Prasad Anupama, Joseph Abraham *

Department of Chemistry, University of Calicut, Calicut University P O, Kerala, India

ARTICLE INFO

ABSTRACT

Guar Gum (GG), a water-soluble hetero polysaccharide is used for the interaction study on mild steel (MS) in 0.5 N HCl by weight loss, electrochemical methods, surface monitoring studies, and DFT and MC based quantum chemical calculations. 200 to 800 ppm of the inhibitor was introduced to the medium at 303 to 323 K. The maximum inhibition efficiency (IE) was obtained for 800 ppm of GG. The surface monitoring including FTIR, XPS, FESEM, and AFM studies reveal that GG effectively forms an adsorbed inhibitive layer on the MS surface by substituting pre-adsorbed water molecules and adsorption phenomenon follows the Langmuir model. The computational correlations (DFT and Monte Carlo simulations) justify the experimental observations. Thermodynamic adsorption parameters confirmed that the GG is adsorbed by spontaneous mixed physisorption and chemisorption with tending to physisorption process.

© 2020 The Authors. Published by Elsevier B.V. This is an open access article under the CC BY-NC-ND license (http://creativecommons.org/licenses/by-nc-nd/4.0/).

1. Introduction

Carbohydrate polymer-based novel sustainable green inhibitors are commonly used for the protection of commercial metals in aggressive environments [1]. Superior inhibition properties of these biopolymers are attributed to the large molecular size and presence of various functional groups that barriers the metal surface and prevent the diffusion of corrosives. The environmental concern in worldwide promotes biodegradable and nontoxic inhibitors [2]. GG is an important high molecular weight commercial biopolymer with linearly bonded mannose units and alternate lateral branched galactose groups [3]. The presence of a considerable number of flexible hydroxyl groups in the polymeric structure entertain GG and derivatives for [4] drug delivery [5], metal ion sorbents, wound healing applications [6], and as thickeners/emulsifiers in food products [7]. GG can be employed as a green corrosion inhibitor owing to its non- toxic nature, biodegradability, low cost, and metal ion sorbent action [8]. In recent times, a large number of carbohydrate biopolymers and their derivatives have been successfully developed as effective corrosion inhibitors for metals in different aggressive media [1]. Fenugreek Gum acts as an effective inhibitor for Protection of MS in 1 N HCl and offers an inhibition efficiency of 94%. Molecular dynamics simulations, DFT, radial distribution function and Mean square displacement were used to ascertain the adsorption mode of the Fenugreek Gum on the mild steel surface [9], Gum Arabic was evaluated as a mixed type inhibitor for steel inhibition in acidic medium and showed a high efficiency in protecting steel from corrosive medium at its optimum concentration of 1.0 g/L [10], Guar gum act as an effective inhibitor for protecting carbon steel in sulphuric acid and phosphoric acid media [11,12]. Polyacrylamide grafted guar gum with various grafting levels has been tested as potential green inhibitor against corrosion of mild steel in 1 N HCl. 86% grafted copolymer maintains inhibition efficiency higher than 90% for about 50 h of exposure [13]. MS is an important construction material in industrial and domestic metallic infrastructures. MS being less protected by alloying, its iron content easily gets depreciated when subjected to oxidation or if not properly concentrated. Even though the corrosion cannot be ceased, we can control the rate by introducing inhibitors (containing N, O, & S in major), which can replace pre-adsorbed water molecules and thereby generating a protective surface coverage. The polar centres of inhibitor interact with active sites on metal surface via physical or chemical adsorption [14,15]. Acids are industrially used in pickling, heat exchangers, and in oil well acidizing [15–18]. The recommended concentration of HCl for acid pickling is 5–15% [19]. In water, GG is non-ionic, hydrocolloidal, and not affected by ionic strength or p^H, but will degrade at extreme pH and temperature. The rate of guar gum dissolution and viscosity development

* Corresponding author.
E-mail address: abrahamjoseph@uoc.ac.in (J. Abraham).

Enhanced Protection 0f Mild Steel in HCl Using Synergistic Interaction of Guar Gum and Non-Ionic Surfactants

Chapter 6
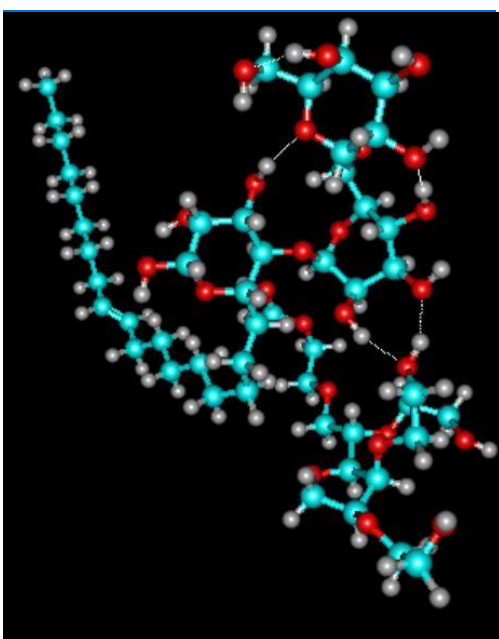
The enhanced corrosion inhibition of guar gum by synergistic interaction with Tween-80 and Triton-X for mild steel in 0.5M HCl is described in this chapter. Various techniques like weight loss study, EIS, PDP, and surface morphological studies were used for monitoring corrosion inhibition mechanism. Quantum chemical studies including NBO and MC simulation studies were also used to confirm the mechanism of corrosion inhibition.

CONTENTS

6.1. Introduction

Synergism is considered as an effective method to improve the performance of solo inhibitors and the synergistic interaction can withstand at higher temperatures for substantial period of time [1]. The synergistic pair of a carbohydrate polymer with other inorganic or organic compounds offered enhanced performance for different metals in various aggressive media[2-4]. The use of surfactants can improve the corrosion inhibition of some synthetic and natural polymers[5, 6]. Mobin et al reported corrosion inhibition of MS via synergistic action of xanthan gum with cationic, anionic, and non-ionic surfactants in 1M HCl[2]. The addition of different surfactants to hydroxyethyl cellulose have significantly increased the inhibition efficiency of carbon steel in 1M HCl solution[3]. Corrosion inhibition of MS in 0.1M H_2SO_4 using starch and surfactants has also been studied by Mobin et al[7]. Herein, the synergistic effects of two non-ionic surfactants (Tween-80 and Triton-X) on the corrosion inhibition performance of GG were studied for MS in 0.5M HCl solution adopting both experimental and theoretical methods.

6.2. Result and Discussion

6.2.1. Weight loss measurement

The corrosion inhibition of MS in 0.5M HCl in the absence and presence of GG, Tween-80 (T-80), Triton-X (T-X), GG: Tween-80 (GT-80), and GG: Triton-X (GT-X) was investigated via weight loss measurement. The corrosion rate and percentage inhibition efficiency (IE) were

tabulated in Table 6.1. Corrosion rate decreases and IE enhances with the addition of GG and 5 ppm of surfactants. When concentration increases greater number of GG molecules are adsorbed on the MS surface by replacing the pre-adsorbed water molecules, that shield the MS surface from the corrosive ions. As the time of immersion extended, the desorption of the inhibitor molecule from the metal surface happens and is responsible for the decrease in IE. It is noticed that the GT-80 or GT-X increases the IE more than either GG or surfactants alone, indicating synergism between GG and surfactants. The synergistic interaction of GG and surfactants causes an increase in IE to 98.10% in the case of GT-80 and 97.95% with GT-X. The synergistic coefficient (S) at different temperatures proposed by Murakawa et al [8] was calculated for describing the combined corrosion inhibition performance of GG with T-80 and T-X

$$S = \frac{1 - IE_{A+B}}{1 - IE'_{A+B}} \qquad (6.1)$$

where $IE_{A+B} = $ (IE$_A$+IE$_B$), IE$_A$ is the IE of GG, IE$_B$ is the IE of surfactant and IE'_{A+B} is the measured IE for GG and surfactant together. If the values of S are greater than 1 which discloses the synergistic action. The synergism parameter in Table 6.1 indicated the strong synergistic interaction between GG and surfactants. The GT-80 is found to be more effective as an inhibitor owing to its large molecular size and electron-donating substituents for MS than GT-X.

Table 6.1. Weight loss data of MS in 0.5M HCl after 24 and 48 hours of immersion

Inhibitor (ppm)	Surfactant (ppm)	Weight loss (g)		CR (mg cm^{-2} hr^{-1})		IE (%)		Synergism parameter	
		24 h	48 h	24 h	48 h	24 h	48 h	24 h	48 h
-	-	0.5334	0.6245	6.173	3.614	-	-	-	-
200	-	0.0715	0.0953	0.8275	0.5515	86.59	84.73	-	-
400	-	0.0540	0.0832	0.6250	0.4814	89.80	86.67	-	-
600	-	0.0212	0.0798	0.2453	0.4618	96.02	87.22	-	-
800	-	0.0144	0.0681	0.1666	0.3940	97.30	89.09	-	-
-	5 T-80	0.1845	0.2548	2.135	1.474	65.41	59.19	-	-
200	5 T-80	0.0235	0.0341	0.2719	0.1973	95.59	94.53	1.596	1.528
400	5 T-80	0.0154	0.0293	0.1782	0.1695	97.11	95.30	1.604	1.536
600	5 T-80	0.0122	0.0228	0.1412	0.1319	97.71	96.34	1.659	1.525
800	5 T-80	0.0101	0.0207	0.1168	0.1197	98.10	96.68	1.665	1.539
-	5 T-X	0.2166	0.2441	2.506	2.777	59.49	54.23	-	-
200	5 T-X	0.0317	0.0569	0.6585	0.3292	94.05	90.88	1.559	1.535
400	5 T-X	0.0192	0.0331	0.2222	0.1915	96.40	94.69	1.554	1.493
600	5 T-X5	0.0132	0.0305	0.1527	0.1765	97.52	95.11	1.601	1.494
800	5 T-X	0.0109	0.0251	0.1261	0.1452	97.95	95.98	1.606	1.498

6.2.2. EIS measurements and corrosion control

The kinetics of electrochemical processes occurring at the MS/electrolyte interface can be analysed with the EIS studies. The impedance values were measured at the OCP. Figure 6.1 shows the EIS plot of MS at the corrosion potentials after one-hour immersion in 0.5M HCl solution containing no inhibitor, T-80, T-X, GG, GT-80, and GT-X at different temperatures (303K- 323K). The Nyquist plots of MS in the absence and presence of inhibitor show single depressed capacitive semicircles and the EIS data were fitted by one -time constant electrical equivalent circuits indicate the charge transfer controlled mechanism of corrosion. Moreover, the semi-circular shapes of the Nyquist plots were secure when GG combined with T-80 and T-X implying that the mechanism of corrosion doesn't altered but better surface coverage has been attained. The impedance data obtained from the Nyquist plot by fitting with an equivalent circuit using Z simp win and are given in Table 6.2. Compared with the blank solution, the diameter of the Nyquist plot increases with the addition of T-X, T-80, and GG. However, the diameter of the Nyquist plot increases intensely in presence of 800ppm of GG and 5ppm of surfactants, showing a better inhibition achieved by the synergistic effect. Higher molecular size and high electron density on the adsorption centres are responsible for the enhanced corrosion inhibition efficiency of GT-80 at all studied temperatures. The decrease in values of double layer capacitance at MS/electrolyte interface of the inhibited solution can be ascribed to the decrease in dielectric constant and/or increase in the double layer thickness due to the better adsorption of GG and surfactants on the surface of MS. R_{ct} values increase with increasing GG concentration [9]. The addition of neutral surfactants to the GG causes a further increase in R_{ct} values. The observed increase in

R_{ct} confirmed the inhibitory action of GG and surfactants through synergistic interaction. The addition of 5 ppm of T-X and T-80 to 800ppm of GG at all studied temperatures causes a decrease in C_{dl} values. The decrease in values of C_{dl} in presence of T-X and T-80 suggests blocking of the active surface of MS.
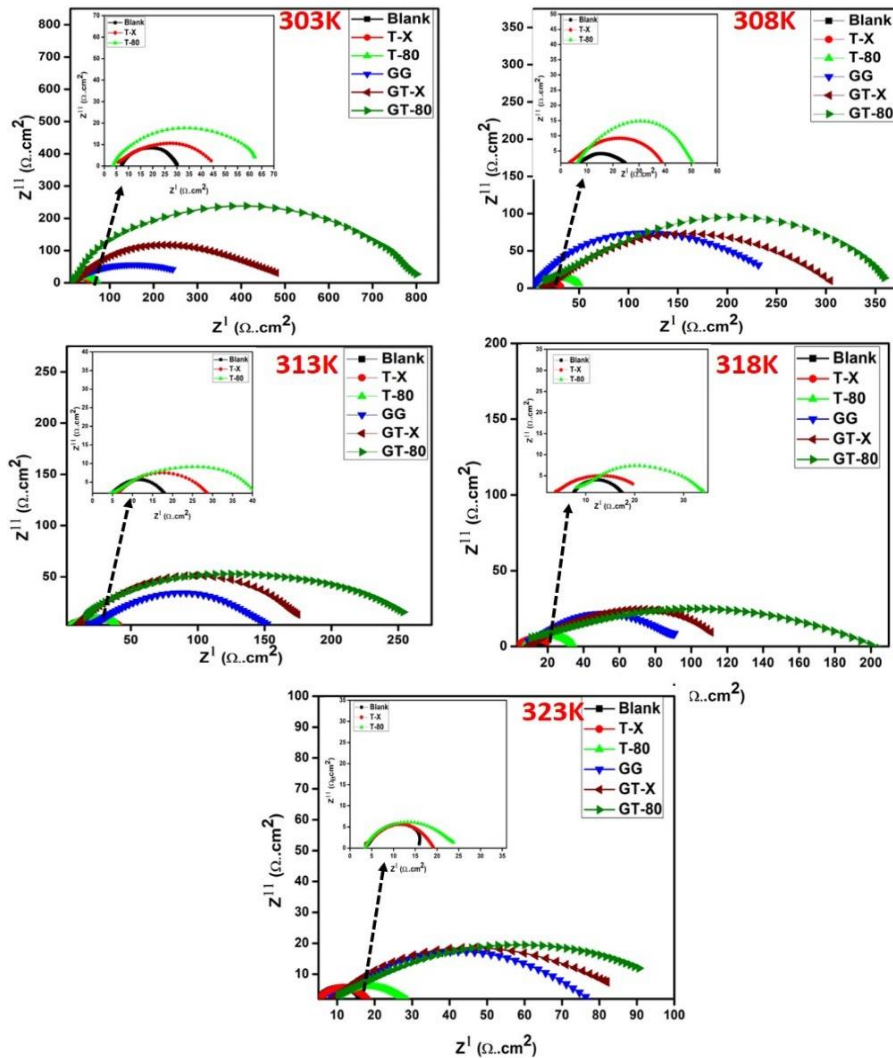
Figure 6.1. Nyquist plot of MS in 0.5M HCl with Blank, T-X, T-80, GG, GT-X, and GT-80 from 303K to 323K

Table 6.2. EIS parameters for corrosion of MS in 0.5M HCl from 303K to 323K

Temperature	Inhibitor	R_s (Ω cm^2)	R_{ct} (Ω cm^2)	n	$Q_{dl} \times 10^{-4}$ S^n Ω^{-1} cm^{-2}	C_{dl} (μF cm^{-2})	CR (mpy)	IE (%)	S
	Blank	7.01	22.84	0.80	10.59	417.6	13.24		
	T-80	3.18	60.03	0.75	3.7604	228.9	4.935	61.95	
	T-X	6.75	41.64	0.80	4.481	271.4	6.460	45.14	
303K	GG	6.85	314.7	0.80	0.79	31.35	1.186	92.74	
	GT-80	9.72	798.3	0.87	0.1570	3.231	0.3787	97.13	1.598
	GT-X	8.31	508.2	0.80	0.1930	6.073	0.594	95.50	1.512
	Blank	5.67	20.50	0.80	14.31	592.2	14.79		
	T-80	6.74	46.4	0.74	7.542	252.4	6.504	55.81	
	T-X	3.82	30.30	0.80	4.021	293.2	7.778	32.34	
308K	GG	2.63	255	0.80	2.90	151.22	1.186	91.96	
	GT-80	8.75	372	0.83	0.3075	8.111	0.816	94.48	1.574
	GT-X	8.80	293.9	0.80	0.4535	15.40	1.029	93.02	1.502
	Blank	5.02	18.91	0.80	15.4	636.1	15.99		
	T-80	2.37	40.42	0.70	3.333	272.55	7.480	53.21	
	T-X	4.04	26.21	0.80	9.930	398.8	11.54	27.85	
313K	GG	15.5	140.7	0.78	2.90	117.6	2.149	86.56	

	GT-80	9.65	255.1	0.82	0.5713	17.05	1.185	92.58	1.515
	GT-X	7.34	175.1	0.81	0.6012	17.92	1.727	89.20	1.468
	Blank	4.40	15.92	0.80	16.25	651.5	18.99		
	T-80	7.05	28.49	0.81	8.946	328.1	10.13	44.12	
	T-X	7.01	20.31	0.78	9.585	423.9	13.05	21.61	
318K	GG	6.64	91.84	0.77	3.37	119.3	3.292	82.66	
	GT-80	10.1	198.8	0.80	0.6200	20.65	1.521	91.99	1.382
	GT-X	10.2	118.3	0.64	0.6411	73.17	2.556	86.54	1.207
	Blank	3.57	13.19	0.78	16.57	757.1	22.92		
	T-80	8.86	21.55	0.80	9.006	336.1	14.03	38.79	
323K	T-X	3.20	16.11	0.78	11.770	516.7	18.73	18.12	
	GG	7.81	62.81	0.79	5.663	269.8	4.814	79.00	
	GT-80	11.5	98.36	0.80	0.9891	31.06	3.093	86.69	1.362
	GT-X	8.79	90.56	0.80	1.959	84.40	3.339	85.46	1.138

6.2.2.1. Effect of temperature on corrosion and activation parameters

The performance of inhibitor and synergistic pairs were studied at elevated temperature up to 323K. The temperature rise may cause the decomposition of protective layer, surface etching and the desorption of inhibitor molecule thereby increasing corrosion rate[10]. The activation energy (Ea) obtained from the Arrhenius plot (Figure 6.2A) of synergistic pairs have much higher values than corresponding blank solutions owing to the better surface coverage which increase the energy barrier for corrosion events to take off and are given in Table 6.3. GT-80 (67.91kJmol^{-1}) holds the highest Ea value and better adsorption is achieved through the more electron rich centres.

Table 6.3. Activation parameters of MS in the absence and presence of inhibitors in 0.5M HCl

Inhibitor	Ea (kJmol^{-1})	ΔH (kJmol^{-1})	ΔS (kJmol^{-1})
Blank	18.54	16.44	-50.08
T-80	36.84	34.35	3.787
T-X	34.98	32.83	-3.767
GT-80	67.91	65.43	84.10
GT-X	62.56	59.39	67.52

The thermodynamic parameters like the entropy of adsorption (ΔS), enthalpy of adsorption (ΔH) for the corrosion process were obtained from the Transition state plot (Figure 6.2B). Higher positive values for ΔH in presence of inhibitor/synergistic pair implies the endothermic nature of metal dissolution and hence difficult to trigger the process[11]. GT-80 have the highest ΔH value (65.43 kJ/mol) and is the most efficient synergistic pair. Also, the high positive values of ΔS indicate

that in the rate determining step, the activated complex undergoes dissociation and disordering during its conversion from the reactants to activated complex[12].
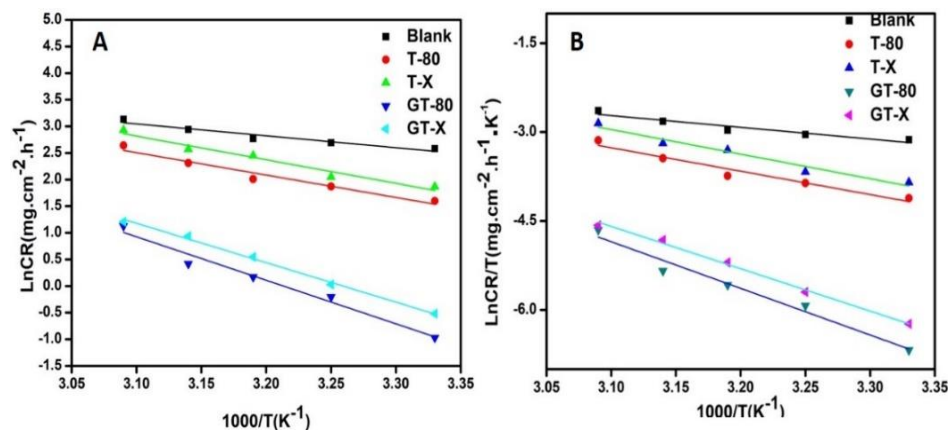

Figure 6.2 A) Arrhenius and B) Transition state plots of MS in 0.5M HCl in the absence and presence of inhibitors

6.2.3. Tafel polarization study (PDP)

Corrosion inhibition of MS using the inhibitor and synergistic pairs was also investigated using the PDP study to complement and confirm the data obtained from weight loss and EIS study. Figure 6. 3 shows the PDP plot of MS at the corrosion potentials after one-hour immersion in 0.5M HCl solution without inhibitor, with T-80, T-X, GG, GT-80, and GT-X at different temperatures (303K- 323K). The PDP parameters obtained in 303K-323K are shown in Table 6.4. The values of I_{corr} decreased continuously with increasing concentration of GG, and further decreased in the presence of surfactants. The maximum IE of 90.85% was observed at GG concentration of 800 ppm indicating that a

higher coverage of GG on the MS surface. The addition of surfactants further improved the IE of GG. The combination of 5 ppm of T-X and T-80 to 800 ppm of GG enhanced the IE to 95.52 and 96.90% at 303K. This value is higher than GG, T-80, and T-X, alone indicating the synergism between GG and surfactants. At higher temperatures also the synergism was sustained with good inhibition efficiency for MS compared to GG and surfactants alone. To effectively evaluate synergistic inhibition, the synergism parameter (S) was calculated using equation 6.1 and the value obtained is greater than one (S >1) at all studied temperatures. The polarization resistance (R_p) values calculated using the Stearn-Geary equation gradually increase from blank to electrolyte having different inhibitor concentrations. The synergistic effect of surfactants is further evident from the fact that the addition of surfactants to GG enhances the value of R_p. The high R_p value of GG with surfactants indicated both GT-80 and GT-X in the acid solution got firmly adsorbed at the MS/electrolyte interface which inhibits polarization of the MS. The Rp value of GT-80 is more pronounced than GT-X which is ascribed due to the better interaction via hydrogen bond between GG and T-80. The results of PDP data are consistent with the result of EIS and weight loss data.
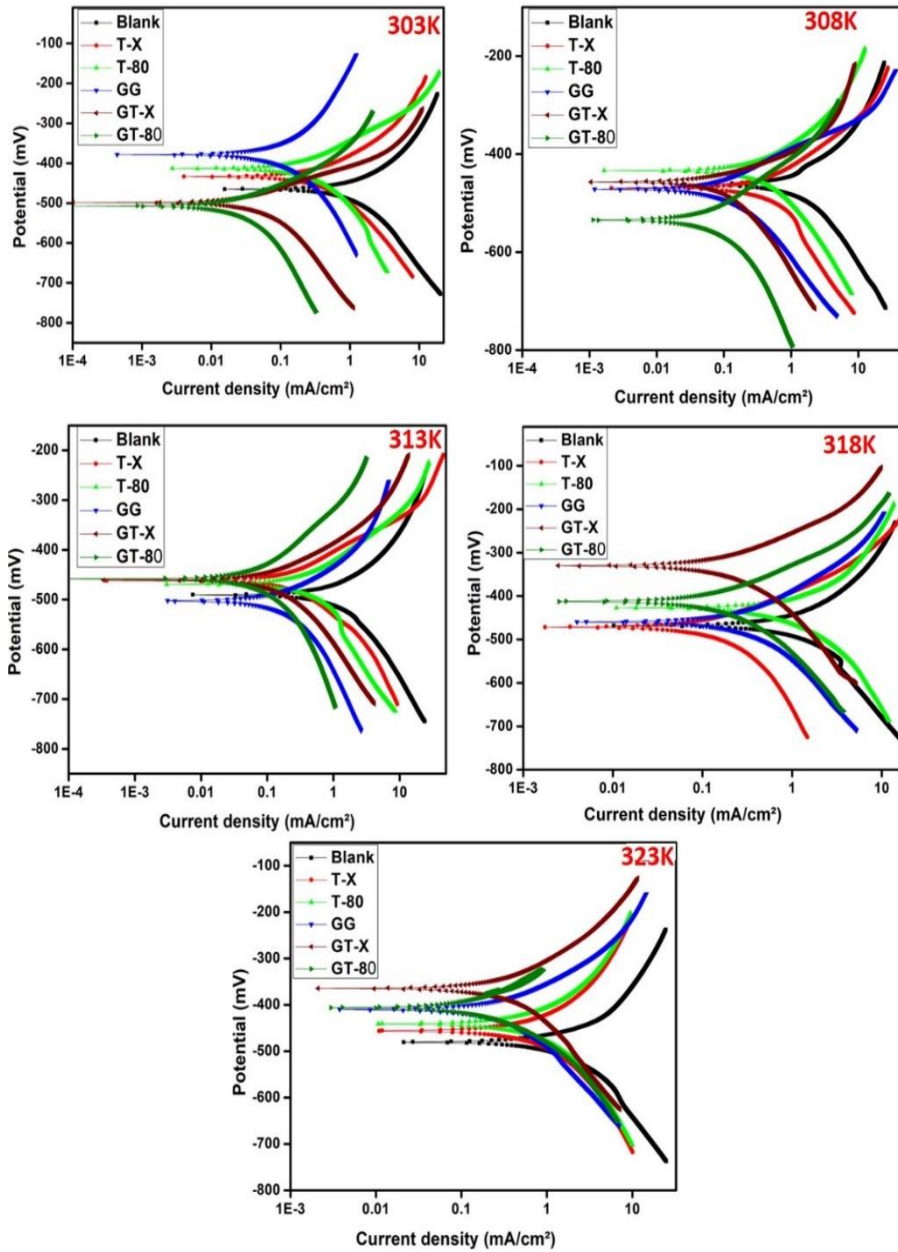
Figure 6.3. PDP plot of MS in 0.5M HCl with Blank, T-X, T-80, GG, GT-X, and GT-80 from 303K to 323K

Table 6.4. PDP parameters of MS in 0.5M HCl from 303K to 323K

Temperature	inhibitor	I_{corr} (mA/ cm^2)	$-E_{corr}$ (mV)	β_a (mV/ dec)	$-\beta_c$ (mV/ dec)	R_p (Ω cm^2)	CR (mpy)	IE (%)	S
	Blank	1.297	460.6	120.7	223.0	26.21	24.37	-	
	T-80	0.2906	413.2	115.3	165.4	101.5	12.61	77.59	
	T-X	0.5207	434.2	138.5	201.1	68.41	12.69	60.91	
303K	GG	0.1186	377.9	200.7	204.7	371.0	2.073	90.85	
	GT-80	0.0401	506.4	117.9	275.5	894.1	1.527	96.90	1.745
	GT-X	0.0580	497.5	78.96	194.8	420.6	1.736	95.52	1.595
	Blank	1.3627	460.2	125.6	157.2	22.25	26.04		
	T-80	0.4095	462.2	92.83	167.3	63.30	14.67	69.94	
	T-X	0.7886	469.5	114.1	205.3	40.38	16.93	42.12	
308K	GG	0.1653	470.8	92.81	157.8	153.5	2.848	87.86	
	GT-80	0.0768	452.1	107.0	190.2	387.2	3.025	94.36	1.679
	GT-X	0.1107	457.2	63.30	179.3	183.5	5.483	91.87	1.419
	Blank	1.4328	471.1	121.0	182.3	22.04	28.06		
	T-80	0.4935	433.7	118.3	181.1	62.95	18.78	65.55	
	T-X	0.9015	462.2	145.3	190.9	39.27	22.37	37.08	
313K	GG	0.2046	394.3	90.64	252.5	141.5	9.383	85.72	
	GT-80	0.0930	457.9	137.3	191.1	373.1	5.583	93.50	1.624

	GT-X	0.1746	459.7	97.03	170.7	153.8	8.019	87.81	1.403
318K	Blank	1.5543	447.6	140.4	182.0	22.14	32.19		
	T-80	0.9065	422.5	152.3	202.9	41.66	22.80	41.67	
	T-X	1.2698	440.4	134.5	240.3	29.55	28.67	18.30	
	GG	0.3421	459.2	140.0	194.3	103.3	9.785	77.99	
	GT-80	0.1553	504.5	129.2	191.2	215.5	6.034	90.01	1.333
	GT-X	0.2016	331.3	108.4	150.8	135.8	8.987	87.02	1.131
323K	Blank	1.8923	475.8	125.6	214.4	18.17	36.70		
	T-80	1.1903	440.4	201.8	239.8	39.97	25.11	37.09	
	T-X	1.6254	426.5	169.2	238.5	26.44	32.00	14.10	
	GG	0.4701	408.7	112.8	195.2	66.05	11.43	75.15	
	GT-80	0.2108	406.9	86.72	185.5	121.7	6.413	88.86	1.266
	GT-X	0.4099	363.6	136.2	205.6	86.79	9.980	78.33	1.141

6.2.4. XPS and surface monitoring

XPS spectra of MS dipped in 0.5M HCl containing the most efficient synergistic pair GT-80 was taken after 24-hour immersion. The coupons were taken out from the electrolyte and rinsed with distilled water to remove electrolyte adhering on the metal surface. Elemental profile on the metal surface is estimated using the wide-scan and the high-resolution XPS spectra. The C1s correction was set at 284.8 eV to calibrate the binding energies. The XPS spectra encounters (Figure 6.4) the peaks of C1s, O1s, and Fe2p. C1s and O1s are mainly attributed to the presence of inhibitors on the metal surface, and the signal of Fe2p arises due to the MS substrate and its corrosion product. The deconvolution of the high peak resolution of Fe 2p spectrum exhibits peak at 710.39eV, 712.50eV, 718.40eV, 723.70eV, and 725.92eV. The first peak at 710.39eV is attributed to ferric compounds such as Fe_2O_3. The peak at 712.50eV is due to FeOOH. The satellite peak of Fe_2O_3 appeared at 718.40eV. Fe2p1/2 of FeO appeared at 723.70eV. Finally, the peak at 725.92eV is attributed to $Fe2p_{1/2}$ due to Fe_3O_4 or FeOOH. The deconvoluted C 1s spectrum for MS in the presence of GT-80 attribute three peaks indicating three chemical forms of C atom present on the MS surface as shown in Figure 6.4(C). The peak at a binding energy of 284.79eV was attributed to C-C or C-H bond in GT-80. The peak at 286.46 eV attributed due to alcohol and ether (C-O-X) in GT-80. The peak at 288.53 eV ascribed to the presence of the carbonyl group probably due to the O-C=O group in tween-80. The O 1s spectra also deconvoluted into three components. The peak at 529.89 eV was attributed to a Fe-O bond. The peak at 531.35eV is attributed to the C-

O bond in C-O-C. The peak at 532.49eV is due to the C-O bond in O-C-O of GG or C=O bond in tween-80[13-17]. The results obtained by XPS analysis supporting the adsorption of inhibitor (GT-80) on the MS surface.
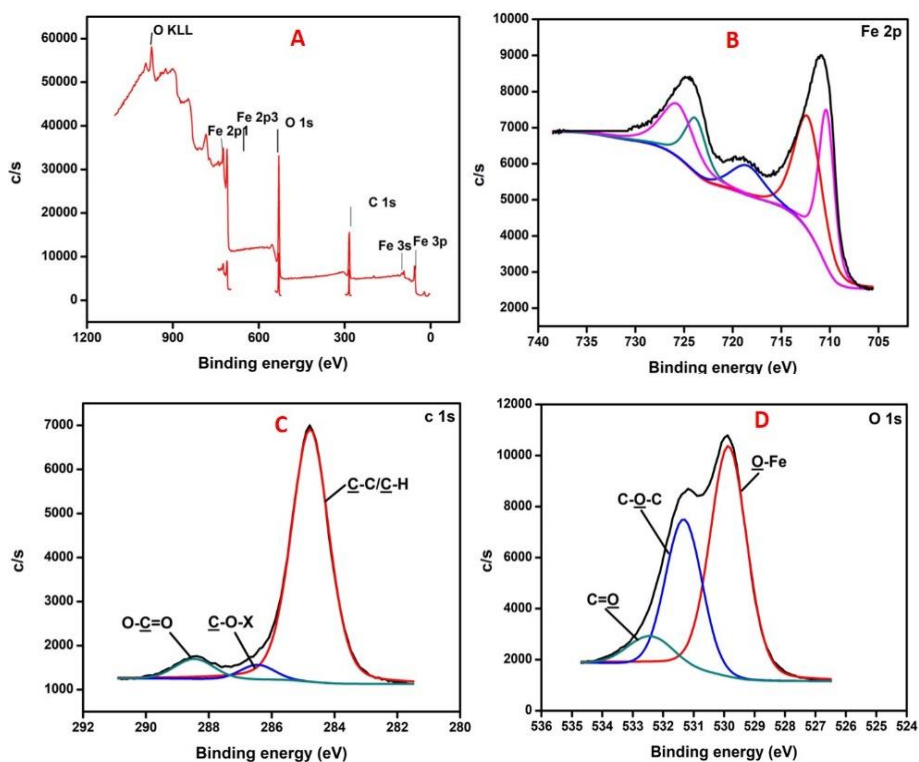

Figure 6.4. The XPS (A) survey scan spectrum and deconvoluted profiles of (B) Fe 2p, (C) C 1s, and D) O 1s for GT-80 treated MS after 24 hours of immersion in 0.5M HCl

6.2.5. Computational quantum studies

Quantum chemical calculations were used to analyse the inhibitor action of GG, T-80, T-X, GT-80, and GT-X. The optimised geometry along with FMOs of T-80 and T-X , GT-X and GT-80 are displayed in Figure 6.5, 6.6, and 6.7. E_{HOMO}, E_{LUMO}, ΔE (energy gap between the LUMO

and HOMO), μ and the global descriptive parameters are tabulated in Table 6.5. The ΔE value gives information about the stability of the inhibitor-metal complex formation. As ΔE value decreases, the reactivity of the inhibitor molecule increases, which enhances the adsorption of the inhibitor molecule on the metal surface and consequently an increase in IE[18]. The inhibitor molecule transfers its electron to the metal if it's ΔN>0 and vice versa[19]. Here, GG could donate electrons from ether, free hydroxyl group to the vacant orbital of metal with a ΔN value of 0.2630. In GT-80 and GT-X, the ΔN value became 0.4048 and 0.3556, which suggested better inhibition of GT-80 over GT-X[20]. The higher ΔN value of GT-80 compared to GT-X is attributed to the presence of more electron donor substituent in GT-80.

Table 6.5. Quantum chemical parameters of T-X, T-80, GT-X, and GT-X

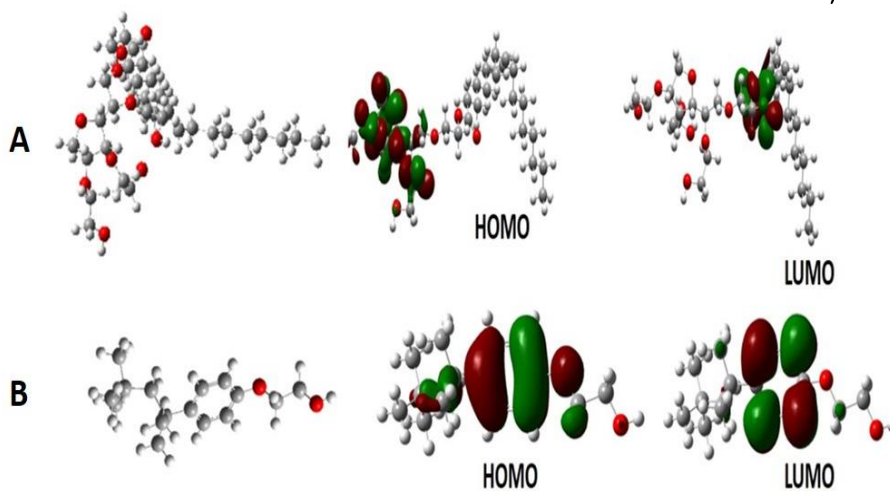| Inhibitor	E_{HOMO} (eV)	E_{LUMO} (eV)	ΔE (eV)	χ (eV)	η (eV)	ΔN
GG	-6.6042	0.9252	7.5294	2.8395	3.7647	0.2630
T-X	-5.9582	0.3227	6.2809	2.8177	3.1405	0.3197
T-80	-6.1117	0.6327	6.7444	2.7395	3.3722	0.3085
GT-X	-5.6589	0.1535	5.8124	2.7527	2.9061	0.3556
GT-80	-5.3715	0.3935	5.7650	2.4801	2.8825	0.4048

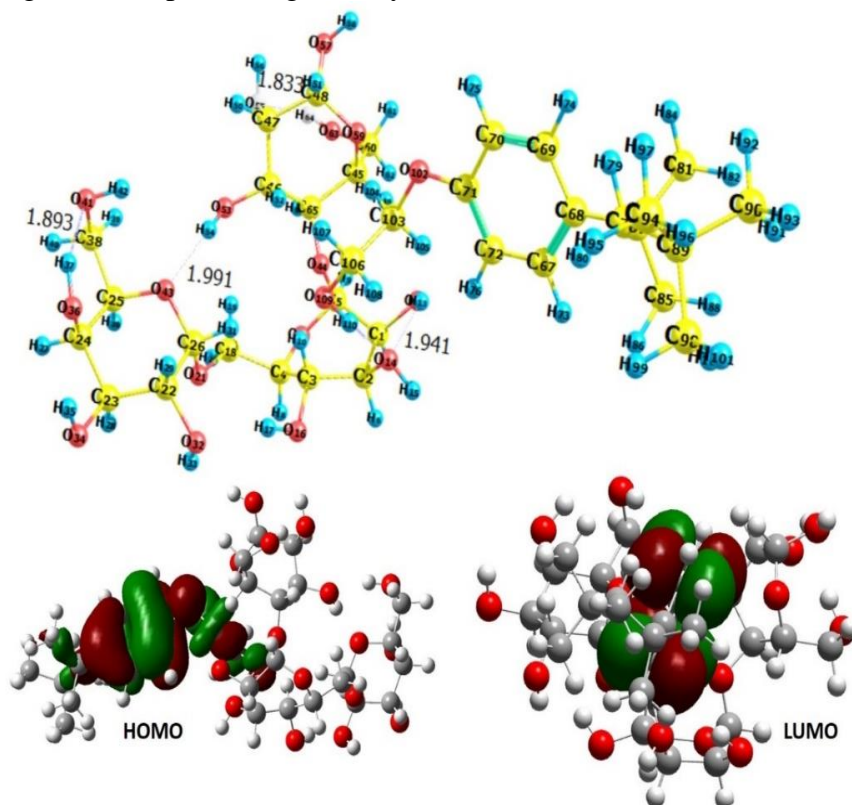Figure 6.5. Optimised geometry and FMOs of A) T-80 and B) T-X

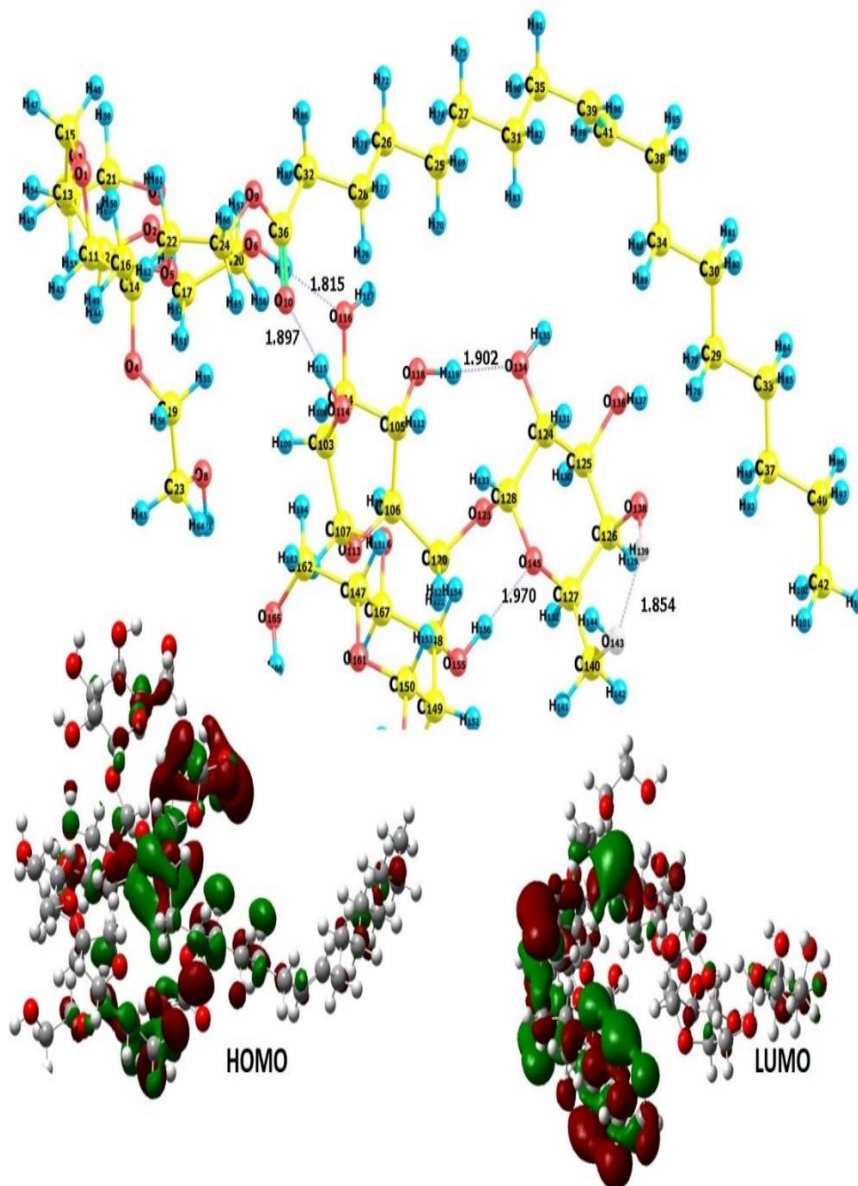Figure 6.6. Optimized geometry with FMO of GT-X

Figure 6.7. Optimized geometry with FMO of GT-80

6.2.6. NBO analysis-Probe of hydrogen bonding

NBO analysis was conducted for GT-80 and GT-X using the DFT/B3LYP/6-31G(d,p) level. The presence of intermolecular

hydrogen bonding between GG and surfactants is clear from the second order perturbation theory from NBO analysis. The hydrogen bond energies are manifested in the form of stabilization energy (E2). As the strength of hydrogen bonding increases, the stabilization energy (E2) also increases. More favourable stabilization energies are achieved in the NBO due to the strong inter and intramolecular hydrogen bond network for GT-80 and GT-X, and the details of intermolecular hydrogen bonding interactions are listed in Table 6.6. The intermolecular hydrogen bonding of GT-80 is established due to the delocalization of the lone pair LP(1) of O10 with an electron density (ED) value of 1.96109e and LP(2) of O10 with ED value of 1.84589e to the σ* bond of O114 - H115 with ED value of 1.99716e, thereby yielding stabilization energies of 6.87 and 7.58 kcal mol^{-1}, respectively. Similarly, the transfer of LP(1) of O116 with ED value of 1.96588e and LP(2) of O116 with ED value of 1.93278e to σ* of O6 - H67 with ED value of 1.99715e yields stabilization energies of 2.14 and 17.50 kcal mol^{-1}, respectively. For GT-X, the network of intermolecular hydrogen bonding is obtained due to LP(1) of O14 with ED value of 1.90435e and LP(2) of O14 with ED value of 1.96788e transferring to the σ* bond of O109 - O110   with ED value of 1.98799e yield stabilization energies of 5.68 and 13.56 kcal mol^{-1}, respectively[21-24]. Thus, these NBO results reveal the presence of strong intermolecular hydrogen bonding in GT-80 and GT-X. Moreover, in GT-80, due to the presence of two strong intermolecular hydrogen bonding more electron-donating substituents donate free electrons to the vacant metal orbital.

Table 6.6. NBO results for GT-80 and GT-X at the DFT/B3LYP/6-31G(d,p) level

Compound	Donor(i)	Type	ED	Acceptor(j)	Type	ED	E(2) kcal/mol	E(j)-E(i) a.u.	F(i,j) a.u.
	O 10	LP(1)	1.96109	O 114 - H 115	σ *	1.99716	6.87	1.18	0.080
	O 10	LP(2)	1.84589	O 114 - H 115	σ *	1.99716	7.58	0.77	0.070
Inter-HB in GT-80	O 116	LP(1)	1.96588	O 6 - H 67	σ *	1.99715	2.14	0.98	0.041
	O 116	LP(2)	1.93278	O 6 - H 67	σ *	1.99715	17.50	0.92	0.114
Inter-HB in GT-X	O 14	LP(1)	1.90435	O 109 - O 110	σ *	1.98799	5.68	1.08	0.070
	O 14	LP(2)	1.96788	O 109 - O 110	σ *	1.98799	13.56	0.85	0.081

ED is electron density, Inter means intermolecular hydrogen bonding, Intra means intramolecular hydrogen bonding, and HB means hydrogen bonding. E (2) is the energy of hyperconjugative interaction (stabilization energy in kcal/mol). E(j)-E(i) is the energy difference between the donor and acceptor i and j NBO orbitals. F(i; j) is the Fock matrix element between the i and j NBO orbitals

6.2.7. Monte Carlo Simulation (MC)

To supplement the experimental result, MC simulation studies has been done to explore the inhibitor-metal interaction in the presence of aqueous electrolytic environment. The final snapshot of each inhibitor on Fe (110) plane from the last step of MC simulations is given in Figure 6.8. In the final simulation snapshots, it is realized that all adsorbed inhibitors aligned almost completely parallel relative to the iron surface, providing good surface coverage which accounts for improved corrosion inhibition [25]. From the adsorption energy values, it is clear that both GT-80 and GT-X firmly adsorbed on the MS surface. Therefore, the synergistic effect of the inhibitors exhibits greater inhibition compared to GG, T-80, and T-X alone. The high adsorption energy of GT-80 (-7.046×10^3 kJ/mol) and better efficiency than GT-X (-6.947×10^3 kJ/mol) may be explained as due to the presence of greater number of functional groups. Further, the differential adsorption energy of GG in GT-80 (-221.97 kJ/mol) is more compared to GG in GT-X (-213.37 kJ/mol), which indicated that GG adsorbs more firmly in combination with T-80 than T-X on the MS surface.
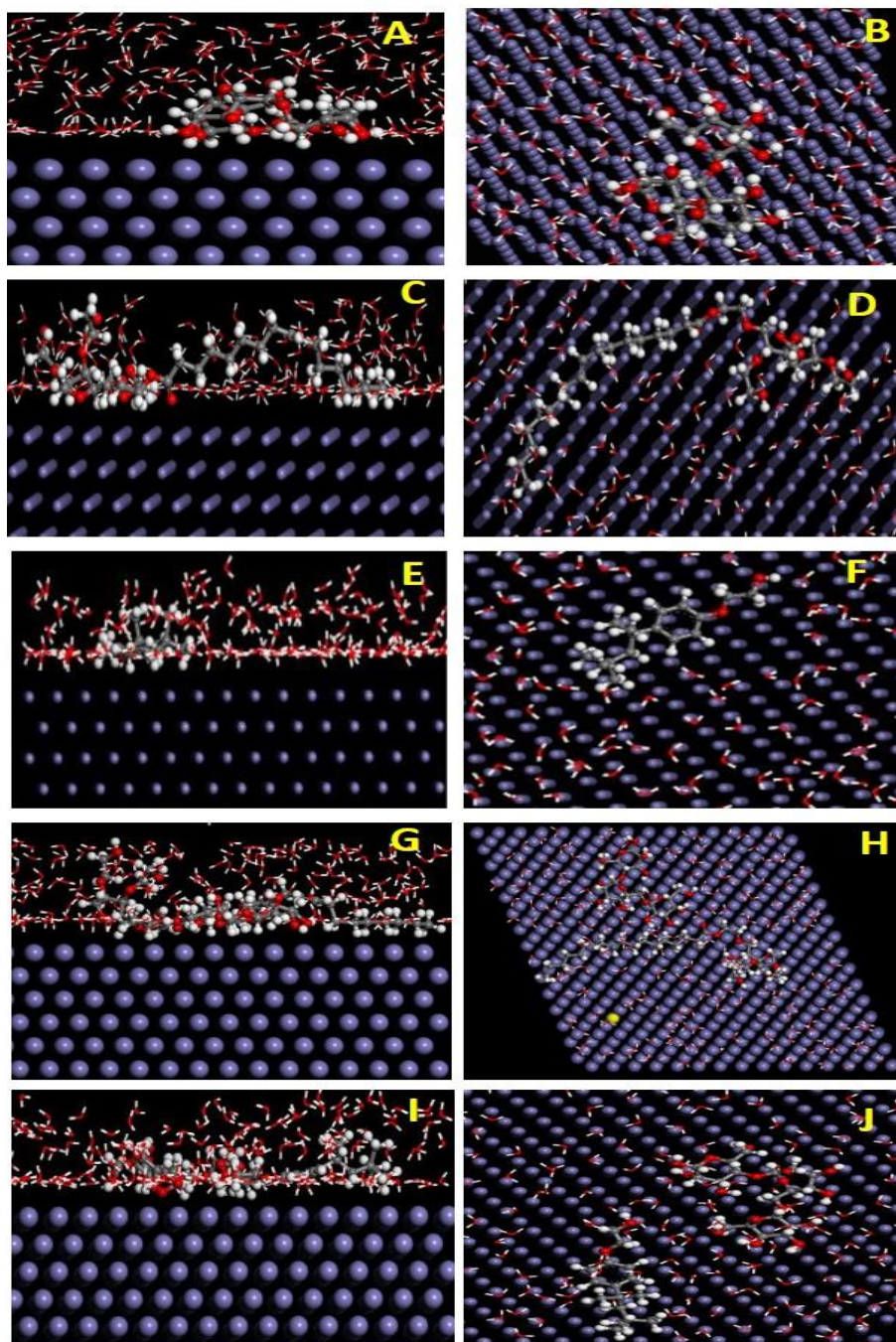
Figure 6.8. Side and top view of (A&B)GG, (C&D)T-80, (E&F)T-X, (G&H)GT-80, and (I&J)GT-X adsorption on Fe (110) surface

6.2.8. Microscopic studies and surface examination (FESEM and AFM)

The changes in surface morphology of the MS sample after 24-hour exposure in 0.5M HCl in the absence and presence of inhibitor combinations were monitored via FESEM micrographs (Figure 6.9). In the absence of inhibitor, more noticeable defects such as cracks and pits were observed on the surface of MS due to severe corrosion whereas in the presence of inhibitor combination the MS surface is found to be more protected and devoid of much defects.
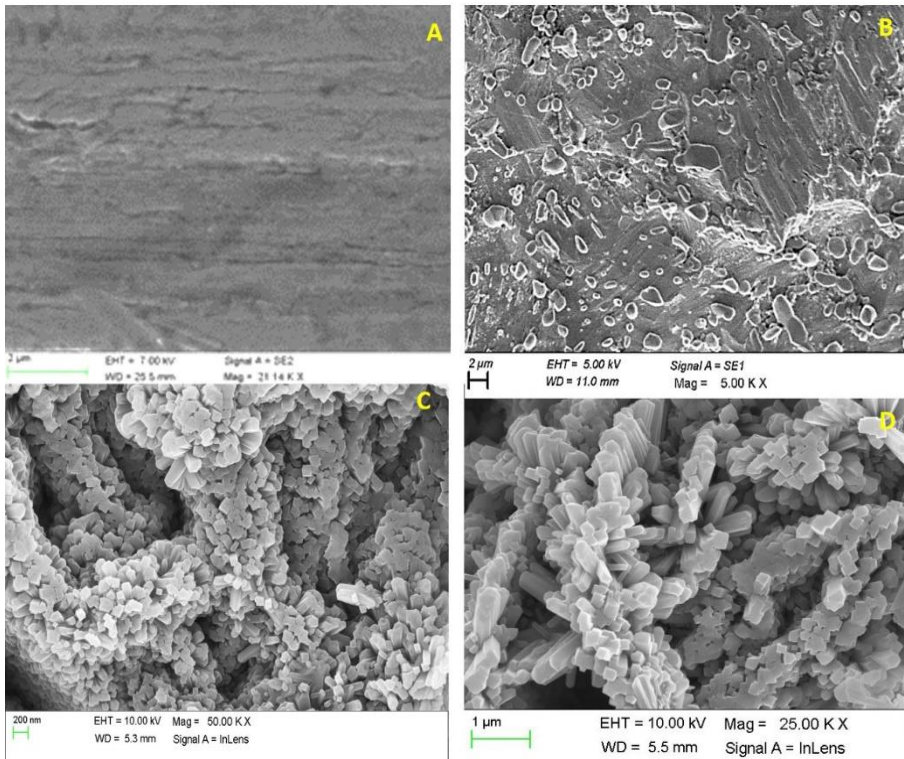

Figure 6.9. FESEM images of A) and B) blank before and after immersion C) GT-80, and D) GT-X of MS in 0.5M HCl after 24-hour immersion

AFM micrographs were recorded to measure surface roughness of the sample in the absence and presence of inhibitors (GT-X and GT-80) in 0.5M HCl after 24 hours of immersion. Figure 6.10 reveals the surface roughness of MS in the absence of inhibitor after 24 hours of immersion as 237.84 nm, 27.2nm with GT-80, and 28.9 nm with GT-X. The lowering of surface roughness in the presence of inhibitor combination indicates the formation of a protective layer on the MS surface by replacing the pre-adsorbed water molecules.
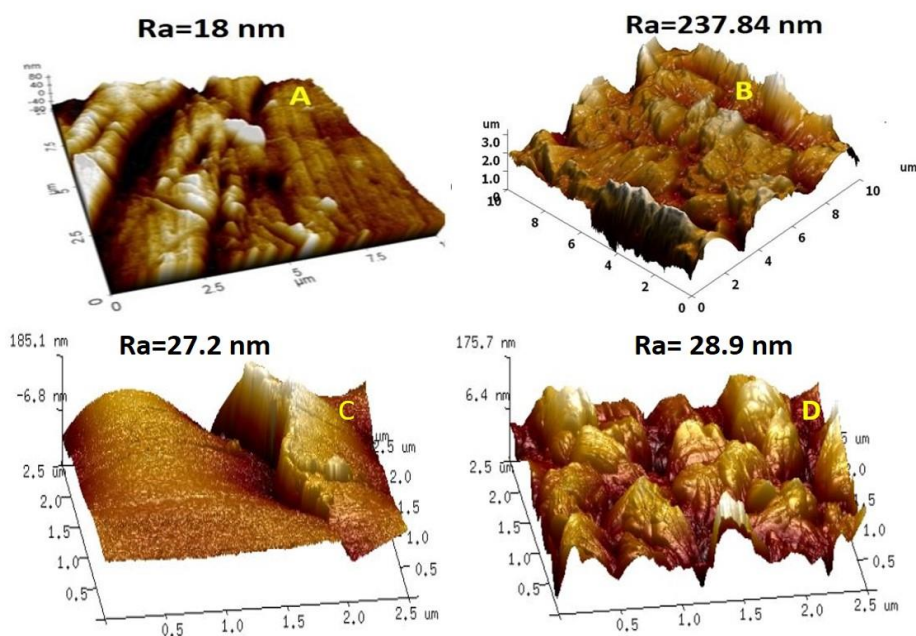

Figure. 6.10. AFM images of A) and B) blank before and after immersion C) GT-80, and D) GT-X of MS in 0.5M HCl after 24-hour immersion

6.3. Conclusions

The addition of two non-ionic surfactants Tween-80 and Triton-X synergistically increased the inhibition efficiency of Guar Gum; the effect of Tween-80 is more pronounced than Triton-X due to the presence of more electron donor substituents. Corrosion inhibition of Guar Gum and surfactants via synergistic interaction was confirmed by weight loss, EIS and PDP measurements. Quantum chemical calculations and Monte Carlo simulation also confirmed that the Guar Gum could cooperate with the two non-ionic surfactants and synergistically inhibit the corrosion of MS in 0.5M HCl. NBO analysis further confirmed the higher inhibition efficiency of GT-80 than GT-X.

References

[1]   K. Ramya, R. Mohan, K. Anupama, A. Joseph, Electrochemical and theoretical studies on the synergistic interaction and corrosion inhibition of alkyl benzimidazoles and thiosemicarbazide pair on mild steel in hydrochloric acid, Materials Chemistry and Physics, 149 (2015) 632-647.

[2]   M. Mobin, M. Rizvi, Inhibitory effect of xanthan gum and synergistic surfactant additives for mild steel corrosion in 1 M HCl, Carbohydrate polymers, 136 (2016) 384-393.

[3]   M. Mobin, M. Rizvi, Adsorption and corrosion inhibition behavior of hydroxyethyl cellulose and synergistic surfactants additives for carbon steel in 1 M HCl, Carbohydrate polymers, 156 (2017) 202-214.

[4]   S. Umoren, I. Obot, E. Ebenso, Corrosion inhibition of aluminium using exudate gum from Pachylobus edulis in the presence of halide ions in HCl, E-Journal of Chemistry, 5 (2008).

[5]   R. Aslam, M. Mobin, J. Aslam, H. Lgaz, I.-M. Chung, Inhibitory effect of sodium carboxymethylcellulose and synergistic biodegradable gemini surfactants as effective inhibitors for MS corrosion in 1 M HCl, Journal of Materials Research and Technology, 8 (2019) 4521-4533.

[6]   M. Mobin, M.A. Khan, Investigation on the adsorption and corrosion inhibition behavior of gum acacia and synergistic surfactants additives on mild steel in 0.1 M H2SO4, Journal of dispersion science and technology, 34 (2013) 1496-1506.

[7]   M. Mobin, M. Khan, M. Parveen, Inhibition of mild steel corrosion in acidic medium using starch and surfactants additives, Journal of Applied Polymer Science, 121 (2011) 1558-1565.

[8]   T. Murakawa, T. Kato, S. Nagaura, N. Hackerman, A contribution to the understanding of the synergistic effect of anions for the corrosion inhibition of Fe by amines, Corrosion science, 8 (1968) 483-489.

[9]   K. Shamsheera, R.P. Anupama, J. Abraham, Computational simulation, surface characterization, adsorption studies and electrochemical investigation on the interaction of guar gum with mild steel in HCl environment, Results in Chemistry, (2020) 100054.

[10]   P.R. Ammal, M. Prajila, A. Joseph, Effect of substitution and temperature on the corrosion inhibition properties of benzimidazole bearing 1, 3, 4-oxadiazoles for mild steel in sulphuric acid: physicochemical and theoretical studies, Journal of environmental chemical engineering, 6 (2018) 1072-1085.

[11]   M.V. Fiori-Bimbi, P.E. Alvarez, H. Vaca, C.A. Gervasi, Corrosion inhibition of mild steel in HCL solution by pectin, Corrosion science, 92 (2015) 192-199.

[12]   F. Bentiss, M. Lebrini, M. Lagrenée, Thermodynamic characterization of metal dissolution and inhibitor adsorption processes in mild steel/2, 5-bis (n-

thienyl)-1, 3, 4-thiadiazoles/hydrochloric acid system, Corrosion Science, 47 (2005) 2915-2931.

[13]   B. Chugh, A.K. Singh, D. Poddar, S. Thakur, B. Pani, P. Jain, Relation of degree of substitution and metal protecting ability of cinnamaldehyde modified chitosan, Carbohydrate Polymers, 234 (2020) 115945.

[14]   W. Zhang, H.-J. Li, M. Wang, L.-J. Wang, Q. Pan, X. Ji, Y. Qin, Y.-C. Wu, Tetrahydroacridines as corrosion inhibitor for X80 steel corrosion in simulated acidic oilfield water, Journal of Molecular Liquids, 293 (2019) 111478.

[15]   M. Ahangar, M. Izadi, T. Shahrabi, I. Mohammadi, The synergistic effect of zinc acetate on the protective behavior of sodium lignosulfonate for corrosion prevention of mild steel in 3.5 wt% NaCl electrolyte: Surface and electrochemical studies, Journal of Molecular Liquids, (2020) 113617.

[16]   Y. Luo, M.-S. Balogun, W. Qiu, R. Zhao, P. Liu, Y. Tong, Sulfurization of FeOOH nanorods on a carbon cloth and their conversion into Fe 2 O 3/Fe 3 O 4–S core− shell nanorods for lithium storage, Chemical Communications, 51 (2015) 13016-13019.

[17]   J. Geng, J. Liu, J. Yan, M. Ba, Z. He, Y. Li, Chemical composition of corrosion products of rebar caused by carbonation and chloride, International Journal of Corrosion, 2018 (2018).

[18]   A. Suvitha, S. Periandy, S. Boomadevi, M. Govindarajan, Vibrational frequency analysis, FT-IR, FT-Raman, ab initio, HF and DFT studies, NBO, HOMO–LUMO and electronic structure calculations on pycolinaldehyde oxime, Spectrochimica Acta Part A: Molecular and Biomolecular Spectroscopy, 117 (2014) 216-224.

[19]   N. Kovačević, A. Kokalj, Analysis of molecular electronic structure of imidazole-and benzimidazole-based inhibitors: a simple recipe for qualitative estimation of chemical hardness, Corrosion Science, 53 (2011) 909-921.

[20]   H. Ju, Z.-P. Kai, Y. Li, Aminic nitrogen-bearing polydentate Schiff base compounds as corrosion inhibitors for iron in acidic media: a quantum chemical calculation, Corrosion Science, 50 (2008) 865-871.

[21]   F. Hammami, H. Ghalla, S. Nasr, Intermolecular hydrogen bonds in urea–water complexes: DFT, NBO, and AIM analysis, Computational and Theoretical Chemistry, 1070 (2015) 40-47.

[22]   T. Polat, F. Bulut, I. Arıcan, F. Kandemirli, G. Yildirim, Vibrational assignments, spectroscopic investigation (FT-IR and FT-Raman), NBO, MEP, HOMO−LUMO analysis and intermolecular hydrogen bonding interactions of 7-fluoroisatin, 7-bromoisatin and 1-methylisatin−A comparative study, Journal of Molecular Structure, 1101 (2015) 189-211.

[23]   B. Shainyan, N. Chipanina, T. Aksamentova, L. Oznobikhina, G. Rosentsveig, I. Rosentsveig, Intramolecular hydrogen bonds in the

sulfonamide derivatives of oxamide, dithiooxamide, and biuret. FT-IR and DFT study, AIM and NBO analysis, Tetrahedron, 66 (2010) 8551-8556.

[24]   A. Saeed, A. Khurshid, M. Bolte, A.C. Fantoni, M.F. Erben, Intra-and intermolecular hydrogen bonding and conformation in 1-acyl thioureas: An experimental and theoretical approach on 1-(2-chlorobenzoyl) thiourea, Spectrochimica Acta Part A: Molecular and Biomolecular Spectroscopy, 143 (2015) 59-66.

[25]   S. Kaya, B. Tüzün, C. Kaya, I.B. Obot, Determination of corrosion inhibition effects of amino acids: quantum chemical and molecular dynamic simulation study, Journal of the Taiwan Institute of Chemical Engineers, 58 (2016) 528-535.

Effect of surfactant addition to Guar Gum and protection of mild steel in hydrochloric acid at high temperatures: Experimental and theoretical studies

K.O. Shamsheera, Anupama R. Prasad, P.K. Jaseela, Abraham Joseph *

Department of Chemistry, University of Calicut, Calicut University, Kerala, India

A B S T R A C T

Guar Gum (GG) is an established green inhibitor for mild steel (MS) corrosion in acidic media. The inhibitor action of GG is enhanced by the synergistic interaction with two non-ionic surfactants (Tween -80 and Triton-X). The synergistic pairs were investigated for MS corrosion in 0.5 M HCl using weight loss and electrochemical methods. The synergistic interactions were monitored via theoretical calculations using NBO analysis implemented in Gaussian-09 packages. AFM, SEM, and XPS spectra were carried out to understand the surface events. Computational calculations (DFT and Monte Carlo simulation) were performed to ensure the synergistic action of GG and surfactants. Experimental results revealed that GG:Tween -80 offers 97.13% and GG:Triton-X has 95.50% inhibition efficiency when used in 800: 5 ppm ration at 303 K. The synergistic pairs exhibited remarkable efficiencies at elevated temperatures also.

© 2021 Elsevier B.V. All rights reserved.

1. Introduction

Due to excellent mechanical properties and cost-effectiveness, mild steel is extensively used as construction and engineering material in a variety of chemical and petrochemical industries [1,2]. During applications, it is often exposed to aggressive acid solutions and corrodes heavily. Owing to the consequential economic and environmental impact the acid corrosion of mild steel needs to be controlled by adopting appropriate prevention strategies. Various types of inhibitor molecules and their combinations are usually practiced to address the issue. Carbohydrate polymers can prevent corrosion of mild steel in different corrosive environments owing to their electron-donating functional groups and large molecular size [3]. Guar Gum is a natural non-ionic polysaccharide with linearly bonded mannose unit and lateral branched galactose groups linked through glycosidic linkages. Structurally GG consists of D-mannopyranosyl backbone (β-1 → 4 glycosidic linkage) along with D-galactopyranosyl side branching (α-1 → 6 glycosidic linkages) in a ratio of 1.5 to 2. The existence of significant number of hydroxyl groups in the GG polymer accounts for the inhibitor action [4]. Synergism is an effective method to improve the performance of a solo inhibitor and the synergistic action can withstand at higher temperatures [5]. The synergistic pairs of a carbohydrate polymer with other inorganic or organic compounds offered enhanced performance for different metals in variable aggressive media [6–8]. The use of

surfactants can improve the corrosion inhibition of some synthetic and natural polymers [9,10]. Mobin et al. reported corrosion inhibition of mild steel via synergistic action of xanthan gum with cationic, anionic, and non-ionic surfactants in 1 M HCl [6]. The addition of different surfactants to hydroxyethyl cellulose have significantly increased the inhibition efficiency of carbon steel in a 1 M HCl solution [7]. Corrosion inhibition of mild steel in 0.1 M H_2SO_4 using starch and surfactants has been studied by Mobin et al. [11]. Herein, the synergistic effects of two non-ionic surfactants (Tween-80 and Triton-X) on the corrosion inhibition performance of GG were studied for mild steel corrosion in 0.5 M HCl solution via experimental and theoretical evaluations. In our previous work, GG could protect mild steel from an acidic environment. However, at elevated temperatures, the inhibition efficiency was decreased gradually [12]. Synergism is an effective method to improve the performance of a solo inhibitor and the synergistic action can withstand at higher temperatures. To the best of our belief this is the first report on the synergistic interaction of two bulk molecules involving theoretical calculations and its correlation with experimental results.

2. Materials and method

2.1. Materials

Analytical reagent grade Guar Gum powder extracted from the endosperm of guar bean of the family *leguminosae* is obtained from Himedia Laboratories Pvt. Ltd., Mumbai, India (Mw = 3.0 × 10⁶ g/mol). It possesses the galactomannan ratio of >70%, moisture content

---

* Corresponding author.
  E-mail address: abrahamjoseph@uoc.ac.in (A. Joseph).

Protection of Mild Steel in HCl using Pectin Isolated from Jack Fruit Waste Products

Chapter 7
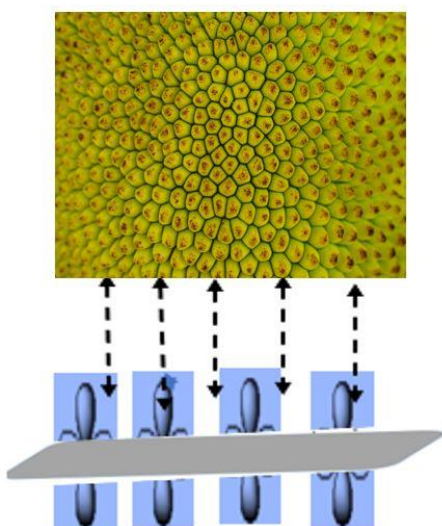
This chapter illustrates the corrosion inhibition performance of pectin isolated from jack fruit peel waste for mild steel in 0.5M HCl. Weight loss, EIS, and PDP measurements were used for the monitoring of corrosion. FESEM and AFM were used to judge the adsorptive nature of the pectin in the acid solution. The electronic and structural information of pectin was disclosed by DFT and Monte Carlo simulation studies.

CONTENTS

7.1. Introduction

Jack fruit (*Artocarpus heterophyllus),* known as the poor man's fruit is one of the largest edible fruits grown worldwide. But a significant amount of jack fruit peel is discarded as waste, leading to environmental problem. Recovery of the useful compounds from agricultural waste and by-product is a novel research movement. Pectin is a valuable by-product that can be isolated from jack fruit waste using different techniques[1]. The purpose of this study is to utilize jack fruit peel waste as a potential source for pectin production and as MS corrosion inhibitor that is beneficial to our environment and economy. It also concerning global environmental issues to encourage the use of renewable resources. The extraction of pectin from jackfruit peel waste is given in chapter 2 (sec. 2.4.6).

7.2. Result and discussion

7.2.1. Pectin yield

Antony et al could isolate about 39.05% of pectin from jack fruit waste using 0.05N oxalic acid at 90°C for 60 minutes. But in this study, the yield of pectin isolated using the same condition as that of Antony et al was only 35.05% determined using equation 2.1. The low yield of pectin might be due to environmental growth conditions and the variety of jack fruit.

7.2.2. FTIR

The FTIR spectra of jack fruit pectin (JP) and JP scratched from the surface of MS after 24 hours of immersion are given in Figure 7.1.

Absorption about 3426cm^{-1} arises due to the O-H stretching frequency of polysaccharide. The peak at 1744cm^{-1} was ascribed to the carbonyl stretching frequency of the methyl ester group in pectin. The carbonyl stretching frequency of the carboxyl group in galacturonic acid appeared at 1639cm^{-1}. The asymmetric and symmetric C-H stretching frequency of methyl esters of galacturonic acid appeared at 2924cm^{-1} and 2830cm^{-1}. The spectra of JP adsorbed on MS surface shows a decrease in intensity of O-H stretching and bending frequency due to the association of JP molecule with the MS surface[2-4]. The intensity of carbonyl stretching frequency of acid and ester group in JP at 1744cm^{-1} and 1639cm^{-1} get decreased upon complex formation with the metal atom.
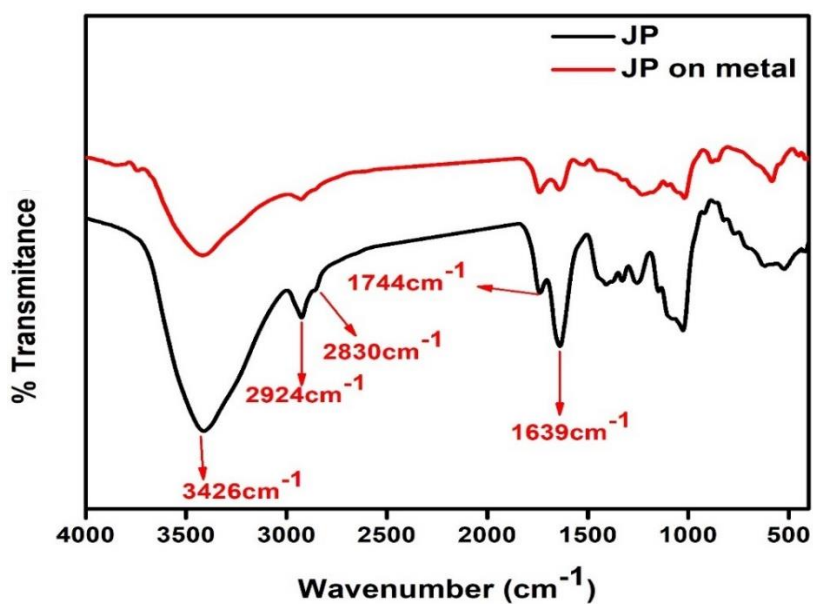

Figure 7.1. FTIR spectra of JP and JP on MS after 24 hours immersion in 0.5M HCl

7.2.3. Weight loss measurement

The CR and IE of MS obtained from weight loss study for the various concentration of JP are exhibited in Table 7.1. The data indicated that CR of MS decreased with an increase in the concentration of JP molecule. The inhibition of MS corrosion in the presence of JP is attributed to the adsorption of the inhibitor molecule on the surface of the metal atom by replacing pre-adsorbed water molecules, which isolates the MS from corrosive ions. JP could be adsorbed on the surface of MS by the interaction between lone pair of electrons on oxygen atoms and vacant orbital of the metal atom. At higher concentration, the inhibitor molecule could form a protective film of JP which inhibit the diffusion of electrolyte from aggressive media onto the metal surface. Maximum IE and hence maximum surface coverage were observed at 1000ppm of pectin.

Table 7.1. Weight loss data of MS in 0.5M HCl in the absence and presence of JP after 24 hours of immersion

Concentration of Pectin (ppm)	Weight loss (g)	CR (mg cm^{-2} hr^{-1})	IE (%)	(θ)
Blank	0.4256	4.925	-	-
250	0.1256	1.453	70.49	0.7049
500	0.0862	0.9976	79.74	0.7974
750	0.0443	0.5127	89.59	0.8959
1000	0.0343	0.3969	91.94	0.9194

7.2.4. EIS measurements

The electrochemical corrosion study of MS in 0.5M HCl in the absence and presence of varying concentrations of JP from 303-323K was investigated using the EIS technique as shown in Figure 7.2. To establish which equivalent circuit best fits the experimentally obtained data, the EIS results were fitted with an appropriate equivalent circuit using Zsimp win software. The decrease in C_{dl} values of MS in the presence of JP compared to the uninhibited solution is due to decreased dielectric constant at the metal electrolyte interface and hence better adsorption of JP on the surface of MS. Effective corrosion resistance is associated with low C_{dl} value and high R_{ct} values. The EIS data reported in the Table 7.2 showed that R_{ct} value increases with increasing the concentration of JP, and C_{dl} values tend to decrease, which indicated that IE increases with an increase in JP concentration. At 1000ppm the JP molecule forms a protective film on MS surface and blocking the diffusion of aggressive ions from the electrolyte. Moreover, with an increase in temperature from 303K to 323K, the C_{dl} values increases, and R_{ct} values decreases, and hence IE decreases, which is attributed to the desorption of JP molecule from the MS surface at higher temperatures. 1000ppm of pectin extracted from jack fruit peel could provide 87.53% efficiency at 303K in 0.5M HCl.
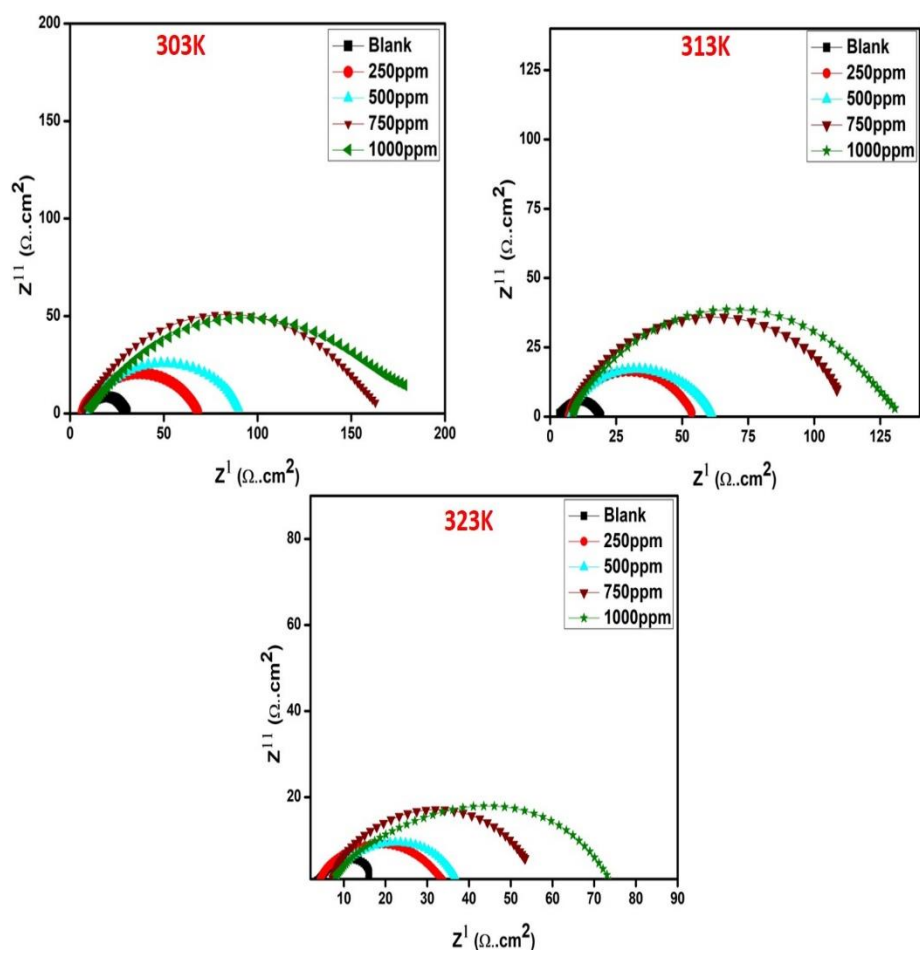
Figure 7.2. EIS plot of MS in 0.5M HCl in the absence and presence of different concentrations of JP from 303-323K

7.2.4.1. Adsorption isotherm

The corrosion inhibition of metal atom depends on the tendency of an inhibitor molecule to adsorb on the MS surface by replacing pre-adsorbed water molecules. JP donates its free electrons to the vacant d orbital of the metal atom and hence the formation of an adsorbed protective layer [5]. Data obtained from the EIS study were used graphically for fitting various isotherm including Frumkin, Temkin, and Langmuir. For JP the Langmuir adsorption isotherm gave the best fit (Figure 7.3). The degree of surface coverage (θ) increases with increasing the concentration of JP and decreases on raising the temperature from 303K to 323K. From the intercept of the Langmuir adsorption isotherm, K_{ads} was calculated for the adsorption of JP on the MS surface. The value of K_{ads} may be taken as a strength of the adsorption forces between the metal surface and the inhibitor molecule. The high value of K_{ads} (6.05) at 303K shows effective adsorption of JP on the surface of MS and gets decreased when the temperature is raised (4.24 at 323K). The value of ΔG^0 and K_{ads} at studied temperatures are listed in Table 7.3. The negative value of ΔG^0 ensures the spontaneous adsorption of JP on the MS surface. In general, the value of ΔG^0_{ads} around -20 kJ/mol or lower are considered as physisorption, and around -40 kJ/mol or more negative are considered as chemisorption[6]. So, it can be realized from the ΔG^0 values that the JP adsorbed physically on the MS surface.

Table 7.2. Parameters obtained from EIS plot of MS in 0.5M HCl in the absence and presence of different concentration of JP from 303-323K

Temperature	Concentration of JP (ppm)	R_s (Ωcm^2)	R_{ct} (Ωcm^2)	n	$Q_{dl} \times 10^{-4}$ $S^n\,\Omega^{-1}\,cm^{-2}$	$C_{dl}(\mu F\,cm^{-2})$	CR (mpy)	IE (%)
	Blank	7.01	22.84	0.80	10.59	417.6	13.24	
	250	6.24	62.51	0.80	6.257	278.2	4.837	63.46
	500	7.69	84.63	0.79	5.399	275.0	3.573	73.01
303K	750	7.65	159.7	0.77	3.961	271.9	1.893	85.69
	1000	7.8	183.3	0.77	3.631	253.1	1.649	87.53
	Blank	5.02	18.91	0.80	15.4	636.1	15.99	
	250	6.80	47.29	0.76	6.125	366.9	6.393	60.01
313K	500	7.74	56.20	0.77	5.665	313.4	5.578	66.35
	750	7.42	105.3	0.76	4.293	295.9	2.871	82.04
	1000	7.73	123.7	0.76	3.794	264.6	2.440	84.71
	Blank	3.571	13.19	0.78	16.57	757.1	22.92	
	250	7.84	29.98	0.76	9.530	568.3	10.08	56.00
323K	500	7.19	33.81	0.74	5.590	345.0	10.01	60.98
	750	6.78	49.43	0.77	6.125	337.4	6.117	73.31
	1000	7.34	67.94	0.75	4.511	304.1	4.450	80.58

Table 7.3. Adsorption parameters from Langmuir adsorption isotherm for the adsorption of JP on the MS at various temperature

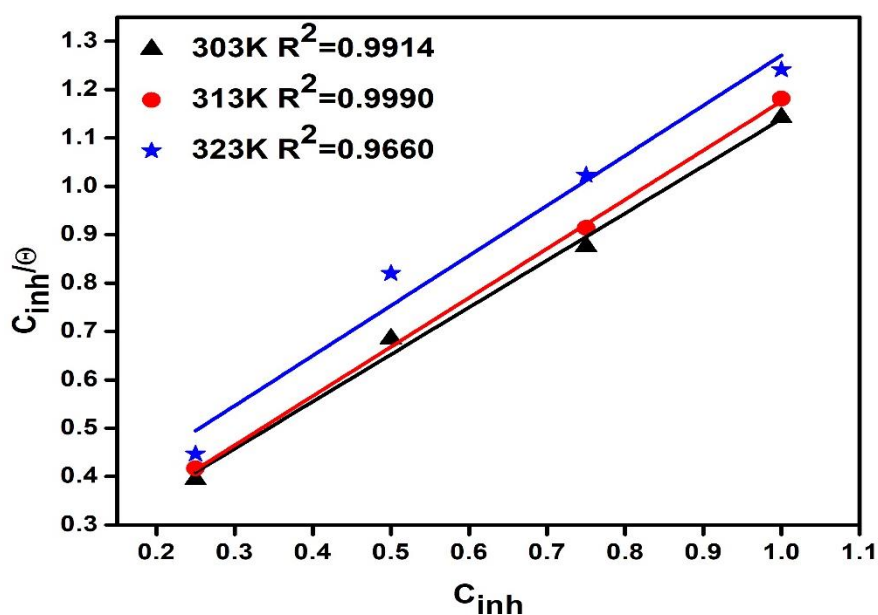| Temperature	K_{ads}	$-\Delta G^0$
303K	6.049	21.93
313 K	6.246	22.74
323 K	4.939	22.84

Figure 7.3. Langmuir adsorption isotherm for MS at different temperature in 0.5M HCl

7.2.4.2. *Thermodynamic and activation parameters*

To evaluate the mechanism of the adsorption process of the studied inhibitor on the MS surface, thermodynamic parameters of adsorption were calculated using the CR from the EIS measurements at temperature ranging from 303-323K. The temperature rise may cause the

decomposition of the protective layer, surface etching, and the desorption of the inhibitor molecules from the MS surface, thereby increasing the corrosion rate[7]. The value of apparent activation energy (Ea) of the corrosion process obtained from the Arrhenius plot (Figure 7.4) are given in the Table 7.4. The Ea value of the corrosion process of MS in the presence of JP is higher than the uninhibited acid solution. The higher Ea observed for 1000ppm of JP discloses good surface coverage via strong adsorption of JP molecules and increases the energy barrier for the corrosion process.

To further elucidate the inhibitive mechanism, thermodynamic parameters like the entropy of adsorption (ΔS) and enthalpy of adsorption (ΔH) for the corrosion process were derived from the Transition state plot. Higher positive values for ΔH in presence of 1000ppm of JP imply the endothermic nature of metal dissolution and difficulty in triggering the reaction [8]. Also, the high positive values of ΔS for 1000ppm of JP indicate that in the rate- determining step, the activated complex signifies dissociation and disordering has taken place from the reactants to the activated complex[9]

Table 7.4. Activation parameters of MS in the absence and presence of JP in 0.5M HCl

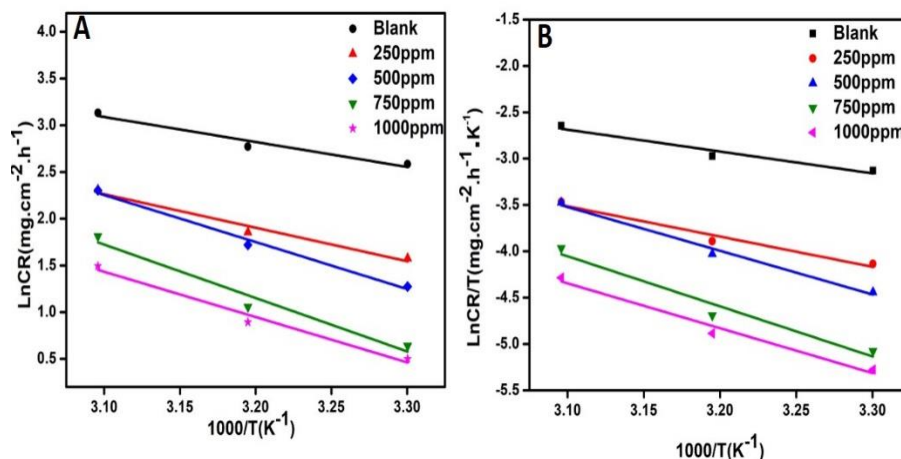| Concentration of pectin (ppm)	Ea (kJmol^{-1})	ΔH (kJmol^{-1})	ΔS (kJmol^{-1})
Blank	22.25	19.61	-39.97
250	29.81	27.17	-23.41
500	41.85	39.22	13.88
750	47.54	44.95	27.23
1000	48.60	48.56	35.17

Figure 7.4. A) Arrhenius and B) Transition state plots of MS in 0.5M HCl with various concentrations of JP

7.2.5. Potentiodynamic polarization study

The corrosion performance of MS in the absence and presence of a varying concentration of JP from 303-323K was also investigated using the PDP technique and is given in Figure 7. 5. The various parameters deduced from the PDP analysis are given in Table 7. 5. The data reveals that the value of CR and I_{corr} decline with an increase in the concentration of JP, indicating that the JP molecule could inhibit corrosion by adsorbing firmly on the MS surface and blocking the diffusion of corrosive ions from the electrolyte. The I_{corr} value obtained for MS in the presence of JP (0.1329mA/cm^2 at 1000ppm) is very lower compared to the blank solution(1.2973mA/cm^2). With increasing the temperature from 303K to 323K, the I_{corr} and CR increases, which can be attributed to the desorption, dissociation, and rearrangement of the inhibitor on the surface of MS. It was also observed that the addition of the JP affects both the anodic metal dissolution and cathodic hydrogen

188

evolution, which implies that JP is a mixed type corrosion inhibitor for MS in 0.5M HCl. The magnitude of the shift in E_{corr} values (<85mV) further corroborates the mixed type corrosion inhibition performance of JP.
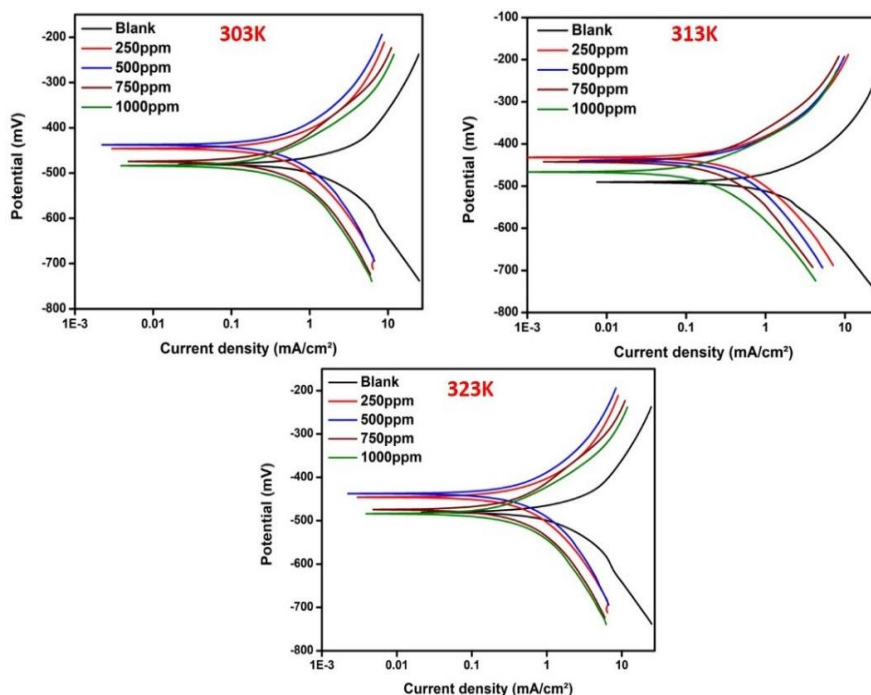

Figure 7.5. PDP plot of MS in 0.5M HCl in the absence and presence of different concentrations of JP from 303-323K

The maximum inhibition efficiency of 89.75% was observed at the JP concentration of 1000ppm at 303K. Upon increasing JP concentration, the value of polarization resistance increases. A high value of R_p (285.8 Ω cm^2) was noted for 1000 ppm of JP indicates that the inhibitor passivates the active site on MS surface. At higher temperatures, lower R_p values are attained due to the diffusion of the corrosive medium into the active site which follows MS corrosion.

Table 7. 5. Parameters obtained from PDP plot of MS in 0.5M HCl in the absence and presence of different concentration of JP from 303-323K

Temperature	Concentration of JP (ppm)	I_{corr} (mA/cm^2)	$-E_{corr}$ (mV)	β_a (mV/dec)	$-\beta_c$ (mV/dec)	R_p (Ω cm^2)	CR (mpy)	IE (%)
	Blank	1.2973	460.56	120.7	223.0	26.21	24.37	
	250	0.4082	440.42	132.3	215.8	87.26	9.703	68.53
303K	500	0.3590	430.95	157.4	226.1	112.3	8.313	72.32
	750	0.1450	467.6	107.5	132.0	177.4	5.029	88.82
	1000	0.1329	446.8	191.6	161.0	285.8	2.392	89.75
	Blank	1.4328	471.15	151.6	207.2	26.53	28.06	
	250	0.5315	431.6	138.9	214.9	68.94	11.91	62.90
313K	500	0.4550	438.7	133.1	230.4	80.51	10.39	68.24
	750	0.3140	442.3	143.9	221.4	120.6	8.224	78.08
	1000	0.2160	466.2	116.7	177.2	141.4	6.549	84.92
	Blank	1.8923	475.8	125.6	214.4	18.17	36.70	
	250	0.7571	445.8	193.2	254.2	62.95	15.16	59.99
323K	500	0.6330	438.4	172.5	200.1	63.54	11.84	66.54
	750	0.4812	472.9	158.1	184.6	76.84	10.82	74.57
	1000	0.4450	484.9	155.0	165.9	78.18	9.229	76.48

7.2.6. Computational study

To explore the corrosion inhibition ability of JP and to correlate their molecular structure with efficiency, DFT calculations were done. The optimized geometry, FMOs, and electrostatic potential (ESP) map of the JP are presented in Figure 7.6. Some of the calculated quantum chemical indices of JP in both the gas and water phase are presented in Table 7.6. It is postulated that the inhibitor molecule donates their bonding and non-bonding electrons to the d orbital of Fe atom and simultaneously the back donation of electrons from the filled orbital of metal to the antibonding molecular orbital of the inhibitor molecule causes a synergistic electron transfer between the metal and the inhibitor molecule. Therefore, an inhibitor with a high value of E_{HOMO} and low value of E_{LUMO} favours strong adsorption leading to better inhibition efficiency. The energy gap (ΔE) is another reactivity parameter that gives an idea about the adsorption tendency and chemical reactivity of the inhibitor molecule[10, 11]. In this study, E_{HOMO}, E_{LUMO}, and ΔE values indicate that the JP molecule can act as a good corrosion inhibitor for MS in 0.5M HCl by adsorbing firmly on the surface of the metal. Moreover, the ΔN values of pectin 0.1212 in the gas phase and 0.1049 in the water phase proposes the donation of the bonding and non-bonding electrons to the d orbital of the metal atom. Concerning the dipole moment values, the μ of pectin (4.4902 Debye) is higher as compared to μ of water (1.85 Debye) which discloses that the JP could adsorb firmly on the surface of the MS by replacing pre-adsorbed water molecules. The electrostatic potential (ESP) map of JP in the gas phase was used as a visual tool to estimate the electron density at different

regions and to determine the more reactive centres in the JP molecule. In the ESP map (Figure 7.6B) the blue colour indicates the most positive (electrophilic) electrostatic potential region and red colour for the most negative (nucleophilic) electrostatic potential region and the zero electrostatic potential region indicated by green colour [12, 13].

Table 7.6. Quantum chemical parameters of JP in gas and water phase

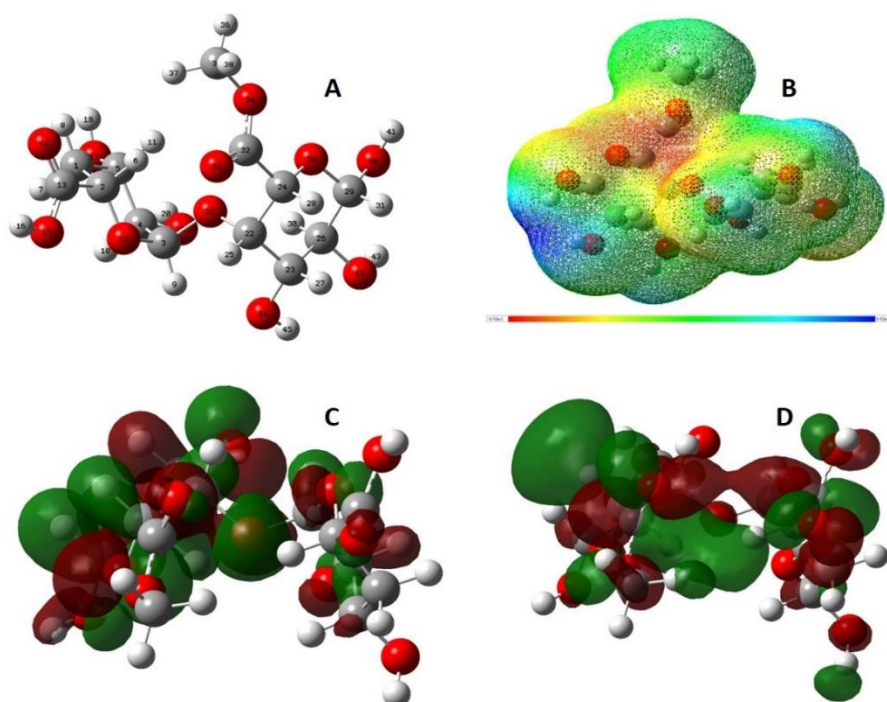| Inhibitor	E_{HOMO} (eV)	E_{LUMO} (eV)	ΔE (eV)	χ (eV)	η (eV)	ΔN
JP (gas phase)	-7.430	-0.5388	6.891	3.984	3.446	0.1212
JP (water phase)	-7.601	-0.5611	7.040	4.081	3.520	0.1049

Figure 7.6. A) Optimized geometry, B) ESP map, C) and (D) FMO of JP.

192

7.2.6.1. Fukui indices

The Fukui functions provide information about the reactive centres in a molecule towards electrophilic and nucleophilic attack. The atomic site for electrophilic attack carrying a positive dual descriptor and nucleophilic attack is controlled by the negative dual descriptor[14, 15]. The values of the condensed Fukui functions for electrophilic and nucleophilic attack in the pectin molecule are given in the Table 7.7. From the analysis of the result, it is clear that O (39) will be the most reactive centre for the electrophilic attack while C (29) will be the most reactive site for the nucleophilic attack from NBO analysis.

Table 7.7. The Fukui indices of JP

Fukui In atom	f^+	f^-	Fukui In atom	f^+	f^-
C (1)	0.0381	0.000	C (23)	0.0131	-0.0065
C (2)	0.0096	0.0046	C (24)	0.0506	-0.0124
C (3)	-0.0001	-0.0112	C (26)	0.0082	0.0043
C (4)	-0.0008	-0.0101	**C (29)**	**0.1906**	-0.011
C (5)	0.1567	0.0088	C (32)	0.0241	-0.0125
O (12)	0.0036	0.0036	O (33)	0.0207	0.029
C (13)	0.0259	-0.0015	O (34)	-0.002	0.0064
O (14)	0.0236	0.0975	C (35)	0.0526	-0.0005
O (15)	0.0146	0.0255	**O (39)**	-0.0013	**0.1246**
O (17)	0.0406	0.0296	O (40)	0.0285	0.0279
O (19)	0.0084	0.0691	O (42)	0.0083	0.069
O (21)	-0.0094	0.0763	O (44)	0.0054	0.0798
C (22)	0.0007	0.0021			

7.2.7. Monte Carlo Simulation

To explore the JP adsorption in gas and water phase on MS in the atomic scale, MC simulation has been carried out. The geometry optimized pectin molecule obtained from quantum mechanical calculation via Gaussian 09 was placed above the (110) plane of Fe. The final snapshot of the top and side view from the last step of MC simulation is given in Figure 7.7. The final visualized snapshots in the gas and water phase designated that the JP molecule could adsorb on the metal surface by aligning parallel to the Fe (1 1 0) surface and thereby establish a corrosion-protective film of JP. The adsorption energy values are tabulated in the Table 7.8 qualitatively state their adsorption capability and further corrosion inhibition performance in both phases. The high negative differential adsorption energy of JP (-143.4 kJ/mol) compared to water molecules (-33.25 kJ/mol) in the water phase indicates the strong adsorption capacity of pectin by replacing the water molecules from the MS surface leading to the formation of a stable corrosion-protective layer[13].

Table 7.8. Energy parameters attained from Monte Carlo simulations for the adsorption of JP on Fe (110) surface in water and gas phase

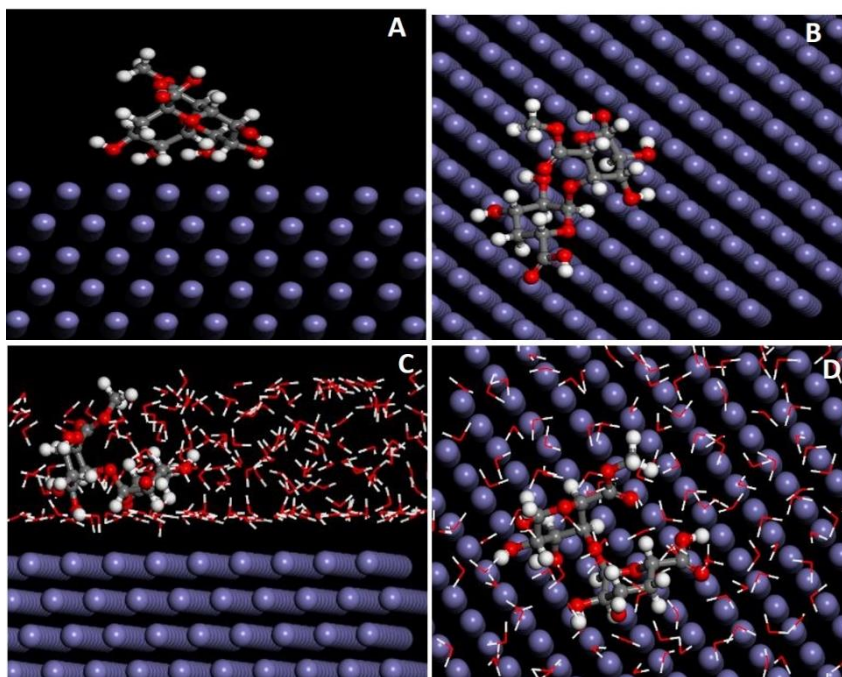| Phase	Total Energy (kJ/mol)	Adsorption Energy (kJ/mol)	Rigid adsorption energy (kJ/mol)	Deformation Energy (kJ/mol)	JP: dEad/dNi (kJ/mol)	Water: dEad/dNi (kJ/mol)
Water	-2.62×10^3	-6.58×10^3	-2.84×10^3	-3.74×10^3	-143.3	-33.25
Gas	-89.53	-163.8	-160.4	-3.338	-163.7	-

Figure 7.7. Side and top view of JP adsorption on Fe (110) surface (A and B) in gas and (C and D) in water phase

7.2.8. FESEM and AFM

To provide visual evidence on the corrosion inhibition performance of the inhibitor JP on MS in 0.5M HCl, surface characterization was carried out using FESEM and AFM analysis. The morphological changes of the sample after 24 hours of immersion in 0.5M HCl in the absence and presence of 1000ppm of pectin was monitored via FESEM micrographs (Figure 7.8). As the figure shows, the MS in the absence of inhibitor is highly damaged with cracks and pits due to the direct attack of corrosive ions. While in the presence of inhibitor the flower-like morphology of polymeric pectin protects the MS from the diffusion of electrolyte.
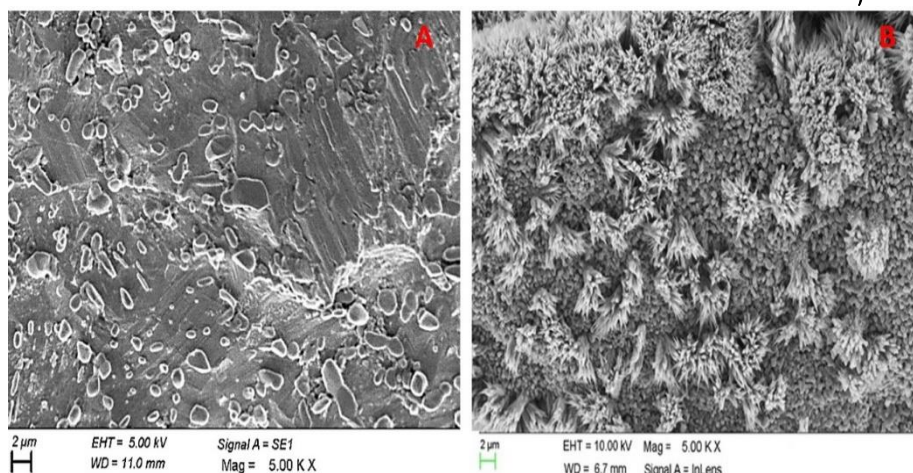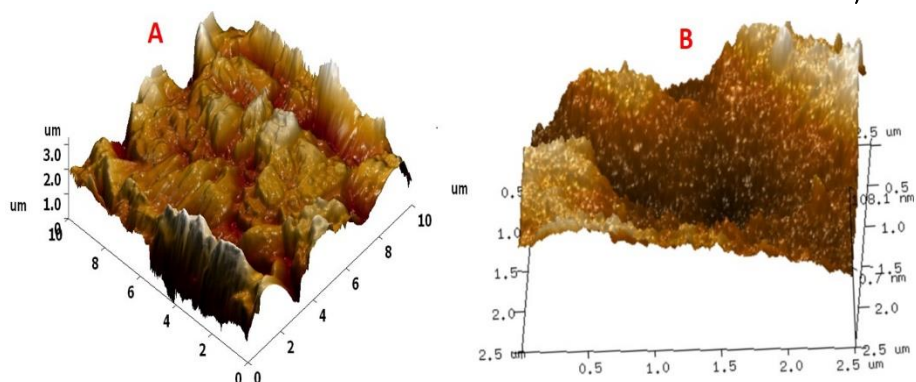
Figure 7.8. FESEM images of MS A) in the absence and B) in the presence of 1000ppm of JP after 24 hours of immersion in 0.5M HCl

To measure surface roughness of the MS sample after 24 hours of exposure to corrosive medium in the absence and presence of pectin, AFM micrographs were recorded (Figure 7.9). The surface roughness of MS after 24 hours immersion in acid solution was 237.84 nm in the absence of pectin and 25.36 nm with 1000 ppm of pectin. The lowering in surface roughness in the presence of the pectin designates the development of protective film on the MS surface by replacing the pre-adsorbed water molecules.

Figure 7.9. AFM images of MS A) in the absence and B) in the presence of 1000ppm of JP after 24 hours of immersion in 0.5M HCl

7.3. Conclusions

Pectin isolated from the jack fruit peel waste acted as a green corrosion inhibitor of MS in 0.5M HCl and the IE was influenced by temperature and concentration of the inhibitor. JP adsorbed on the metal surface in accordance with Langmuir adsorption isotherm. Thermodynamic adsorption parameters established that the JP is adsorbed on MS by a spontaneous mixed chemisorption and physisorption process tending towards the physisorption process. The interaction between the MS surface and JP are well supported by FTIR, SEM, and AFM studies. Quantum chemical studies provided a more detailed interpretation of the mode of donor-acceptor interaction between JP and the metal surface. MC simulation study also confirmed that the JP adsorbed on the MS surface by their horizontal orientation and could inhibit the MS corrosion by replacing the pre-adsorbed water molecule.

References

[1]   F. Akter, M. Haque, JACKFRUIT WASTE: A PROMISING SOURCE OF FOOD AND FEED.

[2]   A.N. Grassino, J. Halambek, S. Djaković, S.R. Brnčić, M. Dent, Z. Grabarić, Utilization of tomato peel waste from canning factory as a potential source for pectin production and application as tin corrosion inhibitor, Food hydrocolloids, 52 (2016) 265-274.

[3]   D. Govindaraj, M. Rajan, A.A. Hatamleh, M.A. Munusamy, From waste to high-value product: Jackfruit peel derived pectin/apatite bionanocomposites for bone healing applications, International journal of biological macromolecules, 106 (2018) 293-301.

[4]   E.C. Arollado, K.M.G. Ponsaran, M.M. Loquias, Isolation and Characterization of Pectin from the Ripe Fruit Peels of Jackfruit (Artocarpus heterophyllus Lam.), Acta Medica Philippina, 52 (2018).

[5]   A. Fekry, R.R. Mohamed, Acetyl thiourea chitosan as an eco-friendly inhibitor for mild steel in sulphuric acid medium, Electrochimica Acta, 55 (2010) 1933-1939.

[6]   K. Shainy, P.R. Ammal, A. Joseph, Development of passive film and enhancement of corrosion protection of mild steel in hydrochloric acid through the synergistic interaction of 2-amino-4-methyl benzothiazole (AMBT) and (E)-2-methylbenzo [d] thiazol-2-yl) imino-4-methyl) phenol (MBTP, Egyptian journal of petroleum, (2017).

[7]   P.R. Ammal, M. Prajila, A. Joseph, Effect of substitution and temperature on the corrosion inhibition properties of benzimidazole bearing 1, 3, 4-oxadiazoles for mild steel in sulphuric acid: physicochemical and theoretical studies, Journal of environmental chemical engineering, 6 (2018) 1072-1085.

[8]   M.V. Fiori-Bimbi, P.E. Alvarez, H. Vaca, C.A. Gervasi, Corrosion inhibition of mild steel in HCL solution by pectin, Corrosion science, 92 (2015) 192-199.

[9]   F. Bentiss, M. Lebrini, M. Lagrenée, Thermodynamic characterization of metal dissolution and inhibitor adsorption processes in mild steel/2, 5-bis (n-thienyl)-1, 3, 4-thiadiazoles/hydrochloric acid system, Corrosion Science, 47 (2005) 2915-2931.

[10]   T. Arslan, F. Kandemirli, E.E. Ebenso, I. Love, H. Alemu, Quantum chemical studies on the corrosion inhibition of some sulphonamides on mild steel in acidic medium, Corrosion Science, 51 (2009) 35-47.

[11]   I. Obot, N. Obi-Egbedi, Theoretical study of benzimidazole and its derivatives and their potential activity as corrosion inhibitors, Corrosion Science, 52 (2010) 657-660.

[12]   K. Shamsheera, R.P. Anupama, J. Abraham, Computational simulation, surface characterization, adsorption studies and electrochemical investigation

on the interaction of guar gum with mild steel in HCl environment, Results in Chemistry, (2020) 100054.

[13]   S. Kaya, B. Tüzün, C. Kaya, I.B. Obot, Determination of corrosion inhibition effects of amino acids: quantum chemical and molecular dynamic simulation study, Journal of the Taiwan Institute of Chemical Engineers, 58 (2016) 528-535.

[14]   K. Ramya, R. Mohan, K. Anupama, A. Joseph, Electrochemical and theoretical studies on the synergistic interaction and corrosion inhibition of alkyl benzimidazoles and thiosemicarbazide pair on mild steel in hydrochloric acid, Materials Chemistry and Physics, 149 (2015) 632-647.

[15]   C. Verma, L.O. Olasunkanmi, E.E. Ebenso, M.A. Quraishi, I.B. Obot, Adsorption behavior of glucosamine-based, pyrimidine-fused heterocycles as green corrosion inhibitors for mild steel: experimental and theoretical studies, The Journal of Physical Chemistry C, 120 (2016) 11598-11611.

Summary and Future Outlook

The thesis evaluates the usage of some carbohydrate polymers like chitosan, guar gum, and pectin isolated from the jackfruit peel waste to control the mild steel corrosion in acidic and saline media. To enhance the protection efficiency of hydrophilic chitosan coating, stearic acid has been grafted into chitosan via a coupling reaction. The developed coating act as a protective shield for mild steel in 0.5M HCl and 3.5% NaCl. Further enhancement in corrosion protection has been observed when chitosan film is preloaded with mesoporous hydrophobic silica and grafting with stearic acid. Guar gum offered good corrosion inhibition for mild steel in 0.5M HCl. The inhibition efficiency is more enhanced when two non-ionic surfactants (Tween -80 and Triton-X) has been used as additive in very small amounts. The isolated pectin from jackfruit peel waste also offered good corrosion inhibition for mild steel. Corrosion monitoring techniques like weight loss method, potentiodynamic polarization (PDP), and electrochemical impedance spectroscopy (EIS) were employed to study the corrosion prevention behaviour of these carbohydrate polymers. Techniques like FTIR, XPS, FESEM, AFM, etc were used to ensure the presence of corrosion formulations on the metal surface. Theoretical quantum chemical calculations (DFT and Monte Carlo simulation) were also done to corroborate the experimental findings.
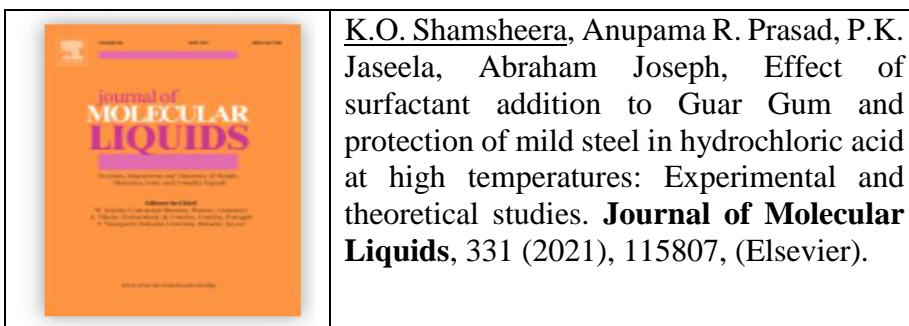
Scope for the future work

The present work has led to the development of some new carbohydrate polymers/derivative as corrosion formulations for mild steel in 0.5M HCl and 3.5% NaCl. However, in order to make these carbohydrate polymers more versatile and robust the following is proposed for future consideration.

- To evaluate the enhancement in corrosion inhibition of guar gum by the addition of ionic surfactants.
- To develop some carbohydrate polymer nanocomposite as corrosion resistant coating
- To evaluate the studied carbohydrate polymer-based corrosion formulations for other active metals/corrosive medium.

List of Publications

	<u>Shamsheera K O</u>, Anupama R Prasad, Julia Garvasis, Sabeel M Basheer & Abraham Joseph, Stearic acid grafted chitosan/epoxy blend surface coating for prolonged protection of mild steel in saline environment, **Journal of Adhesion Science and Technology,** 33 (2019), 2250-2264, (Taylor and Francis).
	<u>Shamsheera K O</u>, Anupama R. Prasad, Jaseela PK and Abraham Joseph, Development of self-assembled monolayer of stearic acid grafted chitosan on mild steel and inhibition of corrosion in hydrochloric acid, **Chemical Data Collections**, 28 (2020), 100402, (Elsevier).
	<u>K.O. Shamsheera</u>, R. Prasad Anupama, and Joseph Abraham, Computational simulation, surface characterization, adsorption studies and electrochemical investigation on the interaction of guar gum with mild steel in HCl environment, **Results in Chemistry**, 2 (2020), 100054, (Elsevier).
	<u>K.O. Shamsheera</u>, Anupama R. Prasad, Abraham Joseph, Extended protection of mild steel in saline and acidic environment using stearic acid grafted chitosan preloaded with mesoporous-hydrophobic silica (mhSiO$_2$), **Surface and Coatings Technology**, 402 (2020), 126350, (Elsevier).

	K.O. Shamsheera, Anupama R. Prasad, P.K. Jaseela, Abraham Joseph, Effect of surfactant addition to Guar Gum and protection of mild steel in hydrochloric acid at high temperatures: Experimental and theoretical studies. **Journal of Molecular Liquids**, 331 (2021), 115807, (Elsevier).

Under Review/Revision:

- A sustainable method of mitigating acid corrosion of mild steel using J-Pectin as green inhibitor-New Journal of Chemistry

Other Publications

	Anupama R Prasad, <u>Shamsheera K O</u>, Julia Garvasis, & Abraham Joseph, Bio-inspired green synthesis of zinc oxide nanoparticles using ABELMOSCHUS ESCULENTUS mucilage and selective degradation of cationic dye pollutants, **Journal of Physics and Chemistry of Solids,** 127 (2019), 265-274, (Elsevier).
	Anupama R Prasad, <u>Shamsheera K O</u>, Anagha M, & Abraham Joseph, Bio-fabricated ZnO nanoparticles: direct sunlight-driven selective photodegradation, antibacterial activity, and thermoluminescence-emission characteristics, **New Journal of Chemistry,** 44 (2020), 8273-8279, (RSC)
	Jaseela P K, <u>Shamsheera K O</u>, Mathew Kuruvilla, Chinju Jacob, Linda Williams, & Abraham Joseph, Excellent protection of mild steel in sodium chloride solution for a substantial period of time using a hybrid nanocoating of poly vinyl alcohol and Titania, **Arabian journal of Chemistry**, 13 (2020), 6921-6930, (Elsevier).
	Julia Garvasis, <u>Shamsheera K O</u>, Anupama R Prasad, Jaseela P K, & Abraham Joseph, Efficient removal of Congo red from aqueous solutions using phytogenic aluminum sulfate nano coagulant, **Materials Chemistry and physics,** 251 (2020), 123040, (Elsevier).

	P.K. Jaseela, <u>K.O. Shamsheera</u>, & Abraham Joseph, Mesoporous Titania-Silica nanocomposite as an effective material for the degradation of Bisphenol A under visible light, **Journal of Saudi Chemical Society**, 24 (2020), 651-662, (Elsevier).
	P.K. Jaseela, <u>K.O. Shamsheera</u>, & Abraham Joseph, HMDS–GPTMS Modified Titania Silica Nanocomposite: A New Material for Oil–Water Separation, **Journal of Inorganic and Organometallic Polymers and Materials**, 30 (2020), 2134–2141, (Springer).
	Anupama R Prasad, Linda Williams, Julia Garvasis, <u>K.O. Shamsheera</u>, Sabeel M. Basheer, Mathew Kuruvilla & Abraham Joseph, Applications of phytogenic ZnO nanoparticles: A review on recent advancements, **Journal of Molecular Liquids**, 331 (2021), 115805, (Elsevier).

Under Review/ Revision:

- Protective coating of PVA@3WGO offers enhanced corrosion resistance to mild steel in acidic and saline environment: surface examination and electroanalytical studies- Results in Surfaces and Interfaces

- Long-term protection of mild steel in hydrochloric acid using mercaptobenzimidazole loaded zinc-ceria (ZnO-CeO2) coating – Electrochemical, mass loss and surface studies- Results in Surfaces and Interfaces

List of Presentations

- **Corrosion protection of mild steel in hydrochloric acid using stearic acid grafted chitosan film: Electroanalytical and surface studies,** International seminar on Emerging Frontiers in Chemical Sciences- EFCS, 23-25 September 2017, Organized by Post Graduate and Research department of Chemistry, Farook College.

- **Development and electrochemical screening of Chitosan/SiO2 based anticorrosive nanocomposite film on mild steel**, National seminar on Medicinal Chemistry, 24th & 25th July 2017, Organized by Post Graduate Department of Chemistry, KAHM Unity Women's College, Manjeri. **ISBN: 978-93-5279-420-1.**

- **Development of hydrophobic stearic acid grafted chitosan film as a protective shield for mild steel in hydrochloric acid environment,** National seminar on Frontiers in Chemical Sciences-FCS, 26-28th February 2018, Organized by Department of Chemistry, University of Calicut.

- **Enhancement of corrosion resistance of chitosan film using stearic acid grafting with preloaded mesoporous-hydrophobic silica in 0.5M HCl, National conference on** Emerging Frontiers in Chemical Sciences- EFCS, 4-5 December 2020, Organized by Post Graduate and Research department of Chemistry, Farook College.